# ENVIRONMENTAL TRACERS IN GROUNDWATER OF THE SALT BASIN, NEW MEXICO, AND IMPLICATIONS FOR WATER RESOURCES

By

SOPHIA CARMELITA SIGSTEDT

Master of Science in Hydrology

New Mexico Institute of Mining and Technology

Socorro, New Mexico

2010

Submitted to the Faculty of the
Earth and Environmental Science Department of the
New Mexico Institute of Mining and Technology
in partial fulfillment of
the requirements for
the Degree of
MASTER OF SCIENCE IN HYDROLOGY
August, 2010

ENVIRONMENTAL TRACERS IN GROUNDWATER

OF THE SALT BASIN, NEW MEXICO, AND

IMPLICATIONS FOR WATER RESOURCES

Thesis Approved:

Dr. Fred M. Phillips

Thesis Adviser

Dr. Penelope J. Boston

Dr. Mark Person

Dr. David B. Johnson

Dean of Graduate Studies

# ACKNOWLEDGMENTS

My thanks go out to my field partner Andre Ritchie who braved the dust storms, gas leaks, flat tires, javalinas, and all the other unexpected obstacles the Salt Basin had to throw at us.

I want to thank my Advisor Dr. Fred Phillips who gave me the wonderful opportunity of working on this adventurous project. I truly appreciate his attention to detail and ability to patiently explain everything from comma placement to cosmic rays.

Thanks to my committee members, Dr. Mark Person and Dr. Penny Boston, for their encouragement and perspective.

A special thanks to Stacy Timmons and Lewis Land, from the New Mexico Bureau of Geology and Mineral Resources, particularly for their guidance with sampling during the early stages of the field work for this project.

I want to thank Andy Campbell not only for the many water analyses he ran for this project, but also for his availability to answer questions and guide me toward the next step.

Thanks to my research group for their input and support. I especially want to thank Jeremiah Morse who was working on a similar project when I started and kept me going in the right direction. I also want to thank Marty Frisbee for being so generous with his time and ideas.

This Salt Basin study is part of a much larger project to assess the Salt Basin Aquifer system. It was really interesting working on a project being analyzed from so many different angles. I want to thank everyone we worked with: Bill Miller (Engineers), Craig Roepke (ISC), John Kay (D&B Stephens), David Jordan (Intera), Penny Boston (NMT), Todd umstot (D&B Stephens), Jan Hendrickx (NMT), Anne Tillery (USGS), and Steve Finch (Shomaker & Assoc.)

TABLE OF CONTENTS

Chapter Page

Chapter Page

LIST OF TABLES

Table Page

LIST OF FIGURES

Figure Page

Figure Page

Figure Page

# CHAPTER I

# INTRODUCTION

## Section 1.1: Present Investigation/Purpose and Scope

The Salt Basin in southern New Mexico (fig. 1.1) is an example of a groundwater system that is heavily pumped, primarily for agricultural purposes, while the recharge rates and storage capacity of the basin are not fully understood. Current figures for recharge to the Salt Basin groundwater system range from 15,000-100,000 acre-ft/yr. These estimates came out following the designation of the Salt Basin by the State Engineer in 2000. They are based on a series of studies which were compiled, along with each author's estimate, primarily in two reports: one by John Shomaker & Associates, Inc., and the other by Sandia National Labs and the USGS (Finch, 2002; Huff and Chace 2006). South of the New Mexico portion of the Salt Basin, just below the NM-TX state line, is the Dell City Irrigation District. In 2000 as much as 210,000 acre-ft of water was used to irrigate about 50,000 acres of farm land in Dell City (Chace and Huff, 2006). While current rates of pumping in Dell City are at least half that, competing interests have arisen in the basin as a future water source. resulting in three applications over the appropriation of the Salt Basin groundwater; two of which ask the Office of the State Engineer for the designation of almost 100,000 acre-ft/yr, each (Buynek, 2007). It is apparent that the large uncertainty regarding the amount of recharge to the Salt Basin constitutes a serious impediment to proper resource management, for which the amount of recharge as well as spatial distribution need to be better constrained.

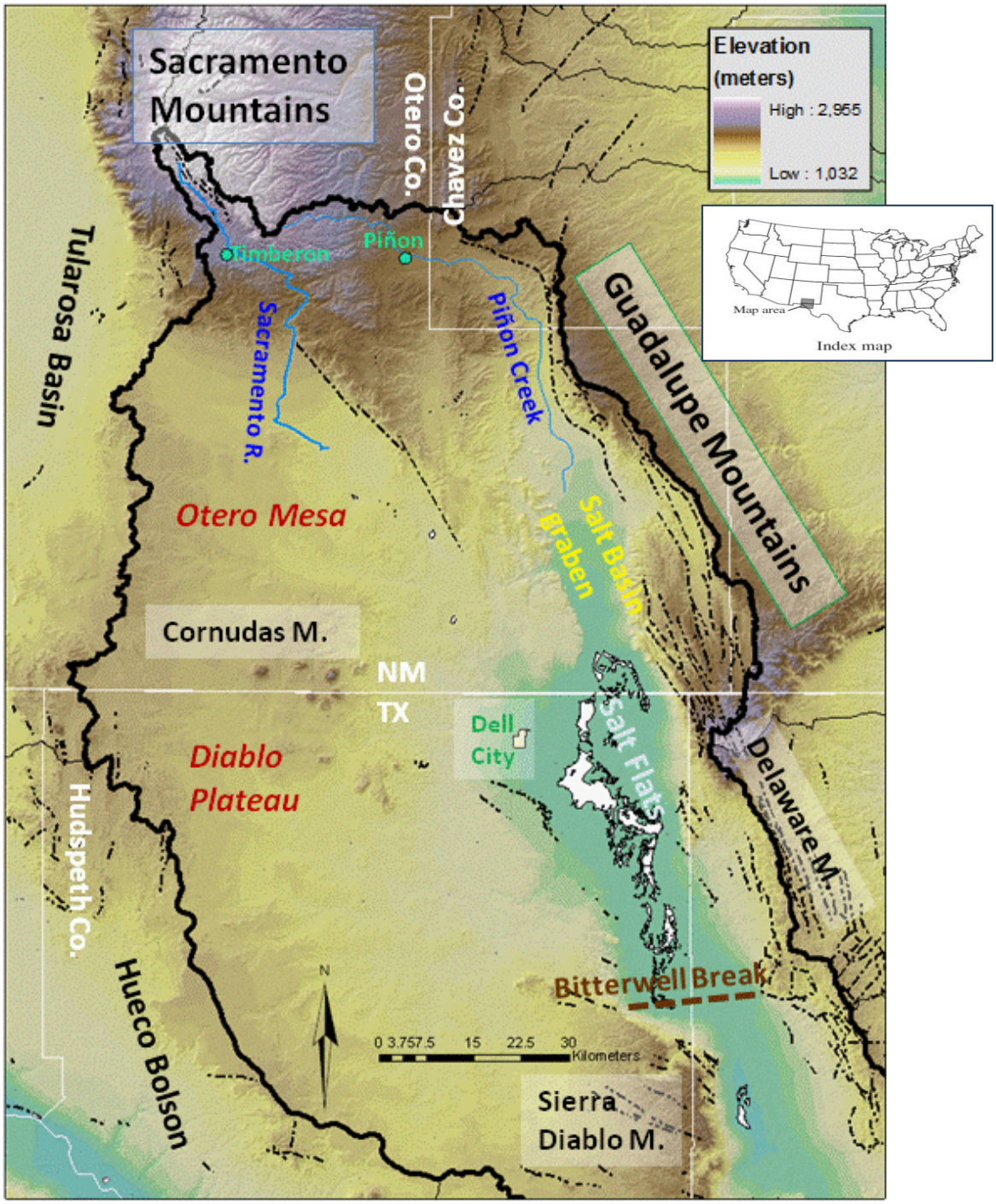


**Figure 1.1** Salt Basin study area with important physiographic features and locations. Outlined in black is the Salt Basin Watershed. Hydrographic features sourced from the National Hydrography Dataset (NHD). Dashed lines represent faults. Elevation coverage from National Elevation Dataset (NED). Map made with ArcGIS.

A regional scale integrated, conceptual model of the Salt Basin groundwater system is lacking. The Salt Basin can generally be typified as a karstic aquifer, for which flow paths and permeability are difficult to quantify because of extensive small-scale variability in porosity and fracture-dominated connectivity (Bakalowicz, 2005). Understanding dominant trends in basin-scale permeability associated with the tectonic forcing and depositional environment during the formation of the Salt Basin is a critical foundation for the hydrogeologic conceptual model. However, due to the small number of wells and high degree of natural variability in permeability and other hydrologic properties, well hydraulics are of limited utility in basin analysis. In this situation, basin-scale hydrodynamics of the system can be effectively characterized by means of environmental tracers. These are naturally present in the groundwater system and can illustrate integrated hydrologic behavior along flow paths. In this study, a suite of environmental tracers have been quantified in the Salt Basin groundwater system in order to obtain information on sources of recharge, estimates of recharge rates, flow paths, flow rates, and sources of solutes in the groundwater.

Groundwater chemistry evolves with time and distance along a flow path. The chemical evolution is determined by geochemical mass transfer between the groundwater and the lithology of the aquifer units. Understanding the dominant controls on this chemical evolution can elucidate flow path directions as well as sources of solutes in the groundwater.

Two important tracers we have employed are the stable isotope ratios of oxygen ($^{18}O/^{16}O$) and deuterium ($^{2}H/^{1}H$). These isotopes, present in the molecules of groundwater that originate as atmospheric precipitation, are a function of precipitation

conditions such as amount of precipitation, elevation, and temperature, and are thus a reflection of the conditions under which recharge occurs. This connection allows for their application in determining sources of recharge, as well as flow paths from the source and evaporation effects. Stable isotope ratios of $^{18}O/^{16}O$ ($\delta^{18}O$) and $^{2}H/^{1}H$ ($\delta D$) have also been used in groundwater studies to reveal evidence for the presence of very old water recharged into the aquifer during very different local climate conditions such as during the Pleistocene.

Recharge estimates for the Salt Basin will primarily be determined by dating the groundwater using carbon-14 which is subject to radioactive decay. For the most accurate apparent ages the carbon-14 measured from the groundwater needs to be corrected for the dilution of atmospheric $CO_2$ by rock/water interactions with dead rock carbon along the flow path. Geochemical mass transfer reactions are defined based on an understanding of the mineralogy of the aquifer units, as well as the geochemical evolution of the Salt Basin groundwater. Subsurface reaction models based on the geochemistry can be used to correct the carbon-14. Seepage velocities can be estimated using groundwater residence times determined from the radiocarbon dating along well defined flow paths. With estimates for flow velocity and porosity groundwater flux can be calculated across a given subsurface cross-section. This in turn, can be related to the recharge flux entering the Salt Basin along primary flow paths. Understanding rates of recharge in the Salt Basin is a critical component for sustainable resource management.

## Section 1.2: Study Area

The northern portion of the Salt Basin (fig 1.1) is located primarily in southeastern Otero County New Mexico, and Hudspeth County Texas. At the northern boundary of the Salt Basin are the Sacramento Mountains which extend slightly into the basin. The western margin of the Salt Basin in New Mexico is located where the Otero Mesa uplift meets the Tularosa Basin; in Texas the western margin is the Diablo Plateau. To the east the Salt Basin is bounded by the Guadalupe Mountains and Brokeoff Mountains in New Mexico; these extend south into the Delaware Mountains in Texas. The southern boundary for the New Mexico portion of the Salt Basin, based on its designation for the N.M. State Engineer's Office is the New Mexico, Texas state line. However, hydrologically, the southern boundary for the northern portion of the Salt Basin is better defined by the beginnings of the Sierra Diablo Mountains in Texas, which represent a surface-water drainage divide and a fault zone which divides the subsurface flow (Kreitler, 1990). In its entirety, the Salt Basin extends through Texas and into Mexico. Because the northern portion of the Salt Basin is a hydrologically closed basin, natural groundwater discharge takes place north of the groundwater divide in a series of playas known as the Salt Flats.

### Section 1.2.a: Physiography

Most of the defining topographic features are a result of crustal extension associated with the North American Basin and Range Province; of which the Salt Basin (fig 1.1) is part of the eastern extent. The typical east-west crustal deformation results in downfaulted valleys, or grabens, and upfaulted mountains. The Salt Basin graben that

lies between the Sacramento Mountains, the Guadalupe Mountains and the Otero Mesa, is a result of this type of tectonic activity. The floor of the Salt Basin graben is almost planar, dipping gently to the south between the elevations of about 1,000 and 1,100 m (Mayer, 1995). The elevations of the surrounding uplands are at about 2,500-2,900 m for the Sacramento Mountains, 1,500-2,100 m for Otero Mesa, and 1,400- 2,600 m for the Guadalupe Mountains. The southern extension of the Sacramento Mountain uplift that lies east of Otero Mesa and meets the northern boundary of the Salt Basin graben is the Chert Plateau (Mayer, 1995). The topography of the Chert Plateau and eastern Otero Mesa is characterized by many low elevation hills that focus surface water flow, creating distinct draws that wind through the hills. These shallow, broad, natural watercourses open out and disappear as they meet the flats of the Salt Basin graben. West of the Salt Basin graben, in the southern extent of the Otero Mesa, are several Tertiary igneous intrusions known as the Cornudas Mountains that form distinct and isolated peaks rising to about 2,100 m.

**Section 1.2.b: Climate**

North in the Salt Basin, in the region associated with the southern Sacramento Mountains, temperatures range from minima (fig 1.2) of -9 to -6 °C (15-20 °F) to maxima (fig 1.3) of 21 to 23 °C (60-70 °F) with an average (fig 1.4) around 6 to 9 °C (43 to 50 °F). The lowlands in the southern Salt Basin exhibit characteristically semiarid climate conditions. The range of temperatures throughout the year is from minima (fig 1.2) of about -4 to 1 °C (25-33 °F), to maxima (fig 1.3) of about 29-36 °C (85-97 °F), with an average (fig 1.4) of about 12-17 °C (53-63 °F); typically with large temperature shifts between the day and night.

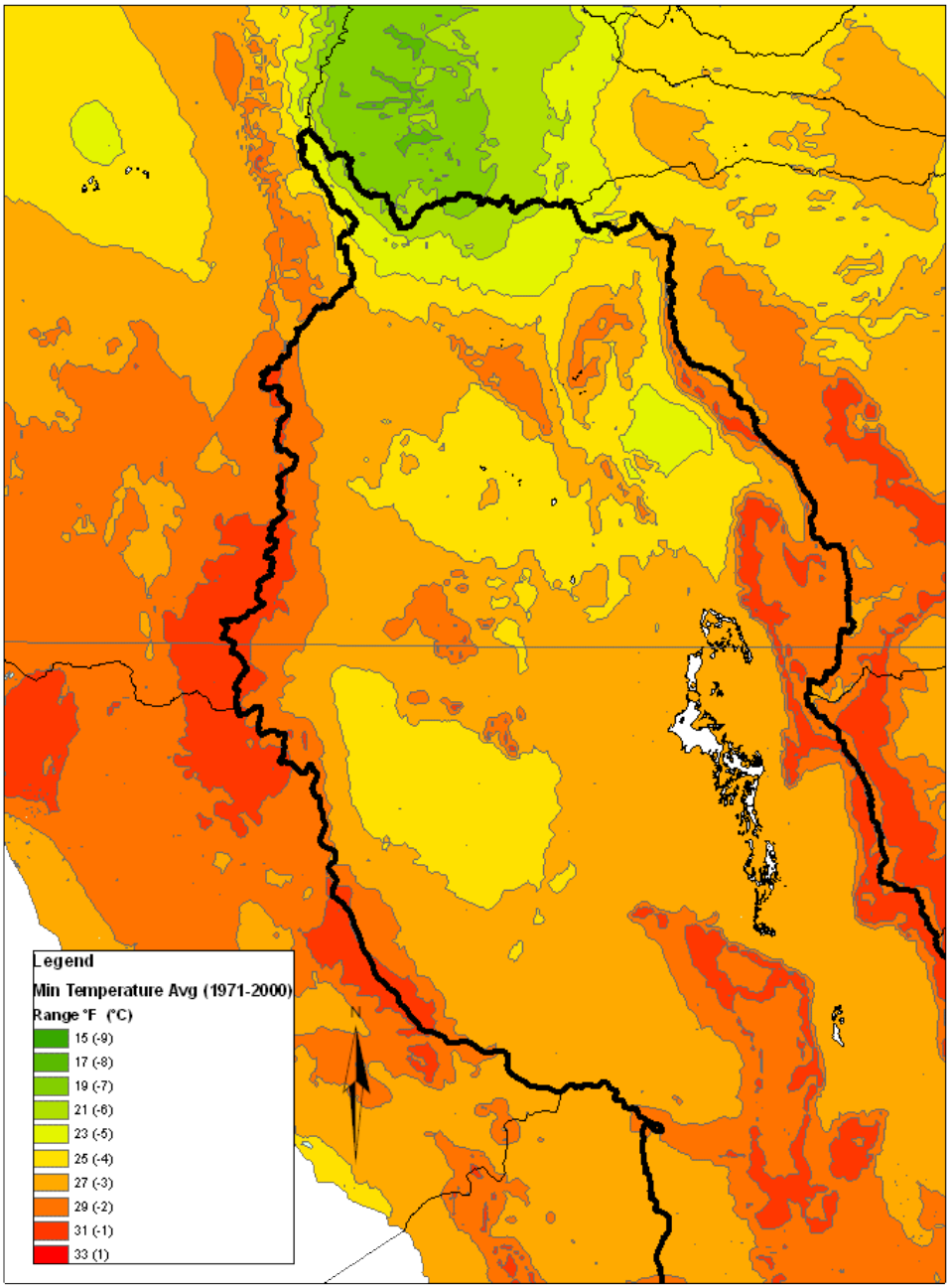


**Figure 1.2** Minimum annual temperature distribution in the Salt Basin. Source is USDA which presents averages over the years 1971 to 2000.

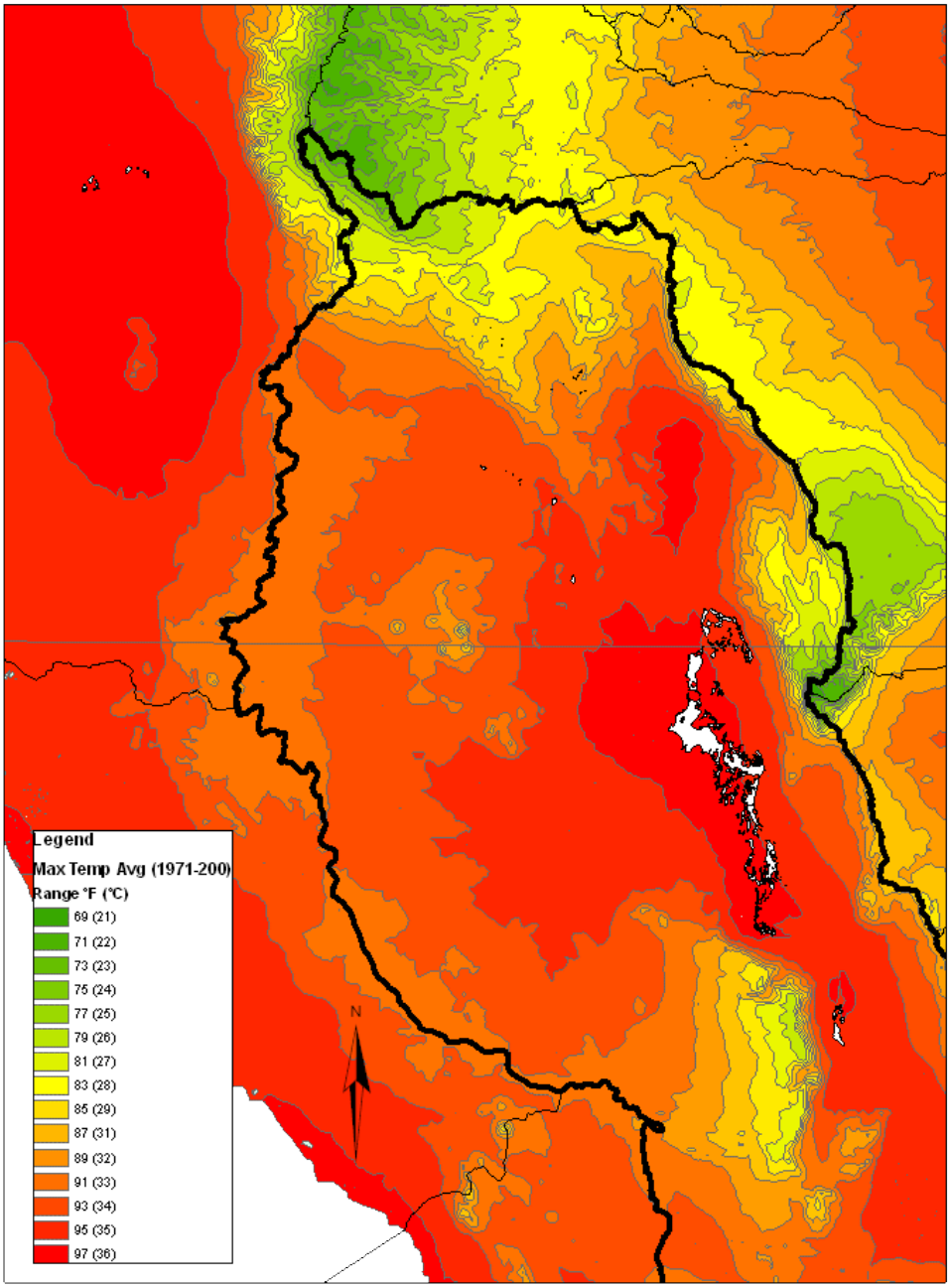


**Figure 1.3** Maximum annual temperature distribution in the Salt Basin. Source is USDA which presents averages over the years 1971 to 2000.

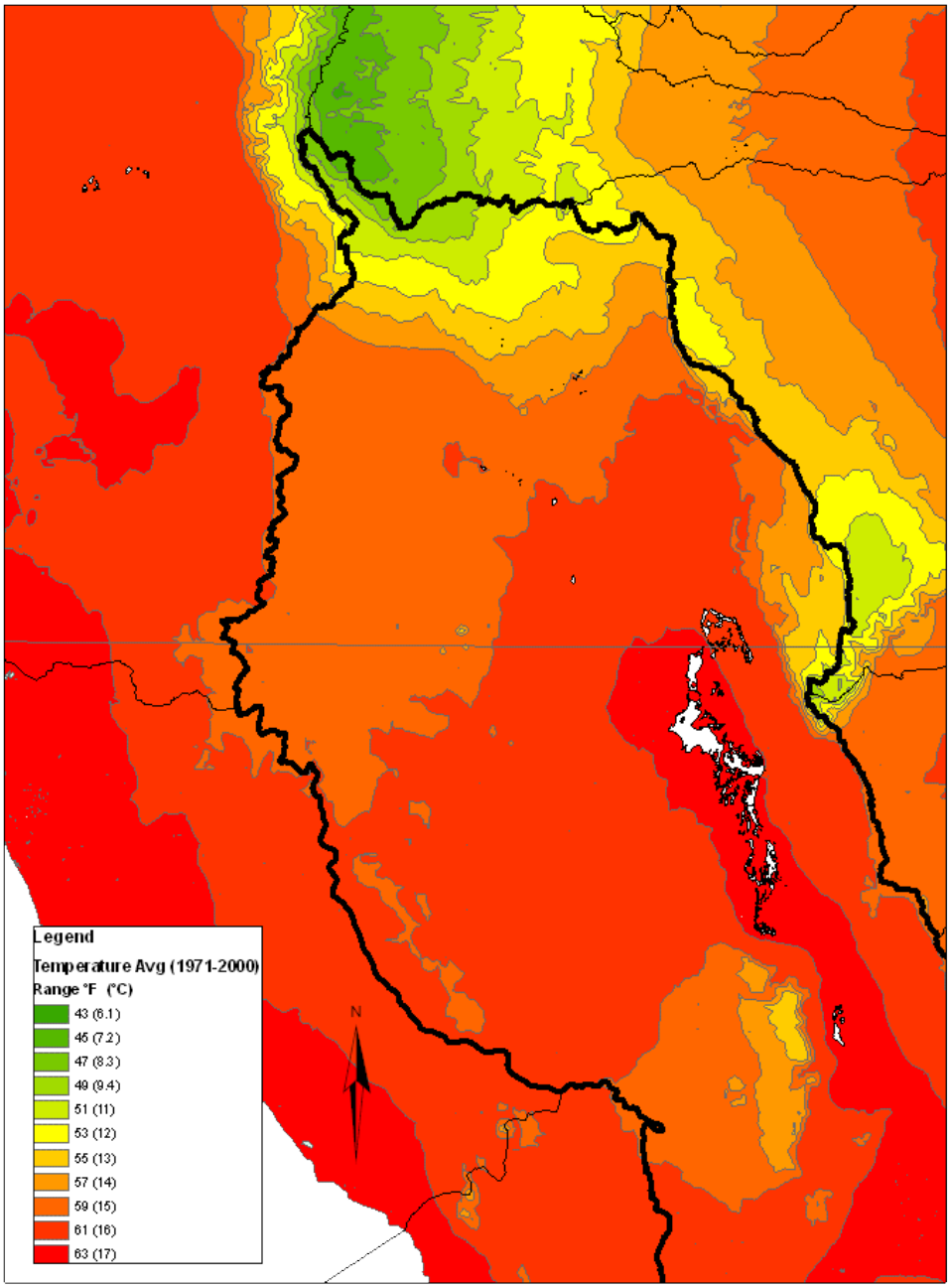


**Figure 1.4** Average annual temperature distribution in the Salt Basin. Source is USDA which presents averages over the years 1971 to 2000.

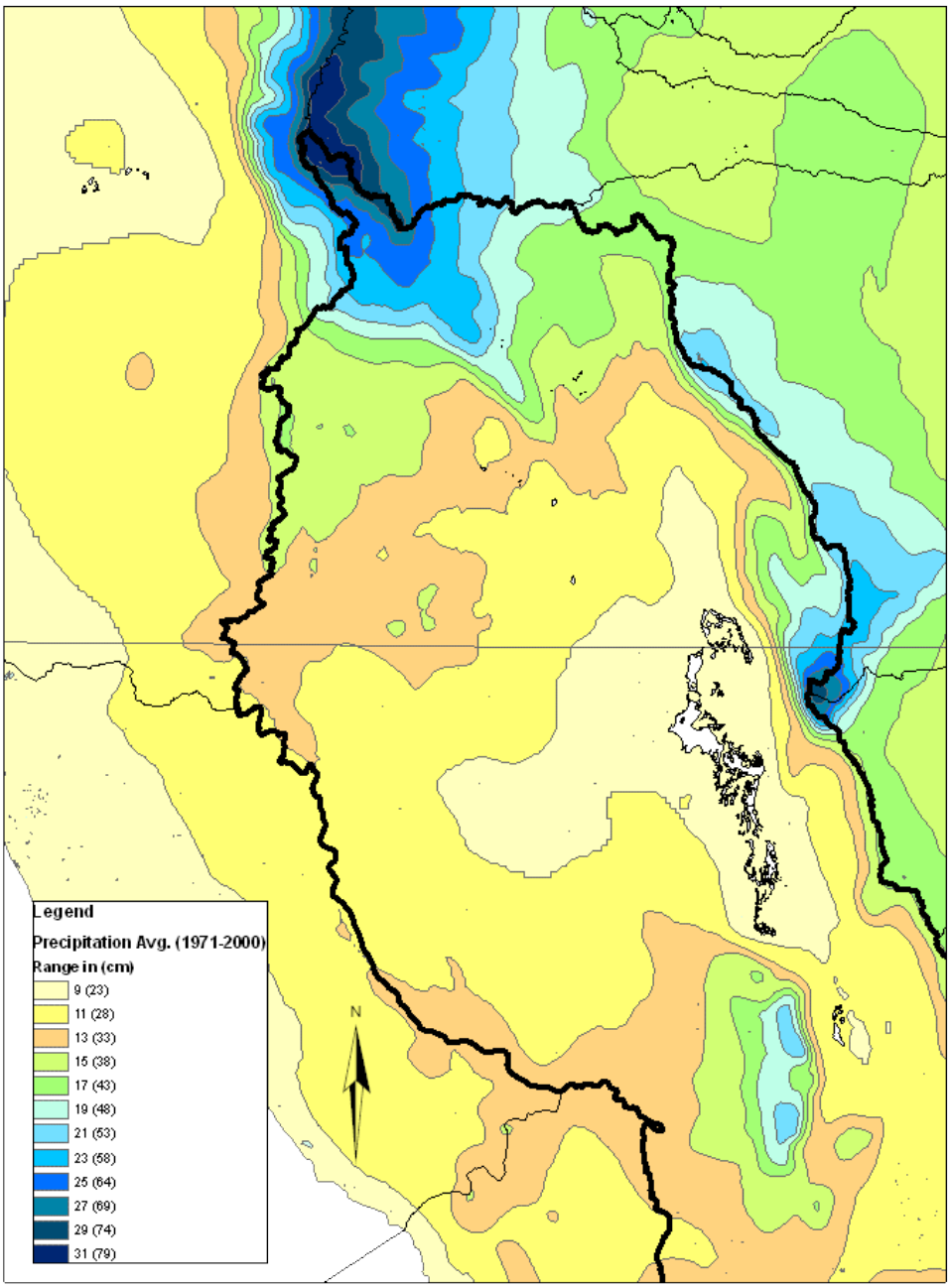


**Figure 1.5** Average annual precipitation in the Salt Basin. Calculated from averages of mean monthly precipitation using PRISM. Source is USDA which presents averages over the years 1971 to 2000.

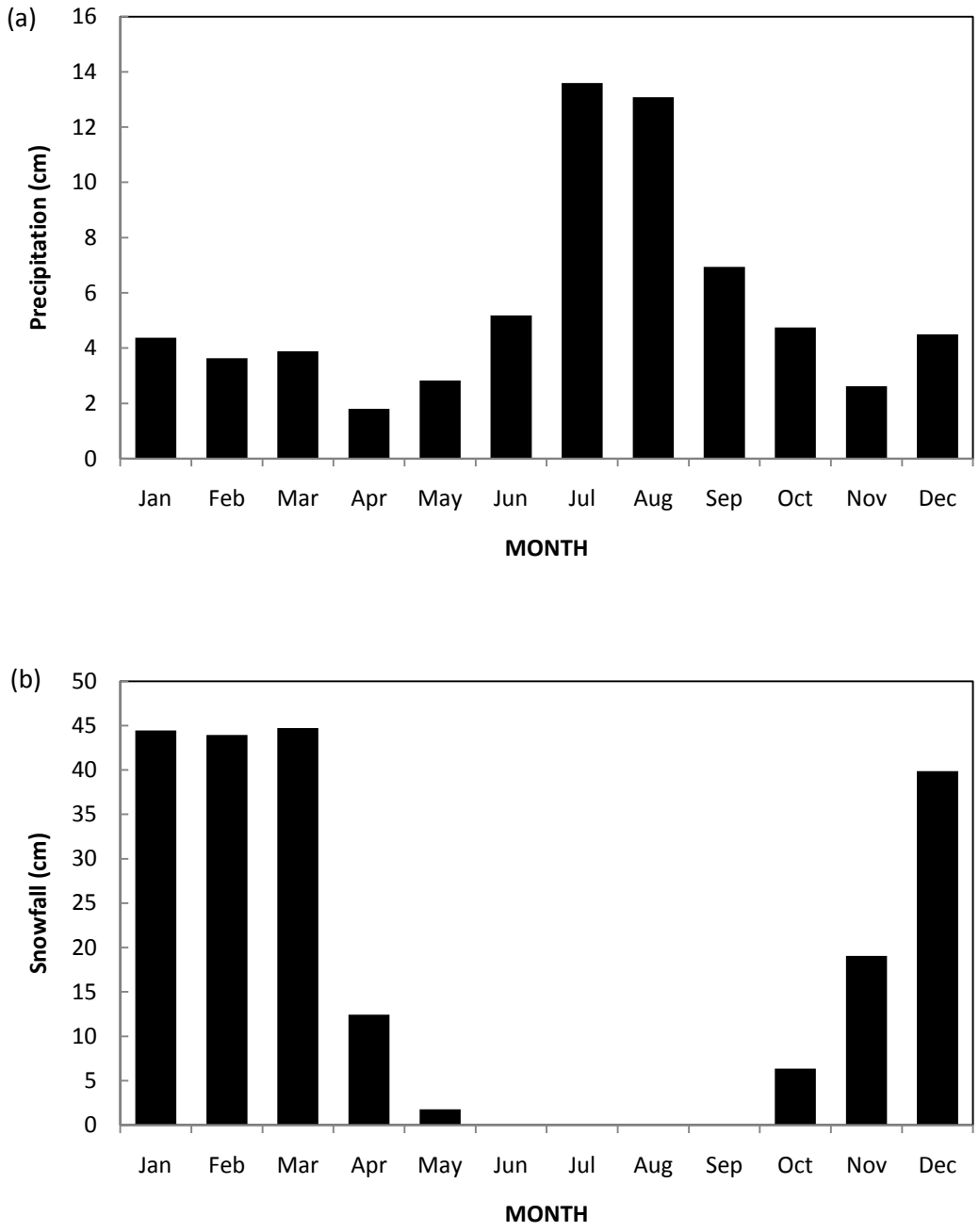


**Figure 1.6** Sacramento Mountains, Cloudcroft NM, monthly climate record. (a) Average total precipitation (1914-1987) (b) Average total snowfall (1914-1987). Western Regional Climate Center

The amount of rainfall received throughout the Salt Basin (fig 1.5) is quite variable with a range from about 79 cm/yr (31 inches/yr) to about 23 cm/yr (9 inches/yr). There is a strong correlation between precipitation and elevation as rainfall is primarily due to orographic effects. The majority of the rainfall in the Salt Basin is associated with the monsoon season from May to October (fig 1.6.a.). In the southern Sacramento Mountains snowfall (fig 1.6.b) during the winter is a significant contribution to the annual precipitation.

**Section 1.2.c: Ecosystem**

The ecoregions for the Salt Basin (fig 1.7) are based on the EPA's level IV designation. The highest elevations with the coolest temperatures are characteristic of the Rocky Mountain Conifer Forest ecoregion. In this region flora, fauna, and water characteristics resemble the southern Rocky Mountains. Ponderosa pine, douglas fir, and where it is especially cool and moist, blue spruce, are present. Typically, thick understory is prevalent and pine needles and other organic matter litter the ground resulting in high soil moisture. The ecosystem characteristic of the lower elevation, southern Sacramento Mountains is the Madrean Lower Montane ecoregion, which is also characteristic of most of the Guadalupe Mountains. In this ecoregion winters are mild and summers are wet. Juniper and piñon pine trees are interspersed between desert grasses.

The climate and ecoregions in the Salt Basin lowlands are a reflection of dry semiarid conditions. There is sunshine most days of the year and mild winters that lead to extended growing seasons. However, high temperatures and near-surface evaporation

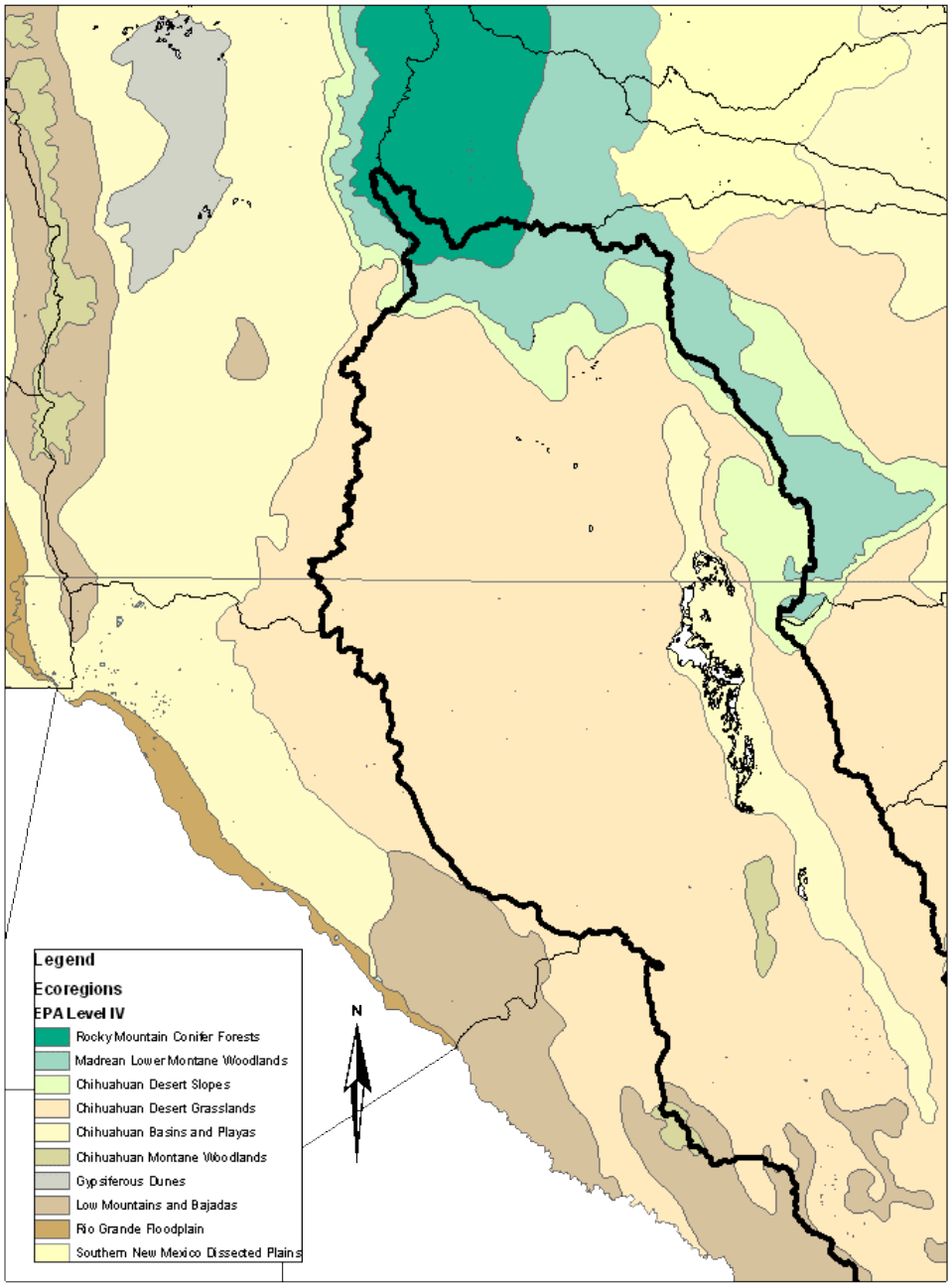


**Figure 1.7** Eco-Regions of the Salt Basin. Source is EPA where level IV designations are illustrated here.

rates mean that irrigation is necessary for plant growth, with the exception of xerophytes of the Chihuahuan desert vegetation. The transition from higher elevation mountains to the Salt Basin lowlands make-up the Chihuahuan Desert Slope ecoregion. This ecoregion extends from the southern Sacramento Mountains as disjunct hilly areas with mixed geology that includes soil, exposed bedrock, and coarse rocky substrates. Similarly, this ecoregion characterizes the slopes of the Guadalupe Mountains, where the alluvial fans of rubble and sand and gravel build up at the base of the mountains. Vegetation is mostly creosote, yucca, and prickly pear with some desert grasses. The Chihuahuan Desert Slope grades into the Chihuahuan Desert Grasslands that encompass the majority of the Salt Basin. Rainfall is slightly elevated in this region compared to the Chihuahuan Basin and Playa ecoregion, generally as a result of slight heightened elevations such as plateaus or mesas surrounding the basin lows. The Chihuahuan Basin and Playa ecoregion represent some of the hottest and most arid in the state of New Mexico. The sparse vegetation must be specifically adapted to withstand large seasonal and diurnal fluctuations in temperature, low available soil moisture and high evapotranspiration rates.

**Section 1.2.d: Land and Water Use**

The New Mexico portion of the Salt Basin is a sparsely populated region, where the small communities of Timberon and Piñon, population ~300 and ~100 respectively (U.S. Census Bureau 2000), in the southern Sacramento Mountains represent the largest populations. Throughout the basin, southeast of the Sacramento Mountains, vast tracts of land are privately owned, primarily by small-time cattle ranchers and sheep farmers. These ranchers use relatively insignificant amounts of groundwater to water their

livestock. The western portion of the Salt Basin is largely a Military Reservation used as a firing range where access is restricted. At the very southern extent of the New Mexico portion of the basin, at the New Mexico, Texas state line is the Dell City Irrigation District. This area has been heavily irrigated since the 1950's yielding considerable crops of cotton and alfalfa, as well as additional crops including: peppers, melons, onions and garlic. Over a forty year period (1950's-1990's), monitoring of the potentiometric surface in this region shows on average a 30-40 ft drop, with a decline in water quality over this period also observed (Sharp, 1993). This area of commercial agricultural with irrigation by groundwater pumping represents the vast majority of the anthropogenic groundwater discharge in the Salt Basin.

**Section 1.3: Previous Work**

Because of the oil and gas potential for the Salt Basin region there have been a number of comprehensive studies addressing the structure, stratigraphy and depositional environment for the area. King and Harder (1982) reported on the oil and gas potential of the Tularosa Basin-Otero Platform area of Otero County, NM. Additionally the authors published a similar report including the Salt Basin graben area for New Mexico and Texas in 1985. These reports layout the dominant physiographic features of the Tularosa and Salt Basin, as well as the geologic history for the region. Black's (1973) dissertation on the geology of the northern and eastern parts of the Otero Platform presents depositional and structural basin analysis. Black later published a paper in 1975 focused on generalized structure and mechanical origins and the stratigraphy of the Otero Platform. Broadheads' (2003) NM Bureau of Geology and Mineral Resources report on the petroleum geology of the McGregor Range presents a detailed stratigraphic column,

and descriptions of the structure and stratigraphy of the region. Characterization of the structure and faulting specifically for the Salt Basin graben is presented in Goetz's (1977) M.S. thesis.

There have been several previous investigations into various aspects of the water resources in the Salt Basin region. One of the earlier investigations was by Bjorklund (1957). It focused on water levels and some general water quality observations in the Crow Flats area. Sharp and others (1993) reported on hydrogeologic trends in the Dell City area. This paper reported information on historic water level changes as a response to groundwater pumping, as well as variability in water quality. Sharp and Mayer published on the role of fractures in the regional groundwater flow in the Salt Basin in 1995. Mayer published his dissertation in 1995, also focused on fracture flow, but included a large set of groundwater chemistry for the Salt Basin. He characterized possible rock/water interactions responsible for the chemical trends, as well as identified some regions of similar water chemistry within the basin. Boyd's (1982) Master thesis dealt with hydrogeologic trends in the northern Salt Basin. She focused on the geochemical trends as groundwater moved toward the salt flats from the surrounding uplands such as the Guadalupe Mountains. Chapman's (1984) Master thesis built upon Boyd's geochemical evolution focusing on the hydrogeochemistry and hydrodynamics at the Salt Flats. The hydrogeology of the Diablo Plateau was characterized by Kreitler in 1990. Hydraulic characteristics of the Permian Yeso Formation were reported by Wasiolek (1991) based on aquifer tests within the upper Rio Hondo Basin and eastern Mescalero Apache Indian Reservation. Huff and Chace (2006) summarized reports on the characterization of the Salt Basin groundwater system, as well as identified areas in

need of future investigation for resource management. In 2002 Finch published work the hydrogeologic framework of the Salt Basin and the development of a 3-dimensional groundwater flow model for the region. Rawling (2009), in a New Mexico Bureau of Geology and Mineral Resources report, characterized the hydrogeology of the Sacramento Mountains.

# CHAPTER II

# HYDROGEOLOGIC FRAMEWORK

## Section 2.1: Depositional Environment and Stratigraphy

The Salt Basin is part of a larger physiogeographic province, known as the Permian Basin. The Permian Basin formed as a consequence of the major continental collision of the North and South American plates during the late Mississippian to early Pennsylvanian time (Mazzullo, 1995). The onset of the Pennsylvanian Ouachita-Marathon orogeny reactivated older, north-south to northwest-southeast oriented, basins and uplifts (Ross, 1986; Goetz, 1985). Rapid subsidence during the Permian resulted in extensive deposition in the platform and basin environments, which left the dominant imprint on the geology of the Permian Basin today (Mazzullo, 1995). Subsidence ceased at the end of the Permian. Extensive periods of erosion followed with intermittent terrestrial and marine deposition of the Triassic and Cretaceous, respectively (Mazzullo, 1995). The block-faulting, volcanism, along with, uplift and eastward tilting of the region that gives the basin its present structure coincided with the Laramide orogeny starting in the late Cretaceous (Mazzullo, 1995).

Broadhead (2003) presents a stratigraphic column for the region spanning the Precambrian to the end of the Cenozoic (fig 2.1). Based on the work of King (1982), the oldest known Precambrain bedrock in the Salt Basin region is 1.35 Ga, Chaves Granitic

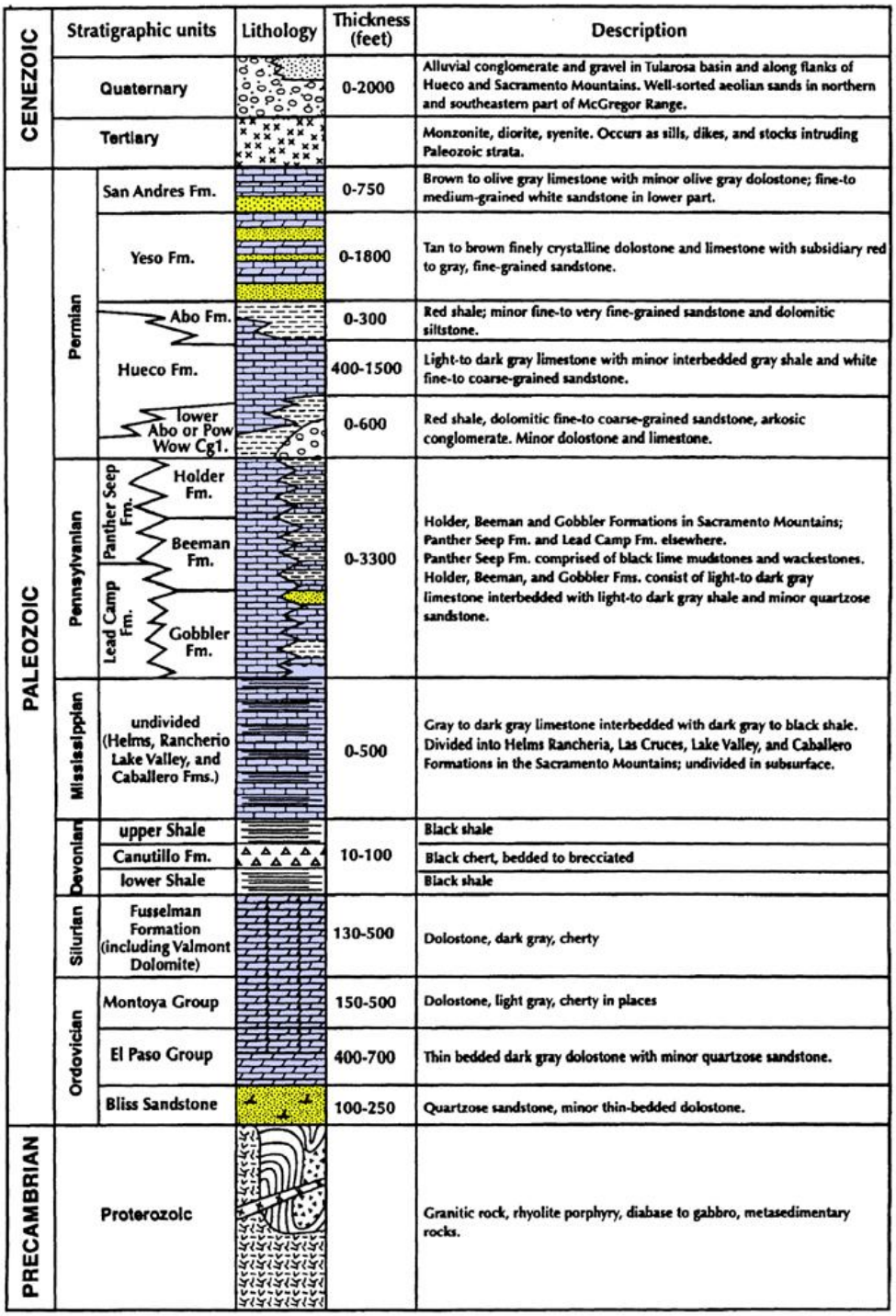


**Figure 2.1 G**eneral stratigraphic column for the Salt Basin region (Broadhead 2003).

Terrane across which later Precambrain sediments were deposited. These later sediments were eventually metamorphosed and underwent subsequent igneous intrusions. The Precambrain formations may have undergone further alteration from additional episodes of burial and uplift until eventually the area was deeply eroded to a surface over which the lower Paleozoic rocks were deposited (King 1982). The Cambrian-Ordovician seas spread throughout the region depositing the basal arkosic Bliss Sandstone. King (1983) describes this sequence followed by Ordovician and Silurian carbonate deposition of the El Paso, the Montoya, and the Fusselman Formations. While rocks older than the Permian are rarely considered significant contributors of water within the region, the Silurian Fusselman dolomite has been reported by the oil and gas exploration industry as having "fresh water" in the Otero Mesa/Diablo Plateau areas (Finch, 2002). This formation is generally found at depths greater than 2,000 ft below the land surface (Black, 1975).

By the Devonian the region was predominantly a shallow sea where dark organic deposits of mud and silt formed (King, 1982). In the Mississipian the sea levels had advanced leaving a variety of carbonate deposits. However, within the region the Mississipian rock are mostly missing due to erosion during the Pennsylvanian (Black, 1973). By the middle of the Pennsylvanian the Pedernal uplift became a dominant structural feature in the region. The southern extension of this positive feature and the subsequent formations of lowlands on either side played a significant role in the deposition of the middle to late Pennsylvanian sediments (King, 1982). King interprets one of the primary results of this uplift to be the transition from the Hueco Formation of

calcareous marine facies into the terrestrial redbed facies of the later Abo Formation. By the Wolfcampian all of the Pedernal was buried beneath the Abo redbeds (Black, 1973).

The Permian limestone of the San Andres and Yeso are the dominant stratigraphic outcrops covering much of the extent of the Salt Basin (fig 2.2). The Yeso Formation of interbedded gypsum, dolomitic calcareous mud, and pinkish silt mud was deposited inland over the Abo Formation (King, 1982). The Yeso is a very heterogeneous stratigraphic unit, ultimately composed of sandstone, limestone, dolomite, siltstone, shale and evaporites. In later deposits the Yeso sediments slightly interfinger with the San Andres deposition, which often makes distinguishing the contact difficult (King, 1982). The Yeso and the San Andres Formations are the uppermost stratigraphic units and are believed to be deposited throughout the Leonardian to the Guadalupian (King, 1982). Dolomite is prevalent throughout the San Andres Formation (Wasiolek 1991). The conditions necessary for seawater to evaporate to the extent of dolomitizing calcite are characteristic of a supratidal flat environment. This is where the shore level is immediately marginal to and slightly above the high tide level (Milner 1976). Depositional facies in the Yeso and San Andres units show successions of low-stand sea level conditions where aqueous or subaqueous sandstones are preceded by high-stand conditions under which limestone and dolomites are deposited (Broadhead, 2003). Following the final gypsum deposits of the upper San Andres Formation the Permian seas retreated, upon which exposure led to dissolution of gypsum and limestone in the San Andres Formation creating a karst environment (King, 1982).

The Tertiary, now only classified as the Paleogene to the Neogene (Gibbard, 2009), can be characterized by the onset of igneous activity. The most significant

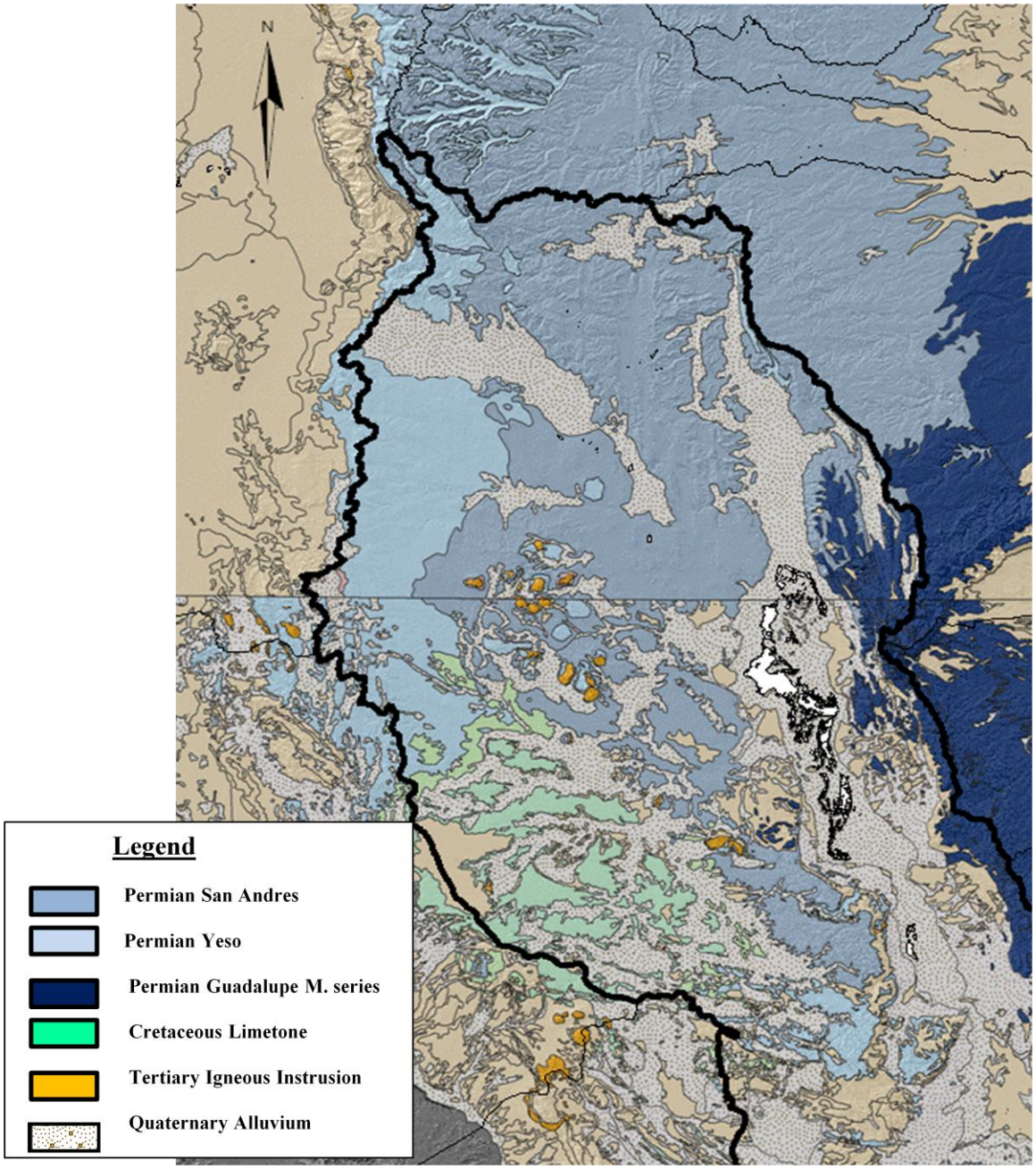


**Figure 2.2** Surface geology of the northern Salt Basin. Geology from Stoeser et al. (2005), with location of alkali flats/playa lakes for New Mexico taken from NHD.

igneous features in the Salt Basin are the Cornudas Mountain intrusions, which are exposed laccoliths and sills predominantly syenite in composition (King, 1982). The Pleistocene marks a time of predominant erosion with some Holocene lake-bed deposits forming in the small, closed basin and playas between the uplifts (Black, 1973). Black also discussed terracing, slumping and solution collapse during the Holocene, along with alluvial fan, arroyo and streambed deposition. Due to the nature of its origin, the alluvium is primarily composed of broken-up limestone, which can be clearly observed in the field.

**Section 2.2: Structure**

King (1982) discussed the general structure of the Salt Basin in relation to different periods of deformation from the Pennsylvanian to the Neogene. He attributes most of the primary folding and faulting at crests of anticlines to deformation during the uplift of the Pedernal landmass in the late Pennsylvanian time. The buried Pedernal landmass (fig 2.3) is a north-south trending feature which is structurally dominant in Otero Mesa (Black, 1975). The buried Pedernal uplift is also of importance in how rock yielded later during the Laramide deformation. During east-west compression the uplift may have acted as a buttress against which the Otero folds were pushed. Rocks overlying the Pedernal and the areas to the east of the feature were less deformed.

Mid- to late- Permian structural features include: the Otero fault, Bitterwell Break, Babb and Victorio flexures (fig 2.3). The Babb and Victorio flexures are northeast-southeast trending monoclines with a northeastward dip (King, 1948). The Babb flexure and the more easterly-trending Victorio flexure cut through the basement

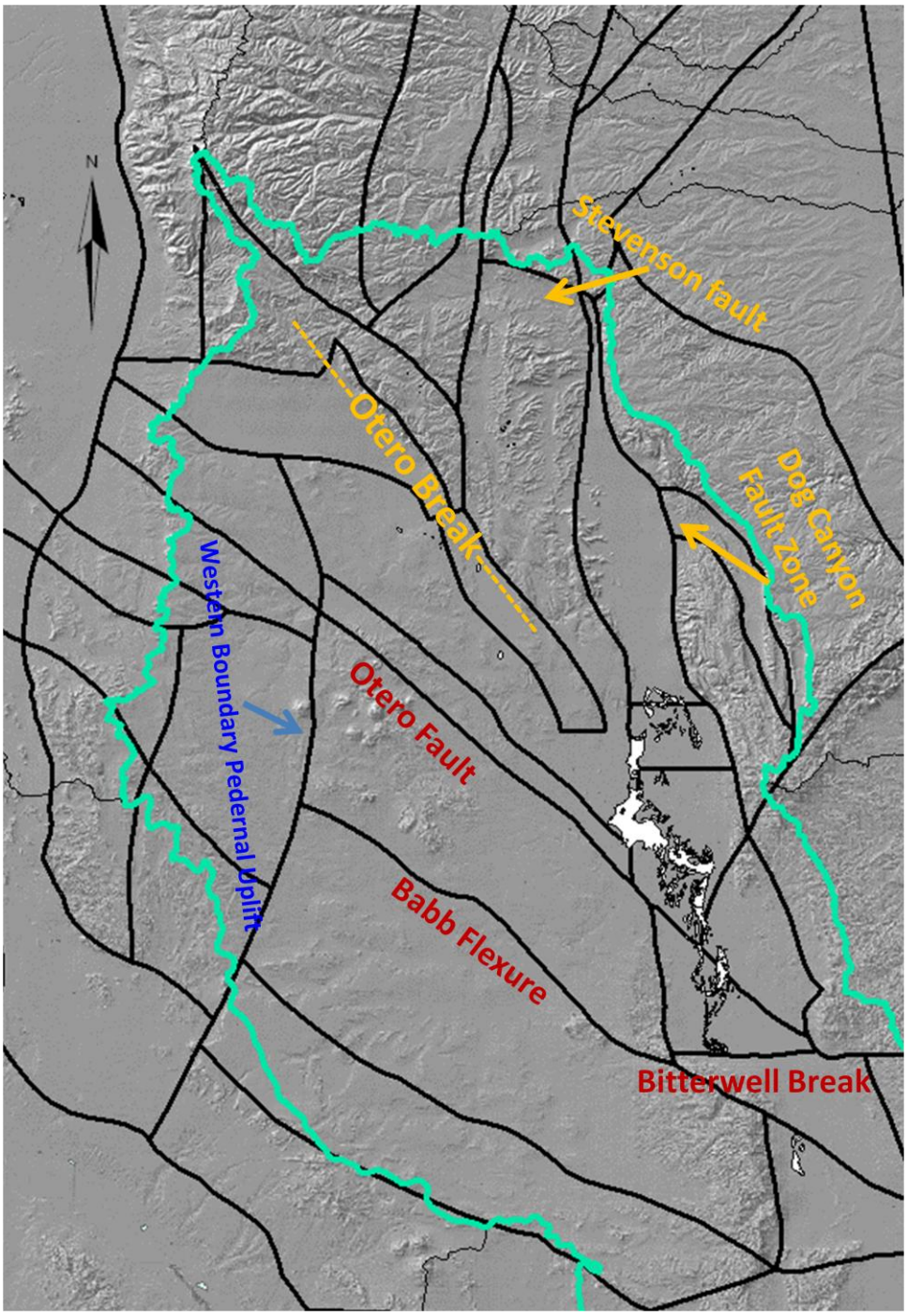


**Figure 2.3** Structural and fault zones for the Salt Basin (Ritchie, 2010). Structural features important for discussion are labeled. Blue label marks Pennsylvannian to early Permian, red label marks mid to late Permian structures, orange label marks Cenozoic features.

blocks of the Salt Basin graben, and intersect on the east side of the graben (Goetz, 1980). Both flexures are ringed by reefs of Leonardian age (King, 1948). The Otero fault is a northwest-striking fault with displacement down to the northeast (Goetz, 1985). The fault cuts through Otero Mesa and continues southeast towards Dell City along the northeast side of the Cornudas Mountains (Goetz, 1985). The Bitterwell Break is a fault in the basement blocks of the Salt Basin graben that trends east-west from the Babb Flexure to the Delaware Mountains (Goetz, 1985). The trend corresponds to the northern boundary of the Sierra Diablo where the down-to-the-north displacement (Goetz,1980) results in a groundwater divide for the northern portion of the Salt Basin (Sharp, 1985).

Subsequent Laramide deformation during the late Cretaceous created many of the northwest and north trending folds that are relatively symmetrical, gently dipping and commonly double plunging (King, 1982). These include the Otero and Cornucopia folds as well as possibly the Jernigan wash anticline, and subtle Chert Plateau folds (Black, 1975). High-angle normal faults are common along the crest and steep west flanks of major anticlines in the Salt Basin (fig 2.4). In addition to the faults associated with the anticlines, north-trending high-angle normal faults of the Cornucopia Hills (fig 2.4) likely underlie the alluvial cover in both Cornucopia Draw and Jernigan Wash (Black, 1975).

Neogene tectonics associated with basin-and-range provinces has resulted in a series of tilted fault blocks, each progressively less deformed and uplifted to the south and east, that characterize the present structure (King, 1982). The Guadalupe fault zone and its possible westward extension known as the Stevenson fault that bounds the northeast and east edges of the Salt Basin are some of the most prominent Cenozoic structures (fig 2.3). The imposing west-facing escarpment of the Guadalupe Mountains is

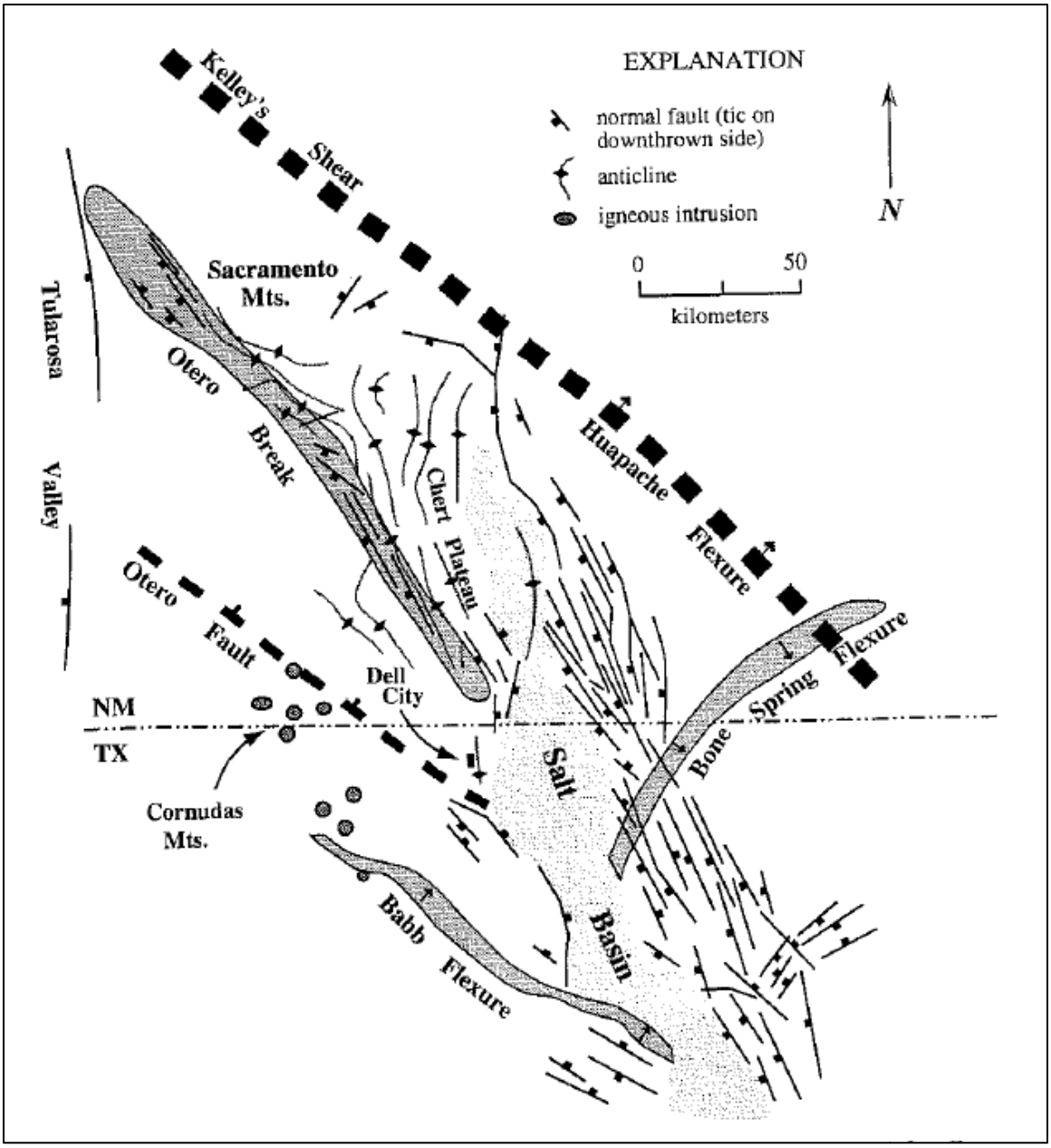


**Figure 2.4** Tectonic structural features of the Salt Basin during the Cenozoic (Goetz, 1986, Black, 1975)

a result of the closely spaced high-angle normal fault zone where the alluvium meets the foot of the Guadalupe rim (Black, 1975). The Sacramento and Orendorf anticlines and intervening Sacramento River and Otero syncline, McGregor anticline, Prather anticline and syncline are all primarily caused by drapefolding over deep-seated fault blocks which have been gently titled to the northeast (Black, 1975). West-oriented extension during the Neogene turned these into a series of west dipping normal faults (fig 2.4) extending northwest to southeast from the Sacramento Mountains, known as the Otero Break (Goetz, 1985; Mayer, 1995).

# CHAPTER III

# WATER RESOURCES

## Section 3.1: Surface Water

The major watersheds within the Salt Basin are the Sacramento River and Piñon Creek. The Sacramento River (fig 3.1), which originates in the Sacramento Mountains, is the only perennial surface water in the basin. The flow is perennial only on relatively limited distances of the river before infiltrating to the shallow groundwater (Rawling, 2009). The headwaters of these perennial reaches are commonly associated with minor wetlands, also present around springs in the Sacramento Mountains. Wetlands are likely to be sites of groundwater recharge as they are permanently saturated, indicating hydraulic connectivity with the shallow water table in the region. The locations, flow directions and interactions with groundwater of the Sacramento River and other headwaters within the Sacramento Mountains are influenced by the structural features of the region. Uplift of the Sacramento Mountains produced an eastward dip of both the geologic layers and the topographic surface (Rawling, 2009). Intersection of this surface with the down-faulted western edge of the range created a crest that forms a drainage divide between streams flowing to the east in the Pecos River and drainage to the west to the Tularosa Basin. The Sacramento River is an exception as it flows southeast into the Salt Basin graben. Near the headwaters the daily mean stream flow of the Sacramento River ranges from 2-13 cubic feet per second (USGS database). With increasing distance

from the headwaters the ephemeral reaches of the Sacramento River diffuse out to join the lower channel networks present in the Salt Basin.

Significant ephemeral flow channels throughout the Salt Basin (fig 3.1) include Piñon Creek, Cornucopia Draw, Big Dog Canyon, and Shiloh Draw. A recent USGS investigation based on channel geometry, reported estimates (table 3.1) for the annual flow and infiltration contribution to the Salt Basin from the major channel networks. For the Sacramento River, Piñon Creek, Cornucopia Draw, Big Dog Canyon an estimated total of about 60,000 acre-ft of annual flow with between 27 to 56 percent loss by infiltration was reported (Tillery, 2010).

**Table 3.1** Flow losses and associated distances for the four major subbasins studied in the Salt Basin (USGS; Tillery, 2010)

| Subbasin | Maximum annual-flow estimate, in acre-ft | Most downstream annual flow estimate, in acre-ft | Difference between maximum annual flow and downstream annual flow, in acre-ft | Flow loss, in percent | Stream miles over which losses occur |
|---|---|---|---|---|---|
| Sacramento River | 10,866 | 6,013 | 4,853 | 45 | 16.0 |
| Cornucopia Draw | 15,212 | 6,737 | 8,475 | 56 | 16.4 |
| Piñon Creek | 29,700 | 21,723 | 7,977 | 27 | 9.2 |
| Big Dog Canyon | 4,636 | 2,970 | 1,666 | 36 | 6.1 |

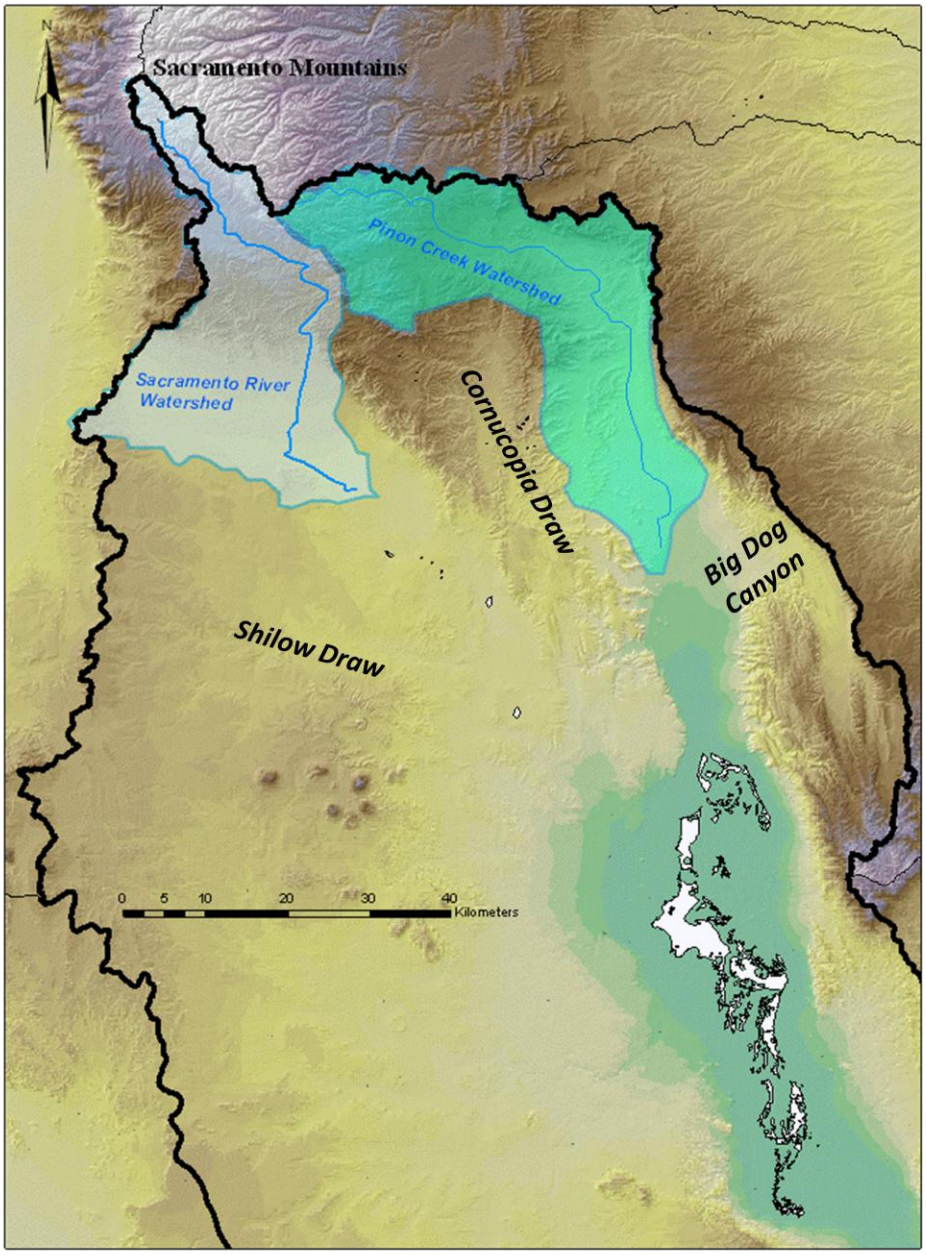


**Figure 3.1** Salt Basin sub-watersheds. Modified from Huff and Chace (2006).

## Section 3.2: Groundwater Aquifer System

The carbonate formations of the Permian are attributed as the major aquifers within the Salt Basin. These are primarily carbonate and mixed carbonate/evaporite sequences formed in shelf-margin to basinal marine depositional environments (Mazzullo, 1995). In the New Mexico portion of the Salt Basin the significant Permian carbonate aquifer is formed by the San Andres and Yeso Formations (Huff and Chace, 2006). Some previous work on developing groundwater flow models of the Salt Basin suggested that these Permian carbonates act as a single hydraulic unit (Mayer, 1995). The eastern reef formations of the Guadalupe Mountains were recognized as a possible exception to this interconnectivity. The vertical connectivity of the deeper, possible aquifer units of the Hueco and the Abo formations, with the primary aquifer is also unknown.

### Section 3.2.a: Hydrostratigraphic Units

#### -Abo and Hueco Formations

Typically groundwater wells do not penetrate past the Yeso formation so the hydraulic characteristics of the Abo and Hueco formations are poorly known. However, some outcrops of the formations in New Mexico are said to be a source for wells (Huff and Chace, 2006). Based on stratigraphy, the Abo can be separated into three distinct sequences, described by Black (1975). The lower Abo is conglomerate redbed. The middle sequence is known as the Hueco, which thickens to the south and is a dark-gray, fine grained, thin to medium-bedded fossiliferous limestone. The upper Abo sequence

consists of reddish-brown mudstone, fine-grained sandstone and siltstone, with a southward-thickening tongue of gray shale, limestone and dolomite (King, 1982).

**-Yeso Formation**

The Yeso Formation is composed of a variety of lithologic types including limestone and dolomite; red, yellow and gray shales and siltstones; evaporites, primarily gypsum/anhydrite and minor halite; and yellow, fine-grained sandstone (Black, 1975). The Yeso was deposited on the Abo where the contact is defined by the presence of gypsum or lowest pinkish clastic bed (Black, 1975). The formation is approximately 1,000 feet thick, the lower 500 ft is associated with more evaporites and siltstones (Kelly, 1971). This depositional trend means that most well that produce water from the Yeso Formation penetrate the upper 500 ft in the fractured limestone and dolomite where the permeability is higher due to dissolution and fractures. In the southern reaches of the Sacramento Mountains wells drilled in the lower Yeso Formation generally yield less than 5 gallons per minute (gpm) while wells in the upper portion of the formation have yields greater than 20 gpm (Finch, 2002). Wasiolek (1991) reported that the hydraulic conductivity determined by deep aquifer tests on Yeso formation under the Mescalero Apache Indian Reservation averaged $7.0 \times 10^{-8}$ m/s (0.02 ft/d) for unfractured siltstone and gypsum beds. The average hydraulic conductivity for the Yeso formation, where flow is preferentially through fractures and dissolved limestone beds, ranged from $2.1 \times 10^{-6}$ to $5.3 \times 10^{-6}$ m/sec (0.6 to 1.5 ft/d). This indicates that, for the Yeso formation in this region, limestone beds with secondary permeability have orders of magnitude higher hydraulic conductivities than those of unfractured beds (Wasiolek, 1991).

**-San Andres Formation**

Like the Yeso Formation, water movement through the San Andres Formation is largely facilitated through fracture flow and dissolution channels in the limestone/dolomite bedding. The lower contact of the San Andres is formed by gradational interfingering of Yeso and San Andres carbonate rocks (Black, 1975). The interfingering can make distinguishing between the two units difficult. The San Andres Formation is primarily light-olive-gray dolomite and dolomite limestone with sandstone and shale lenses. The San Andres carbonates are highly jointed meaning, fractures are slightly displaced perpendicular to the fracture surface and not in any other direction (Rawling, 2009). The bedding of the formation is quite variable, with bedding thickness commonly between 2-5 feet, while massive bedding can sometimes be as great as 20 feet. Sharp and Mayer (1995) quantified estimates of the extent of the preferential flow through fractures zones using a basin scale flow model for the Salt Basin. The flow model generated the best fit of the potentiometric surface in the Salt Basin assuming an average hydraulic conductivity of $10^{-4}$ m/s within fracture zones and an average of $10^{-6}$ m/s outside the fracture zones. Groundwater flow through fractures was also attributed with significant differences in well production during the development phases of Dell City. In the drilling of irrigation wells it was observed that approximately 50 percent of the wells drilled were high yield (>1000 gpm) while the other half were relatively low yield (<500 gpm), even in very close vicinity, as close as 100 ft (Scalopino, 1950). In general, the aquifer in the Dell City region is a considered to have high transmissivity. Kreitler (1990) observed that extensive groundwater production,

approximately $10^8$ $m^3$/yr (98,500 acre-ft/yr) pumped for irrigation for 30 years, resulted in only 10 m (33 ft) of drawdown.

**- Cretaceous Limestone**

In the Diablo Plateau, Cretaceous limestone is considered part of the aquifer, in addition to the Permian aquifer system. These sequences are characterized by yellowish-tan to light-gray nodular, fossiliferous limestone and brownish-tan to orangish-tan sandstone and siltstone. Like the Permian aquifer system in the Dell City area, the Cretaceous limestone aquifer across the Diablo Plateau is also considered to have high transmissivity. Kreitler (1990) reported the hydraulic gradient for the Diablo Plateau aquifer as approximately 1m/km (5 ft/mi), which is relatively low considering the 400 m (1,300 ft) of relief.

**Section 3.2.b: Source, Occurrence and Movement of Groundwater**

The northern portion of the Salt Basin is a hydrologically closed basin with about 12,000 $km^2$ of surface area drainage. The Sacramento Mountains to the north of the basin constitute a high mountain environment that is a significant source of recharge to the Salt Basin. Winter snowfall (fig 1.6.b) that infiltrates into the spring/stream systems is the dominant source of recharge to the regional aquifer system during average precipitation years (Rawling, 2009). The streams distribute the recharge over a larger area than the winter snow pack (Rawling, 2009). Thus, one of the most significant sources of recharge to the aquifer system underlying the Salt Basin is likely infiltration of stream flow from the Sacramento River and Piñon Creek watersheds (fig 3.1) which originate in the Sacramento Mountains (Finch, 2002; Mayer, 1995; Sharp, 1993). The

infiltration can take place directly within the Salt Basin watershed or act as a source of recharge as an underflow flux across the northern surface-water divide from the Sacramento Mountains.

Precipitation falling anywhere within the Salt Basin surface water divide can infiltrate to the groundwater system as long as precipitation and infiltration rate exceed the rate of evaporation. However, across most of the Salt Basin precipitation is so low and evaporation rates so high that only high intensity storm events have the potential for recharge. Canyon systems and ephermal drainage networks off the steep western face of the Guadalupe Mountains focus runoff to the bajadas. The bajadas are a sequence of alluvial fans spreading onto the Salt Basin floor where the shallow slopes and coarser grained material facilitate recharge to the aquifer system. Otero Mesa and Diablo Plateau are also sources of recharge to the Salt Basin. Recharge is thought to infiltrate over the entire plateau ~approximately 7,500 $km^2$ (Mullican, 1987; Kreitler, 1990). The recharge infiltrates through fractures along arroyos during storm events and flooding, rapidly entering the aquifer system. Ephermal watercourses such as Eightmile Draw, drain the majority of the Diablo Plateau where dendritic drainage networks converge to enter the Salt Flats 15 km south of Dell City (Goetz, 1977). Historic flood events can result in standing surface water on the Salt Flats (Chapman, 1984).

The regional groundwater flow (fig 3.2) is south-southeastward from the recharge area of the Sacramento Mountains and eastward from the Otero Mesa/Diablo Plateau toward the Salt Basin graben and Dell Valley (Mayer, 1995; Sharp, 1993). Groundwater flows from the Sacramento Mountains into the Dell Valley area to the Salt Flats through a set of northwest-southeast trending fractures (Mayer and Sharp, 1995). Groundwater

flow from the Otero Mesa generally follows the structural dip which is gently east-sloping toward the Salt Basin graben (Mayer, 1995; Kreitler, 1990). The groundwater divide is close to the southern edge of the Diablo Plateau from which groundwater flows southwest to northeast. Like the Otero Mesa this groundwater is thought to flow down the structural dip of the monocline, with only a minor amount flowing south-westward into Hueco Bolson (Kreitler and Mullican, 1990). Water entering the northern portion of Salt Basin graben is hydrologically isolated from the extension of the southern Salt Basin graben by the Bitterwell Break (fig 3.2). This is a Neogene normal fault that deforms the sediments of the Salt Basin and produces a groundwater divide (Sharp, 1985; Boyd, 1986). This southern boundary extends west to the Babb flexure, a northwest-southeast trending, north-side-down monocline, as previously discussed. The Salt Flats (fig 3.2) are a series of gypsum playas along the eastern margin of the Salt Basin graben that constitutes the natural discharge point for this closed basin (Chapman, 1984; Boyd, 1982). However irrigation near Dell City began around 1950's and has since been a significant amount of the groundwater discharge (Sharp and Mayer, 1993).

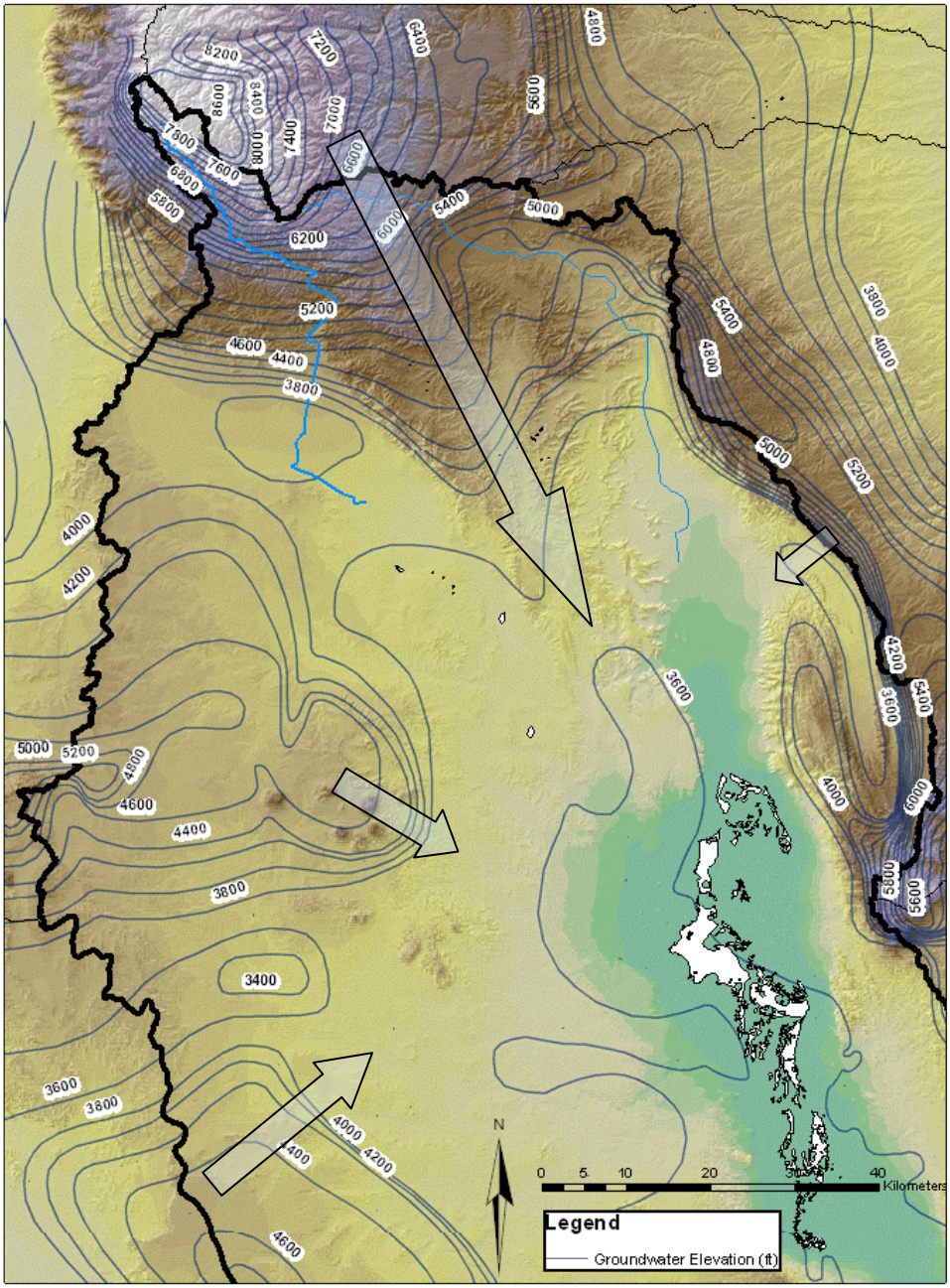


**Figure 3.2** Groundwater movement and groundwater elevation contours (ft). Groundwater contours taken from (Ritchie, 2010).

# CHAPTER IV

# METHODS AND ANALYTICAL TECHNIQUES

## Section 4.1: Groundwater Chemistry Dataset

To obtain a better spatial distribution of the groundwater chemistry in the Salt Basin, data collected specifically for this study of the Salt Basin were supplemented with data obtained from previous studies (fig 4.1). Supplementary data were obtained from two main sources: spring and well samples from the Sacramento Mountains collected by the New Mexico Bureau of Geology and a general chemistry dataset from wells throughout the Salt Basin compiled by Mayer for his 1995 dissertation. Specifics of sample collection and analysis are discussed below for each data source.

## Section 4.2: Current Salt Basin Study

Twenty five water chemistry samples from groundwater in the Salt Basin were collected during a series of field trips in 2008—2009 (fig 4.2). Wells were sampled along regional flow paths (fig 3.2), east of the Otero Break, starting in the southern Sacramento Mountains and ending near Dell City and the Salt Flats. Samples from these sites were analyzed for a wide variety of constituents: major- and minor-element chemistry, oxygen-18 ($\delta^{18}O$) and deuterium ($\delta D$) content, carbon-13 ($\delta^{13}C$) and carbon-14 ($\delta^{13}C$) content of dissolved inorganic carbon, sulfur-34 ($\delta^{34}SO_4$) content of dissolved sulfate, and tritium ($^{3}H$). Water analyses are tabulated in table 5.1 and Appendix A.

Groundwater sampling sites for the Salt Basin study were selected primarily on the basis of location in an attempt to attain the most comprehensive geochemical evolution along the given flow paths. Choice of sampling sites was limited primarily due to access issues. For example, private land owners denied permission to take a water sample, or in the case of most of the western side of the Salt Basin access is limited due to the military reservation, as previously discussed.

Of the 25 wells that were sampled, 4 were domestic wells (wells used to supply water to fewer than 3 households), 3 were irrigation wells (wells used for commercial agricultural production), 2 were powered by windmills (wells having a piston mechanism to lift water, which is used primarily to water stock), 3 were powered by solar panels (wells where solar panels powered submersible pump, which is used primarily to water stock), 1 well was spring fed (shallow well directly drilled into a spring), and 12 were classified as other (wells with submersible pumps, where water is used primarily to water stock). Well depths ranged from about 60 to 1600 ft, with an average of about 630 ft. Information on well depth, depth to water and screened interval was obtained from the landowner and was often limited or approximate. Sampling site locations (fig 4.2) were taken using a Garmin 60 GPS unit.

**Section 4.2.a: Collection of Groundwater Chemistry**

**Purging the well** insures that water samples collected are not from water stored in the well bore volume. Ideally, if the column depth and well casing radius were known the well bore volume could be calculated and at least 2 well bore volumes were discharged and field parameters (specific conductance, water temperature, pH, and dissolved-oxygen concentration) were allowed to stabilize before sample collection. If

there was limited information on the well, the wells were pumped in such a way that discharge could be collected in buckets and measurements were taken until field parameters had stable readings over a significant volume of water. Generally, some estimate for bore volume could be made. The **general chemistry** water samples were collected in 250 ml nalgene polyethylene bottles. For **trace metals** 125 ml of water was collected which needed to be filtered (0.45 micron filters) and kept on ice with the general chemistry samples until delivered for analysis. The **oxygen ($\delta^{18}O$) and hydrogen isotope ($\delta D$)** samples were collected in small (~25 ml) glass vials, underwater to prevent contact with the atmosphere. There should not be air bubbles present in the collected samples and freezing and sun exposure were avoided. For the **sulfur isotopes ($\delta^{34}SO_4$)** measured from sulfate in the groundwater; two 500 ml nalgene polyethylene bottles were collected. Groundwater samples for **tritium ($^3H$) content** were collected in two 500 ml nalgene polyethylene bottles that were filled, underwater to prevent contamination. It was critical to remove wristwatches where glow in the dark dials can have traces of tritium that can contaminate the sample. The **carbon-14 ($\delta^{14}C$) and carbon-13 ($\delta^{13}C$)** samples were collected in a 1 liter nalgene polyethylene bottle. To prevent contamination of the sample in this case, it was very important that gloves be worn during the collection. In every case the sample bottles and caps were rinsed 2-3 time in well water before collection of the actual sample.

### Section 4.2.b: Precipitation Collection

In addition to groundwater samples, four precipitation collectors were set-up throughout the eastern side of the Salt Basin and analyzed for stable isotopes of oxygen-

18 ($\delta^{18}O$) and deuterium ($\delta D$). Precipitation collectors employed are referred to as PVC collectors (Earman, 2006). The PVC (polyvinyl chloride) collector consists of a 19-cm-diameter plastic pipe, approximately 1.25 m high, sealed at the bottom, and mounted to a stake about 1 m off the ground, with a layer of mineral oil in the bottom of the collector. The mineral oil prevents evaporation of the precipitation in the collector. The precipitation collectors were placed in the open, away from trees or structures that might prevent interference. The precipitation was collected seasonally to be analyzed for the stable isotope content.

### Section 4.2.c: Analytical Techniques

#### General chemistry

Analysis of major- and minor elements for the Salt Basin study was performed by the New Mexico Bureau of Geology and Mineral Resources Chemistry (and water quality analysis) Lab. Water chemistry was analyzed using the United States Environmental Protection Agency (USEPA) Clean Water Act Analytical Methods (USEPA, 2010). The analyses include conductivity, alkalinity, pH, total dissolved solids (TDS), hardness, bromide, chloride, fluoride, nitrate, nitrite, phosphate, sulfate, sodium, potassium, magnesium, and calcium. Conductivity was calculated according to USEPA method 120.1, *Conductance and Specific Conductance*. The pH was calculated according to USEPA method 150.2, *pH, Electrometric (Continuous Monitoring)*. The TDS was calculated using *Standard Methods for the Examination of Water and Water Quality* (1992). The alkalinity was determined according to USEPA method 310.2, *Alkalinity, Colorimetric, Automated Methyl Orange.* Analyses of major cations were performed

according to USEPA method 200.7, *Determination of Metals and Trace Elements in Water and Wastes by Inductively Coupled Plasma-Atomic Emission Spectrometry* Revison 4.4. The inorganic anion chemistry was determined according to USEPA method 300.0, *Determination of Inorganic Anions by Ion Chromatography.* Reporting limits with methods for conductivity and TDS are 10 μS/cm and 10 mg/L, respectively. Anion reporting limits are the typically 1 mg/L (with the exception of bromide 0.1 mg/L, or for low bromide 0.001 mg/L). Cation reporting limits are 0.001 mg/L.

**Trace metals**

Analyses of trace metals were performed by the New Mexico Bureau of Geology and Mineral Resources Chemistry (and water quality analysis) Lab. Trace metal analyses included aluminum, antimony, arsenic, barium, beryllium, boron, cadmium, chromium, cobalt, copper, iron, lead, lithium, manganese, molybdenum, nickel, selenium, silica, silicone, sliver, strontium, thallium, thorium, tin, titanium, uranium, vanadium, and zinc. Trace metals were analyzed using the United States Environmental Protection Agency (USEPA) Clean Water Act Analytical Methods (USEPA, 2010). Specifically, trace metal content was determined by USEPA method 200.8, *Determination of Trace Elements in Water and Wastes by Inductively Coupled Plasma-Mass Spectrometry* Revision 5.4. For this method the reporting limits are typically 0.001 mg/L.

**Oxygen ($\delta^{18}O$) and hydrogen ($\delta D$) isotopes**

Analysis of the oxygen ($\delta^{18}O$) and deuterium ($\delta D$) stable isotope content for the groundwater and the precipitation samples were performed by New Mexico Tech Stable Isotope Laboratory which is directed by Andy Campbell. The $\delta^{18}O$ content of a 1 mL

water sample was determined using the $CO_2/H_2O$ equilibration method as described in Clark and Fritz (1997). The samples react in sealed containers, from which the equilibrated $CO_2$ gas is extracted into the Thermo Finnigan Gasbench operated in continuous flow mode. The δD content of the water sample is analyzed from hydrogen gas generated by metal reduction with powdered chromium at 850 °C in an H-Device (Nelson and Dettman, 2001). The gas entry to the mass spectrometer is regulated by a dual inlet system such that the hydrogen gas from the H-device is stored in a bellows, and run against and standard hydrogen gas stored in another bellows. Both the $CO_2$ and $H_2$ were analyzed on a Thermo Finnigan Delta$^{PLUS}$ XP Stable Isotope Ratio Mass Spectrometer. The stable isotope results are reported with respect to Vienna Standard Mean Ocean Water (VSMOW). The delta value is given by $\delta = \left(\frac{Rx-Rstd}{Rstd}\right) x\ 10^3$, where R is the ratio of the heavy to the light isotope measured from counts by the mass spectrometer (Sharp, 2007).

**$\delta^{34}S$ in $SO_4$**

The analyses of the $\delta^{34}S$ stable isotope content of sulfate from the groundwater samples were performed by the New Mexico Tech Stable Isotope Lab. Sample preparation is performed according to the United States Geological Survey (USGS) *Determination of the $\delta(^{34}S/^{32}S)$ of sulfate in Water: RSIL Lab Code 1951*. The dissolved sulfate from the groundwater sample is precipitated with barium chloride ($BaCL_2$) to barium sulfate ($BaSO_4$). The Elemental Analyzer (EA) is used to convert sulfur in the $BaSO_4$ sample precipitate into $SO_2$ gas. The EA introduces the $SO_2$ gas through continuous flow connected to the Thermo Finnigan Delta$^{PLUS}$ XP Stable Isotope Ratio

Mass Spectrometer which determines the sulfur isotope ratio. $\delta^{34}S$ values are reported relative to the Cañon Diablo Troilite (CDT) standard. The delta value is given by $\delta = \left(\frac{Rx-Rstd}{Rstd}\right) x\ 10^3$, where R is the ratio of the heavy to the light isotope measured from counts by the mass spectrometer (Sharp, 2007).

## $^3$H Tritium

The tritium ($^3$H) analysis was performed by University of Utah Gas Lab. The tritium content of the groundwater samples was determined by helium ingrowth methods. The method begins by degassing the water sample under high-vacuum to extract the dissolved gases. The sample is sealed and sits for 6 to 12 weeks while tritium decays and helium-3 grows. After the sample is decayed, the levels of helium-3, which directly correlate to the amount of tritium decayed, is measured using Mass Analyzers Products-Model 215-50 Magnetic Sector Mass Spectrometer. The system setup and analysis process is designed based on the design described in *A static Mass Spectrometer with Triple Collection for Nitrogen and Neon Samples*, Scripps Oceanographic Institute, S.I.O Reference series #93-11 (1993). The results are reported in tritium units (TU); in water of 1 TU the specific activity is equal to 3.2 picocuries per liter (pCi/L), or 7.1 disintegration per minute per liter (dpm L).

## Carbon-14 ($\delta^{14}C$) and Carbon-13 ($\delta^{13}C$)

The carbon-14 ($\delta^{14}C$) and carbon-13 ($\delta^{13}C$) content of the groundwater samples were determined by Beta Analytic Incorporated. The radiocarbon dating was performed using accelerator mass spectrometry (AMS) counting. First, the dissolved inorganic carbon (DIC) was precipitated as strontium carbonate ($SrCO_3$) using strontium chloride

($SrCl_2$). This was rinsed to a neutral solution and dried. The precipitate was then acidified using 0.5 N $H_3PO_4$ phosphoric acid and the carbon was collected as $CO_2$ gas. The gas is then mixed with hydrogen over a cobalt catalyst and heated to 600 °C reducing the carbon to graphite on the cobalt. The graphite is the analyzed by an AMS and measured for the carbon isotope content. By international convention, the modern reference standard was 95% the $\delta^{14}C$ activity of the National Institute of Standards and Technology (NIST) Oxalic Acid (SRM 4990C).

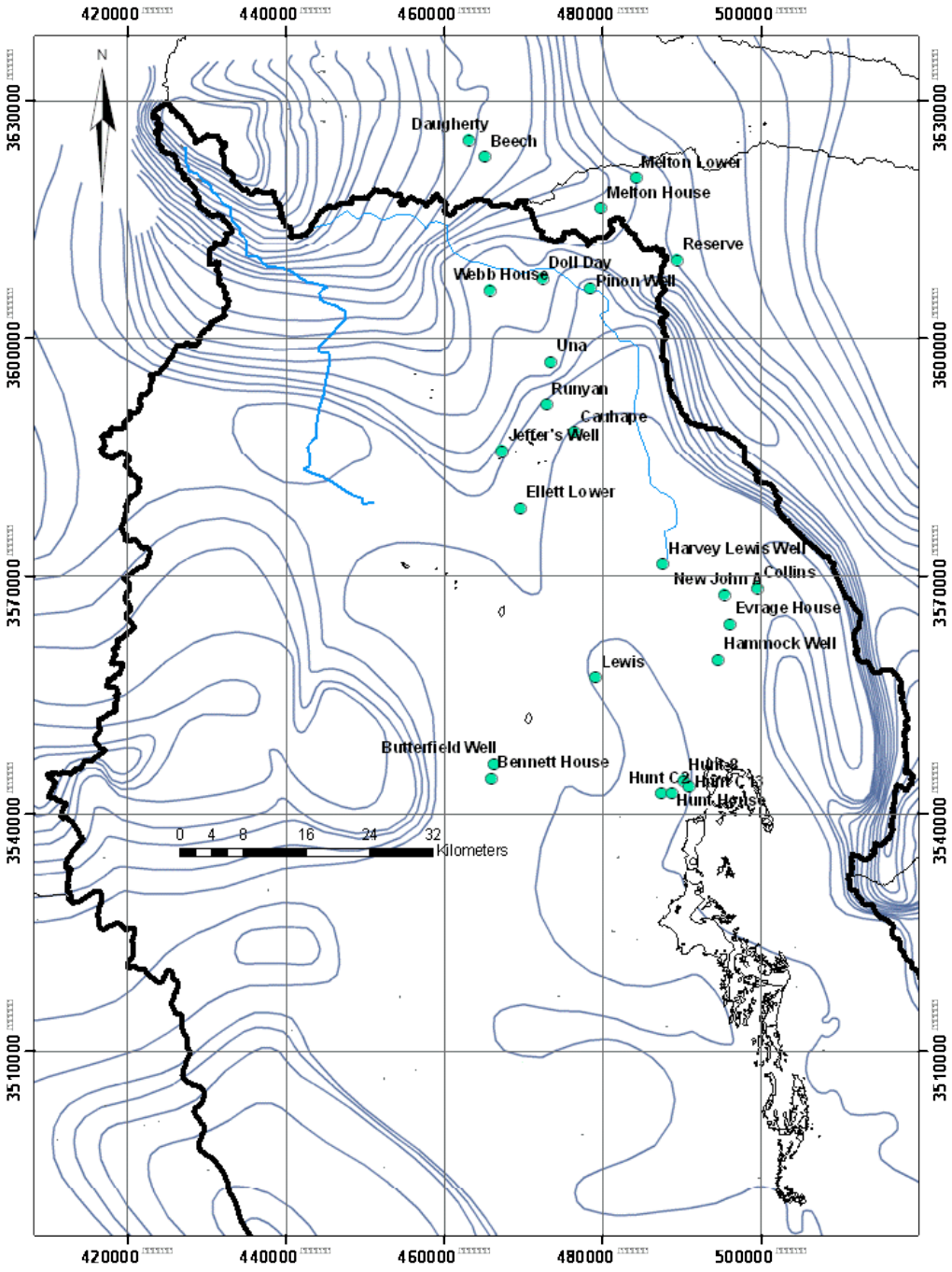


**Figure 4.1** Salt Basin well sample locations. Grid coordinates are in Northing (m) and Easting (m). The water elevations contours are from Richie (2010) refer to figure 3.2.

**Section 4.3: NMBGMR Sacramento Mountain Study Groundwater Chemistry**

The New Mexico Bureau of Geology and Mineral Resources is involved with an ongoing study of the hydrogeology of the Sacramento Mountains in southern New Mexico. The goals of the study are to delineate areas of groundwater recharge, determine directions and rates of groundwater movement, and to characterize the interactions between different aquifers and groundwater and surface-water systems. In the study a variety of techniques are utilized to characterize the regional hydrogeology including water chemistry analyses, isotopic analyses, and groundwater age dating. The dataset for the *Sacramento Mountains Hydrogeology Study* open file report-518 (2009) is available to the public. The preliminary interpretations and dataset from the study was draw on for this Salt Basin study in defining the recharge area of the Sacramento Mountains. Specifically, groundwater chemistry from wells within delineated zones of modernly recharging groundwater were used as initial points in flow paths for geochemical modeling. The database includes latitude and longitude for each sample site (fig 4.1). Samples that did not include at least major- and minor element chemistry were not included in the Salt Basin analysis. The constituents of the chemical analyses from the NMBGMR study (reference numbers are preceded by "SM") are listed in table 5.1 and Appendix B: major- and minor-element chemistry, oxygen-18 ($\delta^{18}O$) and deuterium ($\delta D$) content, carbon-13 ($\delta^{13}C$) and carbon-14 ($\delta^{13}C$) content of dissolved inorganic carbon, and tritium ($^{3}H$). The analytical techniques for the chemical analyses for the water samples are likely similar to those described in sections 4.2.a and 4.2.c as procedures for the Salt Basin study were modeled after procedures of the NMBGMR.

## Section 4.4: Groundwater Chemistry Dataset Compiled by Mayer (1995)

For Mayer's (1995) dissertation on *The Role of Fractures in Regional Groundwater Flow* in the Salt Basin, he compiled a comprehensive dataset of the regional groundwater chemistry. Mayer sampled about 35 well sites throughout the Salt Basin and analyzed them for pH, temperature, alkalinity, conductivity, and the concentration of selected ions ($Ca^{2+}$, $Mg^{2+}$, $Na^{+}$, $K^{+}$, $F^{-}$, $Sr^{2+}$, $Cl^{-}$, $Br^{-}$, $SO_4^{2-}$, $NO_3^{2-}$). The analytical techniques for the water analyses are described in his thesis (Mayer, 1995). He supplemented his work by compiling regional groundwater chemistry from published reports and government records. Sources of chemical data used in his study included Kreitler et al. (1987), Ashworth (1994), and the Texas Water Development Board for the Dell Valley and Diablo Plateau regions; Bjorklund (1957) from the New Mexico State Engineer's Office, and Hudson and Borton (1980) for Crow Flats; and the U.S. Department of the Interior, Bureau of Land Management for wells on federal lands in New Mexico. Mayer discusses the potential complications in using data from different time periods. He makes three main assumptions: (1) apart from irrigated areas (where only predevelopment water chemistry was included) water chemistry has remained constant through time, (2) bias from older analytical techniques are negligible because water analyses are high in total dissolved solids and major constituents are above the detection limits, and finally (3) that pre-1950 pH analyses are likely not reliable as measurement techniques are unknown. For my study, the dataset Mayer (1995) compiled was only used to assess the regional distribution of pertinent ion chemistry and was not used quantitatively for any of the geochemical modeling.

For the maps present in his dissertation Mayer determined well positions from U.S. Geological Survey 7.5 minute topographic maps. Other than his maps of the well locations within in the Salt Basin he did not provide coordinates. To determine latitude and longitude positions for his well locations, I geo-referenced his maps using arcGIS and matched up well locations (fig 4.1) to wells from NWIS database. A few wells did not correspond to wells from the NWIS database and were assigned approximate positions; these exceptions are specified in the data table. Site locations, water analyses, and the source for the well chemistry are listed in Appendix C.

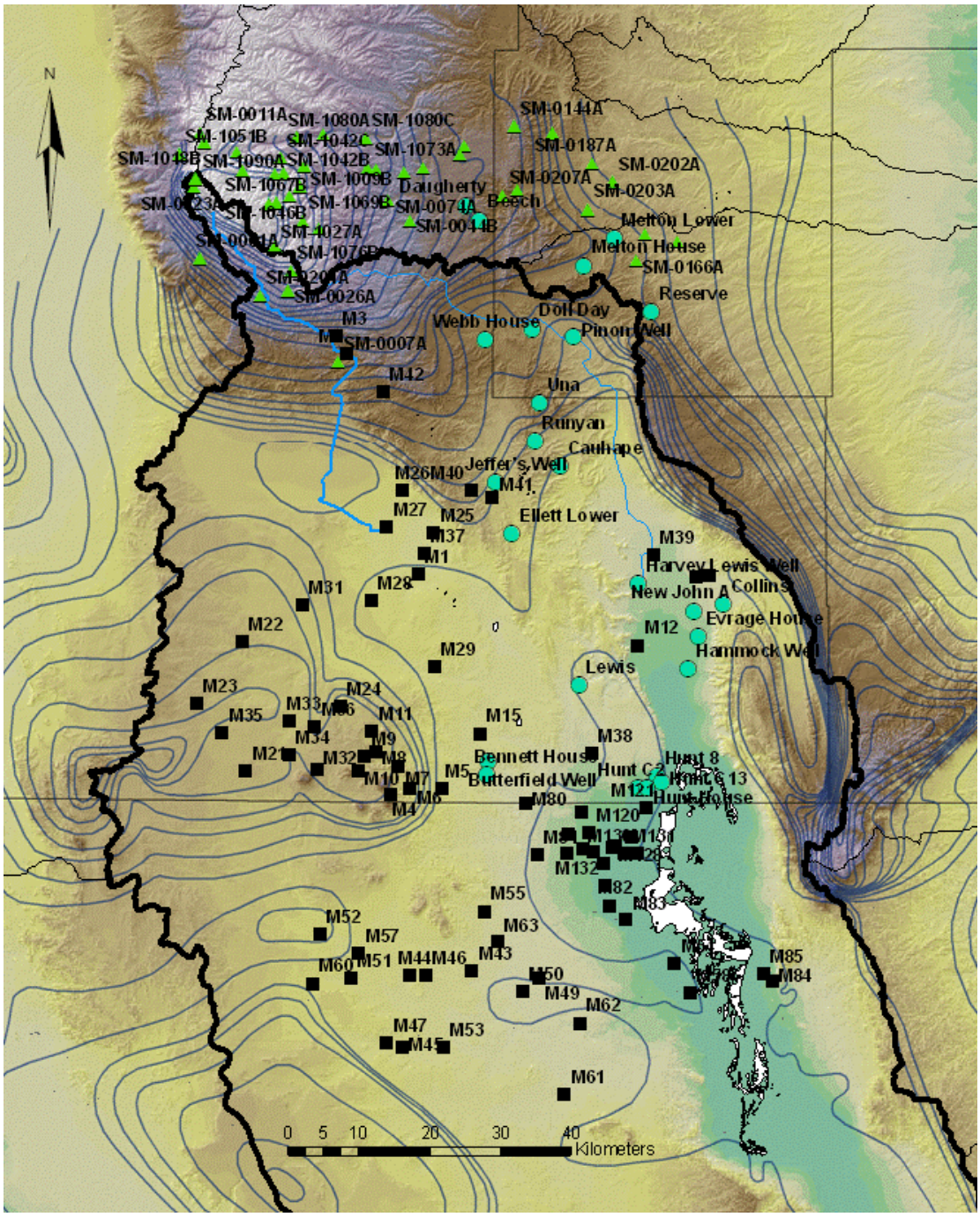


**Figure 4.2** Distribution of comprehensive well water chemistry dataset used for analysis for the Salt Basin. Digital Elevation Map (DEM) provided by the USGS National Elevation Dataset. Water elevation contours are from Ritchie (2010) refer to figure 3.2

# CHAPTER V

## INTERPRETATION OF ENVIRONMENTAL TRACERS IN GROUNDWATER

### Section 5.1: Ion Chemistry as Subsurface Tracers

Specific processes within the hydrologic cycle affect the transport and reactions involving the ion chemistry of natural waters. Fluxes of solutes from rainfall and runoff as well as chemical reactions within the soil and saturated zone operate to increase or decrease the abundance of dissolved constituents in water. For most groundwater, 95% of the ions are represented by 8 major ionic species (Herczeg and Edmunds, 2000). The positively charged cations include sodium ($Na^+$), potassium ($K^+$), calcium ($Ca^{2+}$) and magnesium ($Mg^{2+}$) and the negatively charged anions include chloride ($Cl^-$), sulfate ($SO_4^{2-}$), bicarbonate plus carbonate ($HCO_3^- + CO_3^{2-}$) and nitrate ($NO_3^-$). These species when added up makeup the total dissolved solids (TDS). However, minor constituents such as bromide ($Br^-$), strontium ($Sr^{2+}$) and lithium ($Li^+$) can also be informative of physical or chemical processes (Herczeg and Edmunds, 2000).

Solutes present in groundwater are primarily derived from two main sources: 1) rainfall, and 2) weathering and rock/water interactions (Herczeg and Edmunds, 2000). Precipitation carries solutes of marine origin as well as continental dust picked up as condensed air masses move inland. When the precipitation falls to the land surface these constituents are concentrated through evapotranspiration from soil or surface-water. As the precipitation infiltrates to the subsurface the incorporation of carbon dioxide, from atmospheric and biological processes in the vadose zone, acts as a weak acid driving

mineral dissolution (Herczeg and Edmunds, 2000). Ultimately, as the water moves through the subsurface it records information on the significant reaction minerals and lithology of the aquifer system (Back and Hanshaw, 1970; Back and Freeze, 1983; Edmunds et., 1987). A sequential process of geochemical reactions as water moves down gradient is observed in most aquifers. These means elemental chemistry can often be used to trace flow paths and even as an indicator for maturity and relative residence time (Edmunds and Smedley, 1999).

The rock/water interactions that will dominate in the subsurface as the groundwater flows through the aquifer are controlled by the departure from chemical equilibrium conditions of the water with respect to the minerals present. Deviations from equilibrium chemistry are described in *Fundamentals of Ground Water* (Schwartz and Zhang, 2003). Departure of a reaction from equilibrium can be estimated by the means of the ratio of the ion activity product to the equilibrium constant (IAP/K). The saturation state is often expressed in terms of saturation index (SI), defined as log(IAP/K). When a mineral is in equilibrium with respect to a solution, the SI is zero. Undersaturation with respect to a mineral results in the net dissolution indicated by a negative SI. Supersaturation results in the net precipitation of the mineral and a positive SI.

**Section 5.2: Interpretation of Stable Isotopes Oxygen-18 and Deuterium**

Stable isotope ratios of oxygen and hydrogen from water molecules are useful environmental tracers as tools for tracing precipitation through the hydrologic system. In particular these stable isotopes can be applied to, identifying sources of recharge,

delineation of flow paths, and quantification of mass-balance relationships (relative amounts of water from various sources) in hydrologic investigations (Coplen, 2000).

### Section 5.2.a: Stable Isotope Ratios and Abundance

Isotopes are atoms of the same element that differ in mass due to differences in the number of neutrons that make of the nucleus. For example, the nucleus of most oxygen atoms contains 16 subatomic particles- oxygen-16 or $^{16}O$: 8 protons and 8 neutrons. A small fraction of all oxygen atoms (approximately 2%) contains 10 neutrons, for a total of 18 subatomic particles in the nucleus. This isotope is oxygen-18 or $^{18}O$. Hydrogen atoms typically contain a single proton in the nucleus ($^{1}H$) orbited by a single electron. A small fraction of hydrogen atoms (approximately 0.016%) also contain one neutron in the nucleus, for a total of 2 subatomic particles. The isotope $^{2}H$ is given the name deuterium and symbolized D. Natural abundances for these isotopes are provided by *Principles of Isotope Geochemistry: Hydrosphere chapter 4* (Sharp, 2007). Oxygen-18 and deuterium are referred to as stable isotopes because they are not subject to radioactive decay. As discussed in chapter 4, analytical techniques report the ratio of the heavier isotope to the lighter isotope ($^{18}O/^{16}O$, D/H) as a per mil deviation from an international standard. A negative value means the sample is depleted in the heavier isotope and isotopically lighter than the standard. A positive values means the sample is enriched in the heavier isotope and isotopically heavier than the standard.

### Section 5.2.b Meteoric Water Line (MWL)

There is a linear relationship between $\delta^{18}O$ and $\delta D$ isotopic compositions of precipitation. The function of this relationship on a worldwide basis is called the global

meteoric water line (GMWL). The GMWL can generally be defined by $\delta D = 8*\delta^{18}O + 10$ (Sharp, 2007). The GMWL was generated from thousands of analyses of precipitation samples from the International Atomic Energy Agency network (Rozanski et al., 1993). The intercept is known as the deuterium excess factor and can vary geographically. To compensate for this a 'local' meteoric water line (LMWL) is often defined for a given study area. Because precipitation is the fundamental source for groundwater, the interpretation of stable isotope data is often performed using a δD versus $\delta^{18}O$ plot with the meteoric water line (MWL) as the reference (fig 5.1).

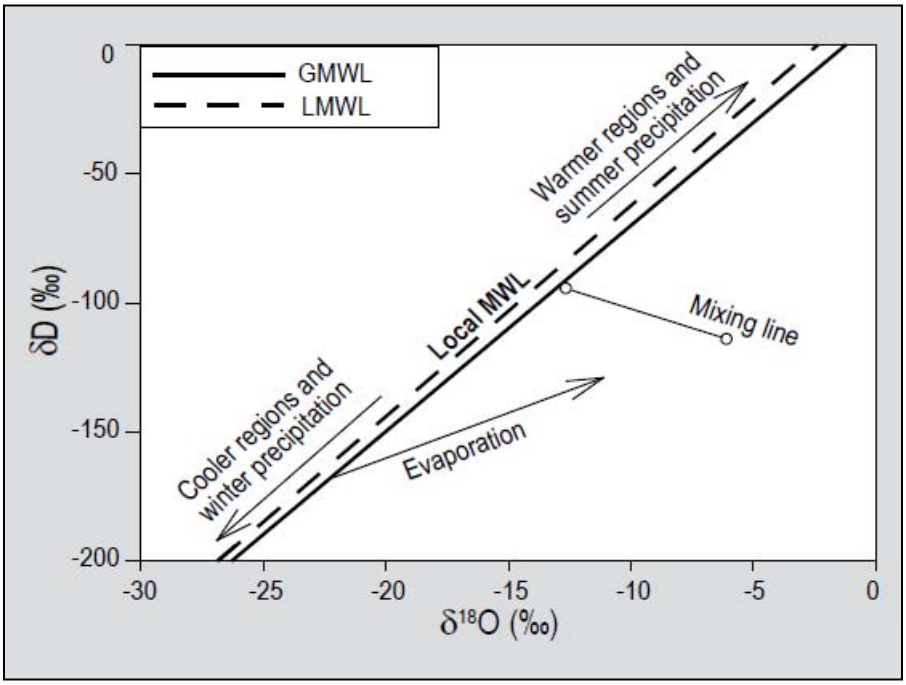


Figure 5.1 The relationship between δD and $\delta^{18}O$ of meteoric water, as well as deviations from the MWL. From NMBGMR (Rawling, 2008).

A general feature of the GMWL is that precipitation in warmer climates will plot toward the heavier end (less negative values), and precipitation from cooler climates plot toward the lighter end (more negative values). Seasonal trends are also commonly observed at a given location with winter precipitation at the lighter end and summer precipitation toward the heavier end. However, this a simplified concept as there are many interrelated factors controlling the isotope composition of precipitation.

A process that will cause water to deviate from the MWL is evaporation. Evaporation is a nonequilibrium process that enriches the residual water such that the $\delta D/\delta^{18}O$ slope is less than 8, and often between 3 and 6 (fig 5.1). The slope of the evaporation line (fig 5.1) is a function of humidity, temperature, salt concentrations and other factors (Coplen, 2000).

Figure 5.1 also illustrates how the mixing of two water sources of distinct isotopic compositions can be evaluated using the $\delta D/\delta^{18}O$ plot. Two mixing waters will plot on a straight line between the water sources end-members. The distance between the mixed water and the end-members is proportionally related to the contribution from each end-member.

**Section 5.2.c: Factors Controlling the Isotopic Composition of Precipitation**

The spatial and temporal variations of the isotope ratios in precipitation have their origin in isotopic fractionation effects involved in evaporation from the ocean and the environment influencing consequential condensation during transport through the atmosphere. The variability is interpreted to be controlled by numerous inter-related factors such as: surface air temperature, relative humidity in the atmosphere, amount of

precipitation, latitude, distance from the coast, seasonal variation and elevation of a given area above sea level. These relationships have been observed by a worldwide survey of isotopic composition of monthly precipitation by the International Atomic Energy Agency in conjunction with the World Meteorologic Organizations, starting in the 1960's (Rozanski, 1997). Each of these factors is in some way related to Rayleigh fractionation during rainout of an air mass. Under Rayleigh conditions, liquid condenses in equilibrium with the isotopic composition of the vapor, but then is removed from the system (i.e. the cloud) as precipitation. The rainout process continually depletes the remaining vapor fraction. Dansgaard (1964) empirically correlated the effect of these factors to the average degree of rainout and the change in isotopic composition of precipitation.

(1) **Altitude Effect** $\delta^{18}O$ and $\delta D$ composition decrease with increasing altitude. Higher altitudes are associated with cooler temperatures so air masses hold less water (lower vapor fraction). Fractionation is also temperature dependant and lower temperatures mean that Rayleigh fractionation is intensified.

(2) **Latitude Effect** $\delta^{18}O$ and $\delta D$ composition decrease with increasing latitude as rainout of air masses increases (lower vapor fraction) and temperature decreases with latitude .

(3) **Continental Effect** $\delta^{18}O$ and $\delta D$ composition decrease as air masses move inland from the coast raining out over the continent (lower vapor fraction). Another control on the continental effect is the $\Delta T$ decreases between the source of the vapor and the precipitation location. During the winter this effect increases.

(4) **Amount Effect** The greater the rainfall the more depleted $\delta^{18}O$ and $\delta D$ composition. Evaporation increases $\delta^{18}O$ and $\delta D$ composition of light precipitation compared to large rainfall events. Large rainout also means lower vapor fraction remaining.

(5) **Temperature** This is so interrelated to the progression of rainout (lower vapor fraction) during transport to higher latitudes (or altitudes) with lower temperature that it is difficult to isolate its effects.

(6) **Seasonal Variation** Winter precipitation is typically depleted in $\delta^{18}O$ and $\delta D$ composition relative to summer rains in mid- and high latitudes. Seasonally changing temperatures affect the extent of rainout (vapor fraction remaining). Sources and travel paths of air masses can also change seasonally that affect isotope compositions due to the continental effect.

The factors controlling isotopic compositions of precipitation are described in *Principles of Stable Isotope Geochemistry: Hydrosphere chapter 4* (Sharp, 2007) and *Environmental Tracers in Subsurface Hydrology: Isotope Engineering chapter 3* (Coplen, 2000).

**Section 5.2.d: Identifying Sources of Recharge**

Because the variability in the isotopic composition of precipitation is dependent on recharge environment, $\delta^{18}O$ and $\delta D$ can act as a fingerprint for sources of recharge to the groundwater system. In a groundwater basin with sources of recharge at different altitudes or with different seasonality for precipitation distinct end-members may be

identified. Different mechanisms of recharge will also affect the isotopic composition of the groundwater. Higher rainfall events resulting in rapid infiltration through fast transport pathways will have depleted isotopic signatures compared to slower infiltration of lighter more scatter precipitation more affected by evaporation (Coplen, 2000). Enrichment by evaporation of surface-water can be used as a trace for surface-water and groundwater interactions (Coplen, 2000). Quantification of the contributing end-members in a groundwater system can be determined based on mixing relationships.

Factors controlling the isotopic composition of precipitation such as changes in temperature and precipitation patterns are also fundamental components to climate change. This means isotopic shifts observed in groundwater can reflect changes in recharge over time. The transition from the late Pleistocene to the present represents a particularly significant shift in climate conditions for temperate-latitude regions. The noble gases (Ne, Ar, Kr, and Xe) as well as oxygen and hydrogen isotopes have been used as indicators for paleo-temperatures relative to present temperatures. Noble gas ratios show evidence for recharge temperatures close to present values during most of the Holocene. Alternatively, noble gas temperatures indicate for the last glacial maximum (LGM) about 5.2 °C cooler temperatures compared to the Holocene (Stute et al., 1995). This temperature shift was observed in a number of studies from Texas, New Mexico, and Arizona. The difference in recharge temperature, as well as possibly other interrelated factors: vegetation type, lower evaporation rates, higher humidity, or more precipitation are shown to affect the oxygen and deuterium composition. In the San Juan Basin, New Mexico, the isotopic composition of Pleistocene-age groundwater average -3 per mil depletion in $\delta^{18}O$ and -25 per mil depletion in $\delta D$ (Phillips et al., 1986). The

difference in $\delta^{18}O$ and $\delta D$, between the late Pleistocene to the Holocene groundwater determined by Andrews and Lee (1979) is about -1.7 per mil in $\delta^{18}O$ and $\delta D$ is depleted by more than -8.4 per mil. These same waters all showed groundwater ages in excess of 10,000 yrs BP, and support evidence for recharge during a colder climate regime.

**Section 5.3: Tritium as an Environmental Tracer**

There are three isotopes of hydrogen. Hydrogen atoms typically contain a single proton in the nucleus ($^1H$) orbited by a single electron, also known as protium. A small fraction of hydrogen atoms also contain one neutron in the nucleus, for a total of 2 subatomic particles, also known as deuterium. Tritium, the third naturally occurring isotope of hydrogen, has one proton and two neutrons for a total of 3 subatomic particles in the nucleus. The additional neutron in tritium imparts instability so that tritium is subject to radioactive decay. Tritium ($^3H$) decays by beta emission to $^3He$ with a half-life of $12.3 \pm 0.02$ years (Unterweger et al., 1980). Tritium can replace hydrogen in water to form HTO (partially tritiated water) or $T_2O$ (tritiated water) (Solomon and Cook, 2000).

Because large amounts of tritium were blasted into the atmosphere during the 1950's-1960's atmospheric nuclear weapons testing, tritium can be used as an environmental tracer to distinguish water recharged before, during or after the atmospheric weapons testing period. Prior to 1950, the only source of tritium in precipitation was from natural production in the upper atmosphere, largely through the bombardment of nitrogen by the flux of neutrons in cosmic radiation. The natural (pre-bomb) level of tritium in rainfall in Europe and North America was estimated by means of measurements on vintage wines to be 3-6 tritium units (TU) in (Soloman and Cook,

2000). These values indicate that water that recharged from precipitation prior to 1950 would have tritium concentrations less than 0.5 TU. There are seasonal varations and latitude dependence on $^{3}H$ levels in precipitation (Fontes, 1980; Gat, 1980). Uncertainty in historical tritium levels mean that $^{3}H$ dating is often relative (i.e. pre-1950, during the nuclear testing, or post-bomb testing). Higher levels of tritium generally indicate water recharged in the last 50 years (Fontes, 1980).

## Section 5.4: Radiocarbon ($\delta^{14}C$) Dating Groundwater

### Section 5.4.a: Natural Abundances of Carbon and $\delta^{14}C$ Radioactive Decay

The three most important isotopes of elemental carbon are carbon-12 , carbon-13, and carbon-14. Carbon-12 is the most abundant isotope of carbon (approximately 98.89 %). Carbon-12 ($\delta^{12}C$) is a stable isotope; the nucleus contains 6 protons and 6 nuetrons for a total of 12 subatomic particles. A small fraction of all carbon (1.1 %) contains 6 protons and 7 neutrons in the nucleus for a total of 13 subatomic particles. This is known as carbon-13 ($\delta^{13}C$) and is also a stable isotope. Carbon-14 is naturally produced in the upper atmosphere by the interactions of nitrogen and the cosmic rays that constantly bombard the earth (Kalin, 2000). Carbon-14 ($\delta^{14}C$) has 6 proton and 8 neutrons for a total of 14 subatomic particles in the nucleus. The additional neutron in carbon-14 imparts instability so that carbon-14 is subject to radioactive decay. Carbon-14 decays according to: $^{14}C \rightarrow {}^{14}N + \beta-$ with a modern half-life of 5,730 ± 40 years (Godwin, 1962). Measurements of $\delta^{14}C$ are reported as percent modern carbon (pmc), determined as the ratio of the sample activity to that of the international standard expressed as a percent.

Most laboratories report $\delta^{14}C$ activity normalized for the isotope fractionation effects of $\delta^{13}C$ with a value of -25 per mil (Stuiver and Polach, 1977). This correction is for more traditional use of radiocarbon dating (i.e. organic matter). In radiocarbon dating groundwater most of the the effects on $\delta^{13}C$ are from rock/water interactions where dissolved inorganic carbon (DIC) is typically enriched compared to $\delta^{13}C$ of -25 per mil. This means radiocarbon dating of DIC in groundwater is better based on actual measured $\delta^{14}C$ activity expressed in non-normalized (pmc). Normalized $\delta^{14}C$ activities can be converted to non-normalized values by the equation 5.1 (Mook and van der Plicht, 1999), for measurements based on the $^{14}C/^{12}C$ ratio,

Equation 5.1 $$pmc = pM\left[\frac{\left(1+{}^{\delta^{13}C}/_{1000}\right)}{0.975}\right]^2$$

In this equation pmc is non-nomalized $\delta^{14}C$, pM is normalized $\delta^{14}C$, and $\delta^{13}C$ is the measured value. The $\delta^{14}C$ pmc in table 5.1 has been de-normalized from the reported values. This in the end is a minor correction only about 1 per mil difference.

**Section 5.4.b: Concepts in Deriving Radiocarbon ($\delta^{14}C$) Age of Groundwater**

The radioactive carbon-14 is quickly oxidized to carbon dioxide ($^{14}CO_2$). The activity of $\delta^{14}C$ in atmospheric $CO_2$ gas is approximately 100 pmc (Fritz and Fontes, 1980). Atmospheric $CO_2$ gas is incorporated into the groundwater system (as bicarbonate

$H^{14}CO_3^-$) during infiltration of recharge through the vadose zone (Kalin, 2000). As the infiltration crosses the water table the dissolved inorganic carbon (DIC) is isolated from the modern $\delta^{14}C$ input from the atmosphere and soil zone reservoirs. As the water travels along flow paths in the aquifer system the $\delta^{14}C$ decays with time. This means the amount of $\delta^{14}C$ measured in the groundwater along a flow path, in association with its half life, gives an age or the approximate time that has passed since the water recharged into the aquifer system (equation 5.2). In relative terms, lower percent modern carbon (pmc) indicates older groundwater. To quantitatively estimate groundwater age, radiocarbon dating techniques interpret the distribution of a radiocarbon species in terms of a first-order kinetic rate law of decay (Schwartz and Zhang, 2003). The groundwater age (t) is determined by:

Equation 5.2: $$t = \frac{t_{1/2}}{\ln(2)} \ln\left(\frac{A_o}{A_{obs}}\right)$$

Where $t_{1/2}$ is the half-life for decay, $A_o$ is the activity assuming no decay, and $A_{obs}$ is the measured $\delta^{14}C$ activity. The rate of decay (~ 5,730 yrs) means that radiocarbon dating can be applied to groundwater from about 1,000 to 40,000 years old.

**Section 5.4.c: Interpretation of Radiocarbon ($\delta^{14}C$) Age of Groundwater**

Carbon-14 ($\delta^{14}C$) is not an ideal environmental tracer in that it is not necessarily conservative in groundwater systems. Some reactive minerals (i.e., calcite) contain inorganic carbon that can be transferred in and out of the groundwater. These interactions act to reduce the $\delta^{14}C$ activity in the water and need to be accounted for in

estimating the age (Shwartz and Zhang, 2003). Any age calculation (eqn. 5.2) is meaningful only as long as $A_o$ and $A_{obs}$ only differ due to the effects of radioactive decay.

$A_o$ (100 pmc) needs to be corrected for processes affecting $\delta^{14}C$ activity in the vadose zone during recharge. Typically two main factors are considered important in the vadose zone. The infiltrating waters interaction with soil $CO_2$ gas that typically has higher pmc than atmospheric $CO_2$ due to biologic activity (Brook et al., 1983). As well as, the effects of dissolved $CO_2$ reacting with carbonate minerals in the vadose zone of the recharge area, resulting in increased dissolved inorganic carbon (Kalin, 2000). The initial $\delta^{14}C$ activity can be estimated using a number of isotope exchange and mass balance approaches [see Kalin's chapter 4 on Radiocarbon Dating in, *Environmental Tracers in Subsurface Hydrology* (2000)]. Alternatively, $A_0$ can be assumed to be 85 ± 5 pmc based on numerous measurements of $\delta^{14}C$ activity of groundwater recharge (Vogel and Ehhalt, 1963; Vogel, 1967, 1970). And finally, $A_o$ can be measured for any given study area assuming confidence in a well delineated recharge area.

The $\delta^{14}C$ activity measured along a flow path ($A_{obs}$) needs to be corrected for the rock/water interactions that act as sources and sinks for carbon-14 as the water travels through the aquifer system (Kalin, 2000). Well defined flow paths and geochemical evolution are critical for accurate estimates of measured $\delta^{14}C$ activity. Due to the many geochemical interactions and hydrologic processes that can act as sources or sinks for $^{14}C$ in a groundwater system, geochemical modeling is often applied in modern approaches to radiocarbon dating. In particular, computer models such as NETPATH (Plummer et al., 1994) can be used to quantify carbon mass transfer for determining the initial $\delta^{14}C$ activity and adjusting the observed $\delta^{14}C$ activity.

Another important consideration in dating groundwater is that any water sample collected contains a huge number of molecules. The path of each molecule containing $^{14}C$ may be different due to dispersion/diffusion processes along the flow path. This means that the measurement of $\delta^{14}C$ activity in a water sample is actually a distribution of all the $\delta^{14}C$ activities from individual molecules. The reported values is the peak of the distribution sometimes termed apparent groundwater age. The concept of an age distribution has been widely applied in hydrology (Hooper, 2003; Loaiciga, 2004, and McGuire and McDonnell, 2006).

### Section 5.5: $\delta^{34}SO_4$ as a Lithologic Tracer

There are four stable isotopes of sulfur ($^{32}S$, $^{33}S$, $^{34}S$, $^{36}S$). The isotopes that are commonly measured are $^{32}S$ and $^{34}S$, because they are the most abundant at 95.03% and 4.19 %, respectively (Sharp, 2007). Often geologic units in an aquifer system contain evaporitic gypsum. This means that the occurrence of groundwater can be traced using the $\delta^{34}S$ isotope content measured in sulfate from the groundwater as the isotopic composition can be diagnostic of particular formations. Recharge enters the basin aquifer system by infiltration of intermittent surface water flows and underflow along stream channels as well as faults and fractures. Sulfate enrichment in the groundwater most likely originate from dissolution of sulfate bearing minerals (gypsum/anhydrite) caused by infiltrating meteoric waters into the extensive carbonate sequences. Dissolution of evaporites does not involve significant sulfur isotope fractionation, thus $\delta^{34}SO_4$ values of the groundwater describe flow paths through isotopic signatures picked up from the formation as the water moves through it (Krouse and Mayer, 2000).

**Table 5.1** Evironmental tracers from groundwater in the Salt Basin and Sacramento Mountains

| Sample Location | Goundwater Sample ID | δD (per mil) | $\delta^{18}O$ (per mil) | Tritium 3H (TU) | $\delta^{13}C$ (per mil) | $\delta^{14}C$ (pmc) | $\delta^{34}SO_4$ (per mil) |
|---|---|---|---|---|---|---|---|
| Salt Basin | Reserve | -58.94 | -9.38 | | | | |
| Salt Basin | Doll Day | -60.87 | -9.57 | 0.55 | -10.30 | 51.74 | 10.26 |
| Salt Basin | Pinon Well | -59.12 | -9.34 | 1.27 | -8.30 | 44.28 | |
| Salt Basin | Webb House | -71.85 | -10.70 | 1.60 | -9.80 | 67.70 | 11.70 |
| Salt Basin | Una | -58.70 | -9.43 | 1.14 | -5.90 | 27.66 | 10.24 |
| Salt Basin | Runyan | -68.44 | -9.54 | | | | 12.07 |
| Salt Basin | Cauhape | -62.13 | -9.94 | 0.27 | -7.90 | 34.82 | 10.78 |
| Salt Basin | Jeffer's Well | -59.96 | -9.57 | 1.40 | -7.80 | 29.04 | 11.28 |
| Salt Basin | Ellett Lower | -62.87 | -9.64 | 0.24 | -5.70 | 14.37 | 9.98 |
| Salt Basin | Harvey Lewis Well | | | 0.03 | -4.50 | 19.74 | |
| Salt Basin | Collins | -65.94 | -9.62 | 0.34 | -5.20 | 19.62 | 11.68 |
| Salt Basin | New John A | -63.19 | -9.30 | | | | |
| Salt Basin | Evrage House | -69.73 | -9.55 | 0.01 | -5.20 | 15.37 | 11.82 |
| Salt Basin | Hammock Well | -68.11 | -9.61 | 0.17 | -2.70 | 22.92 | 11.43 |
| Salt Basin | Lewis | -62.87 | -10.23 | 0.18 | -7.70 | 33.09 | 11.59 |
| Salt Basin | Butterfield Well | -77.89 | -12.15 | 0.11 | -3.70 | 8.19 | 10.85 |
| Salt Basin | Bennett House | -63.47 | -10.26 | | | | |
| Salt Basin | Hunt 8 | -69.97 | -9.96 | 0.10 | -5.20 | 22.52 | |
| Salt Basin | Hunt C13 | -65.53 | -10.04 | 0.00 | -6.00 | 22.50 | |
| Salt Basin | Hunt C2 | -63.64 | -9.91 | 0.00 | -5.40 | 26.09 | 11.35 |
| Salt Basin | Hunt House | -69.01 | -10.03 | 0.10 | -5.30 | 22.78 | 11.85 |
| Sacramento Mountains | SM-0138 | -60.00 | -9.00 | | -8.90 | 85.76 | |
| Sacramento Mountains | SM-0140 | -58.00 | -8.70 | | -8.90 | 80.89 | |
| Sacramento Mountains | SM-0144 | -56.00 | -9.00 | | -8.30 | 70.54 | |
| Sacramento Mountains | SM-0152 | -58.00 | -9.10 | | -8.50 | 65.71 | |
| Sacramento Mountains | SM-1009 | -60.00 | -10.20 | 4.32 | -12.90 | 92.65 | |
| Sacramento Mountains | SM-1073 | -57.00 | -9.80 | 3.49 | -11.00 | 82.93 | |
| Sacramento Mountains | SM-1076 | -67.00 | -11.30 | 5.11 | -12.20 | 89.03 | |

# CHAPTER VI

## GROUNDWATER SYSTEM CHARACTERIZATION

### Section 6.1: Groundwater Chemistry

The groundwater chemistry dataset analyzed for this report is a compilation of about 170 well samples which includes spring and well samples from the Sacramento Mountains collected by New Mexico Bureau of Geology, and a general chemistry dataset from wells throughout the Salt Basin compiled by Mayer for his 1995 dissertation. These two sources supplement groundwater chemistry from about 25 well samples collected for this study during a series of field trips through 2008--2009. See chapter 4 for a discussion on the chemistry datasets and the distribution of sample sites (Fig 4.1). The 25 groundwater samples collected for this study define general flow paths along the eastern side of the Salt Basin (Fig 6.1), starting in the recharge area of Sacramento Mountains and extending south through the Piñon Creek watershed and Cornucopia Draw, down to Crow Flats, and ending near both, the primary anthropogenic discharge area of the Dell City Irrigation District, and the natural discharge area of the Salt Flats. Because groundwater samples along these general flow paths on the eastern side of the Salt Basin were sampled for stable isotopes and carbon-14 in addition to ion chemistry this will be the principal flow path used for geochemical modeling to determine seepage velocities and elucidate other important implications for recharge.

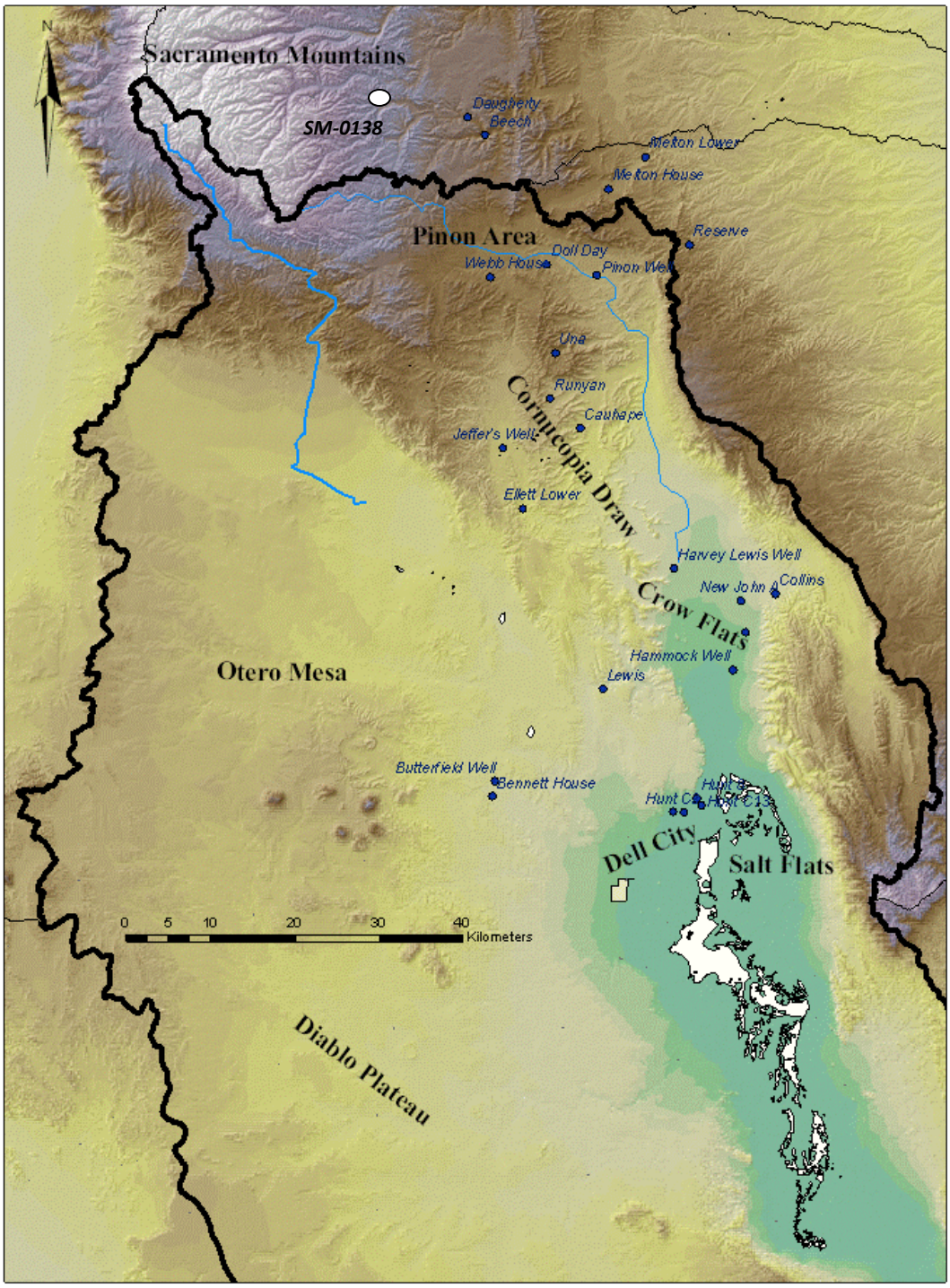


**Figure 6.1** Distribution of sample points: Recharge (white) and Salt Basin(dark blue) wells used for geochemical modeling through general sub-regions in the Salt Basin. Digital Elevation Map (DEM) provided by the USGS National Elevation Dataset.

### Section 6.1.a: Groundwater Temperature, Conductivity, and TDS

The temperature of groundwater in the Salt Basin ranges between 6 °C (in the Sacramento Mountain wells and springs) and 25 °C (in the southern portion the Salt Basin, near the Salt Flats). The average surface air temperature in the Sacramento Mountains is 9 °C; however, mean annual air temperatures vary across the basin, warming to 20 °C as elevation decreases to the south. The groundwater temperature versus surface air temperature plot (fig 6.2) is atypical of shallow aquifers (it shows an anomalously rapid increase of groundwater temperature with flow distance). This is presumably because of the very deep vadose zone over the middle of the study area. The groundwater temperature is roughly equivalent to the surface air temperature in the recharge area where the aquifer is shallower. As the flow paths become deeper the groundwater is heated due to thermal gradients (Reiter and Jordan, 1996). The increasing trend in groundwater temperatures mirrors the increase in surface air temperature (fig 1.4) in its correlation to the topography of the basin (figures 6.3 and 6.4).

Groundwater temperatures near the range of mean annual surface air temperature for the Sacramento Mountains (6-12 °C; fig 1.2) likely delineate recharge areas (fig 6.4). Alternatively, anomalously high groundwater temperatures (i.e. Pinon and Ellett wells) in the Salt Basin (fig 6.4) may indicate warmer deep groundwater upwelling (Reiter and Jordan, 1996). Localized vertical groundwater flow may also affect the groundwater chemistry at a well compared to the regional chemistry.

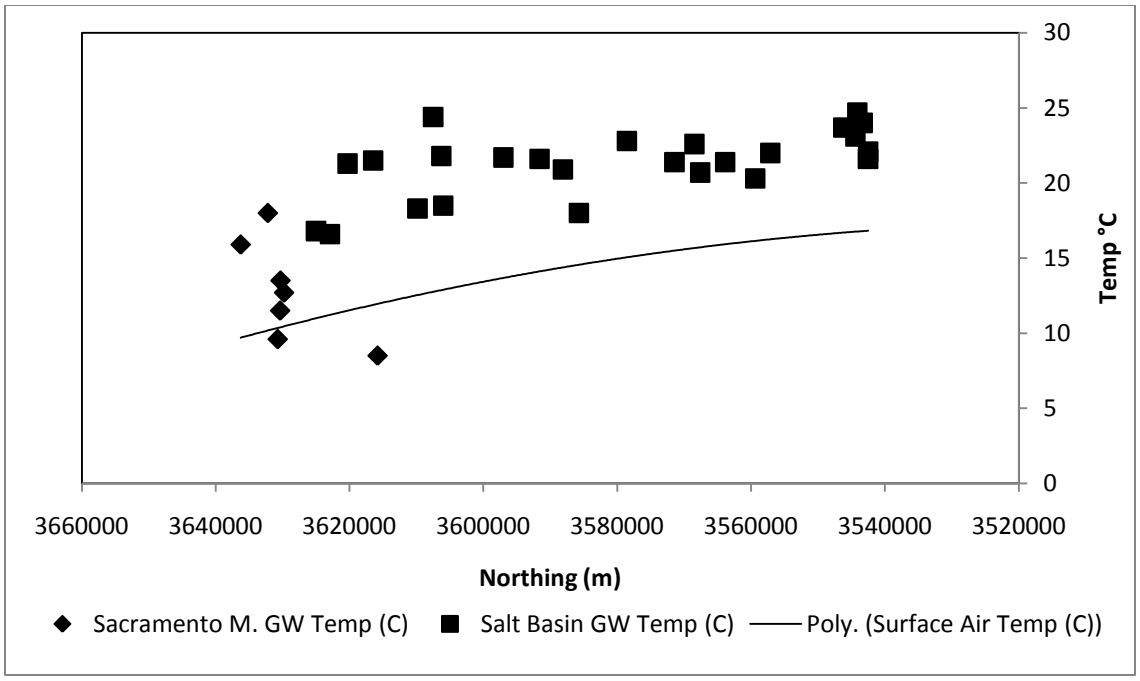


**Figure 6.2** Measured groundwater and surface air temperatures (°C) in relation to northing (m) down the general flow paths on the eastern side of the Salt Basin

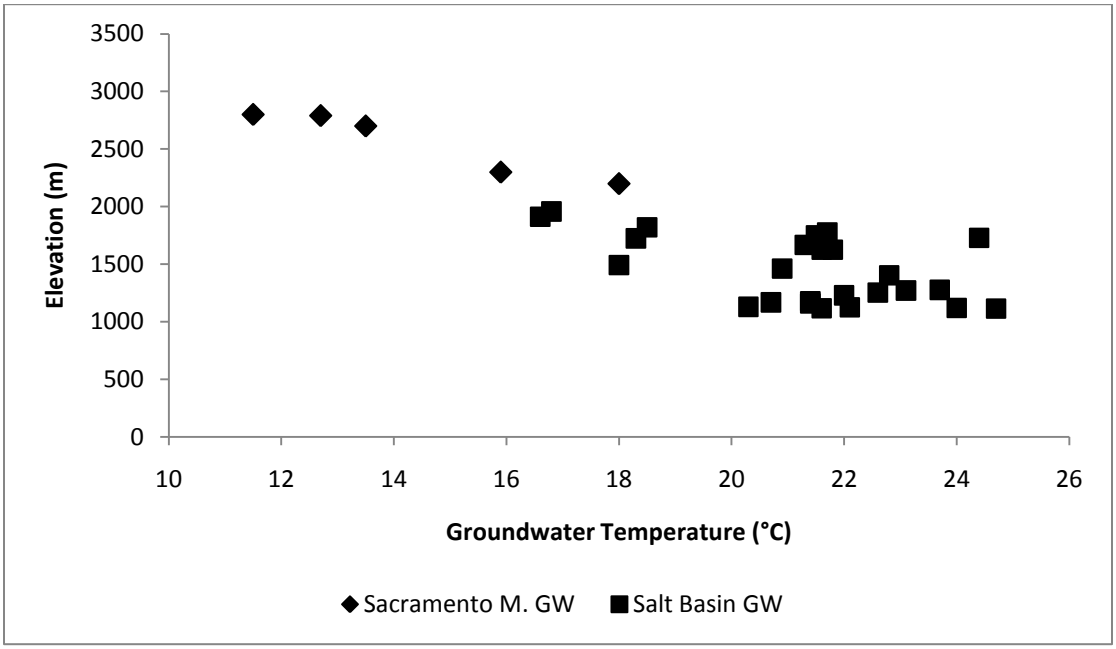


**Figure 6.3** Relationship of measured groundwater temperature ( °C) to elevation (m) at the sample location along general flow paths on the eastern side of the Salt Basin.

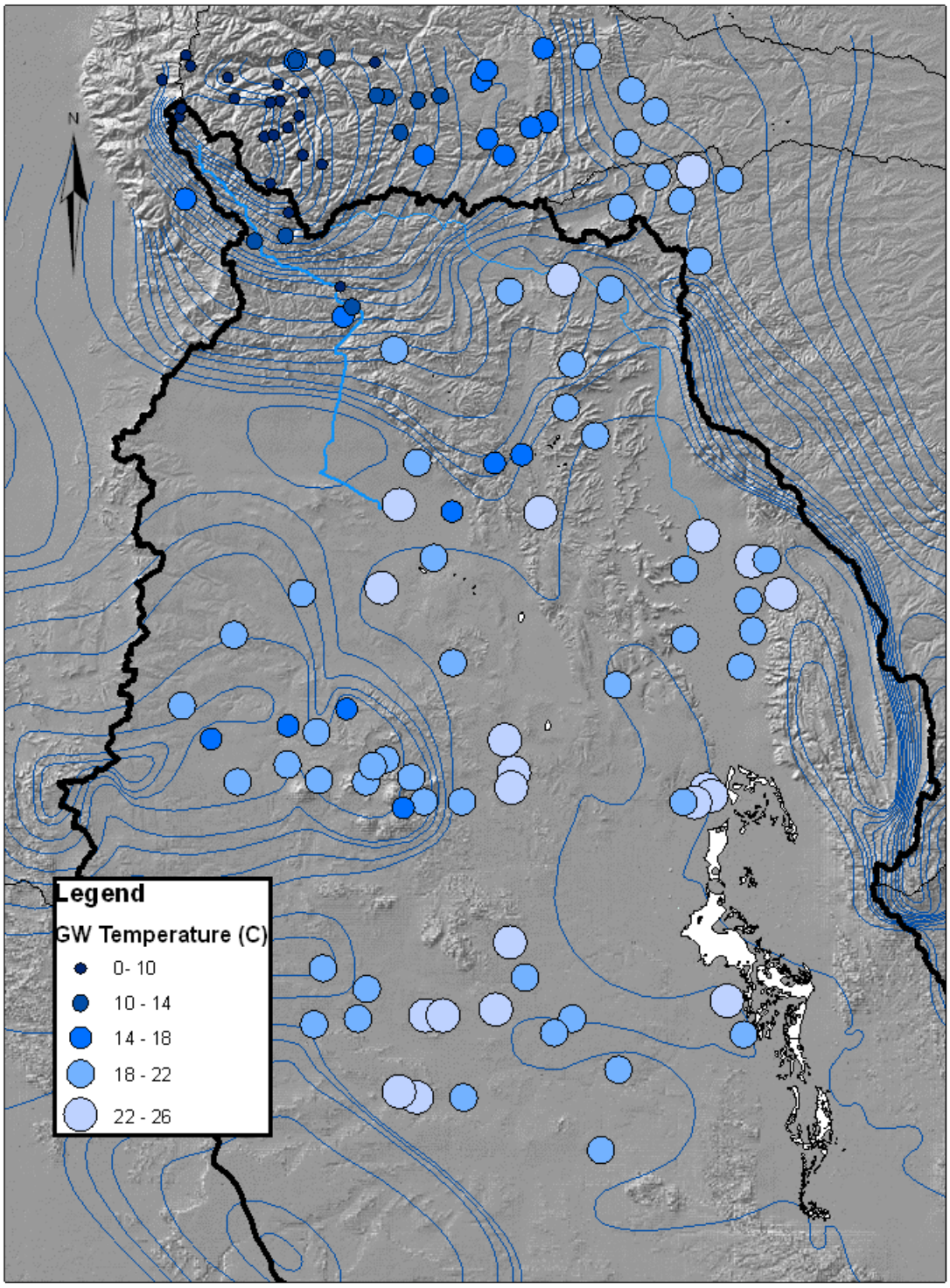


**Figure 6.4** Map of well water temperatures (°C). The symbol size increases with warmer temperatures and the color grades to lighter shades. Digital Elevation Map (DEM) provided by the USGS National Elevation Dataset. Blue lines are groundwater contours refer to figure 3.2 (Ritchie, 2010).

Total dissolved solids (TDS) is a relative measure of the total quantity of ions in solution. Recharge areas will have low TDS (fig 6.5 and 6.6). TDS concentration will increase with increased exposure for rock/water interactions and distance down the flow path. The Otero Break (fig 2.3) corresponds to a zone of low TDS due to high groundwater velocity funneling Sacramento Mountain recharge through the fracture zone (Mayer, 1995).

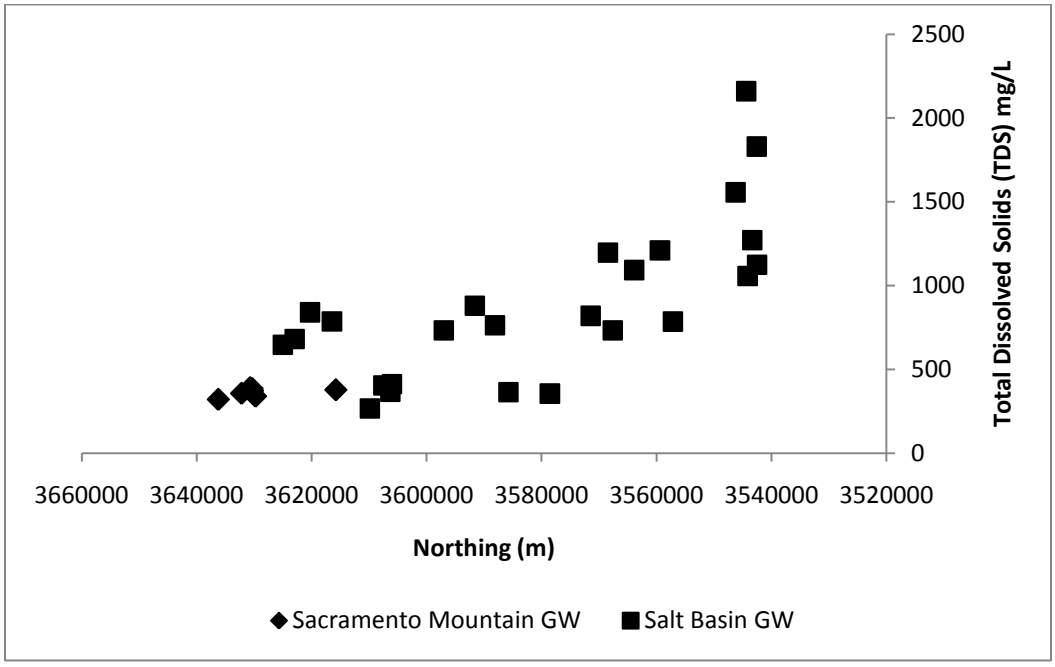


**Figure 6.5** Measured groundwater TDS (mg/L) in relation to northing (m) down the general flow paths on the eastern side of the Salt Basin

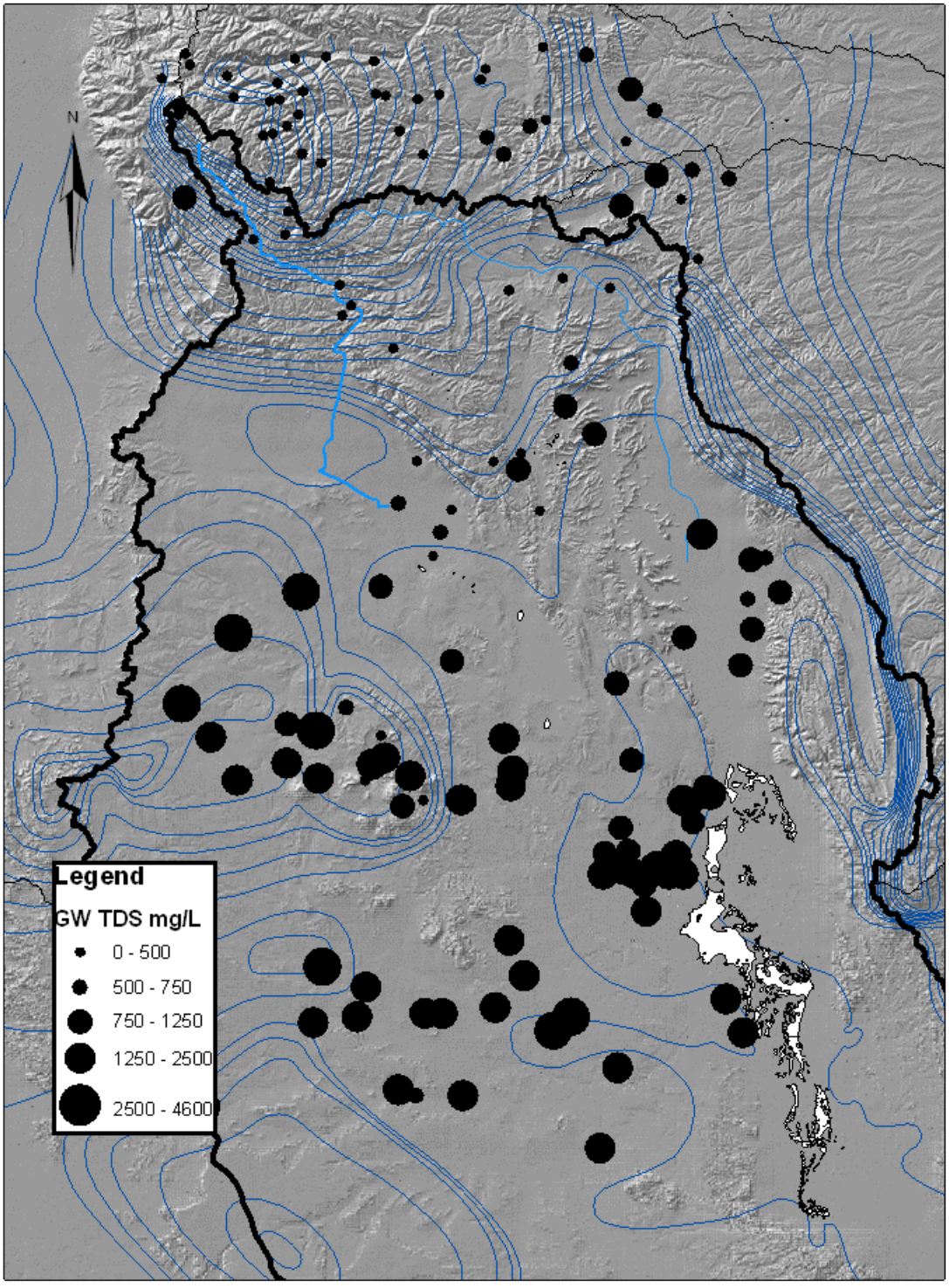


**Figure 6.6** Map of well water TDS concentration mg/L. The symbol size increases with high concentration. Digital Elevation Map (DEM) provided by the USGS National Elevation Dataset. Blue lines are groundwater contours refer to figure 3.2 (Ritchie, 2010).

**Section 6.1.b: Major Cations- Magnesium, Calcium, Sodium and Potassium**

Increases in all the major cations are observed for the groundwater samples along the flow paths on the eastern side of the Salt Basin (from the Sacramento Mountains recharge area southeast to the discharge area of Dell City and the Salt Flats). Magnesium concentrations (fig 6.7) steadily increase from about 10 mg/L to about 100 mg/L. Calcium concentrations (fig 6.8) increase from about 90 mg/L to about 285 mg/L. Sodium concentrations (fig 6.9) increase from about 5 mg/L to about 40 mg/L. A slight overall increase in potassium concentrations (fig 6.10) is also observed from about 0.5 mg/L to about 2 mg/L.

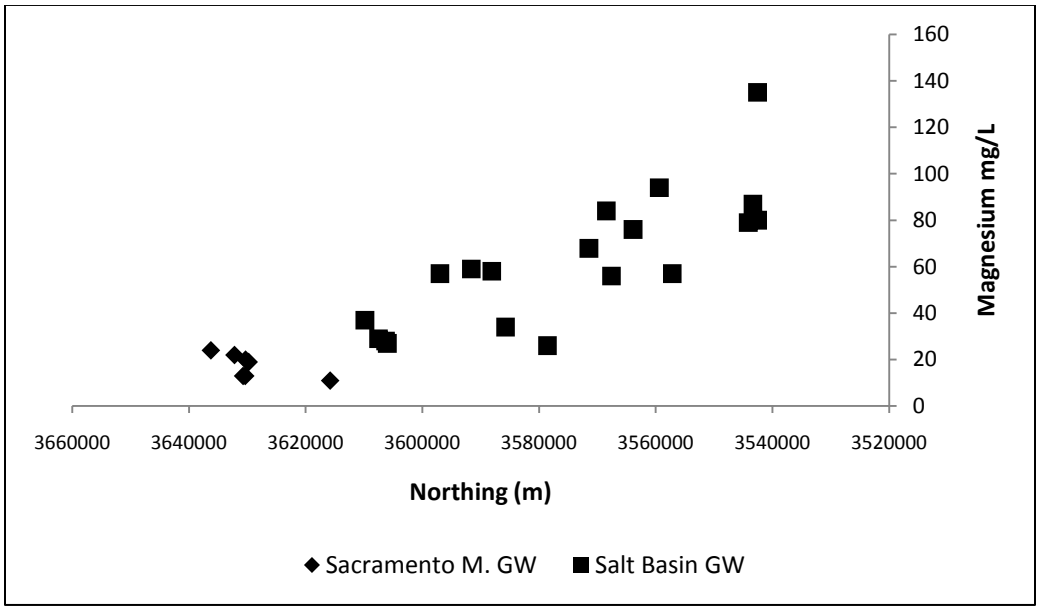


**Figure 6.7** Measured groundwater magnesium concentration (mg/L) in relation to northing (m) down the general flow paths on the eastern side of the Salt Basin

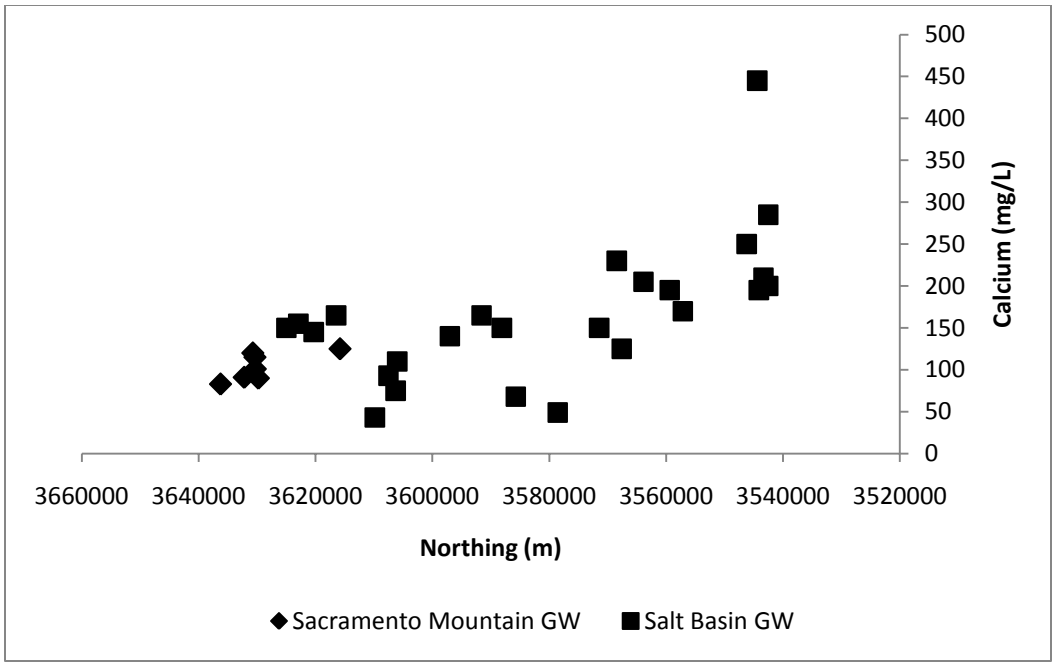


**Figure 6.8** Measured groundwater calcium concentration (mg/L) in relation to northing (m) down the general flow paths on the eastern side of the Salt Basin

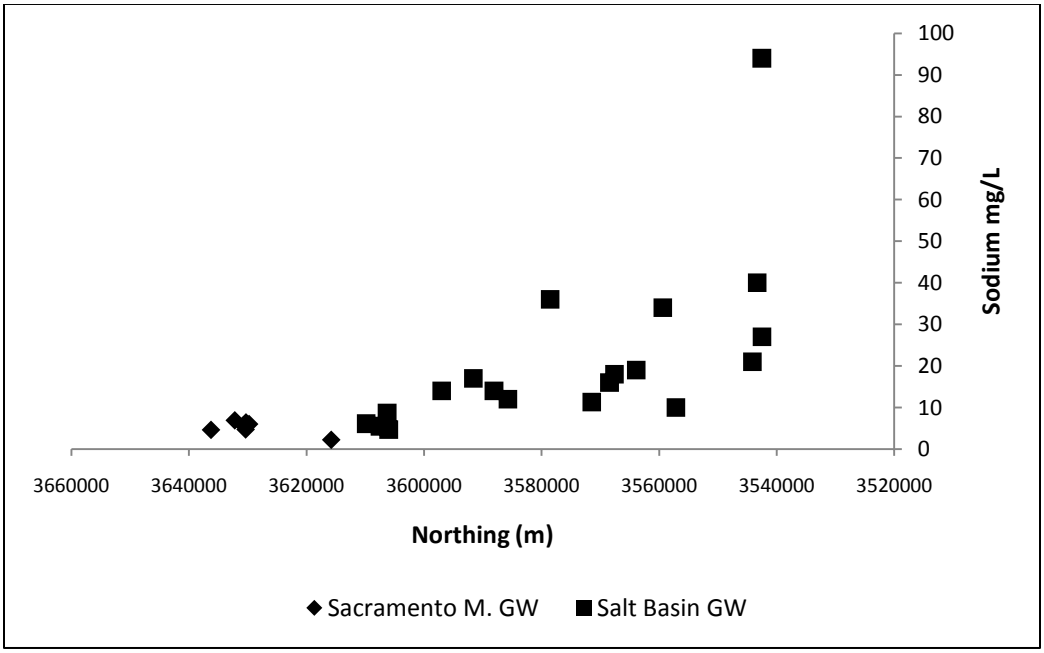


**Figure 6.9** Measured groundwater sodium concentration (mg/L) in relation to northing (m) down the general flow paths on the eastern side of the Salt Basin

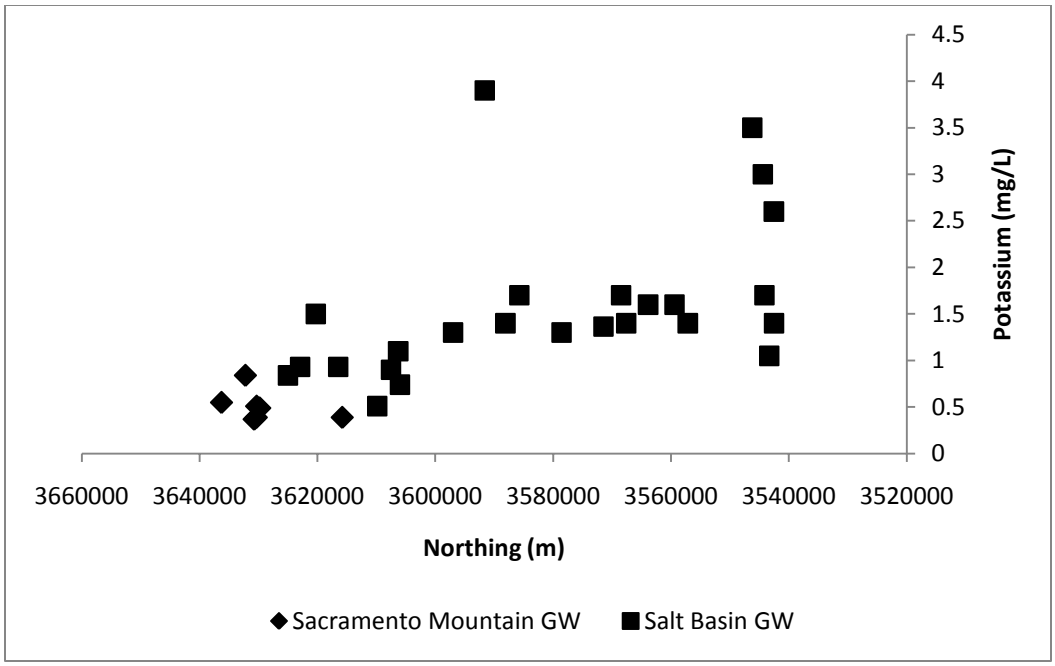


**Figure 6.10** Measured groundwater potassium concentration (mg/L) in relation to northing (m) down the general flow paths on the eastern side of the Salt Basin

The distribution of the major cations from groundwater throughout the Salt Basin is similar to the distribution of TDS content (fig 6.5). Magnesium (fig 6.11), sodium (6.12), and calcium (6.13) concentrations are low through the Otero Break fault zone (fig 2.3). Consistent with the TDS the relatively freshwater appears to be an indication of higher velocity flow paths preferentially channeling recharge from the Sacramento Mountains to the Salt Basin graben (Mayer, 1995). Similar to groundwater concentrations observed in the Sacramento Mountains concentrations through the Otero Break are typically below: 50 mg/L for magnesium concentrations, 25 mg/L sodium concentrations, and 120 mg/L for calcium concentrations.

The cation distribution for groundwater throughout the Salt Basin also mirrors the TDS distribution in the prominent concentration increase in Otero Mesa and Diablo

Plateau. In these regions concentrations are well above those seen on the eastern side of the Salt Basin. Magnesium concentrations are between 100 and 200 mg/L. Sodium concentrations have broad range between 50 and 500 mg/L. Similarly, calcium concentrations are typically from 200 to 600 mg/L. Although higher concentration are characteristic of the majority of groundwater samples in Otero Mesa, for all the major cations there are some wells that have relatively low concentrations. This may be related to some amount of recharge from the Cornudas Mountains, semi-perched aquifer systems, or some kind of preferential flow feature. There is also freshwater associated with the Diablo Plateau but this is likely related to eastward flow from the Hueco Bolson (Kreitler, 1990).

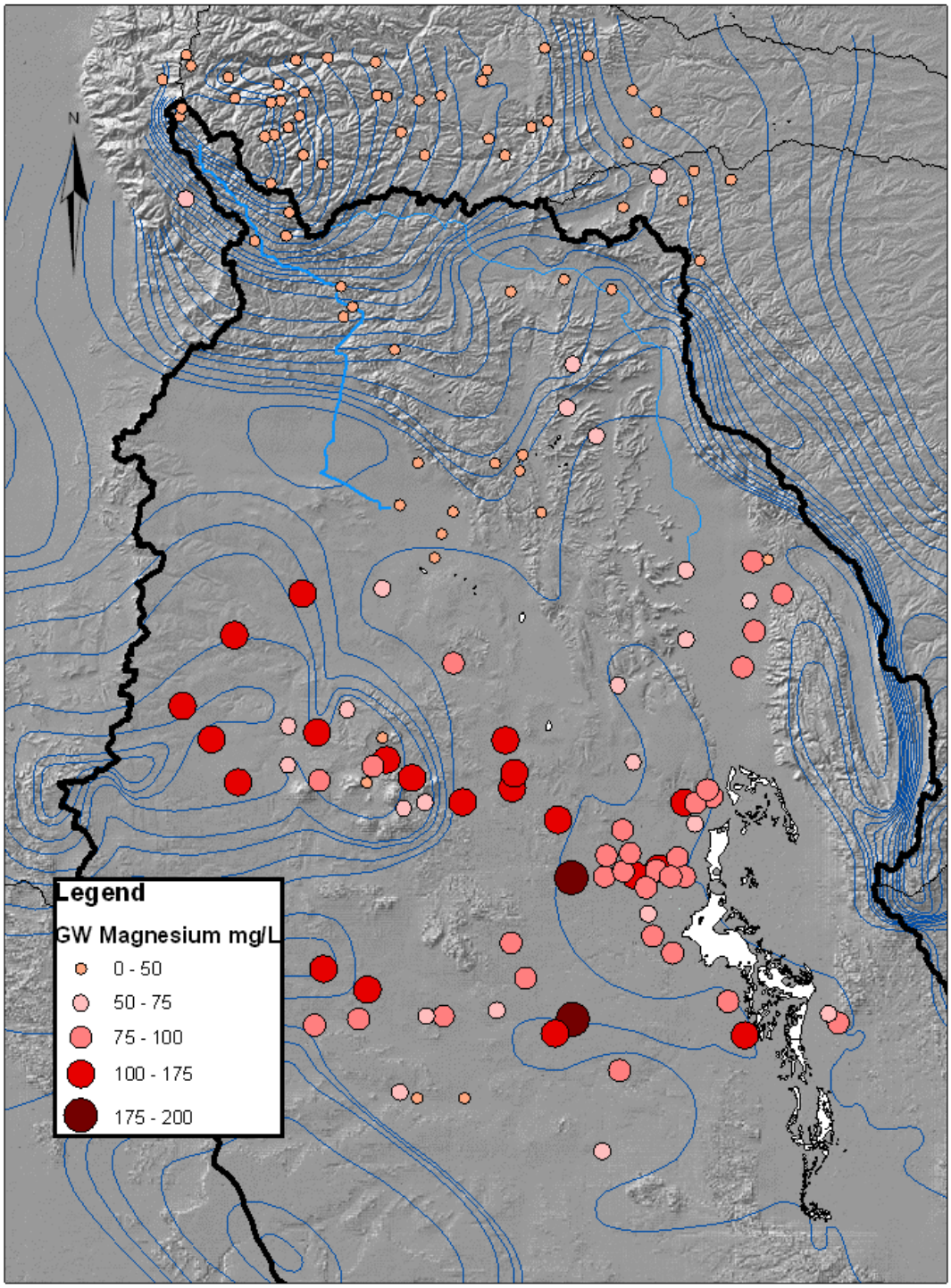


**Figure 6.11** Map magnesium concentration mg/L. The symbol size increases with higher concentrations and the color grades to darker shades. Digital Elevation Map (DEM) provided by the USGS National Elevation Dataset. Blue lines are groundwater contours refer to figure 3.2 (Ritchie, 2010).

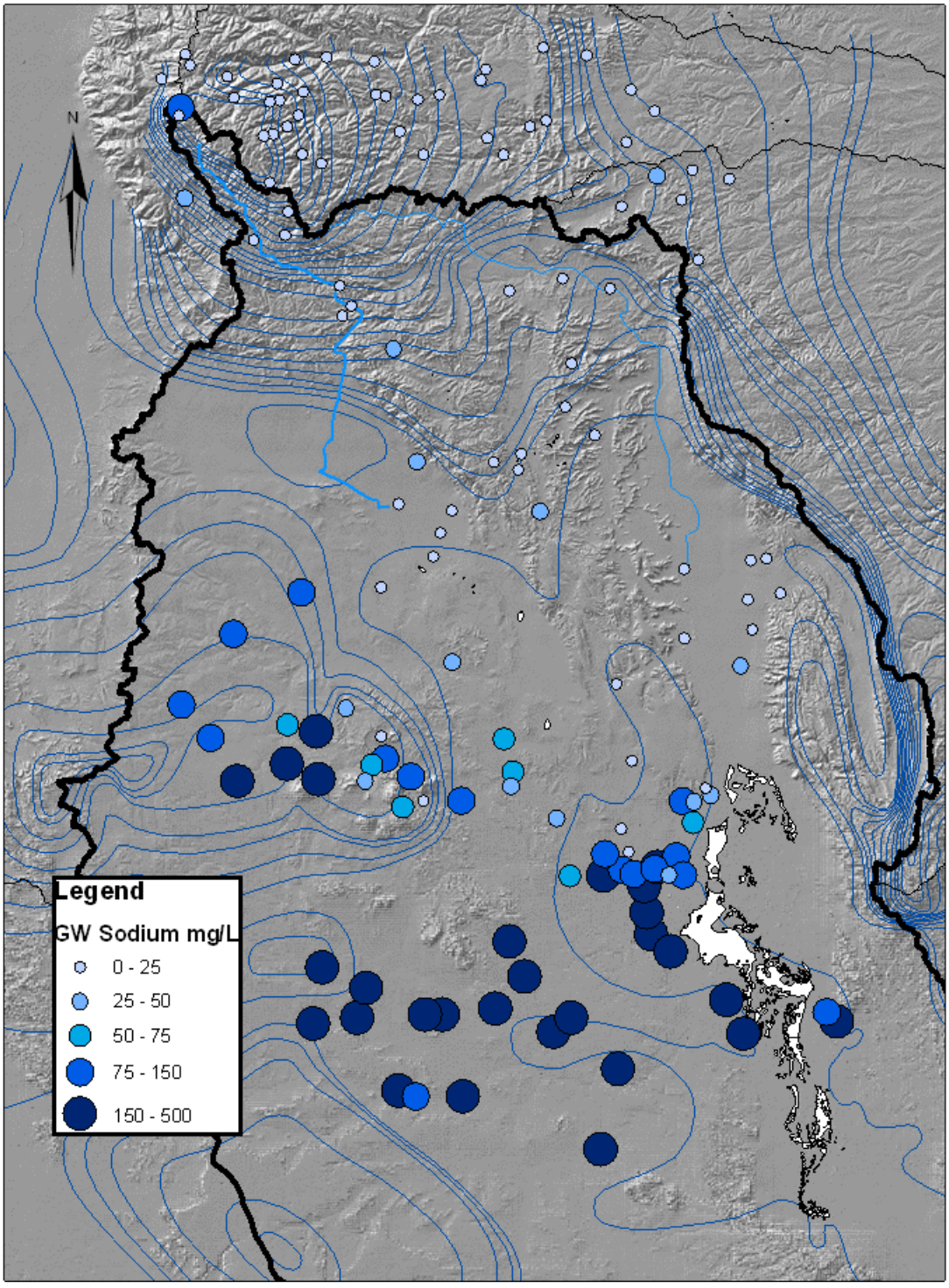


**Figure 6.12** Map sodium concentration mg/L. The symbol size increases with higher concentrations and the color grades to darker shades. Digital Elevation Map (DEM) provided by the USGS National Elevation Dataset. Blue lines are groundwater contours refer to figure 3.2 (Ritchie, 2010).

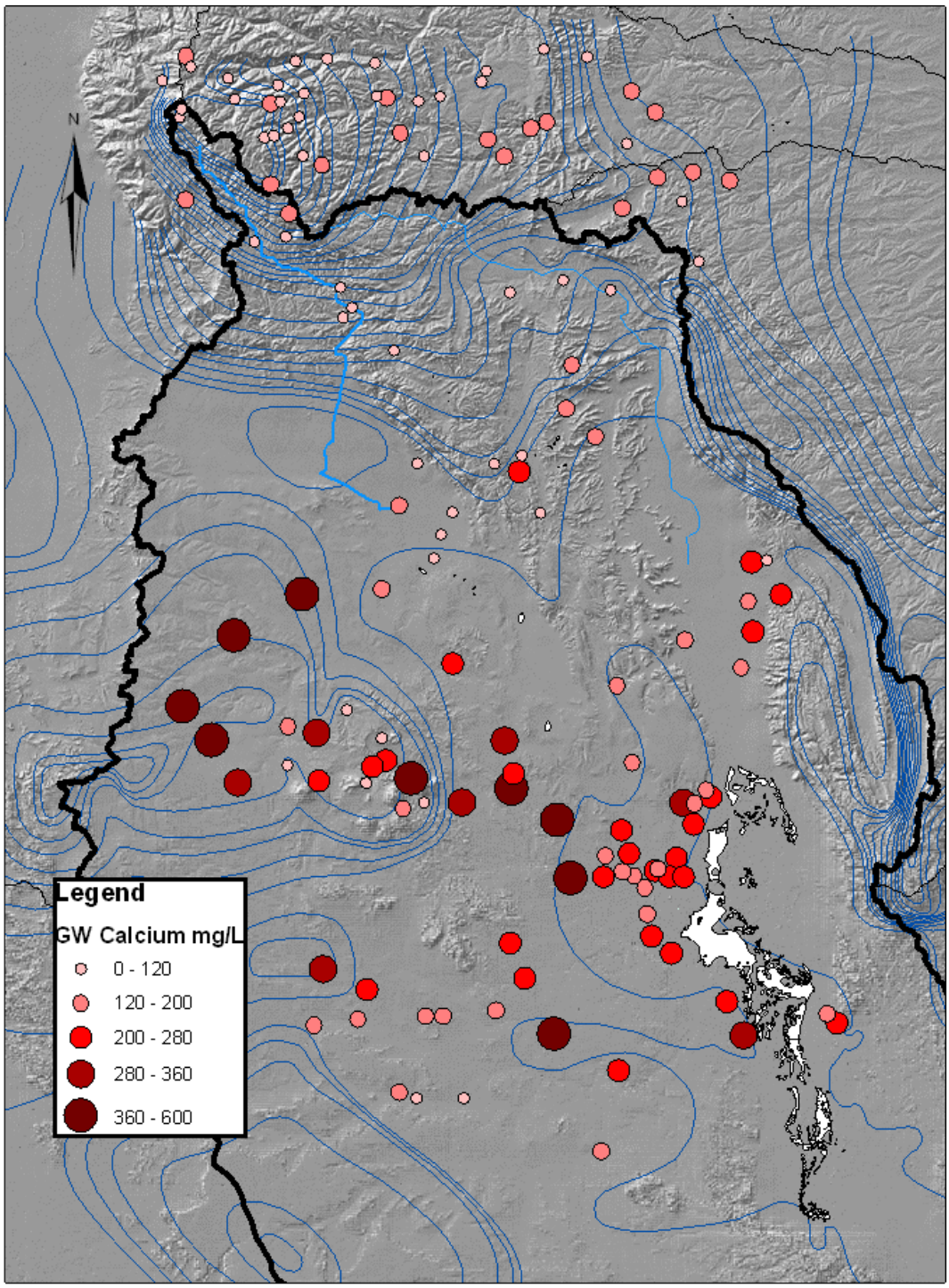


**Figure 6.13** Map calcium concentration mg/L. The symbol size increases with higher concentrations and the color grades to darker shades. Digital Elevation Map (DEM) provided by the USGS National Elevation Dataset. Blue lines are groundwater contours refer to figure 3.2 (Ritchie, 2010).

**Section 6.1.c: Major Anions- Chloride, Sulfate, and Bicarbonate**

Different trends for the major anions were observed for the groundwater samples along the flow paths on the eastern side of the Salt Basin (from the Sacramento Mountains recharge area southeast to the area of Dell City and the Salt Flats). Chloride concentrations (fig 6.14) were relatively stable until rapid increasing near Dell City and the Salt Flats. Sulfate concentrations (fig 6.15) steadily increased from about 20 mg/L to 600 mg/L. Bicarbonate concentrations (fig 6.16) slightly decreased from about 400 mg/L to 200 mg/L.

The trends in the anion distribution throughout the Salt Basin were similar to these trends. Chloride concentrations (fig 6.17) are relatively stable with much higher concentrations near Dell City and the Salt Flats. The sulfate concentrations (fig 6.18) are similar to the TDS distribution. There are low concentrations, similar to values observed in the Sacramento Mountains, through the Otero Break. While Otero Mesa and Diablo Plateau show much higher concentrations than those observed on the eastern side of the Salt Basin. For Otero Mesa concentrations range from 900 mg/L to sometimes greater than 2,000 mg/L. Bicarbonate concentrations (fig 6.19) are highest in the Sacramento Mountains and Otero Mesa/Diablo Plateau and lowest near Dell City and the Salt Flats.

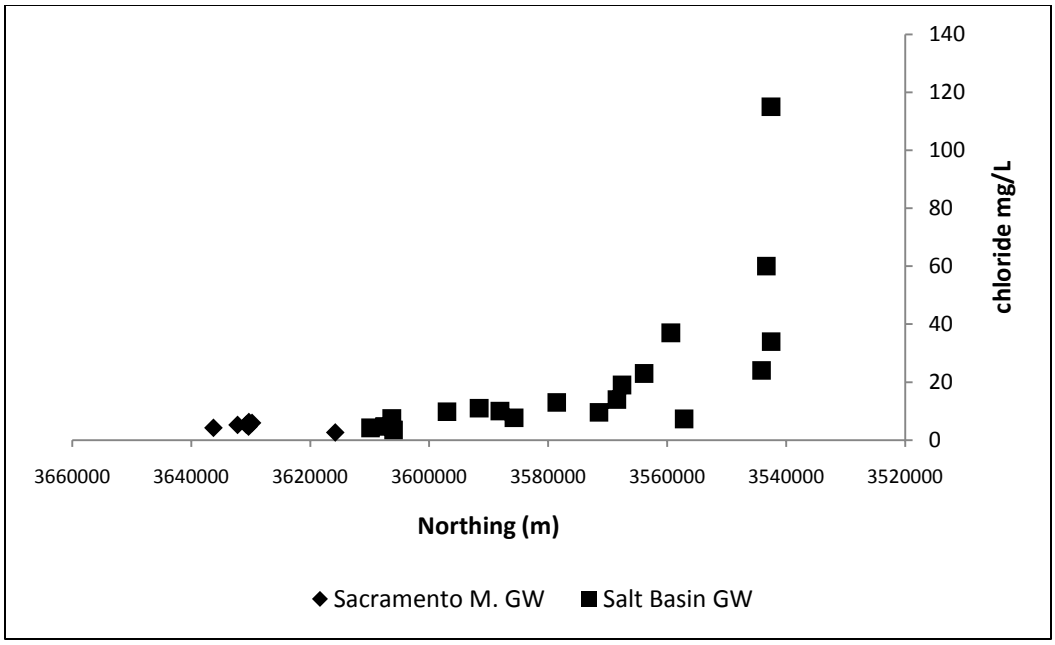


**Figure 6.14** Measured groundwater chloride concentration (mg/L) in relation to northing (m) down the general flow paths on the eastern side of the Salt Basin

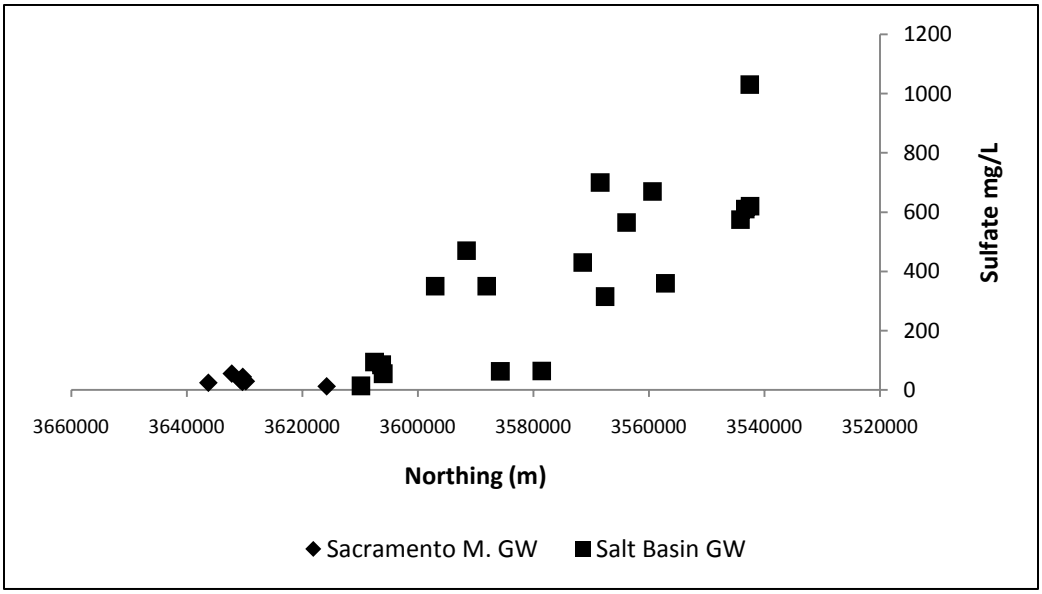


**Figure 6.15** Measured groundwater sulfate concentration (mg/L) in relation to northing (m) down the general flow paths on the eastern side of the Salt Basin

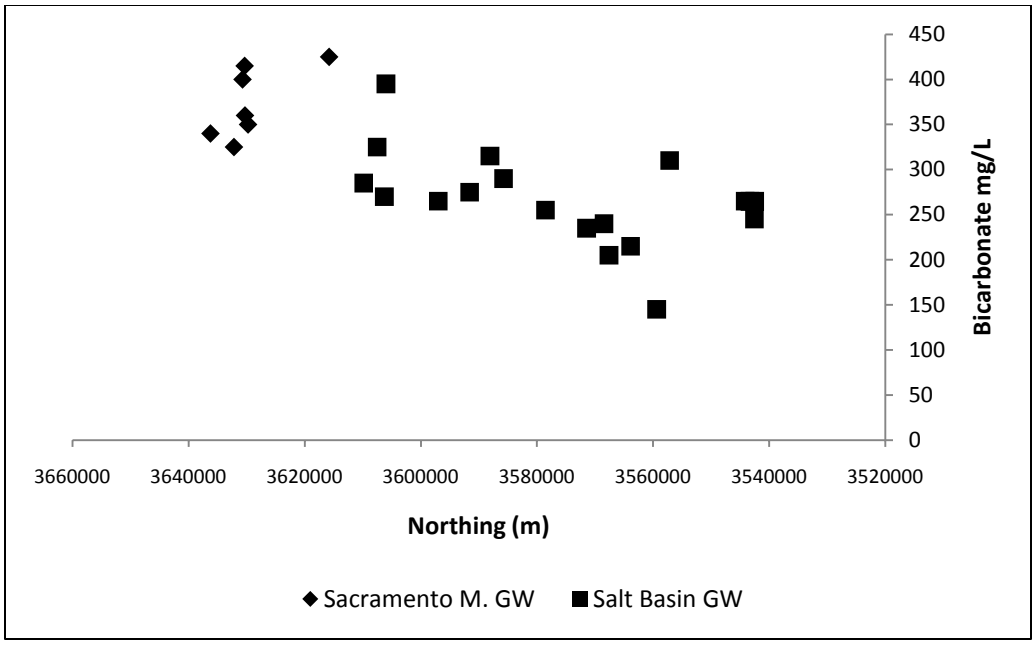


**Figure 6.16** Measured groundwater bicarbonate concentration (mg/L) in relation to northing (m) down the general flow paths on the eastern side of the Salt Basin

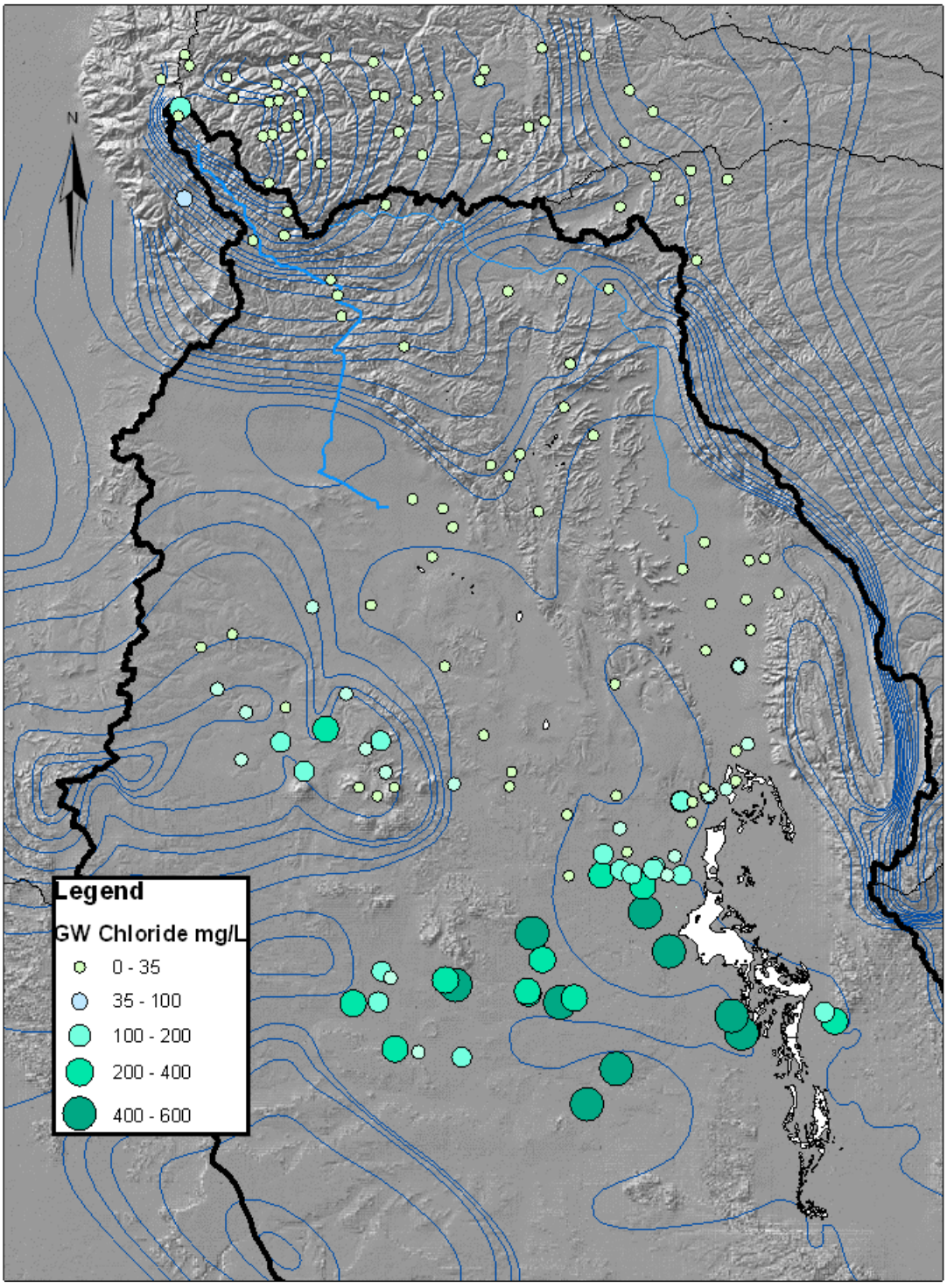


**Figure 6.17** Map chloride concentration mg/L. The symbol size increases with higher concentrations and the color grades to darker shades. Digital Elevation Map (DEM) provided by the USGS National Elevation Dataset. Blue lines are groundwater contours refer to figure 3.2 (Ritchie, 2010).

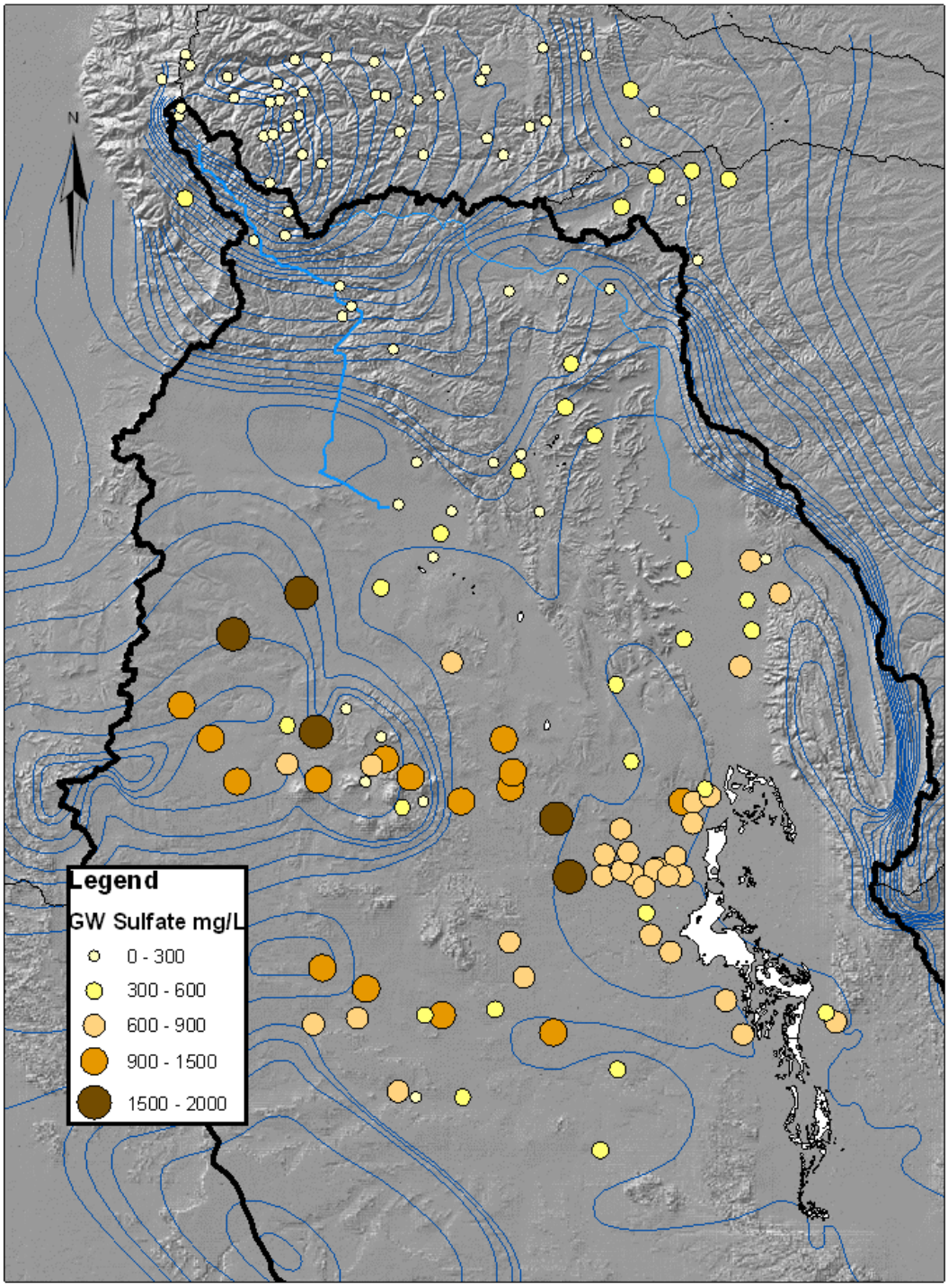


**Figure 6.18** Map sulfate concentration mg/L. The symbol size increases with higher concentrations and the color grades to darker shades. Digital Elevation Map (DEM) provided by the USGS National Elevation Dataset. Blue lines are groundwater contours refer to figure 3.2 (Ritchie, 2010).

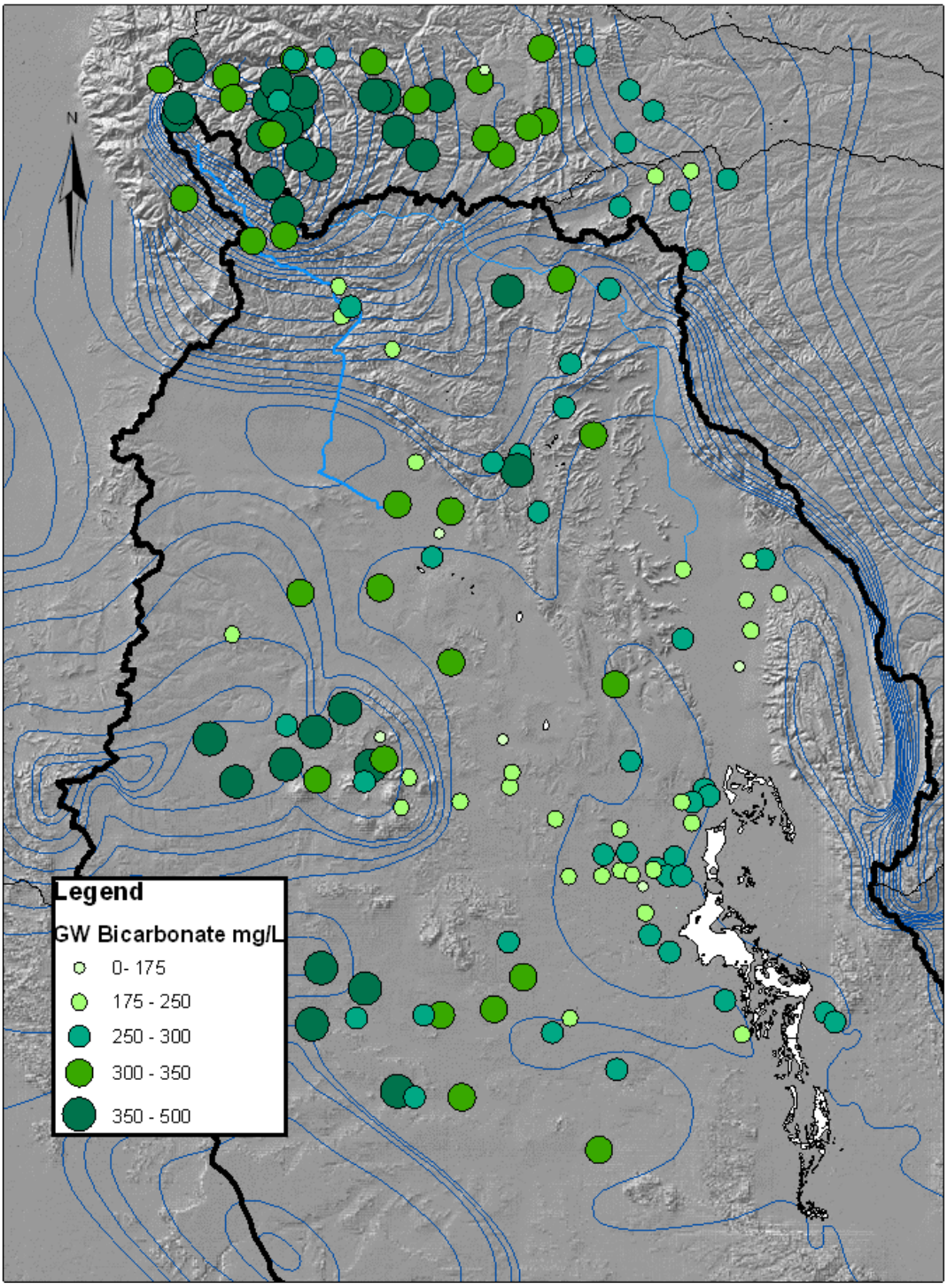


**Figure 6.19** Map bicarbonate concentration mg/L. The symbol size increases with higher concentrations and the color grades to darker shades. Digital Elevation Map (DEM) provided by the USGS National Elevation Dataset. Blue lines are groundwater contours refer to figure 3.2 (Ritchie, 2010).

**Section 6.1.d: Minor Constituents- Fluoride, Silica and Strontium**

The presence of minor constituents in the groundwater can indicate minerals involved in rock/water interactions beyond those identified by the major ion chemistry. Increases in fluoride, silica and strontium were observed for the groundwater samples along the flow paths on the eastern side of the Salt Basin (from the Sacramento Mountains recharge area southeast to the area of Dell City and the Salt Flats). Fluoride concentrations (fig 6.20) increase from about 0.1 mg/L to 1.5 mg/L. Silica content (fig 6.21) increase from 10 mg/L to 20 mg/L. Strontium concentrations (fig 6.22) increase from about 0.3 mg/L to 5 mg/L.

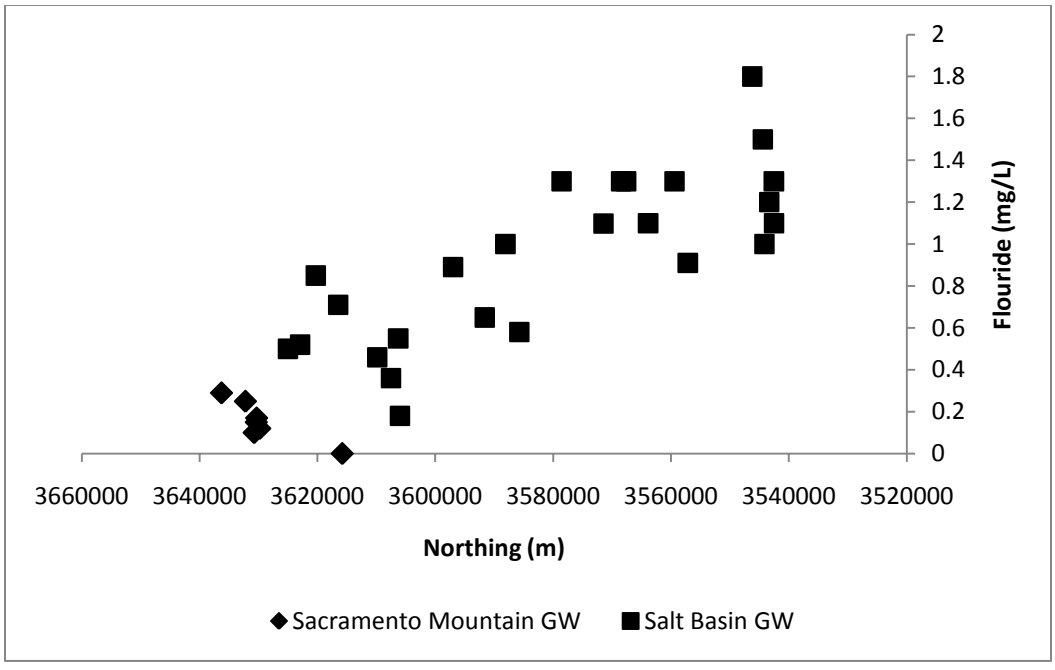


**Figure 6.20** Measured groundwater fluoride concentration (mg/L) in relation to northing (m) down the general flow paths on the eastern side of the Salt Basin

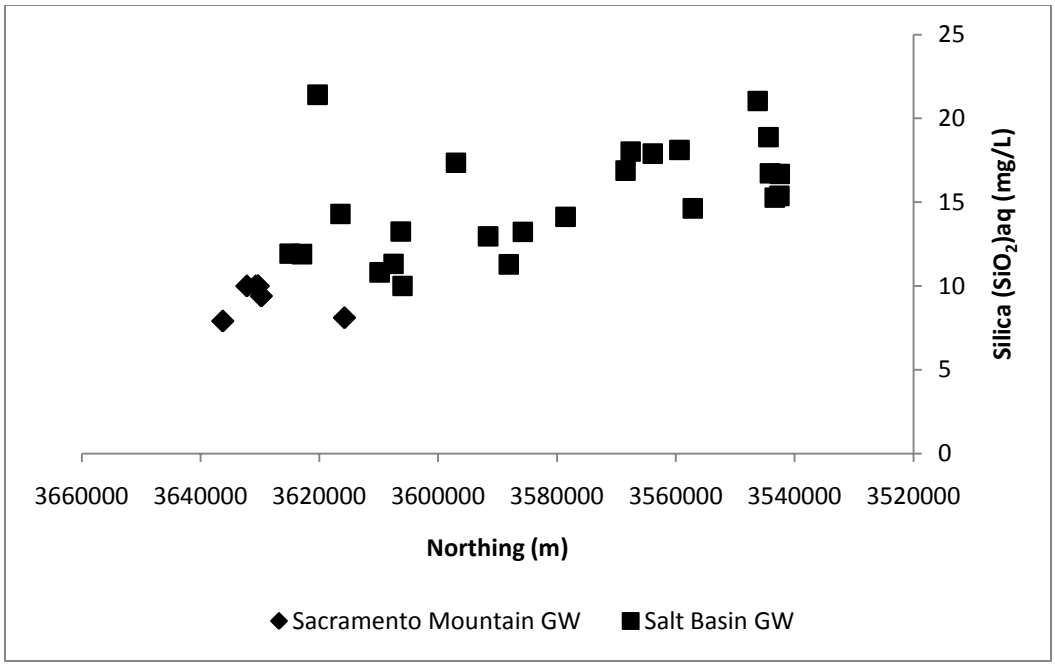


**Figure 6.21** Measured groundwater silica $SiO_2aq$ concentration (mg/L) in relation to northing (m) down the general flow paths on the eastern side of the Salt Basin

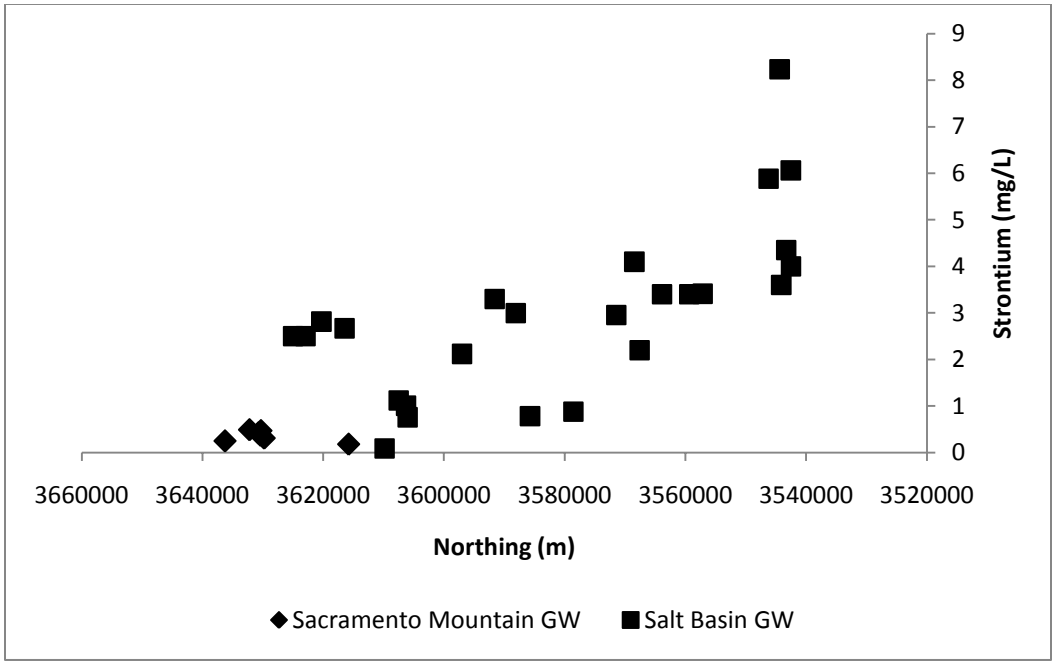


**Figure 6.22** Measured groundwater fluoride concentration (mg/L) in relation to northing (m) down the general flow paths on the eastern side of the Salt Basin

## Section 6.2: Groundwater Chemistry Evolution

### Section 6.2.a: Solute Sources and Sinks in the Aquifer System

As discussed in chapter 5.1, the chemical composition of groundwater is largely a function of the lithology and mineralogy of the aquifer system. Ion chemistry trends are diagnostic of the dominant reaction minerals along the flow paths. Along the flow paths on the eastern side of the Salt Basin as the water evolves ion chemistry shows significant increases in both magnesium and calcium concentration. The Salt Basin is predominantly a carbonate aquifer system where calcite ($CaCO_3$) and dolomite [$CaMg(CO_3)_2$] are prominent components of the Permian San Andres and Yeso formations. Dissolution of these minerals is a likely source for the increase in calcium and magnesium observed down the flow paths.

(1) Calcite Dissolution:

$$CaCO_{3(calcite)} + CO_{2(gas)} + H_20 \longrightarrow Ca^{2+} + 2HCO_3^-$$

(2) Dolomite Dissolution:

$$CaMg(CO_3)_{2(dolomite)} + 2CO_{2(gas)} + 2H_2O \longrightarrow Ca^{2+} + Mg^{2+} + 4HCO_3^-$$

Although, as Mayer (1995) points out in his discussion of the groundwater chemistry for the Salt Basin, if only the dissolution of these two minerals were responsible for the ion chemistry the molar ratio of $(Ca^{2+}+Mg^{2+})/(HCO_3^-)$ should be 1:2. This would also be the ratio expected if weathering of calcium- and magnesium-bearing silicates such as amphiboles pyroxenes were responsible for the increases. However, in the Salt Basin the

molar ratio of $(Ca^{2+} + Mg^{2+})/(HCO_3^-)$ plot above the 1:2 line indicating an additional source of calcium or magnesium.

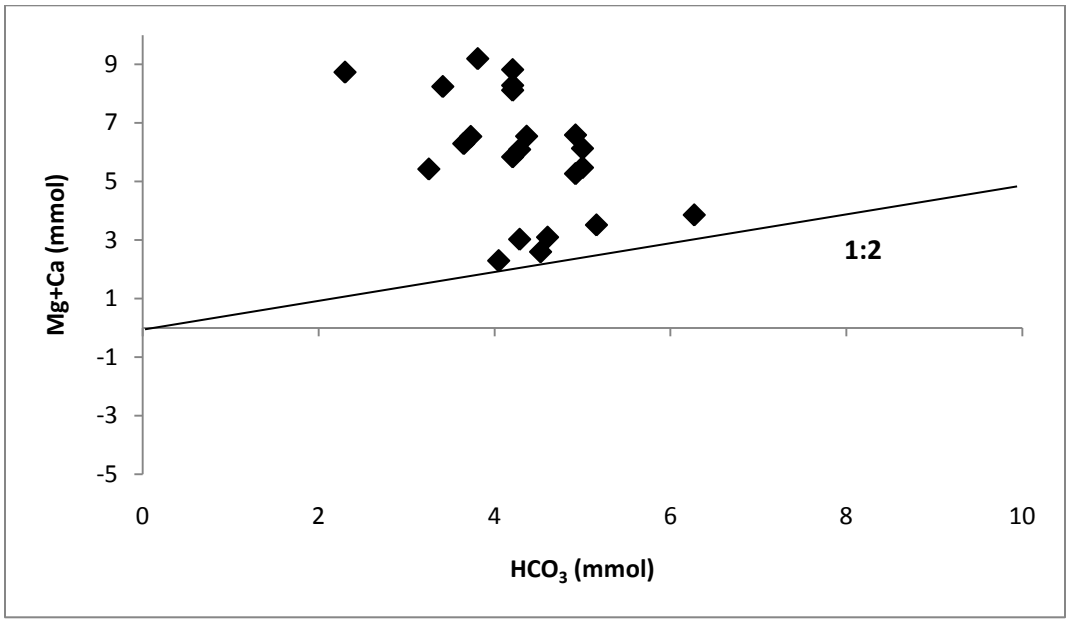


**Figure 6.23** Molar ratios of $Ca^{2+}+Mg^{2+}$ vs $HCO_3^-$. 1:2 line would correspond to the stoichiometric ratio for calcite and dolomite equilibrium reactions.

Although Figure 6.23 only illustrates the chemical evolution along the flow paths on the eastern side of the Salt Basin, Mayer observed similar molar ratios in his analysis (where water chemistry is largely from the Otero Mesa/Diablo Plateau, Crow Flats, and Dell City region). Gypsum is a highly soluble mineral and present in both the San Andres and Yeso formations (although more prevalent in the Yeso). This means the additional source of calcium is likely a result of gypsum dissolution, as previously suggested by Mayer (1995).

(3) Gypsum Dissolution

$$CaSO_4 \cdot 2H_2O_{(gypsum)} \longrightarrow Ca^{2+} + SO_4^{2-}$$

Gypsum dissolution also accounts for the increase in sulfate observed down the flow path (fig 6.15). To account for the additional $Ca^{2+}$ from gypsum dissolution $SO_4^{2-}$ is subtracted from $Mg^{2+} + Ca^{2+}$ and plotted versus $HCO_3^-$. Based on reactions (1), (2) and (3) this should yield a molar ratio of 1:2.

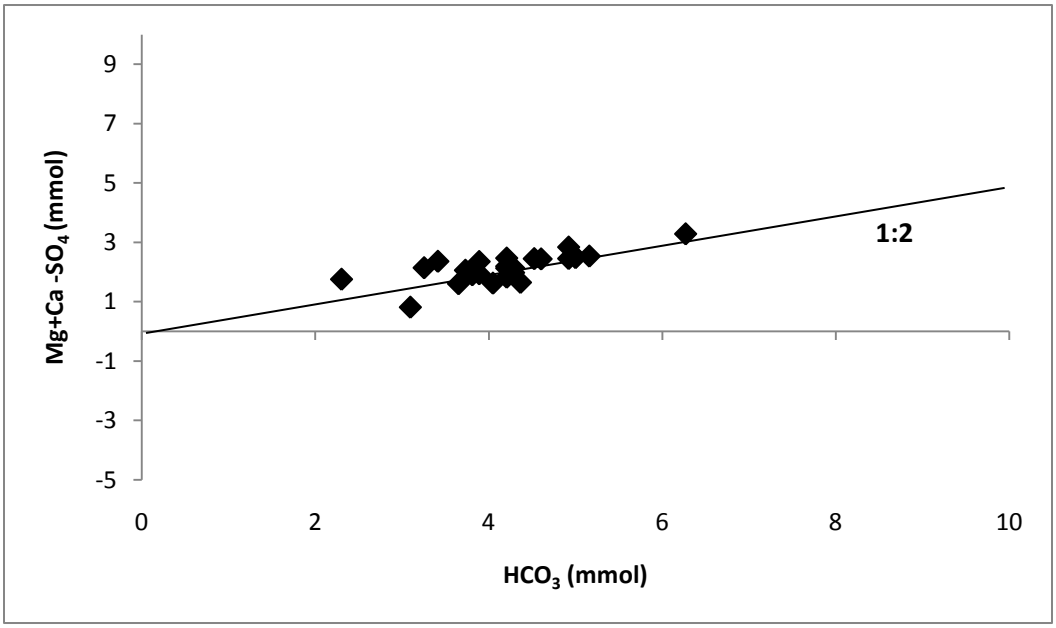


**Figure 6.24** Molar ratios of $Ca^{2+}+Mg^{2+}-SO_4^{2-}$ vs $HCO_3^-$. 1:2 line would correspond to the stoichiometric ratio for calcite, dolomite and gypsum equilibrium reactions.

The dissolution and/or precipitation of calcite, and dissolution of dolomite and gypsum are consistent with the groundwater chemistry along flow paths on the eastern side of Salt Basin (from the Sacramento Mountains recharge area southeast to the area of Dell City and the Salt Flats).

In Mayer's (1995) analysis of the groundwater chemistry he shows that the majority of the well chemistry he compiled plots below the 1:2 line for ($Ca^{2+}$ + $Mg^{2+}$ - $SO_4^{2-}$ ) versus $HCO_3^-$. Mayer (1995) discusses how this indicates an additional sink for $Ca^{2+}$ and/or $Mg^{2+}$, and suggests the possibility of cation exchange with $Na^+$. To test his hypothesis Mayer (1995) compares molar concentrations of $Na^+$ - $Cl^-$ versus ($Ca^{2+}$ + $Mg^{2+}$ - $SO_4^{2-}$ - $HCO_3^-$/2). The quantity $Na^+$ - $Cl^-$ is sodium derived from sources other than halite dissolution, assuming all the chloride is derived from halite dissolution. The quantity ($Ca^{2+}$ + $Mg^{2+}$ - $SO_4^{2-}$ -$HCO_3^-$/2) is the $Ca^{2+}$ and $Mg^{2+}$ from sources other than carbonate and gypsum dissolution. Essentially he quantified the sodium and magnesium plus calcium available for exchange. Mayer (1995) shows that for his chemistry dataset this molar ratio defines a slope of -2 consistent with divalent cation exchange (i.e. $Mg^{2+}$ or $Ca^{2+}$) with $Na^+$ increasing at twice the rate. However, the majority of Mayer's dataset was from groundwater from Otero Mesa and Diablo Plateau (fig 4.2). As discussed in section 6.1 in these regions the groundwater chemistry observed is different than the groundwater chemistry along the eastern side of the Salt Basin. Specifically, there are much higher sodium concentrations in Otero Mesa/Diablo Plateau.

There is increasing in sodium concentration down the flow paths on the eastern side of the Salt Basin (fig 6.9). A plot of the molar ratio of $Na^+$ to $Cl^-$ (fig 6.27), assuming all chloride is the result of halite dissolution, would plot on a 1:1 line if only halite dissolution were taking place down the flow path. There does appear to be a source of sodium not associated with halite dissolution as the groundwater chemistry molar ratios plot above the 1:1 line. However, a plot of $Na^+$ - $Cl^-$ versus ($Ca^{2+}$ + $Mg^{2+}$ -

$SO_4^{2-}$ - $HCO_3^-$/2) shows no correlation for the groundwater chemistry, indicating that cation exchange is not is not responsible for the additional sodium.

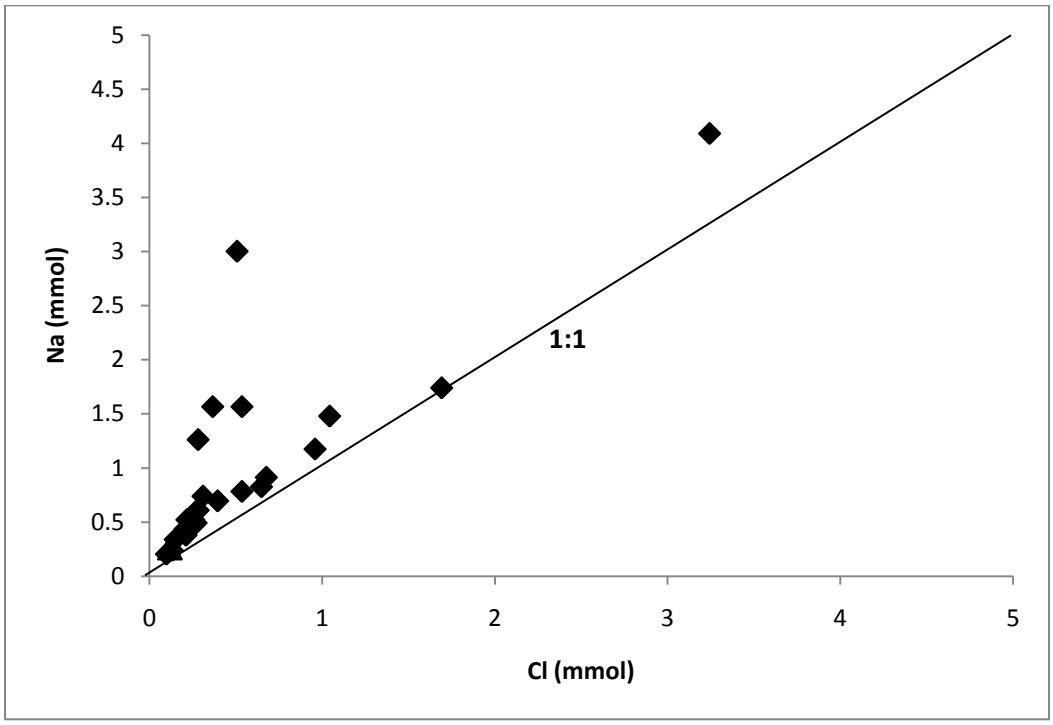


**Figure 6.25** Molar ratios of $Na^+$ vs $Cl^-$. 1:1 line corresponds to the stoichiometric ratio for halite dissolution.

Alternative sources of the sodium could be from dissolution of detrital, plagioclase feldspars (i.e. albite $NaAlSi_3O_8$) likely found within the clastic units of the San Andres and Yeso formations. Typically, the pure potassium endmember orthoclase ($KAlSi_3O_8$) forms in solid solution with albite (Chesterman, 1979) and may be responsible for the increase in potassium (fig 6.10) down the flow path. Dissolution of these feldspars would also explain the increase in silica content (fig 6.23) down the flow path. The silica contents from groundwater on the eastern side of the Salt Basin are

typical (5-14 mg/L) for limestone and dolomites with trace clays and quartz present (Langmuir, 1997).

Increases in minor constituents down the flow path on the eastern side of the Salt Basin indicate the presence of other trace minerals. A trace mineral possibly present in the aquifer system is fluorite ($CaF_2$) due to the increase in fluoride concentration (fig 6.22) down the flow path. Fluorite may be associated with calcite and is a common minor constituent in limestone (Chesterman, 1979). An increase in strontium concentration (6.24) is also observed down the flow path. Celestite ($SrSO_4$) is a likely source of strontium. Celestite is mostly found in sedimentary rocks associated with gypsum, anhydrite, and halite (Chesterman, 1979). Strontianite ($SrCO_3$) could also be present, which is a carbonate mineral with strontium (Langmuir, 1997).

**Section 6.2.b: Evidence for Dedolomitization**

The relative changes in ion chemistry of the groundwater provide information about water-rock interactions that have taken place as the water travels along flow paths, dissolving minerals in the rock. Classifying groundwater samples on a Piper diagram is one way of identifying regions of chemically similar water and defining the evolution in water chemistry along a flow system. Piper diagrams illustrate the distribution of relative concentrations of cations (positively charged ions) and anions (negatively charged ions). The relative abundance of cations with % meq/L of $Mg^{2+}$, $Ca^{2+}$ and $Na^{+} + K^{+}$ are assumed to be equal 100% and are plotted in the bottom left cation triangle. Similarly, the bottom right anion triangle displays the relative abundance of $Cl^{-}$, $SO_4^{2-}$, and $HCO_3^{-}+CO_3^{2-}$.

Straight lines projected from the lower two triangles into the upper diamond define the combined ion distribution.

The significant reaction minerals present in the Salt Basin carbonate aquifer system are calcite ($CaCO_3$), dolomite [$CaMg(CO_3)_2$], and anhydrite/gypsum ($CaSO_4$). This suggests the trends observed in the geochemical evolution illustrated by the Piper diagram (fig 6.28) are diagnostic of dedolomitization taking place. In the Sacramento Mountains the dominant groundwater type is calcium bicarbonate (Ca-$HCO_3$), typical of recharge through a carbonate aquifer system. As the water evolves south down the principal flow path, the ion chemistry shows increases in both magnesium (Mg) and sulfate ($SO_4$), while bicarbonate ($HCO_3$) slightly decreases. Back (1983) describes this process as the dominant control on the chemical evolution of waters in a similar aquifer system the Mississippian Pahasapa Limestone of the Madison aquifer (fig 6.29). His paper shows evidence for how the dedolomitization process can take place across a regional scale like the Salt Basin. Back (1983) summarizes the proposed mechanism for dedolomitization from the explanations of a number of authors. As meteoric water moves through an aquifer; calcite, dolomite, and anhydrite/gypsum go into dissolution at different rates based on their geochemical stability. When the system becomes saturated with calcite and dolomite, its evolution continues to be driven irreversibly by dissolution of gypsum, which causes additional dissolution of dolomite and incongruent precipitation of calcite. This causes increases in magnesium, and sulfate, while bicarbonate slightly decreases. This evolution is consistent with the trends observed in the Salt Basin. With the exception of Ellett well that also showed anomalous temperature (fig 6.4).

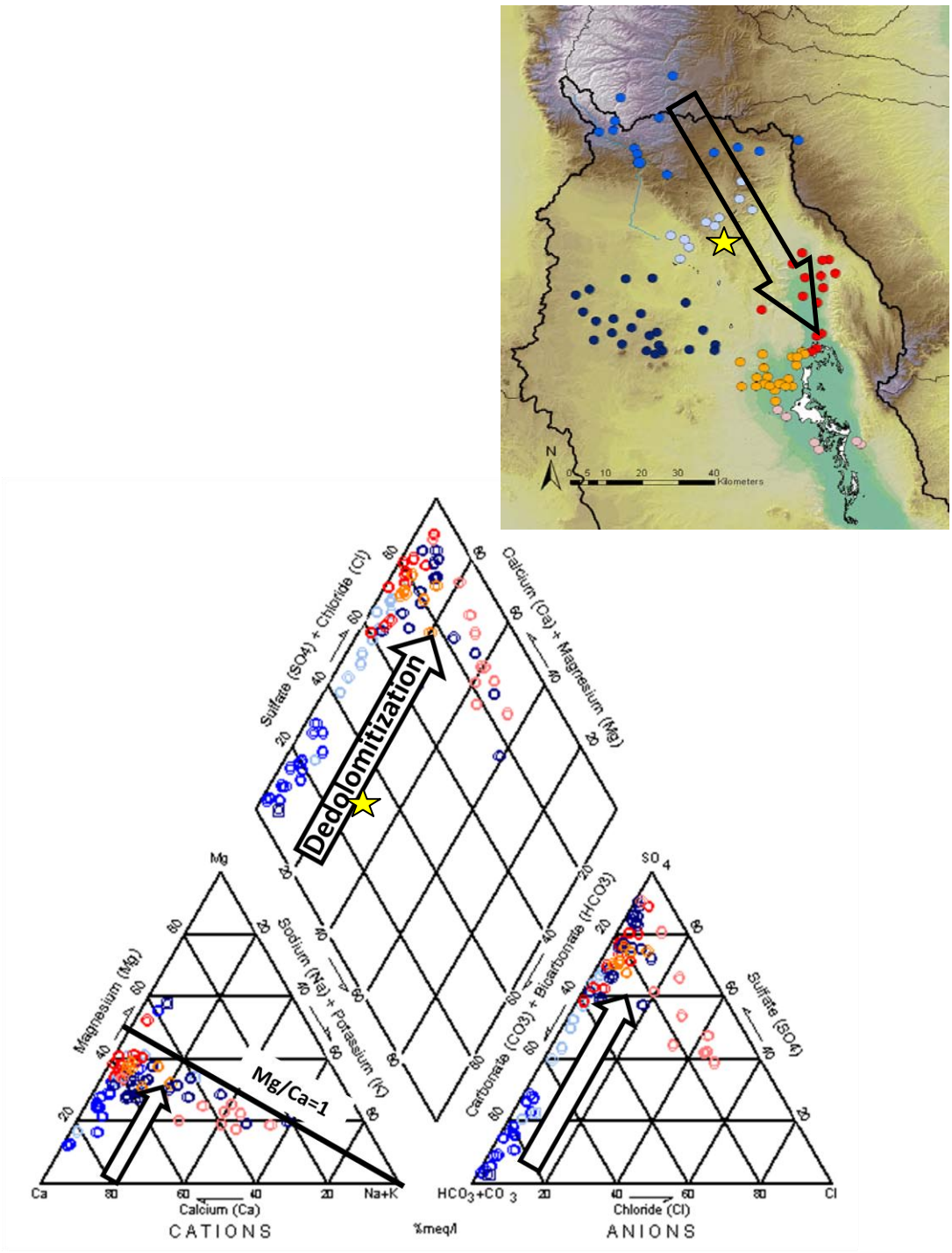


**Figure 6.26** Piper diagram of Salt Basin well chemistry. The sampled well waters plot on a linear trend indicating increasing magnesium and sulfate concentrations. The trend is indicative of dedolomitization as described in Back (1983). The star is an outlier to the trend (Ellett well)

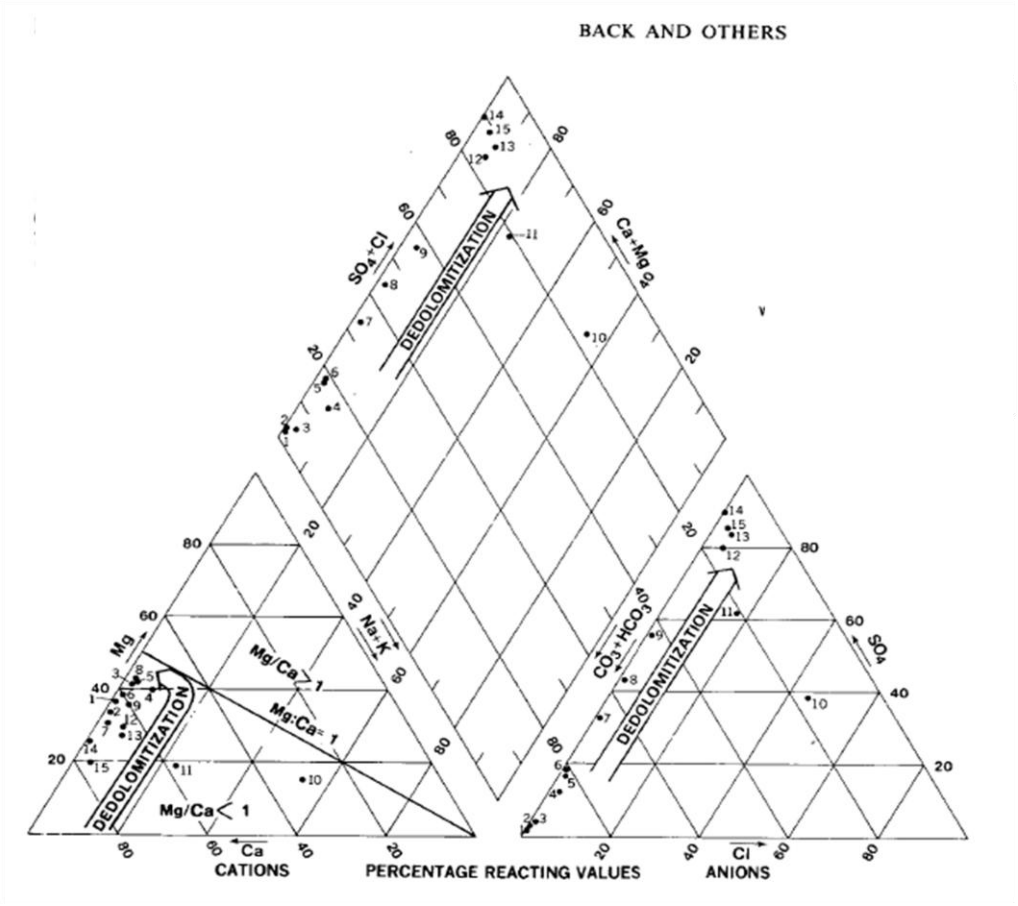


**Figure 6.27** Piper diagram groundwater chemistry of Pahasapa Limestone of the Madison Aquifer. The trend is indicative of dedolomitization as described in Back (1983).

## Section 6.2.c: Water Chemistry of the Otero Mesa

The water chemistry in Otero Mesa reflects significant increases in sulfate, as well as, sodium concentrations. This is evident from the position of the Otero Mesa water chemistry samples on the Piper diagram (fig 6.28) as well as in the maps of sodium (fig 6.12) and sulfate (fig 6.18) concentrations throughout the Salt Basin. The gypsiferous Yeso formation dominates in this region which likely explains the higher sulfate concentrations. In general this region is associated with more evaporitic deposits,

which also explains higher concentrations of chloride compared to other areas in the Salt Basin that are equidistant from the Salt Flats. The introduction of sodium to the groundwater system here may indicate dissolution of carbonate or gypsum minerals accompanying calcium or magnesium exchange with sodium; which was previously discussed (6.2.a). Alternatively, these waters are also in close proximity to the Cornudas Mountains which may mean the introduction of sodium is a result to syenite weathering processes.

**Section 6.2.d: Brine Evolution Effects**

The existence of the Salt Flats is a function of the Salt Basin being a closed un-drained basin. In this type of system, precipitation falling on the mountain front enters the groundwater through fractured rocks, talus slopes, or alluvial fan deposits. Valleys in the basin and range province are tectonic troughs that often lack a subsurface outlet; the water returns to the surface through playas, where it is discharged to the atmosphere by evapotranspiration. Runoff in this system will drain internally, with no outlet except the atmosphere (Duffy 1988). The locally depressed playas or salt flats tend to lie in chains on the east or west edges of the basin; probably originating as shallow or intermittent lakes that filled slight depressions in the valley floor. They often lie along fault trends. The level of the Salt Flats is generally lower than the surrounding ground level, with elevations around 1100 meters, which is about at the water table in the lower Salt Basin. Closed and undrained basins can be considered self-contained hydrologic systems, with water and energy exchange primarily with the atmosphere. These dynamics can result in forced convective flow that leads to a hydrodynamic connection between the groundwater and the atmosphere at the Salt Flats.

As the groundwater in the Salt Basin moves closer to the discharge area at the Salt Flats the effects of brine evolution are evident. When pore fluids are removed by evaporation from the Salt Flats the concentration of dissolved solids increases, such that certain minerals are removed from solution by precipitation and the remaining solution becomes enriched or depleted in one ion or another. The Eugster-Hardy model (1978) does a good job of explaining the Salt Basin brine evolution. Calcite, the least soluble mineral is the first to precipitate removing bicarbonate and carbonate from the water. Gypsum precipitates next, where initial molar ratios dictate sulfate build-up and calcium depletion. Ultimately, relatively dilute inflow waters evolve to water types dominated by chloride and sulfate for the anions, balanced by sodium and magnesium for the cations. This progression can be observed in the Piper diagram trends moving from the Dell City area to the Salt Flat groundwater samples (fig 6.28). The effects of brine evolution are also apparent in the map of chloride concentrations throughout the Salt Basin (fig 6.17). The Salt Flats produce evaporite deposits of gypsum and halite, as well as carbonate minerals such as calcite, dolomite, and magnesite (Boyd 1982). In the Dell City area groundwater is likely influenced by back flushing of salts from irrigation TDS concentrations reach 6500 mg/L (Mayer, 1995). At the Salt Flats where groundwater is discharging through evapotranspiration TDS concentration can be in excess of 250,000 mg/L (Boyd, 1982).

**Section 6.3: Geochemical Reactions and Mass Transfer**

The rock/water interactions that will dominate in the subsurface as the groundwater flows through the aquifer are controlled by the departure from chemical equilibrium conditions of the water with respect to the minerals present, as discussed in

chapter 5. Saturation indices for groundwater down the principal flow path analyzed for the Salt Basin were calculated using the USGS geochemical modeling program NETPATH. Interpretation of the values of saturation index for the important minerals in the system--calcite, dolomite, and gypsum--shows that the significant reactions are consistent with dedolomitization being the dominant control on the water chemistry (Back and Hanshaw, 1971). The saturation index for gypsum/anhydrite (fig 6.30) shows that water is significantly undersaturated in the Sacramento Mountain recharge area; while the saturation index increases progressively with increased distance along the flow path. The saturation indices indicate irreversible dissolution of gypsum/anhydrite; in as much as equilibrium conditions are never reached. The saturation index for dolomite (fig 6.31) indicates that the water in the recharge area is undersaturated, but, that with increasing dissolution of gypsum, the water reaches equilibrium or slightly above equilibrium. The water is close to, or above, equilibrium for calcite (fig 6.32).

If there was no gypsum/anhydrite present in the Salt Basin aquifer system, calcite and dolomite would dissolve to equilibrium. Given only these two phases, at low temperatures, calcite is more unstable than dolomite and would likely attain equilibrium faster. Under these conditions it would be expected that some of the calcite originally dissolved would precipitate when dolomite saturation is approached. However, because gypsum is dissolving the water reaches supersaturation with respect to calcite and dolomite, due to the calcium ions put into solution by the dissolution of gypsum ($CaSO_4$). This constant addition of calcium from the gypsum forces precipitation of calcite ($CaCO_3$) due to the common-ion effect (Back, 1983). When calcite precipitates it causes

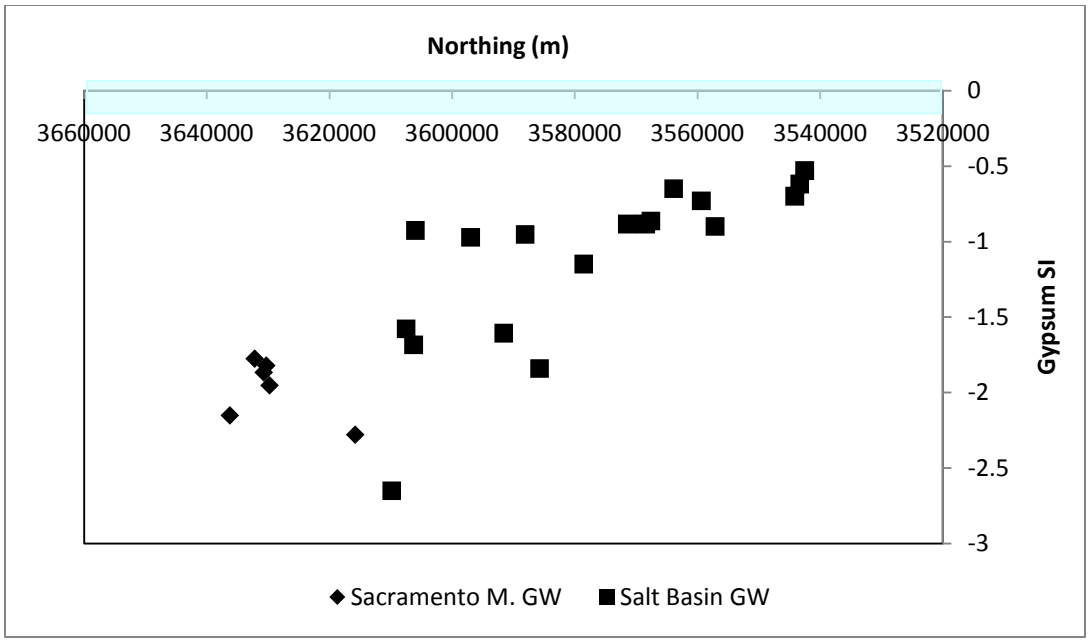


**Figure 6.28** Saturation index [log(IAP/KT)] for gypsum equilibria as a function of distance down flow path for Salt Basin well samples. Shaded blue indicates equilibrium.

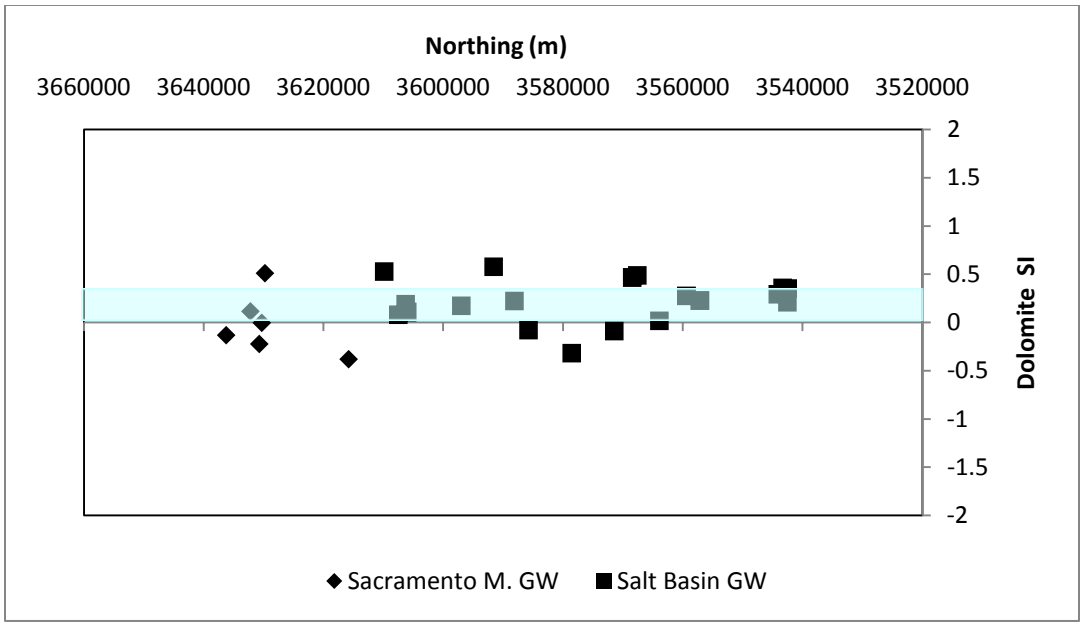


**Figure 6.29** Saturation index [log(IAP/KT)] of dolomite equilibria as a function of distance down flow path for Salt Basin well samples. Shaded blue indicates equilibrium.

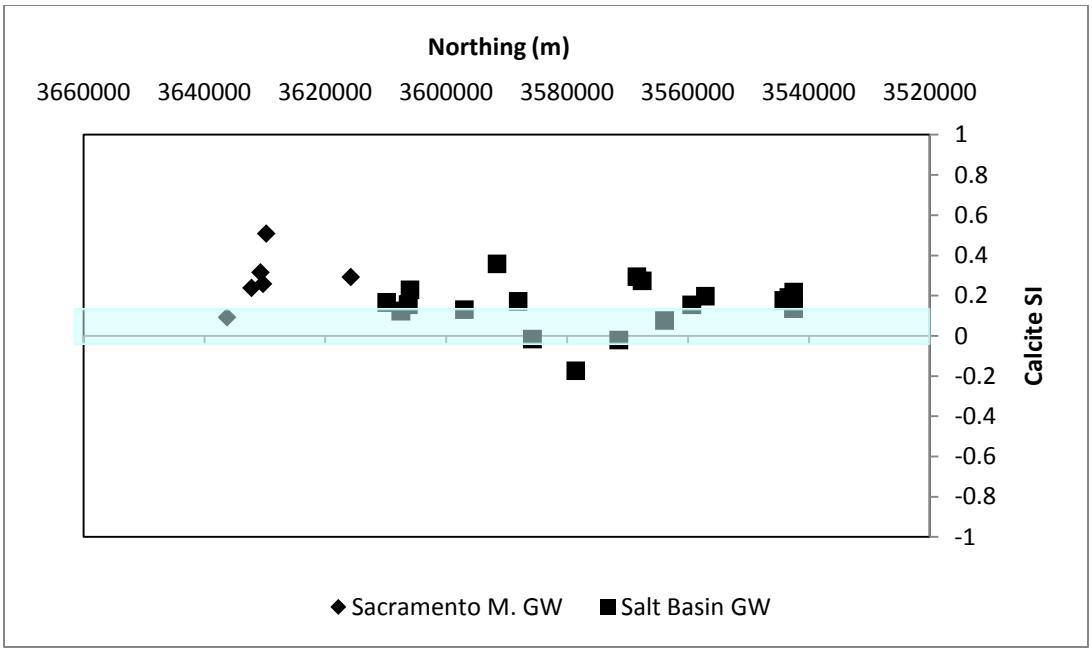


**Figure 6.30** Saturation index [log(IAP/KT)] of calcite equilibria as a function of distance down flow path for Salt Basin well samples. Shaded blue indicates equilibrium.

a shift to lower pH values by removing carbonate from the system which in turn causes dolomite [$CaMg(CO_3)_2$] to go into dissolution. The dolomite dissolution increases the dolomite saturation index toward equilibrium. The process of dedolomitization is critically driven by the dissolution of gypsum and will not proceed in low temperature environments without the presence of gypsum or some other source of additional calcium ions (Back, 1983). The resulting calcite is not only believed to replace dolomite to form dedolomite but may account for some vein calcites and secondary cements. Evidence of these types of secondary calcite features have been observed in the San Andres in studies both in Lincoln County, NM (Milner, 1973) and Eddy County, NM (Muir 1976); two neighboring counties to the Salt Basin. In both cases thin sections were found where calcite was identified to have precipitated into a dolomite matrix where gypsum

dissolution took place (fig 6.33). Although, it should be noted that overall the dedolomitization reaction results in net dissolution which may enhance permeability in the aquifer system.

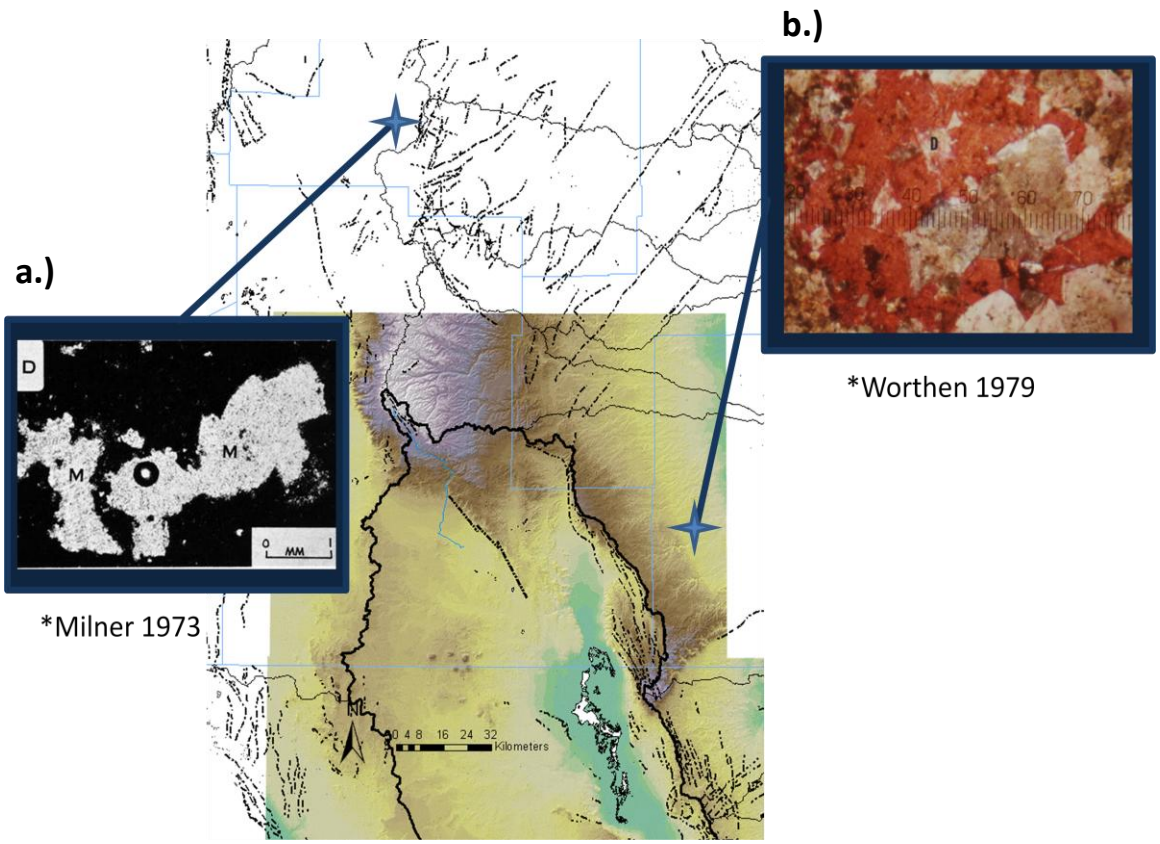


**Figure 6.31** Evidence for secondary calcite replacing gypsum in a dolomite matrix found in the San Andres unit near the Salt Basin. In example a.) the gypsum matrix is black and the white marked M is the secondary calcite. In example b.) the gypsum matrix is red and the small white mineralization marked D is the secondary calcite.

The dedolomitization reaction process is as follows:

(a) $2H_2O + 2CO_{2(gas)} \rightarrow 2H_2CO_3 \rightarrow 2H^+ + 2HCO_3^-$

(b) $2H^+ + 2HCO_3^- + CaSO_{4(gypsum)} + CaMg(CO_3)_{2(dolomite)} \rightarrow 2Ca^{2+} + SO_4^{2-} + Mg^{2+} + 4HCO_3^-$

(c) $2Ca^{2+} + SO_4^{2-} + Mg^{2+} + 4HCO_3^- \rightarrow SO_4^{2-} + Mg^{2+} + 2CaCO_{3(calcite)} + 2H^+ + 2HCO_3^-$

In the Madison aquifer this process was observed to coincide with an increase in $PCO_2$ as well as a decrease in pH (Plummer, 1991). However, in the Salt Basin system the $PCO_2$ (fig 6.34) and pH (fig 6.35) are relatively stable down the flow path.

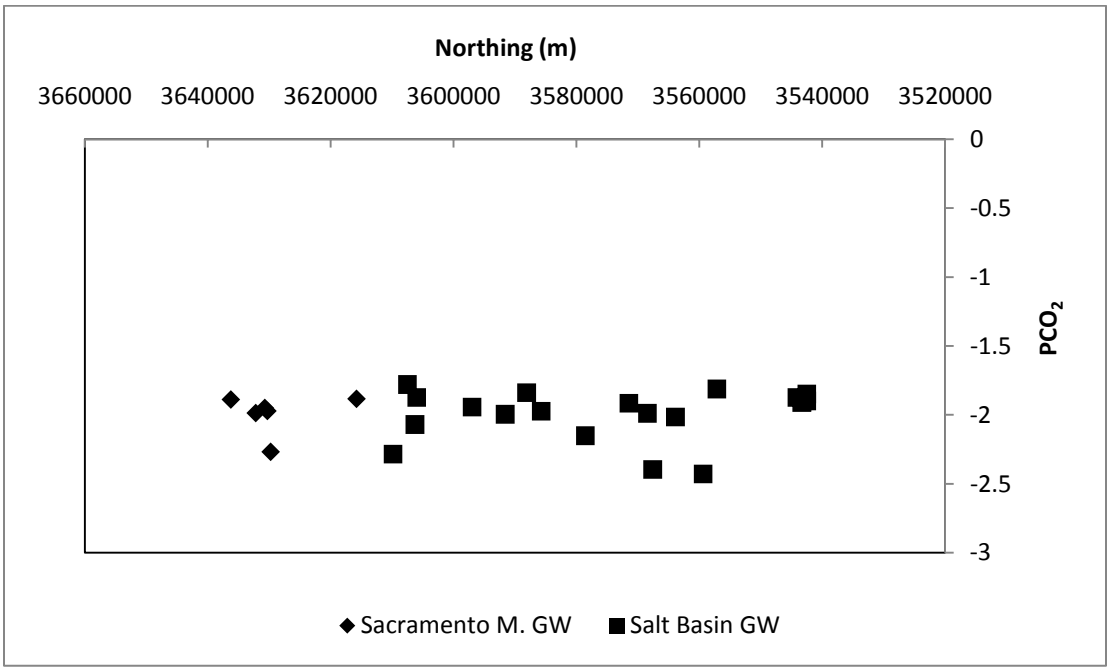


**Figure 6.32** Variation in log partial pressure of carbon dioxide as a function of distance down flow path measured from wells in the Salt Basin.

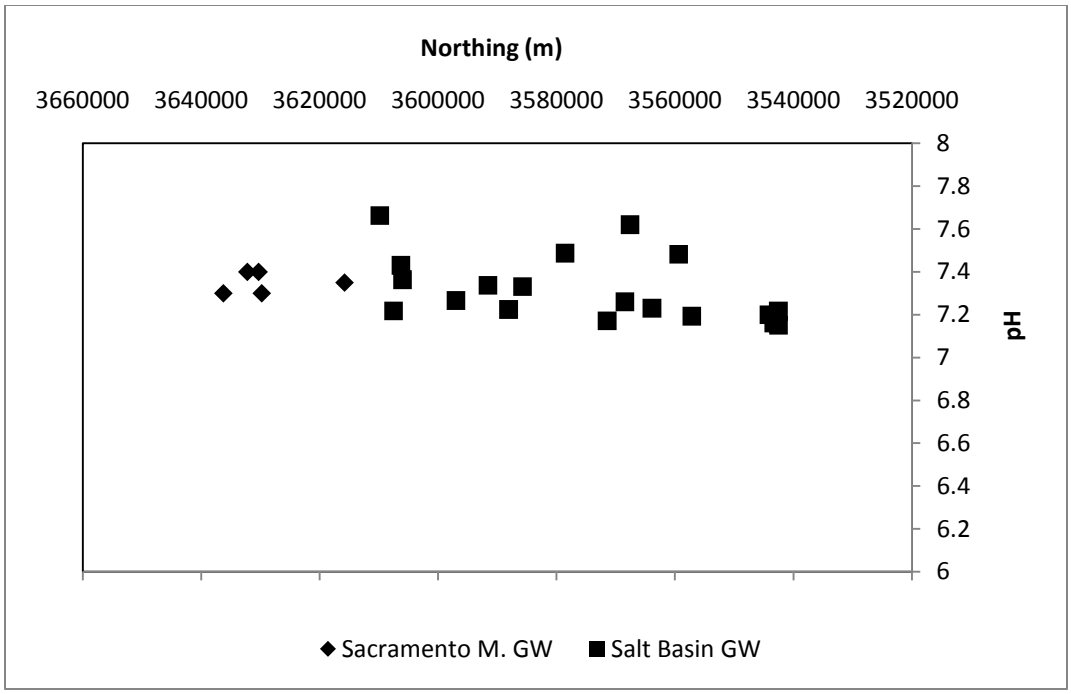


**Figure 6.33** Variation in pH as a function of distance down flow path measured from wells in the Salt Basin.

Another defining characteristic of the dedolomitization reaction process is the Mg/Ca ratio. Dolomite is near equilibrium at 25 °C in low temperature groundwater that is also in equilibrium with calcite and has Mg/Ca ratio equal to one (Hanshaw, 1971). When Mg/Ca ratios are greater than one, dolomite precipitates, and for ratios less than one dolomite goes into dissolution. The significance of this relationship is that it is the mechanism by which gypsum drives the dedolomitization. The dissolution of gypsum introduces the calcium to the system that keeps the Mg/Ca ratio lower than one. The groundwater in the Salt Basin remains consistently below a Ma/Ca ratio of one, as seen in figure 5.17. This coupled with the precipitation of calcite forces dolomite dissolution. If either gypsum dissolution stopped or calcite precipitation stopped the water would attain equilibrium with dolomite and dedolomitization would cease. Equilibrium conditions for

this system are best represented as a range (figures 6.30-6.32) because the temperature dependence of the saturation conditions of dolomite and calcite are not necessarily well constrained, especially in dynamic equilibrium conditions with each other.

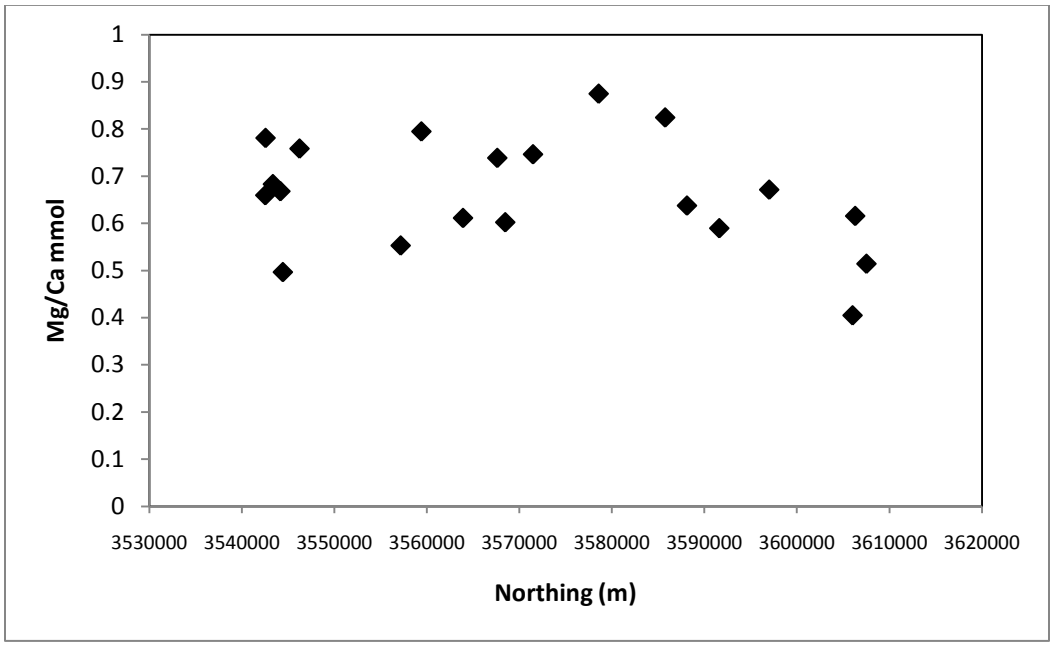


**Figure 6.34** Mg/Ca molar ratio along the groundwater flow path. The Mg/Cl ratio is a significant control for the dedolomitization process.

## Section 6.4: Chemical and Mineralogical Comparison using SaltNorm

SNORM is free USGS software that will calculate a salt norm from the chemical composition of natural water. The salt norm is the quantitative ideal equilibrium assemblage of minerals that would crystallize if the water were evaporated 100% at 25 °C and 1 bar pressure under atmosphere partial pressure of $CO_2$. It quantitatively distributes the program's 18 acceptable solutes into normative salts that are assigned from 63

possible normative salts to allow only stable associations based on the Gibbs Phase Rule, available free energy values, and observed low temperature associations (Bodine, 1986).

SNORM characterization of groundwater samples from the Salt Basin will be used in a comparison between the geochemical evolutions of waters analyzed for the Madison aquifer, as a test for the importance of dedolomitization as a water chemistry control. Different areas within the Salt Basin have distinct water chemistry characteristics that are associated with the groundwater. The water chemistry characteristics of each region are a function of both its evolutionary point along a flow path and rock/water interactions controlled by the lithology. Each unique area might even be considered a hydro-chemical facies. Like a geologic facies it is a distinct unit which forms under certain conditions of sedimentation which reflect a particular process or environment. To illustrate these hydrologic facies spatially within the two basins, water chemistry data was analyzed using Salt Norm. The normative salt compositions were averaged for each region giving distinct distributions based on mineral percent.

In the Salt Basin the normative salt distribution (fig 6.37) for the Sacramento Mountains and Piñon area is largely calcite ($CaCO_3$) , dolomite [$CaMg(CO_3)_2$] , and gypsum/anhydrite ($CaSO_4$). This composition is controlled primarily by $CO_2$-carbonate mineral reactions with some gypsum/anhydrite dissolution as precipitation recharges through the San Andres and/or Yeso formations. As the groundwater flows south through Cornucopia Draw the normative distribution of dolomite increases, while calcite disappears. The appearance of magnesite ($MgCO_3$), like the increase in dolomite, is a reflection of the increase in magnesium as the water evolves. The Crow Flats have water

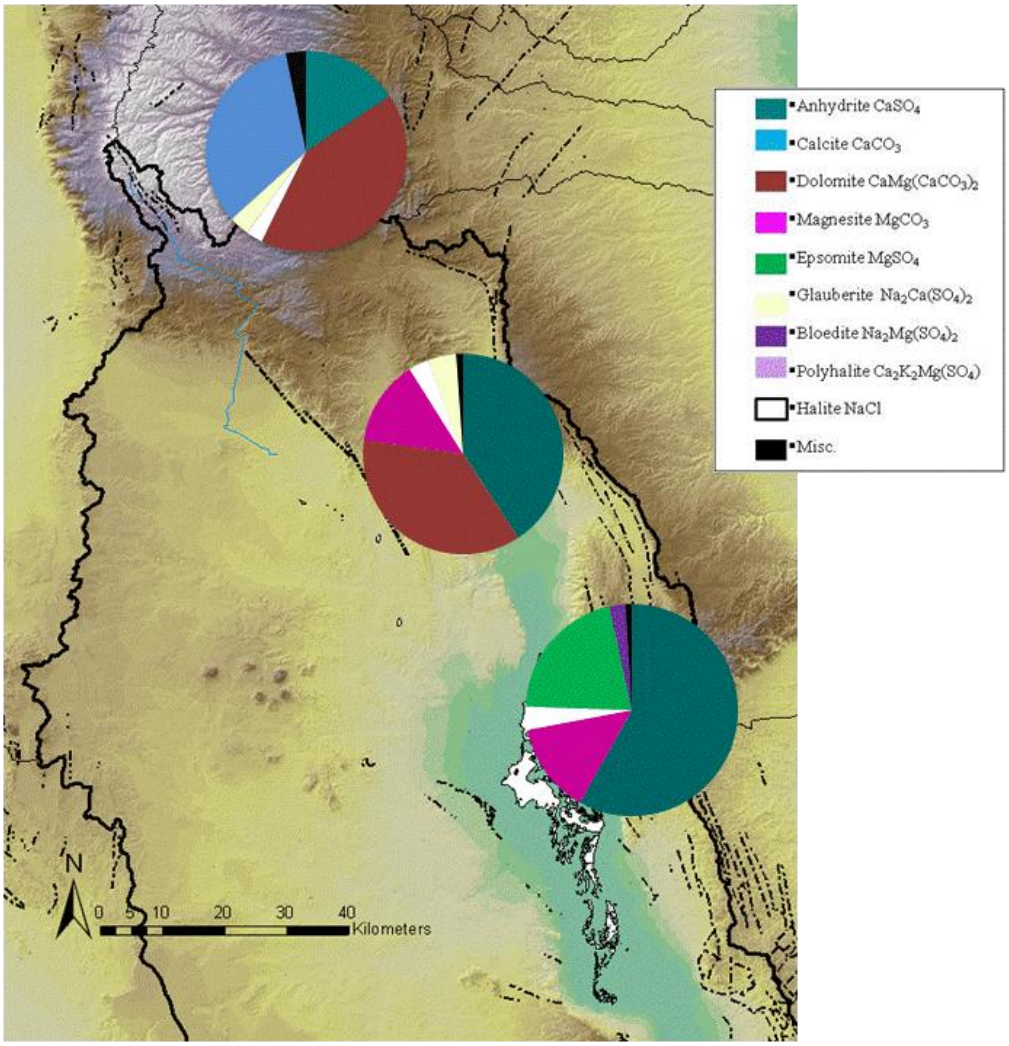


**Figure 6.35** Salt Norm % mineral compositions and their spatial distribution in the Salt Basin. It is a quantitative mineralogic comparison of natural waters. Progression of the mineral compositions down the flow path is consistent with $Ca>Mg:HCO_3$ to $Ca>Mg:SO_4>HCO_3$ to $Na>Ca>Mg:Cl>SO_4>HCO_3$ which describes the dedolomitization reaction path.

chemistry consistent with relatively mature waters in which dissolution of gypsum/anhydrite dominates over dissolution of the carbonate minerals. Dolomite is no longer present in the normative salt distribution, leaving magnesite as the only carbonate-

containing mineral. The percentage of gypsum/anhydrite significantly increases, and the mineral epsomite ($MgSO_4$) appears for the first time in the distribution. For these waters, salts with sulfate present in the mineral compositions make up at least 80% of the total distribution.

The major minerals in the Madison Limestone are calcite, dolomite, and gypsum/anhydrite, like the Salt Basin. The equilibrium speciation calculations for the saturation indices of these minerals (Plummer, 1991) are comparable to those of the Salt Basin. In Plummer's 1991 report of the hydrology of the Madison Limestone he discusses these thermodynamic controls on the trends in the water chemistry that result from the dedolomitization reaction as discussed by Back and others (1983). The full dedolomitization reaction path is described as progressing from predominantly $Ca>Mg:HCO_3$ to $Ca>Mg:SO_4>HCO_3$ to $Na>Ca>Mg:Cl>SO_4>HCO_3$ waters. This evolution is consistent with that of the Salt Basin which is clearly illustrated by comparing the chemical evolution between the two aquifers by the Piper diagrams. The dedolomitization reaction process is also observed in the progression of the mineral compositions calculated using Salt Norm down the Salt Basin flow path as well as that of the Madison Aquifer. Each mineral distribution in the Salt Basin marks a distinct point in the chemical evolution that corresponds to a matching point in the chemical evolution in the Madison Limestone.

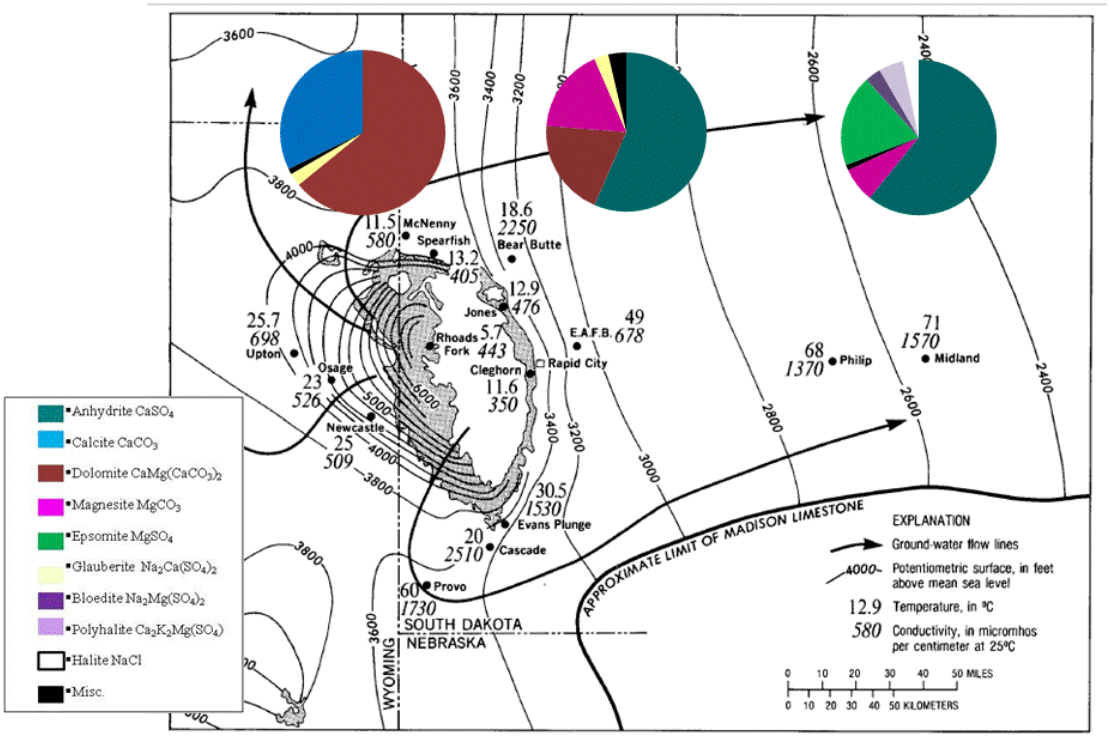


**Figure 6.36** Salt Norm % mineral compositions and their spatial distribution in the Madison Aquifer. Dedolomitization is the dominant control on the geochemical evolution in the Madison Aquifer.

## Section 6.5: Salt Basin Solute Controls by Faults and Structural Features

The Salt Basin is a block-faulted graben, where the central part of the basin is at lower elevation than the surrounding mesas, plateaus, and mountains. The Sacramento Mountains are generally considered the dominant source of recharge for the Salt Basin (Mayer, 1995; Huff, 2006; Sharp, 1995). This means that like many semiarid basins, the most significant contribution to recharge to the basin aquifer is flux across the mountain-front block (Wilson, 2004). Generally, the Sacramento Mountain fault block marks the northern boundary of the Salt Basin groundwater system. Mayer (1995) has discussed how a 300 foot scarp at the boundary of the Otero Mesa and the Tularosa Valley forms a

major surface-water divide and the western margin of the groundwater flow system. He interpreted the eastern boundary of the basin fixed at the graben of the Salt Basin which is juxtaposition between the low-permeability basin fill and highly, fractured carbonates. In Mayer's PhD dissertation (1995) he presents data in support of faulting and fracturing within the structure of the Salt Basin playing a significant role in the control of groundwater movement. In between the Otero Mesa and the Salt Basin graben lies a prominent faulted and fractured south-west facing scarp, known as the Otero Break (Goetz, 1985; Black, 1975). This feature is characterized by a series of west-dipping normal faults that are an extension of the Sacramento Mountains. Otero Break gradually disappears to the southeast. This feature is the result of two stages of deformation: first right-lateral shear and extension during the Paleozoic along northwest-oriented fault zones and second west- oriented extension, beginning during the Neogene (Goetz, 1985). Within the flow system, the groundwater flows preferentially to the southeast, parallel to the high-permeability fracture zone (Mayer, 1995). Groundwater chemistry throughout the basin has been used to identify a broad zone of relatively fresh water (based on TDS) extending from the Sacramento Mountains southeast down to the Salt Flats near Dell City, TX (Mayer, 1995). This trend is present along the Otero Break fracture, which Mayer attributes to large-scale channeling of Sacramento Mountain recharge along faulted and fractured conduits.

Based on the water chemistry evolution defined by the dedolomitization reaction process, there are specific ions present in the groundwater that can be used as a proxy for residence time in the groundwater system. The increase in aqueous magnesium and sulfate in the groundwater is a time-dependent process related to the dissolution of

dolomite and gypsum as the water travels through the aquifer system. Contour plots of the concentrations of these two ions (figures 6.39 and 6.40) illustrate how the groundwater chemistry in the Salt Basin varies systematically in space. These trends identify other structural controls on the movement of the groundwater in the Salt Basin system in addition to the major channeling along the Otero Break.

Structural features that appear to control the movement of groundwater are generally characterized as either a barrier to flow or zones of enhanced permeability. The prominent features that correlate with solute movement in the Salt Basin are the Stevenson fault in the north, the Otero fault and Diablo Plateau in the west, and the Dog Canyon fault zone to the east (fig 2.3). The Otero Break controls the groundwater flow in the center of the basin. Considering that the Stevenon fault is the possible westward extension of the Guadalupe fault zone, it is consistent with the water chemistry that this fault acts as a barrier to flow from the north into the Salt Basin; just as the Guadalupe fault zone marks an eastern boundary for the groundwater system. The Stevenson fault is characterized by high-angle, down-to-the-south normal faulting, as previously cited. This may be responsible for low permeability behavior or act as a short circuit to the flow system as aquifer units may be displaced. At the southern extent of the Guadalupe fault zone, along the Algerita Escarpment of the Guadalupe Mountains is the Dog Canyon fault zone. This corresponds to a region of what appears to be relatively freshwater input to the Salt Basin from the Guadalupe Mountains. It is difficult to say whether this corresponds to groundwater influx from the regional flow system of the Guadalupe Mountains or as surface water infiltration through the Dog Canyon drainage network.

During the Permian, down-to-the-northeast faulting occurred along several northwest trends, one of which is the Otero fault. This feature corresponds to a broad zone of high concentration of the chemical tracers with relatively freshwater channeling along either side. There are two likely scenarios to explain the solute distribution resulting from that of the Otero fault zone. One is enhanced permeability along the western and eastern margins of the fault zone channeling water around what would have to be a relatively low permeability zone in the center caused by the inherent trends in the nature of the displacement (Caine, 1996). Alternatively, Nutt (1997) discusses how this region corresponds to the western edge of the buried Pedernal uplift. This is associated with significant thinning of the Yeso aquifer unit above the buried uplift, where water may preferentially channel around this feature. Solute distributions also show an influx of relatively fresh water moving northeast to the Salt Flats in Texas across the aquifer system of the Diablo Plateau. This is consistent with Krietler and others (1990). This water encounters the Babb flexure where increased permeability could be related to Leonardian reefs that ring the fault deformation, as previously cited.

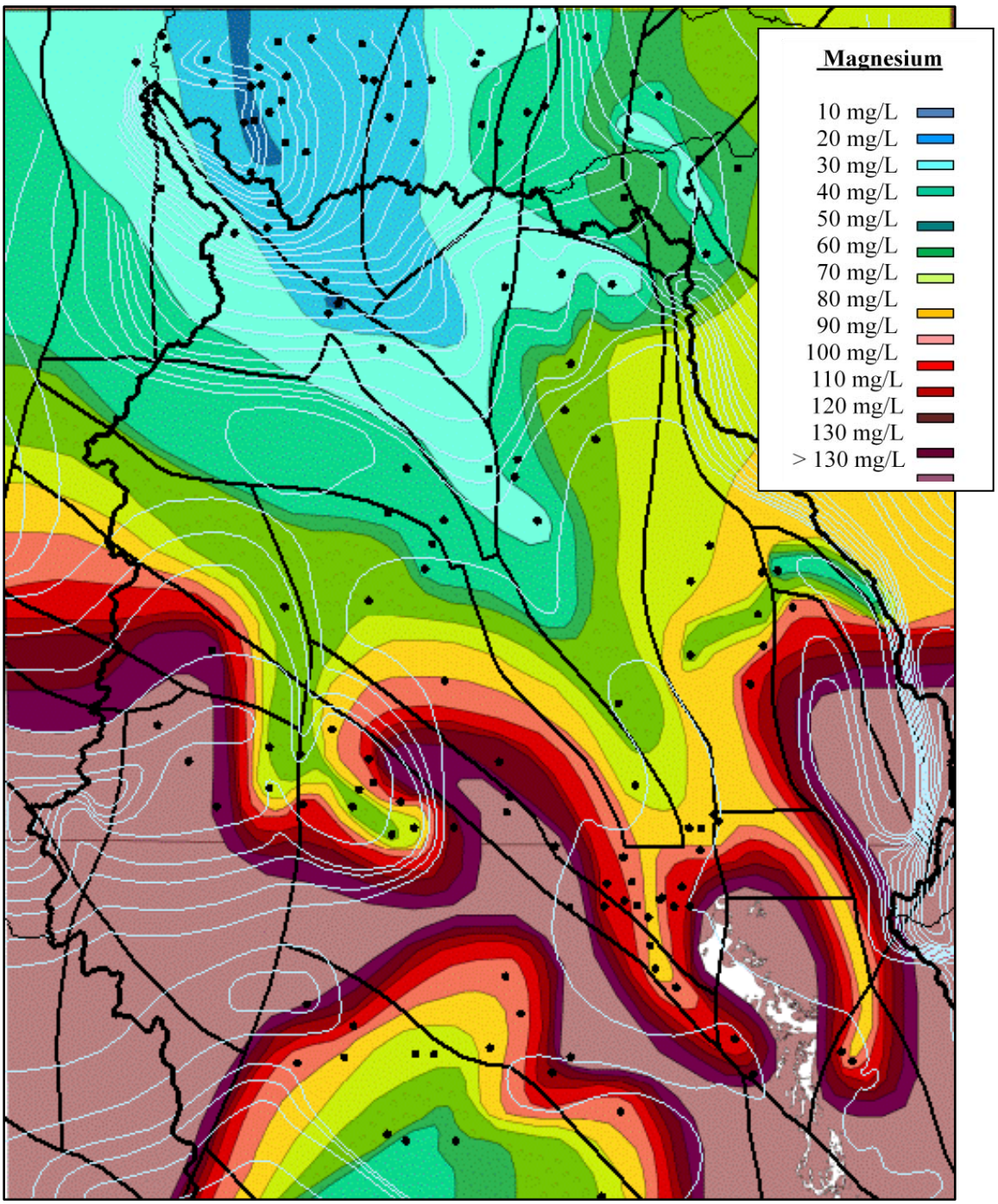


**Figure 6.37** Association of magnesium (Mg) concentration and major faults and structural zones in the Salt Basin. Geochemical evolution demonstrates that increase in magnesium can be related to increased residence time in the aquifer system. Black dots represent control points for the solute contours (Mayer, 1995 and NMBG). Pale blue line are groundwater contours, refer to figure 3.2 (Ritchie, 2010). To identify structural features and faults refer to figure 2.3 (Richie, 2010).

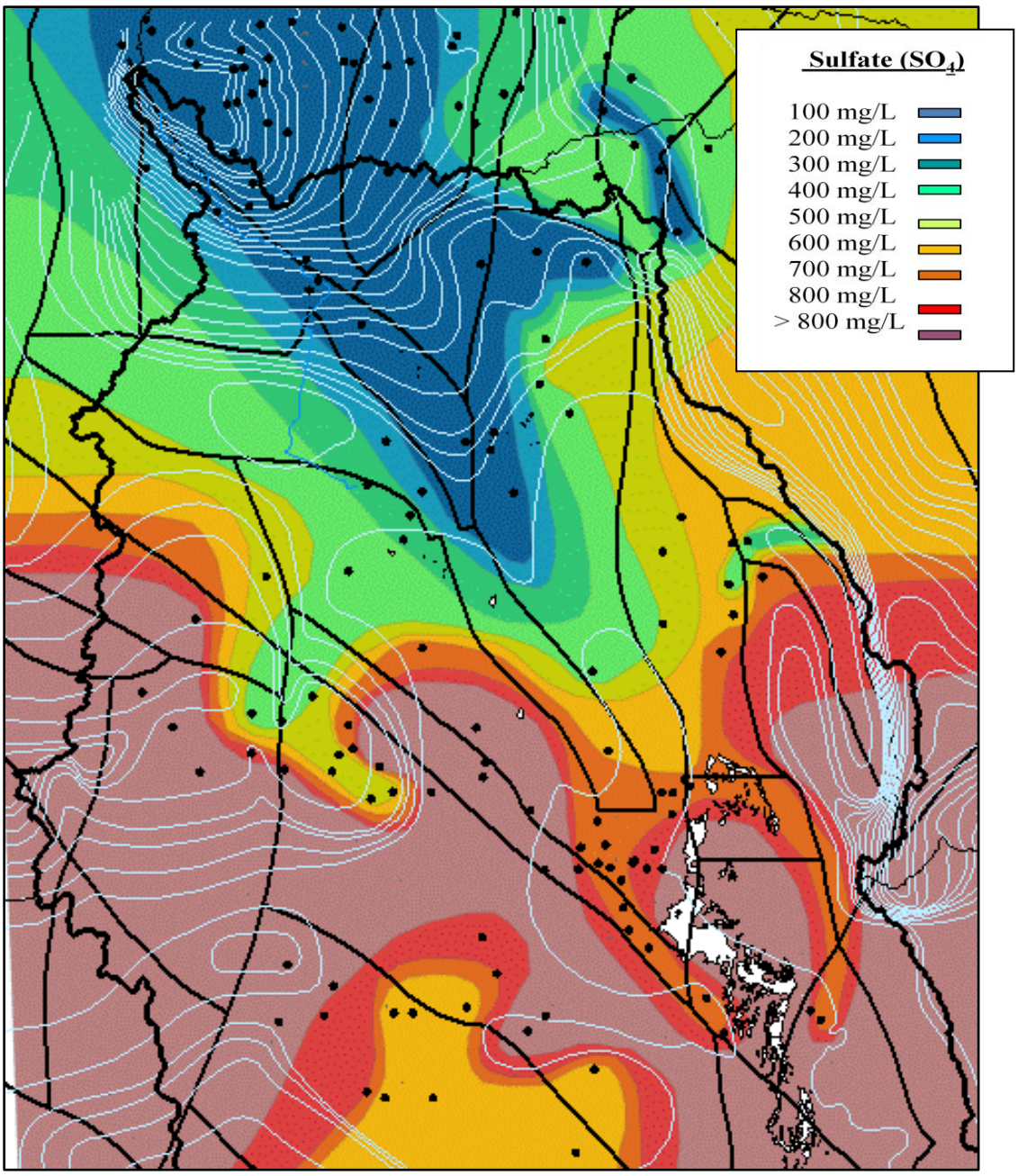


**Figure 6.38** Association of sulfate ($SO_4$) concentration and major faults and structural zones in the Salt Basin. Geochemical evolution demonstrates that increase in sulfate can be related to increased residence time in the aquifer system. Black dots represent control points for the solute contours (Mayer, 1995 and NMBG). Pale blue line are groundwater contours, refer to figure 3.2 (Ritchie, 2010). To identify structural features and faults refer to figure 2.3 (Richie, 2010).

# CHAPTER VII

# STABLE ISOTOPES AND THEIR IMPLICATIONS FOR RECHARGE

## Section 7.1: Recharge Environment

Stable isotope ratios of oxygen ($\delta^{18}O$) and hydrogen ($\delta D$) are useful environmental tracers that can act as a fingerprint for sources of recharge to a groundwater system. As discussed in chapter 5.2, the isotopic composition of precipitation depends on certain conditions of the recharge environment: surface air temperature, relative humidity in the atmosphere, amount of precipitation, latitude, distance from the coast, and elevation of a given area above sea level (5.2.c). For the Salt Basin, this means that precipitation will have different isotopic signatures depending on whether it falls during the summer or winter, and where it takes place in the basin. The mechanism for recharge will also affect the isotopic signature of the groundwater (5.2.d). Understanding these relationships can distinguish between recharge from the Sacramento Mountains, the Guadalupe Mountains, and lowlands in the Salt Basin based on their recharge environment.

The Sacramento Mountains rise to elevations of 2,500 to 2,900 m with average precipitation of about 27 cm/yr. Based on a recent study of the hydrogeology of the Sacramento Mountains by the New Mexico Bureau of Geology, the recharge environment is described as follows (Rawling, 2009). The Sacramento Mountains receive the majority of their rainfall during the monsoon season from May to October.

This rainfall pattern is a result of orographic effects and the higher temperatures associated with these seasons. The precipitation is generated from the forced vertical movement of moist air up the orographic slope caused by the daytime heating of the mountain surface. The air parcels cool and expand as they are lifted, resulting in condensation and potentially precipitation. Winter storms are frontal storms that originate in the eastern Pacific and lose most of their moisture as they travel across the mountains of California and Arizona. Recharge in average precipitation years is largely from snow melt that has infiltrated into the stream/spring system and subsequently undergone evaporation in stream channels and spring-fed wetlands before infiltrating into the groundwater system. There is an additional source of recharge from extreme storm events during some monsoon seasons that contributes to the aquifer system through short, transient flow paths, such as fractures systems, that are not significantly affected by evaporation. The recharge from the Sacramento Mountains enters the Salt Basin aquifer, primarily, as a subsurface flux across the mountain-front-block.

The Guadalupe Mountains are lower in elevation than the Sacramento Mountains. The Guadalupe Mountains border the east side of the Salt Basin with elevations of about 1,400 to 2,600 m with average precipitation of about 19 cm/yr. The mechanisms for recharge from the Sacramento Mountains into the Salt Basin are different than those of the Guadalupe Mountains. Most studies of the groundwater system in the Guadalupe Mountains have concluded that the regional flow is to the east. The mountain front faults adjacent to the Salt Basin graben are generally considered to be barriers to subsurface flow. This means the precipitation entering the Salt Basin from the Guadalupe Mountains will be diffuse near-surface flow that is transmitted along the steep slope via

ephemeral drainage networks such as arroyos; or as subsurface interflow from small catchments along the mountain front.

The elevation of the Salt Basin graben is about 1,100 m with average precipitation of about 10 cm/yr. The little moisture the lowlands do receive is primarily during summer monsoon showers. However, it is likely most of this precipitation is lost to evaporation as spring and summer are characterized by extremely high temperatures, often above 37 °C (100 °F), and severe dust storms. If there was recharge, a significantly evaporated signal would be expected in the groundwater; with the exception of fast-transport infiltration during flood events.

## Section 7.2: Distribution of $\delta D$ and $\delta^{18}O$ in the Salt Basin Groundwater System

Because precipitation is the fundamental source for groundwater, the interpretation of stable isotope data is often performed using a $\delta D$ versus $\delta^{18}O$ plot with the Meteoric Water Line (MWL) as the reference line; This is discussed in chapter 5.3.b. For this study of the Salt Basin it is more informative to use a Local Meteoric Water Line (LMWL), where the slope and y-intercept may vary slightly from the GMWL due to local climatic conditions. In the Sacramento Mountains the LMWL (fig 7.1) is defined by $\delta D = 8.38*\delta^{18}O + 22.77$, based on local precipitation collected regularly since 2006 by the New Mexico Bureau of Geology (Rawling, 2009). The New Mexico Bureau of Geology estimated an evaporation line (5.2.c) for the Sacramento Mountains as $\delta D = 5.47*\delta^{18}O + 12.03$ (fig 7.1), based on surface-water compositions measured from streams and wetlands in the area (Rawling, 2009).

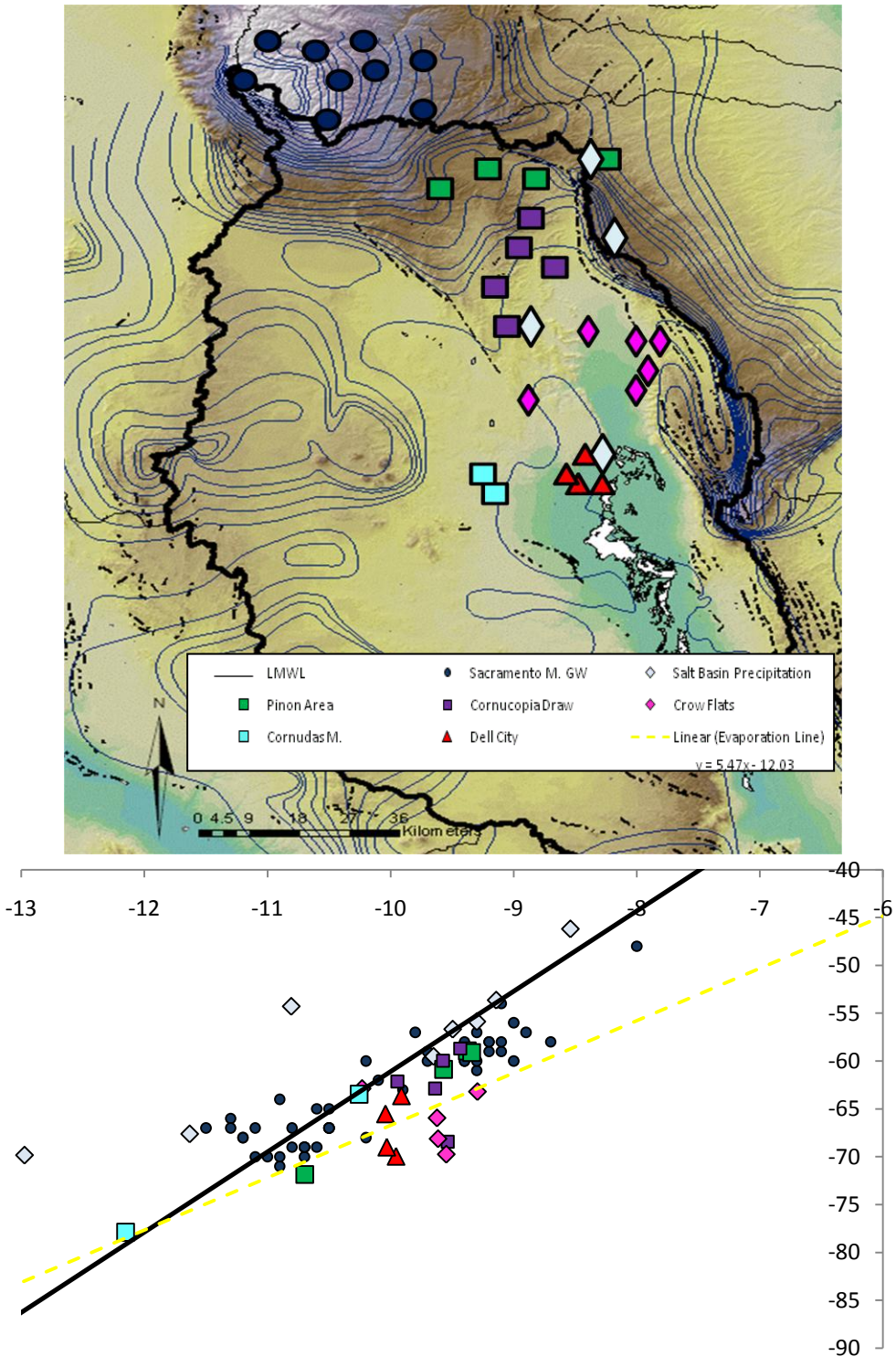


**Figure 7.1** Stable isotopes of oxygen and deuterium from groundwater and precipitation (light blue diamonds) and their distribution throughout the Salt

Typically, winter precipitation is depleted in δD and $\delta^{18}O$ relative to summer rains (5.2.c). This trend is observed in the isotopic composition of precipitation collected in the Sacramento Mountains (Rawling, 2009). However, for many groundwater systems the meteoric δD- $\delta^{18}O$ signature transferred during recharge tends to be an average over the summer and winter isotopic signatures. As rainwater infiltrates into the unsaturated zone, movement and mixing through convoluted paths leads to a smoothing out of the seasonal variations. This is thought to particularly apply to karstic and fractured limestones environments like the Salt Basin. In these types of systems it has been observed that infiltrating water, traversing a 10-15 m thick unsaturated zone retains less than 5% of seasonal variation (Yonge, 1985). This is consistent with groundwater measured for the Sacramento Mountains which generally plots between the seasonal extremes. Most of the Sacramento Mountains groundwater also plots between the LMWL and the evaporation line (fig 7.1, blue circles). This suggests that the mixing process during infiltration also tends to smooth out differences in the signature between waters infiltrating through streams and springs that have an evaporative signature, and fast transport infiltration waters that have not undergone evaporation (Rawling, 2008).

For this study precipitation was collected from four points within the Salt Basin including the Pinon area, the rim of the Guadalupe Mountains, Cornucopia Draw, and near Dell City (fig 7.1, light blue diamonds). The precipitation collected in August is consistent with the isotopic composition of summer precipitation for the Sacramento Mountains and plots between -65 and -55 per mil for δD and -9 and -10 per mil $\delta^{18}O$. The precipitation collected in October show highly variable compositions and all plot left of the LMWL.

Groundwater samples collected along the general flow paths on the eastern side of the Salt Basin system were also analyzed for stable isotope composition. Those in the Piñon area (fig 7.1, green squares), extending down through Cornucopia Draw (fig 7.1, purple squares), plot along with groundwater samples from the Sacramento Mountains. That is between the LMWL and the evaporation line, indicating a mixing process between evaporated and non-evaporated recharge. There are two exceptions in these regions that appear depleted with respect to the others; one from the Piñon area (Webb H. well), and one from Cornucopia Draw (Runyan). The well depth of the Cornucopia Draw sample is quite deep; as it was originally drilled as an oil well. The deeper well may penetrate a deeper long flow path, or maybe a different geologic facies which might explain the discrepancy. There is no well depth information for the Piñon area sample, which makes it more difficult to interpret.

The majority of groundwater samples collected from Crow Flats down to the Dell City area appear isotopically depleted compared to the other waters of the Salt Basin. These waters plot below the evaporation trend for the Sacramento Mountains. If the slope of the evaporation trend has remained constant through time, the original composition of the precipitation (i.e. the intercept with the LMWL) would be significantly depleted compared to that of modern groundwater in the Sacramento Mountains. Two possible scenarios explain the observed depletion in these, as well as the exceptions in the more northern Salt Basin groundwater samples. One is that mountain-front recharge from the Guadalupe Mountains might have entered the southern extent of the basin during extreme winter precipitation events, where surface runoff is transmitted along arroyos and alluvial fans into the Salt Basin at the Crow Flats. In the

case of the northern exceptions, winter floods might have entered through drainage networks extending from the southern Sacramento Mountains. The other explanation is that residence times in the Salt Basin are long, and that some groundwater in the basin may have recharged under a very different climatic environment.

Two other anomalous stable isotope compositions come from the groundwater samples collected in the more western part of the basin, in the vicinity of the Cornudas Mountains. These samples plot directly on the LMWL; but one is significantly depleted compared to the other. This is interesting particularly because of how close (less than a mile) the two wells were to each other. This might seem like an indication that modern recharge is present because of their positions relative to the LMWL and the variability between them. However, this does not seem consistent with the percent modern carbon measured for these wells which was below 14 pmc (table 5.1), generally indicating these are very old waters (5.4). They also lie within the very high concentration regions for magnesium and sulfate which also indicates long older more evolved water (figure 6.39 and 6.40).

**Section 7.3: Implications for Recharge from the Guadalupe Mountains**

Surface runoff from the Guadalupe Mountains during extreme storm events could contribute significant amounts of isotopically light water which would explain the depletion in Crow Flats and Dell City isotope compositions. The factors that would cause this depletion would be related to what is different about this source of recharge compared to that of the Sacramento Mountains. Most importantly, in the case of Guadalupe Mountain recharge, only extreme storm events are being considered

significant sources; in which case the infiltration would be depleted primarily due to the "amount effect" (5.2.c). Additionally, if the storm event was from winter precipitation it would originate over the Pacific Ocean as opposed to monsoon storms which come from the Gulf Coast. This would further deplete the isotopic signature due to the "continental effect" (5.2.c). More intense rainfall events will also be associated with faster infiltration with less evaporation effects also resulting in more depleted the isotopic signature (5.2.b).

The introduction of water with this type of signature along the Guadalupe Mountains bordering Crow Flats could explain the depletion observed in the lower Salt Basin groundwater. Fresh water introduced from the Guadalupe Mountains along the Dog Canyon Fault zone is also consistent with solute distributions for magnesium and sulfate that were used as proxies for residence time. A similar type of recharge might also explain the depletion in the Piñon area well. However, this scenario is less consistent with the depletion observed in the deep (~1000 m) well in Cornucopia Draw.

**Section 7.4: Implications for Paleo-Recharge**

There are a couple of aspects of the groundwater chemistry in the Crow Flats and Dell City region that are not completely consistent with the hypothesis of Guadalupe Mountain recharge during extreme storm events as a significant source to the groundwater. One apparent contradiction to new water recharging into this area is the low tritium levels observed in the groundwater (fig 7.2). Tritium as an environmental tracer is discussed in chapter 5.3. The tritium levels in the Sacramento Mountains range from 2.97 to 10.4 TU (Rawling, 2009). These are consistent with of post-bomb recharge, indicating the groundwater is typically less than 50 years old. The relationship between

tritium concentrations and carbon-14 pmc (fig 7.3) is also consistent with the higher tritium concentrations in the Sacramento Mountains being modernly recharged water whereas the low tritium concentrations have pmc associated with older water. Carbon-14 and groundwater ages are discussed in chapter 5.4.

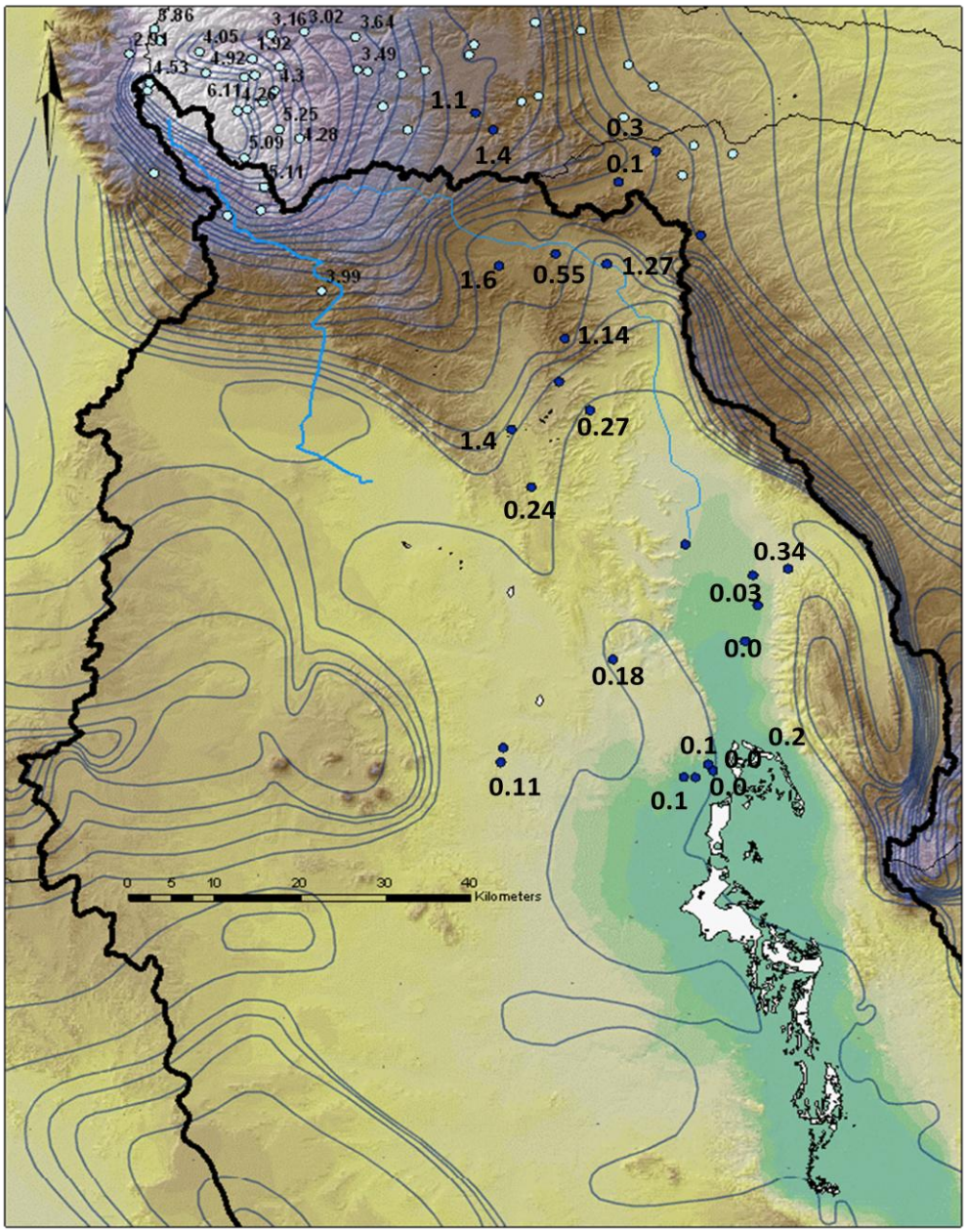


**Figure 7.2** Tritum (TU) distribution throughout the Salt Basin. Light green are from the Sacramento Mountains, blue are from the Salt Basin.

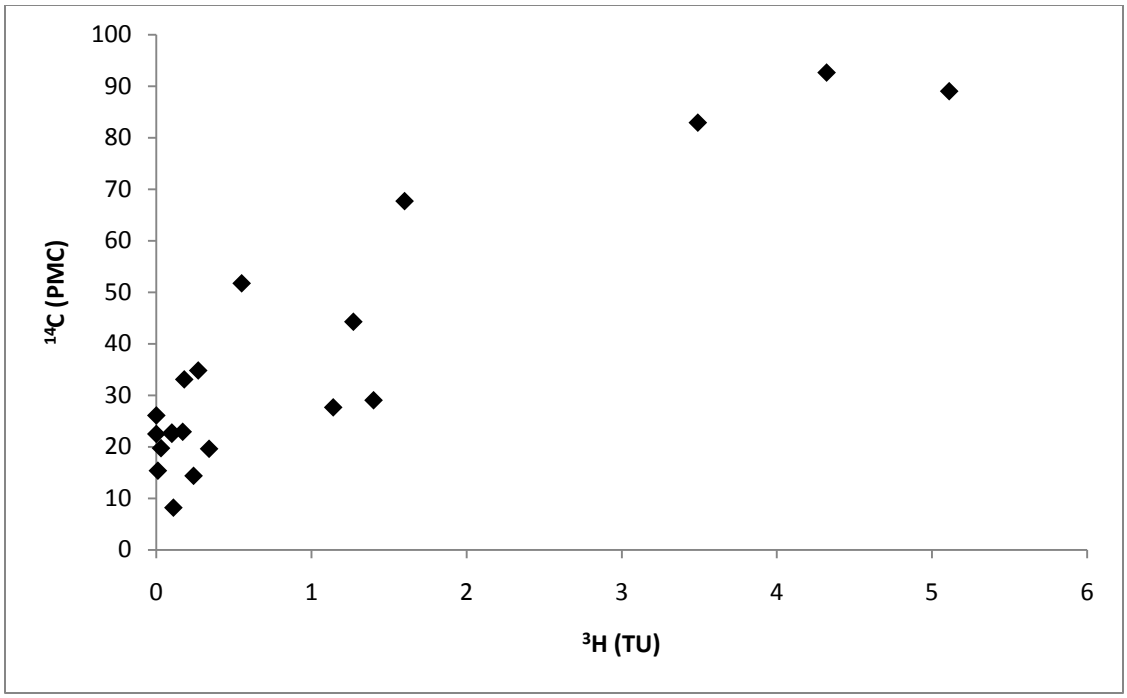


**Figure 7.3** Tritium concentrations in the Salt Basin groundwater as a function of $^{14}C$ pmc

In the Salt Basin, tritium levels fall below 0.5 TU over a relatively short distance as the groundwater flows into the lowlands of the basin, below the Piñon area. At Crow Flats there does not appear to be an influx of modern water, based on the low tritium concentrations. The carbon-14 is also low (<25 pmc) (table 5.1) for the groundwaters of Crow Flats and Dell City. Percent modern carbon versus δD values (fig 7.4) shows a positive correlation between decreasing pmc and depletion in the deuterium values. This evidence is not completely consistent with modern recharge entering the Salt Basin lowlands through runoff from the Guadalupe Mountains. However, the discontinuity in age interpreted using tritium which is limited to less than 50 years old, and carbon-14 which measures on the order of thousands of years old, could mask the presence of recharge from the Guadalupe Mountains due to mixing processes.

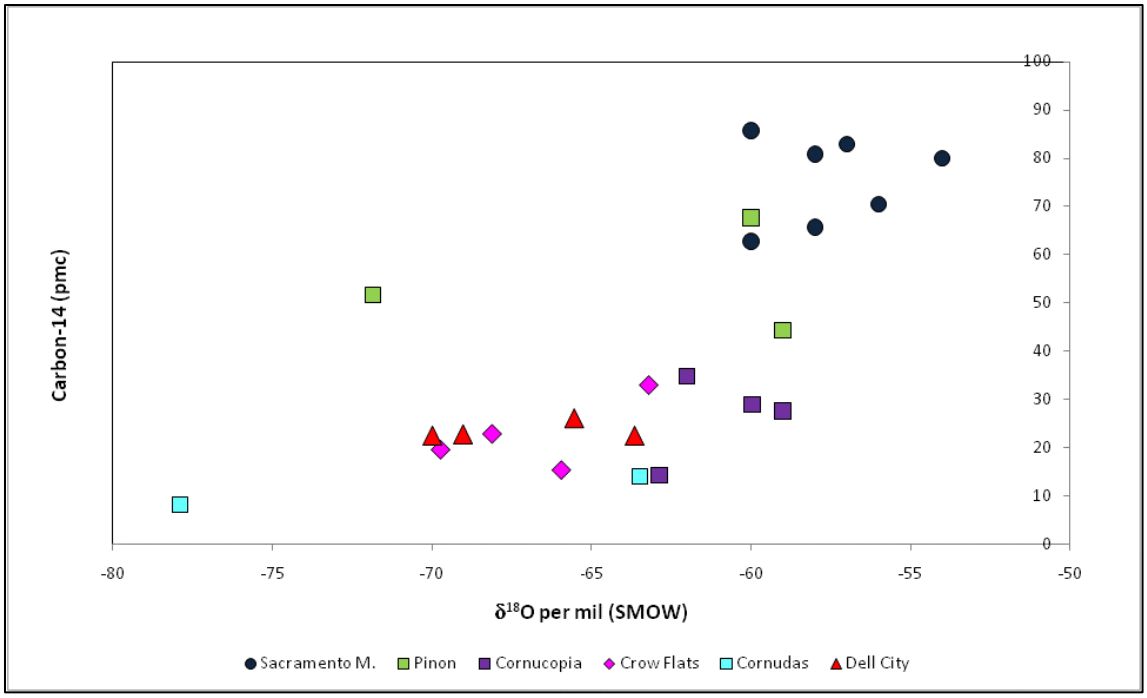


**Figure 7.4** Groundwater carbon-14 pmc as a function of deuterium isotope ratios

The alternative explanation for the depletion in the stable isotope values observed in the lower extent of the Salt Basin would be that discrete water parcels along a flow line may reflect changes in recharge environment over time. As previously discussed (5.2.d), recharge temperatures during the last glacial maximum (LGM) were about 5-6 °C cooler in New Mexico and Texas (Stute et al., 1995). The cooler recharge environment has been shown to correspond to a shift in isotopic composition of Pleistocene aged groundwater to more depleted values. In the San Juan Basin, New Mexico, the isotopic composition of the Pleistocene-age groundwater averages -3 per mil depletion in $\delta^{18}O$ and -25 per mil depletion in δD (Phillips et al., 1986). The extent of the depletion in the Salt Basin groundwater isotope compositions can be analyzed with two basic approaches.

The first is that the slope of the evaporation line is used to project onto the LMWL the reconstructed composition of each Salt Basin sample before evaporation took place (fig 7.5). If groundwater from the lower Salt Basin is paleo-recharge and if the slope of the evaporation trend has remained constant through time, the original composition of the precipitation (i.e. the intercept with the LMWL) would illustrate the depletion of paleo-precipitation compared to modern precipitation in the Sacramento Mountains. The blue field (fig 7.5) is the weighted annual average of the isotopic

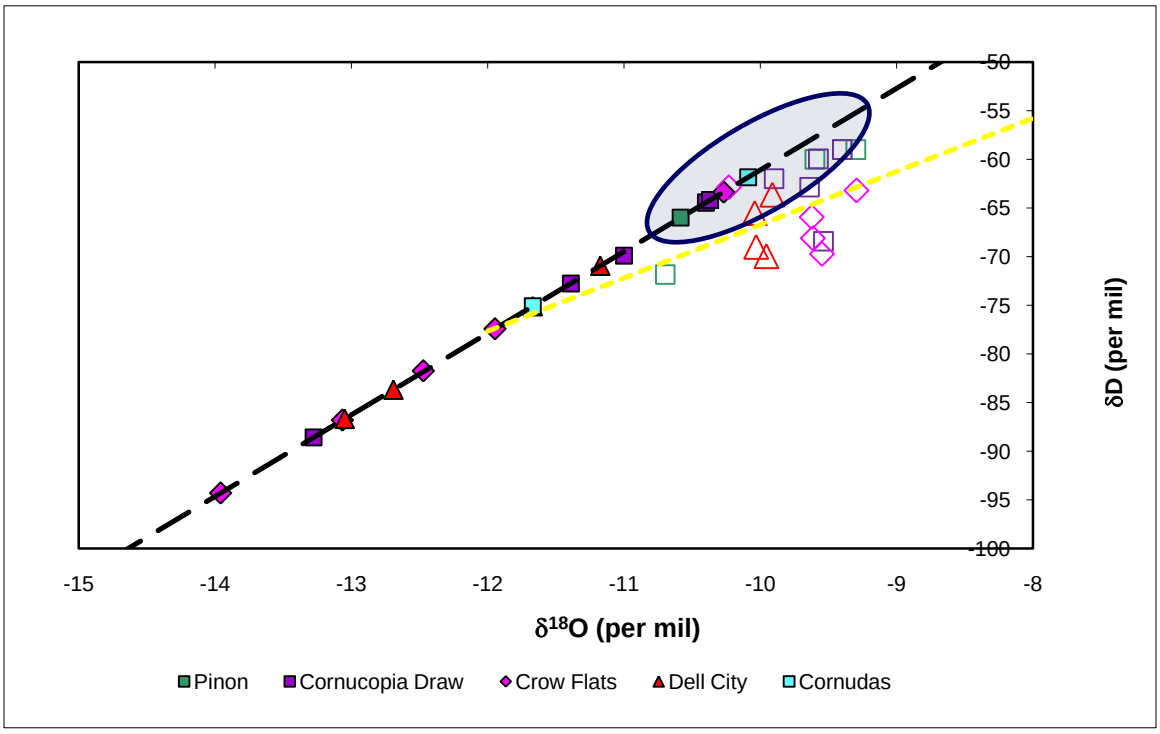


**Figure 7.5** Oxygen and deuterium isotope ratio projected with the slope of the evaporation line to determine intercept with the LMWL. Hollow symbols are measured and solid symbols are projected isotopic composition. Blue field is annually weighted isotopic composition of precipitation from the Sacramento Mountains measured 2006-2008 (NMBGMR; Rawling, 2008)

composition of precipitation from the Sacramento Mountains measured from 2006 to 2008 (NMBGMR; Rawling, 2008). There are large seasonal variations in the isotopic

composition of precipitation measured in the Sacramento Mountains. The annual weighted average isotopic composition is the average of the isotopic values of all samples collected at a single location over one year, weight by the sample volumes. The hollow symbols (fig 7.5) are the measured groundwater isotopic compositions from the Salt Basin and the solid symbols are the projected intercept with LMWL using the evaporation line. Based on the projected compositions, the depletion in precipitation for Crow Flats and Dell City groundwater samples compared to modern precipitation in the Sacramento Mountains range from about -5 to -25 per mil in δD and -1 to -4 per mil in $\delta^{18}O$.

An alternative approach is to compare the $\delta^{18}O$ and δD values from the Sacramento Mountains and the Salt Basin with both modern precipitation and paleo-recharge from the Franklin and Organ Mountains, west of the Salt Basin. In the Hueco Bolson Aquifer (Fig 1.1) groundwater recharged from the Franklin and Organ Mountains show two distinct groupings of $\delta^{18}O$ and δD composition (Eastoe, 2007). The group associated with modern recharge show stable isotope compositions around -9 and -65 per mil $\delta^{18}O$ and δD, respectively. The second group is depleted by about -1 per mil and -10 per mil, for $\delta^{18}O$ and δD, respectively. The carbon-14 data from this study show that the groundwater with the lower stable isotope compositions are most likely late Pleistocene precipitation (Eastoe, 2007). The comparison of shifts in both $\delta^{18}O$ and δD values from modern recharge to paleo-recharge in the Franklin and Organ mountains is pretty comparable to the shift observed in the Salt Basin from the Sacramento Mountains modern precipitation to the groundwater of Crow Flats and Dell City (fig 7.6).

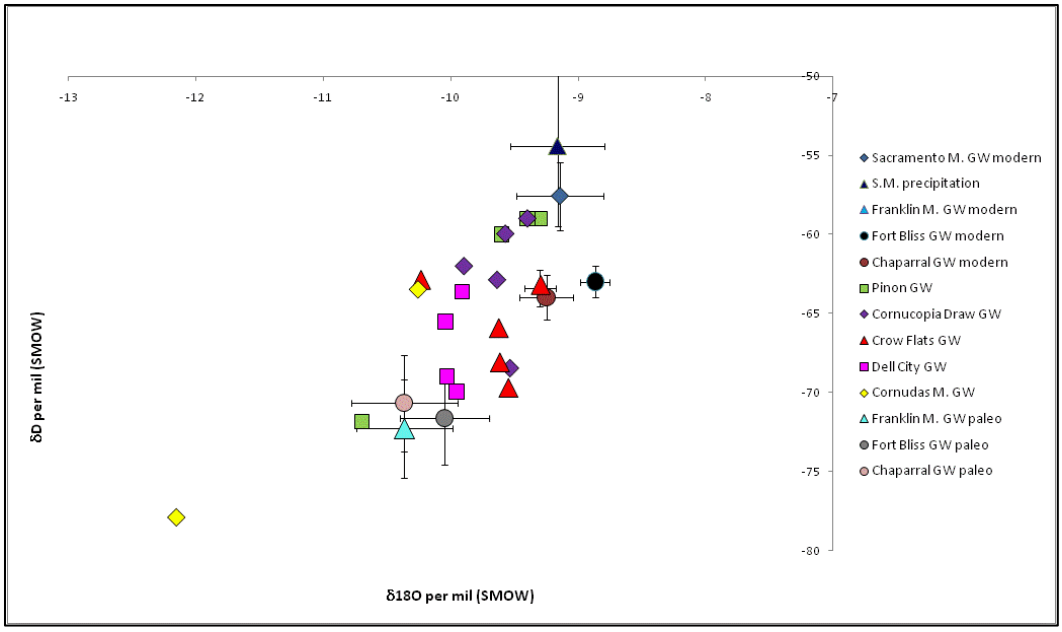


**Figure 7.6** Depletions in $\delta^{18}O$ and $\delta D$ compositions from modern Sacramento Mountain precipitation to groundwater in the Salt Basin compared to the depletions observed between modern precipitation and pale-groundwater in the Franklin and Organ Mountains. Whisker bars are the ±1σ (standard deviation) when averages were used.

The groundwater from the Hueco Bolson Aquifer that correspond to the isotopic composition of modern precipitation from the Franklin and Organ Mountains are labeled "Franklin M. GW modern", "Fort Bliss GW modern", and "Chaparral GW modern". For each of these locations average groundwater values are plotted where whisker bars are the ±1σ (standard deviation). The groundwater from the Hueco Bolson Aquifer that correspond to the isotopic composition of paleo-recharge are labeled "Franklin M. GW paleo", "Fort Bliss GW paleo" and "Chaparral GW paleo". Again for each of these locations average groundwater values are plotted where whisker bars are the ±1σ (standard deviation). The average isotopic composition of modern Sacramento Mountain precipitation is labeled "S.M. precipitation" with whisker bars of the ±1σ (standard

deviation). The average isotopic composition of modern recharge from groundwater in the Sacramento Mountains is labeled "Sacramento M. GW modern" with whisker bars of the ±1σ (standard deviation). The rest of the points are individual measurements from groundwater within the Salt Basin. The groundwater from the southern Salt Basin, such as Crow Flats and Dell City, appear to trend toward the paleo-groundwater compositions observed in the Organ and Franklin Mountains (fig 7.6).

The overall depletion down the flow paths on the eastern side of the Salt Basin (starting in the Sacramento Mountains and moving southeast to Dell City and the Salt Flats) is about -1 per mil in $\delta^{18}O$ (fig 7.7) and -10 per mil in δD (fig 7.8). These shifts are about the same as those between modern recharge and paleo-recharge in the Franklin and Organ Mountains.

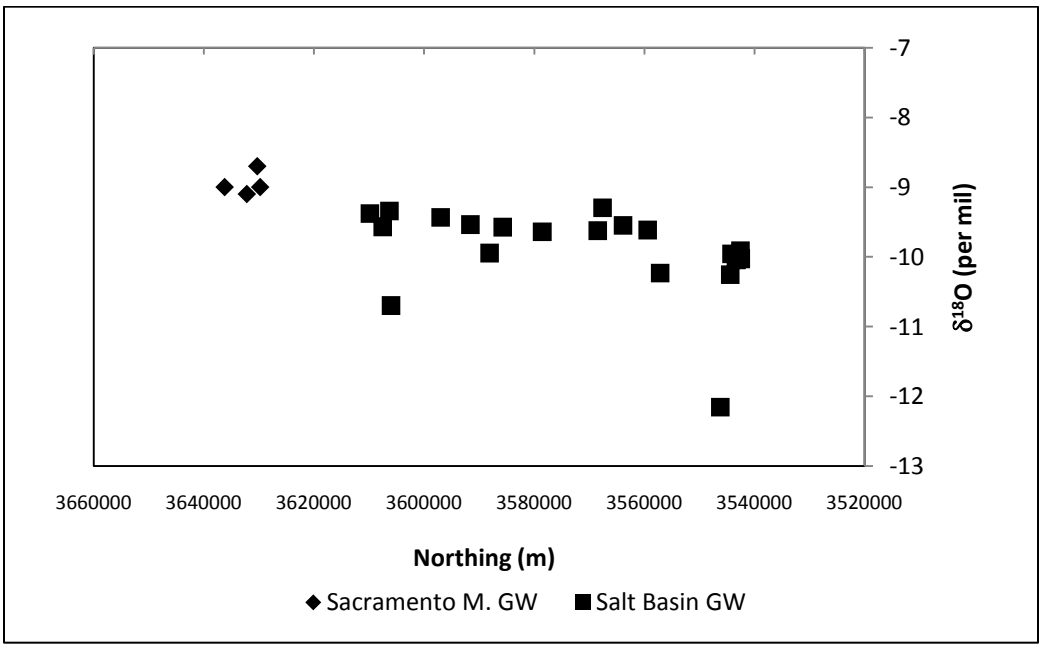


**Figure 7.7** Measured groundwater $\delta^{18}O$ content (per mil) in relation to northing (m) down the general flow paths on the eastern side of the Salt Basin

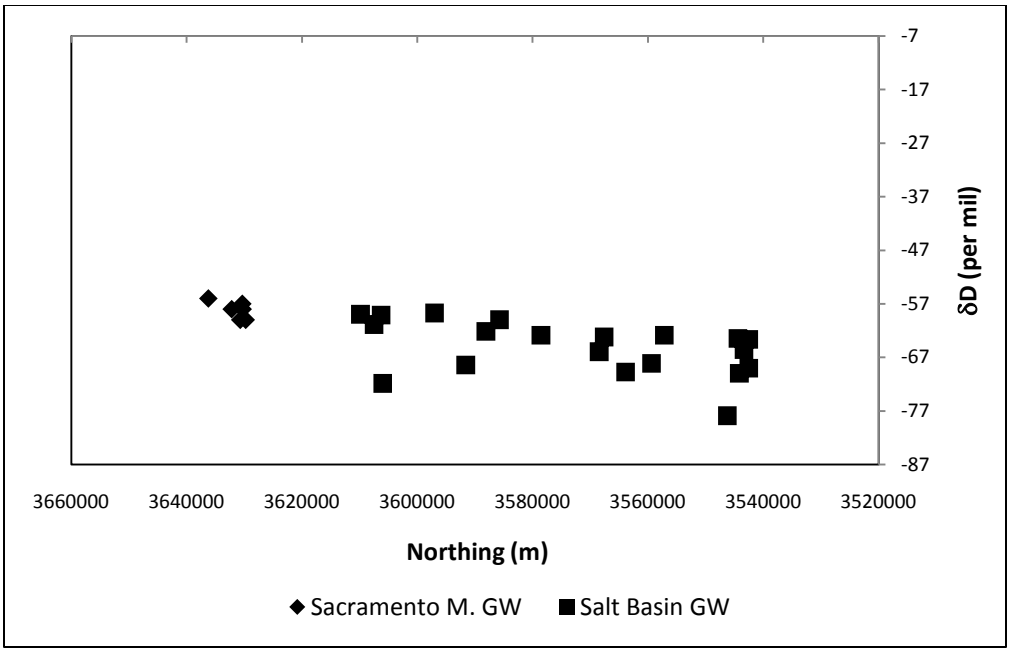


**Figure 7.8** Measured groundwater δD content (per mil) in relation to northing (m) down the general flow paths on the eastern side of the Salt Basin

The stable isotope evidence for the presence of paleo-groundwater in the Salt Basin seems consistent. This hypothesis could also explain the depletion observed in the deep well in Cornucopia Draw. It is possible this well intercepts a deeper, longer, regional flow path along which paleo-groundwater may still be present in the more northern extent of the basin. This hypothesis does not explain the depletion in the Piñon area well, as it has high percent modern carbon, and tritium levels above 1.5 TU. This depletion is more likely evidence for modern recharge in the Sacramento Mountains during extreme storm events where runoff is propagated to at least the foothills in this region before it infiltrates along fast transport-fracture pathways.

## Section 7.5: Principal Component Analysis/End Member Mixing Analysis

This section discusses mixing relationships of stable isotopes determined in order to identify what sources contribute significantly to the Salt Basin groundwater. However, it should be noted, the Salt Basin aquifer is not a well mixed system. Flow in the Salt Basin is dominantly by means of large and small scale fracture systems, leading to limited mixing along the flow paths. As will be discussed further in chapter 8.5.b., this means flow in the Salt Basin more closely follows a piston-flow model compared to a mixed-reservoir model. For the purposes of the end member mixing analysis, mixing refers to: the introduction of new water along flow paths (i.e. Guadalupe Mountain or storm event recharge), the presence of water along piston-flow paths where isotopic compositions reflect change in recharge condition over time, or density driven mixing near the Salt Flats.

Understanding quantitatively how much contribution there is of paleo-groundwater, or even Guadalupe Mountain recharge, to the Salt Basin presents a difficult problem. It has been shown that the mixing of two water sources of different isotopic compositions can be evaluated by looking at a plot of $\delta D$ and $\delta^{18}O$. A water sample that is a mixture of two isotopically distinct waters will have an isotopic composition that plots on a straight line that connects the two end member water sources (5.2.b). For example, how groundwater in the Sacramento Mountains plots between the LMWL and the evaporation line suggesting it is a mixture of evaporated and un-evaporated sources of recharge. The proportion of mixing can be quantified based on where the point lies on the mixing line between the two end members. In the Salt Basin there are more than two end members to consider as contributing sources to the groundwater system. Each

additional end member adds a dimension to the mixing problem creating a more and more complex geometry to solve.

One way to effectively solve this problem is using an End Member Mixing Analysis program (EMMA) which utilizes principal component analysis techniques to simplify datasets so only the chemical constituents and end members that explain the greatest amount of variability are retained in the final analysis (Hooper, 2003; Liu et al., 2008). In the Salt Basin the distribution of the stable isotopes $\delta^{18}O$ and $\delta D$ is what is of interest in terms of mixing processes in the aquifer system. EMMA can be used to determine whether these environmental tracers exhibit conservative behavior and the number of end-members to be retained to sufficiently explain their variability (Hooper, 2003; Liu et al., 2008).

A fundamental requirement in using end member mixing analysis is that geochemically unique end members need to be defined to determine the separation. In the Salt Basin the stable isotope composition of the groundwater is being separated based on the influence of five possible end members; each distinct based on its evolutionary pathway. Sacramento Mountain recharge defined by an average for modern groundwater in the mountains would be one end member. The isotopic composition of rainfall collected from the Piñon area, the rim of the Guadalupe Mountains, Cornucopia Draw, and near Dell City was used to define another end member. This represents runoff infiltration through fast pathway transport through drainage systems in the Salt Basin lowlands during storm events. Recharge from the Guadalupe Mountains is defined based on stable isotope compositions collected from Carlsbad cave systems. The water from soda straws was considered to be the most representative of infiltration because the water

could be collected as soon as it entered the cave, minimizing evaporation and exchange with the cave environment (Ingraham, 1990). The contribution of a paleo-groundwater end member is defined by the average stable isotope compositions of groundwater found in the Franklin and Organ Mountains interpreted to have paleo-origins (Eastoe, 2007). The final end member is that of the Salt Flats. This composition is distinct in its highly evaporated signature and was averaged from pore water collected at 30, 60, 120, 122 cm depth within the playa (Chapman, 1984).

For the Salt Basin a 2-dimensional mixing subspace represents a good model "fit" using $\delta^{18}O$ and $\delta D$ as conservative tracers in the system. This means three end members are required to explain most of the variability in the system. The majority of the Salt Basin groundwater samples fall within a mixing space defined by Sacramento Mountain recharge, rainfall infiltration through lower elevation drainage networks, and paleo-groundwater, figure 7.9. Outliers to this mixing space include groundwater from the Crow Flats which fall into a mixing space defined by Sacramento Mountain recharge, paleo-groundwater, and Guadalupe Mountain recharge, figure 7.10. As well as, the Dell City area groundwater, which is defined by Sacramento Mountain recharge, paleo-groundwater, and the Salt Flats, figure 7.11.

Webb house and Runyan wells are two outliers that can't be defined by any combination of the end member mixing. As previously noted, Runyan is a very deep well which appears to intercept a unique flow path compared to other waters in the system. While Webb house maybe a reflection of a recent localized storm event that affected the well water just prior to collection and can't be matched to more regional compositional trends.

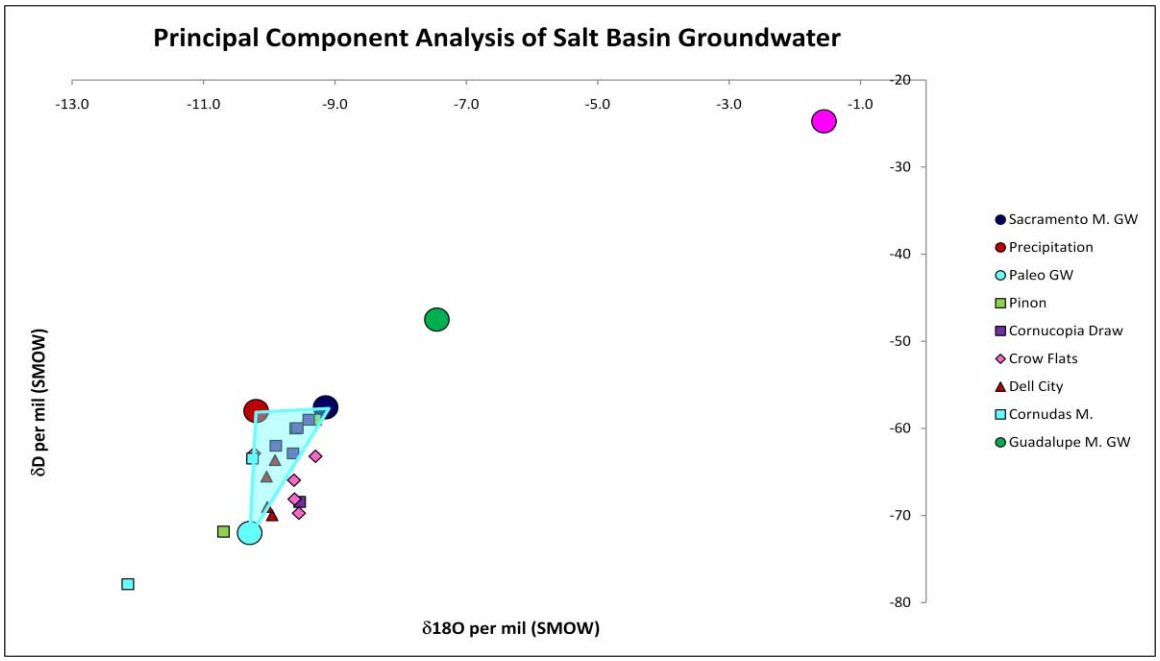


**Figure 7.9** Mixing between Sacramento M. groundwater, Salt Basin precipitation, and Paleo-groundwater end-members. These end-members explain the majority of the variability in $\delta^{18}O$ and $\delta D$ from the Salt Basin well samples.

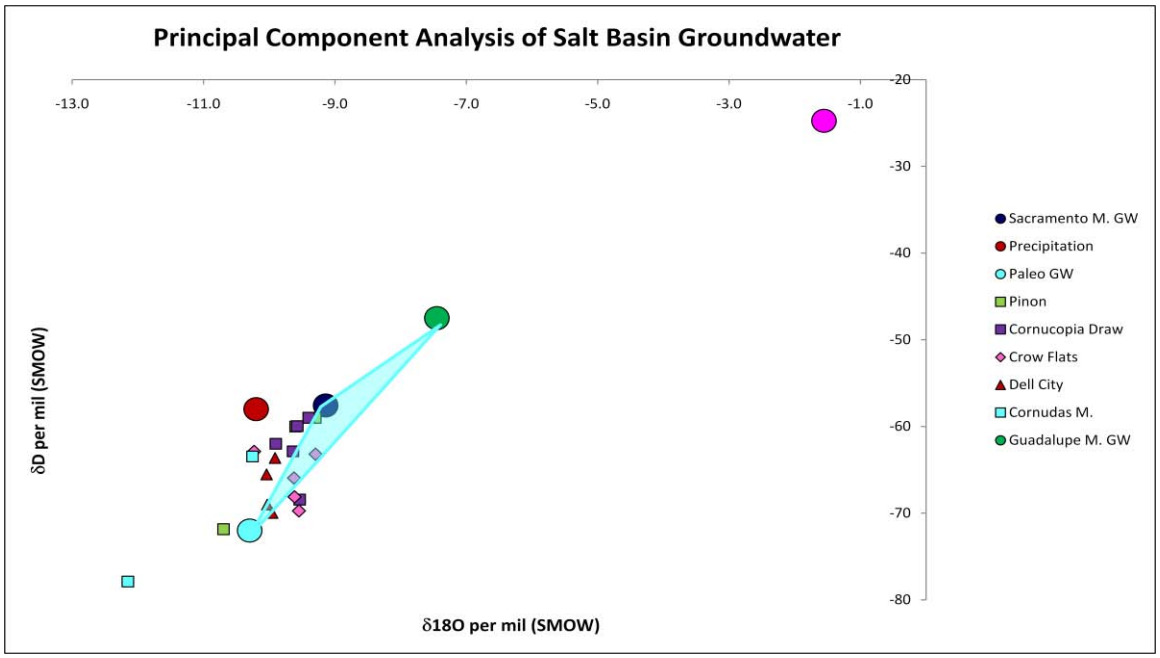


**Figure 7.10** Mixing between Sacramento M. groundwater, Paleo-groundwater, and Guadalupe M groundwater end-members. These end-members explain the variability in $\delta^{18}O$ and $\delta D$ from the Salt Basin well samples in the Crow Flats.

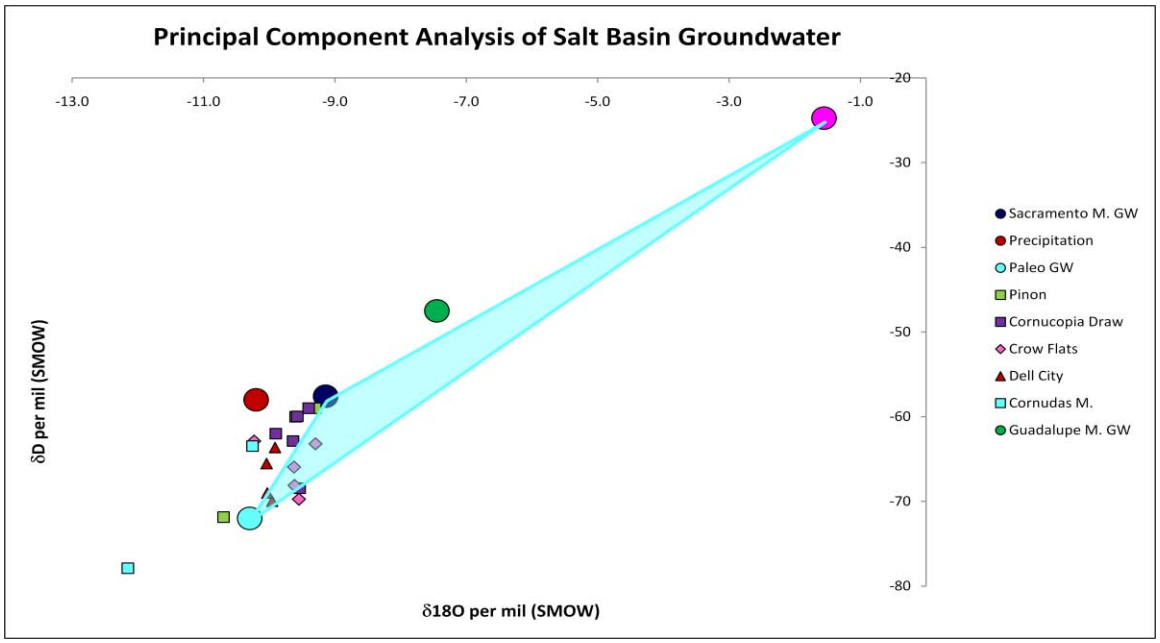


**Figure 7.11** Mixing between Sacramento M. groundwater, Paleo-groundwater, and Salt Flat end-members. These end-members explain the variability in $\delta^{18}O$ and $\delta D$ from the Salt Basin well samples near Dell City.

The percent contribution of each end member in the above mixing spaces is illustrated in figure 7.12. These should not be taken too literally as the end-members are defined more theoretically, especially the paleo-groundwater and the Guadalupe Mountain groundwater. However, in general it looks like wells in the northern extent of the basin are mostly defined by Sacramento Mountain recharge and fast track precipitation events. While the Dell City and Crow Flat waters are more consistent with paleo-groundwater signatures, with only slight influence by the Guadalupe Mountains and the Salt Flats.

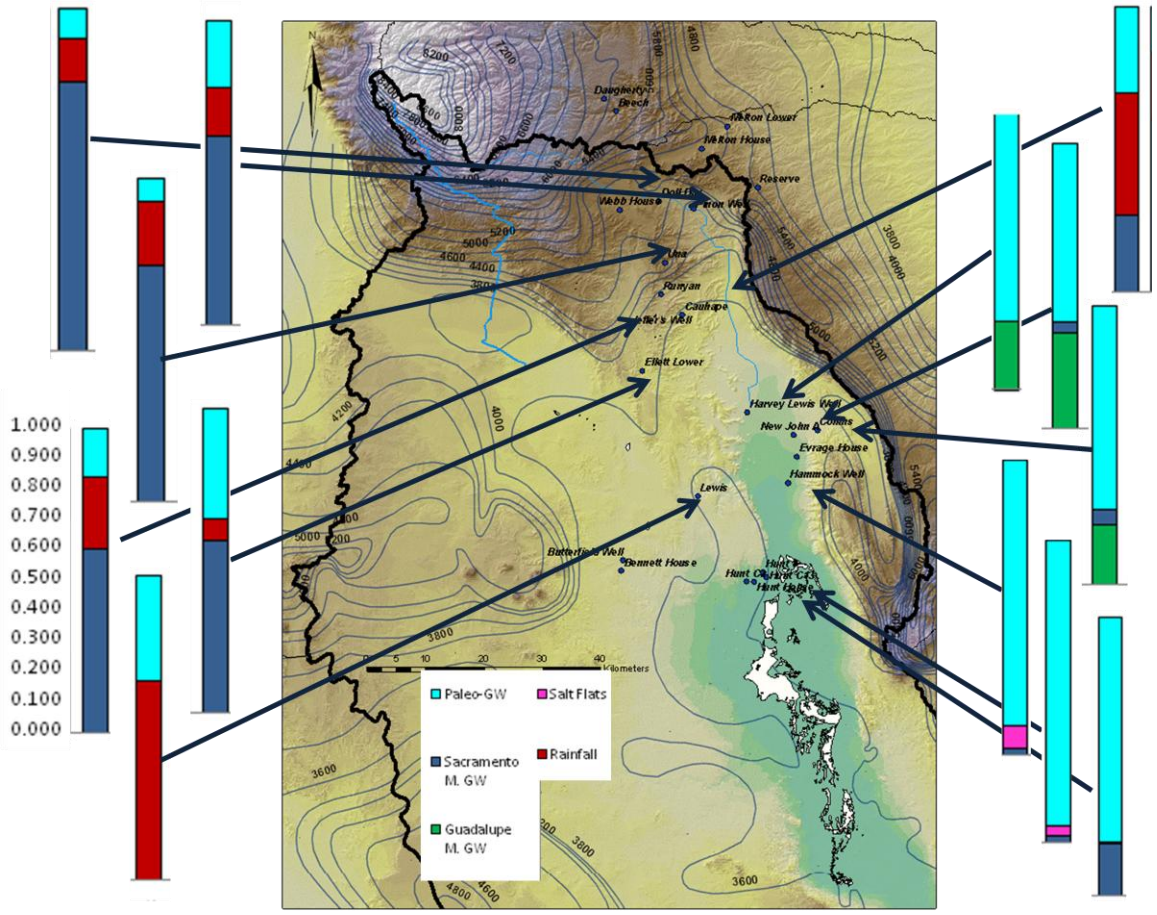


**Figure 7.12** Distribution of the % contribution of the selected end-members for some wells in the Salt Basin based on their $\delta^{18}O$ and $\delta D$ composition as analyzed by End-Member Mixing Analysis (EMMA).

# CHAPTER VIII

# GEOCHEMICAL MODELING TO ESTIMATE RECHARGE USING CARBON-14

## Section 8.1: Radiocarbon Dating in Groundwater Systems

Although certain hydrodynamic and geochemical processes can cause difficulties in the interpretation of groundwater age, many hydrogeologic setting have been investigated where radiocarbon dating has successfully elucidated information on flow velocity and recharge rates based on groundwater ages in an aquifer system (see chapter 5.4 for a discussion on radiocarbon dating systematics). Ideally multiple environmental tracers are used to characterize the residence time of groundwater in an aquifer system where corroboration between a set of tracers overcomes the uncertainties associated with each tracer as an individual.

Due to the many geochemical interactions and hydrologic processes that can act as sources or sinks for $\delta^{14}C$ in a groundwater system, geochemical modeling is often applied in modern approaches to radiocarbon dating. The geochemical modeling techniques employed for the Salt Basin aim to reduce uncertainties in two critical components of $\delta^{14}C$ dating: determination of the initial $\delta^{14}C$ activity of infiltration as it crosses the water table ($A_o$), and the extent of rock/water interactions occurring along flow paths and their effect on the $\delta^{14}C$ activity.

## Section 8.2: Definition of Recharge Chemistry

In the Salt Basin, flow paths used for geochemical modeling begin in the Sacramento Mountains and extend south, to the east of the Otero Break, through Piñon Creek watershed and Cornucopia Draw, through Crow Flats, ending near Dell City and the Salt Flats (fig 6.1). Recharge chemistry for the flow paths is defined by Sacramento groundwater that has recently infiltrated across the water table but has not significantly interacted with the rock matrix. This meant (1) being in an appropriate position of origin relative to the flow direction of the flow paths; (2) temperature measured had to be close to the mean annual surface air temperature of 9 °C; (3) sulfate concentrations had to less than 50 mg/L and magnesium concentrations less than 25 mg/L; (4) the unadjusted $^{14}C$ value had to be above 80 percent modern carbon (pmc); and (5) if it was available tritium had to be higher than 3 TU. These constraints were modeled after criteria used to define recharge chemistry for geochemical modeling using NETPATH in the Madison Aquifer (Plummer, 1991). The criteria were adjusted as to be more specific in terms of delineating Sacramento Mountain recharge zones.

Having measurements of the radiocarbon activity from groundwater in the recharge area of the aquifer system simplifies many of the complexities associated with the determination of initial activity $A_o$ (see chapter 5.4). However, one of the criteria in defining the recharge chemistry was that $\delta^{14}C$ activity had to be consistent with 85 ± 5 pmc (Vogel and Ehhalt, 1963; Vogel, 1967, 1970). This value of $A_o$ was empirically determined to be consistent with the recharge area in a groundwater system.

## Section 8.3: Dedolomitization Reaction Model

The Salt Basin aquifer system primarily consists of carbonate lithologies. Rock/water interactions involving dissolution and precipitation of carbonates will alter the $\delta^{13}C$ and $\delta^{14}C$ composition of the water as it travels through the aquifer system. This means that the $\delta^{14}C$ values measured in the lab need to be adjusted for more accurate estimates of the groundwater age. As previously discussed (6.2.b), the process of dedolomitization is the dominant control on the geochemical evolution of groundwater in the Salt Basin. This reaction initially involves the dissolution of calcite and dolomite resulting in a Ca-Mg-$HCO_3$ water type. This causes an increase in $\delta^{13}C$ and a decrease in the $\delta^{14}C$ activity. The effect on an unadjusted $\delta^{14}C$ age is to bias it toward older ages. As the dedolomitization reaction progresses, gypsum/anhydrite dissolution with concordant calcite precipitation result in a Ca-Mg-$SO_4$-$HCO_3$ water type. This causes a significant decrease in the $H^{13}CO_3^-$ and $H^{14}CO_3^-$ concentrations, but only a small decrease in $\delta^{13}C$ and $\delta^{14}C$ specific activity, in as much as both of these are expressed relative to the $H^{12}CO_3^-$ concentration. However, both are enriched relative to the $\delta^{12}C$ in the calcite cement by isotope fractionation resulting in a decrease of the $\delta^{13}C$ and $\delta^{14}C$ pmc as dedolomitization progresses. The effect on an unadjusted $\delta^{14}C$ ages is again a bias toward older ages. This means corrections using geochemical modeling will only act to make the apparent age distribution for the Salt Basin younger, increasing seepage velocities and improving estimates for recharge rates.

**Section 8.3.a: Modeling Strategy for Dedolomitization Mass Transfer Model**

Based on mass balance relationships as determined by the stoichiometry of the dedolomitization reaction, the activity of $\delta^{13}C$ and $\delta^{14}C$ can be corrected for the extent of the rock/water interactions as the water travels through the aquifer system. A dedolomitization reaction model to correct carbon-14 data was recently applied to a study following flow paths through the San Andres and Yeso formations east from the Sacramento Mountains (Morse, 2010). In this model, the change in moles of $HCO_3^-$ (between an up-gradient and down-gradient well along a flow path) is initially controlled by the dissolution of dolomite: $(HCO_{3\,i}^- \times \delta^{13}C_i) + (\delta^{13}C_{dol} \times 2\Delta Mg)$. Where $HCO_{3\,i}^-$ is the initial moles of bicarbonate, $\delta^{13}C_i$ is the initial $\delta^{13}C$ activity, $\delta^{13}C_{dol}$ is the activity of dolomite in the aquifer, and $\Delta Mg$ is the change in moles of magnesium between the up-gradient and down-gradient wells. As previously discussed (6.3) when the system is saturated with respect to dolomite and calcite, gypsum dissolution drives the incongruent precipitation of calcite. To account for the fraction of bicarbonate ($\Delta HCO_3^-$) leaving the system through calcite precipitation, the term $\left(\frac{\Delta HCO_3^-}{HCO_{3final}^- + 2\Delta Mg}\right)$ is subtracted from the total fraction of bicarbonate which is 1. When calcite precipitates it imparts a fractionation on $\delta^{13}C$ based on the fractionation factor between calcite and bicarbonate $\left(\varepsilon_{HCO_3^- - CaCO_3}\right)$. These terms are combined and divided by the final moles of bicarbonate to adjust the $\delta^{13}C$ activity measured in the down-gradient well for the extent of the dedolomitization that has taken place. This equation is simplified to adjust the $\delta^{14}C$ activity between the up-gradient and down-gradient well because the $\delta^{14}C$ activity of

dolomite in the aquifer is assumed to be zero. Overall the dedolomitization reaction model for $\delta^{13}C$ and $\delta^{14}C$ activity correction is presented in equation 8.1.

Equation 8.1:

$$\delta^{13}C_f = \frac{\left\{\left[\left(HCO_{3i} \times \delta^{13}C_i\right) + \left(\delta^{13}C_{dol} \times 2\Delta Mg\right)\right] \times \left[1 - \left(\frac{\Delta HCO_3}{HCO_{3f} + 2\Delta Mg}\right)\right] - \left[\epsilon_{HCO3 \rightarrow CaCO3} \times (\Delta Mg - \Delta HCO_3)\right]\right\}}{HCO_{3f}}$$

$$PMC_f = \frac{\left\{\left[\left(HCO_{3i} \times PMC_i\right)\right] \times \left[1 - \left(\frac{\Delta HCO_3}{HCO_{3f} + 2\Delta Mg}\right)\right] - \left[\epsilon_{HCO3 \rightarrow CaCO3} \times (\Delta Mg - \Delta HCO_3)\right]\right\}}{HCO_{3f}}$$

**Section 8.3.b: Selection of Modeling Parameters and Constraints**

This dedolomitization model is relatively simplistic in that it only quantifies changes in magnesium and bicarbonate, whereas the actual evolution process involves many more variables. This limitation means that without consistently increasing or decreasing in magnesium and bicarbonate, respectively the model cannot account for forward evolution and an apparent age of the groundwater cannot be determined. Flow in the Salt Basin is dominantly by means of large and small scale fracture systems, leading to limited mixing along the flow path and thus a high degree of variability in chemical composition between consecutive points along a flow path. Linear trend fits through the chemistry data were therefore used to derive the dedolomitization model (figures 8.1-8.5). This allowed the age distribution to be based on regional trends, as well as allowing more well observations to be incorporated into the model.

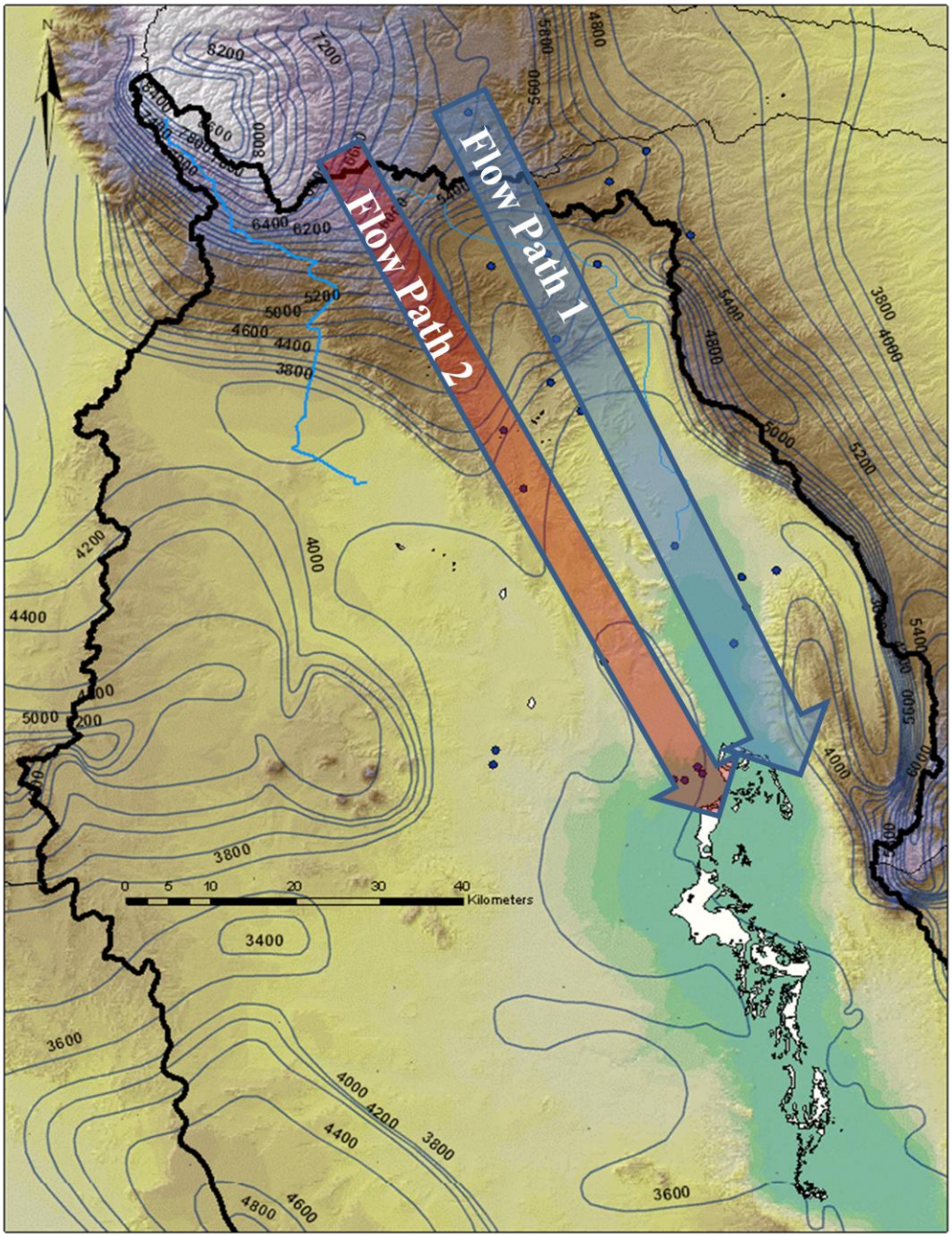


**Figure 8.1** Illustration of the two flowpaths used for $\delta^{14}$ C modeling. Flowpath #1 has 12 well samples and Flowpath #2 has 8 well samples.

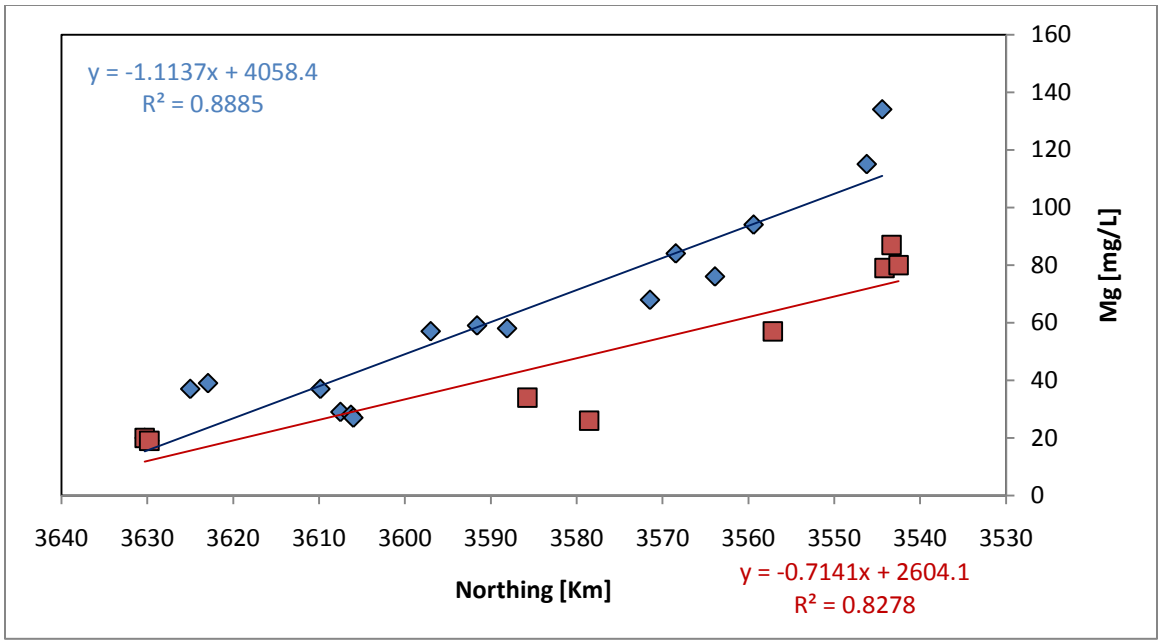


**Figure 8.2** ΔMg as a function of distance down the two flowpaths. Linear trends were used for geochemical modeling with dedolomitization reaction model.

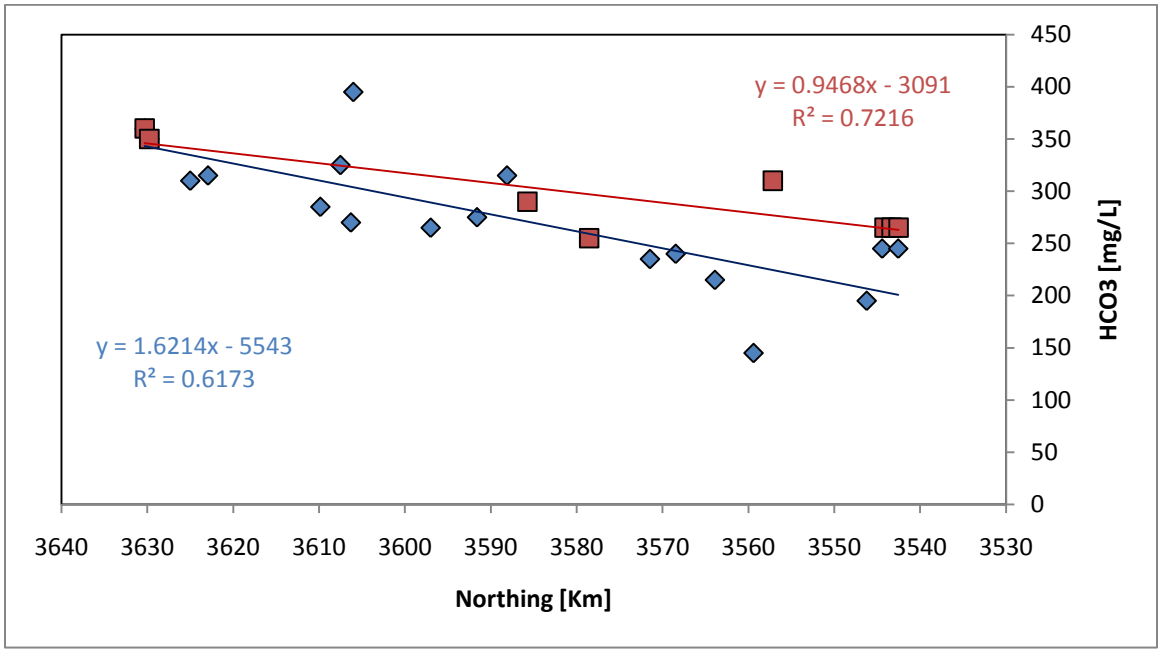


**Figure 8.3** $\Delta HCO_3$ as a function of distance down the two flowpaths. Linear trends were used for geochemical modeling with dedolomitization reaction model.

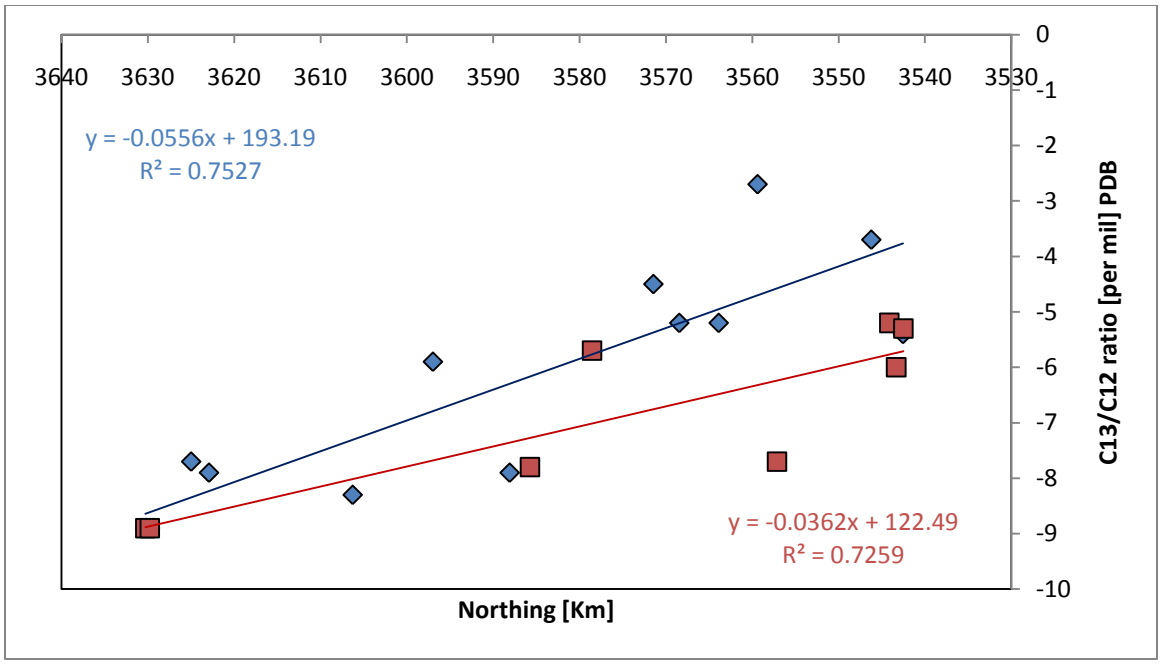


**Figure 8.4** Carbon-13 as a function of distance down the flow paths. Linear trends were used for geochemical modeling with dedolomitization reaction model.

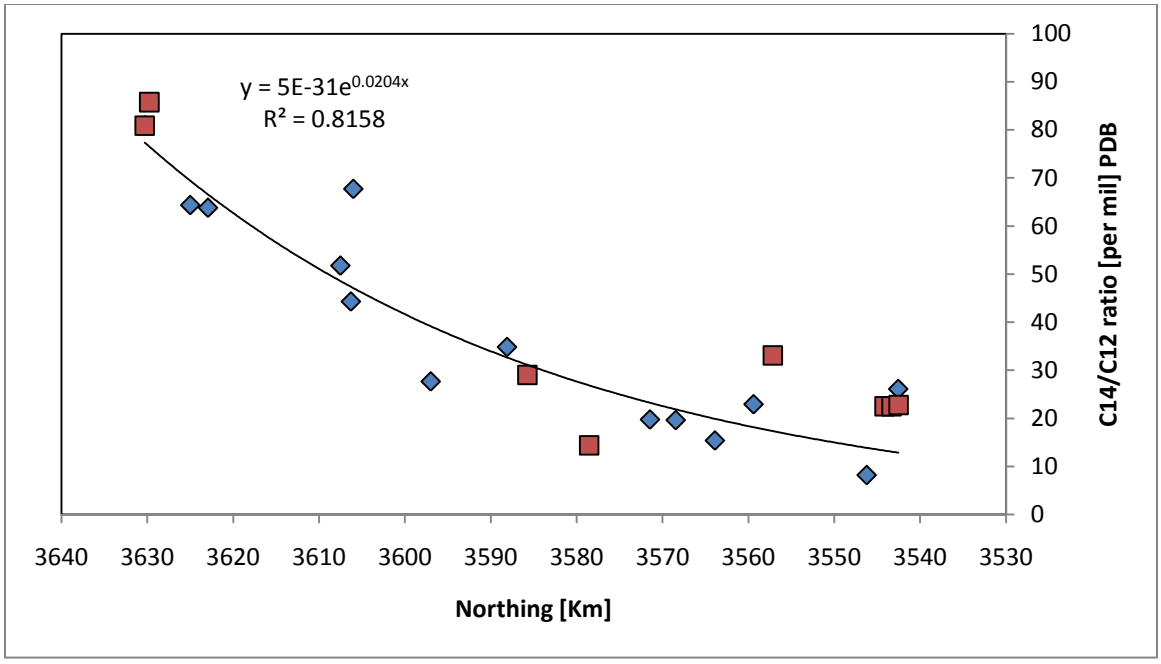


**Figure 8.5** Carbon-14 as a function of distance down the flow paths. Linear trends were used for geochemical modeling with dedolomitization reaction model.

An important model parameter is the isotopic fractionation factor between bicarbonate and calcite. The Fraction fractor $\left(\varepsilon_{HCO_3^- - CaCO_3}\right)$ is temperature dependant as it is related to equilibrium constants for exchange between the two phases. At temperatures typical of groundwater in the Salt Basin the isotopic fractionation factor between bicarbonate and calcite was calculated using Dienes et al. (1974) fractionation equation. A value of 2.13 was used in the dedolomitization geochemical model.

The $\delta^{13}C$ of dolomite is another important factor in the model. Rock cores drilled into the San Andres formation just east of the study area provided a number (~70) of stable isotope values for the dolomite unit (Wiggins, 1993). A well constrained value (1σ ± 0.04) of 5.7 per mil was used in the dedolomitization model for the $\delta^{13}C$ of dolomite ($\delta^{13}C_{dol}$).

**Section 8.3.c: Final Mass Transfer Results/ Groundwater Age Distribution**

The age correction down the flow path is based on sequentially moving along the continuous-curve fit of the wells calculating the corrected carbon-14 activity ($pmc_f$) and carbon-13 activity ($\delta^{13}C_f$). Starting with initial well on the continuous-curve fit, the initial carbon-14 activity ($pmc_i$) is used in the dedolomitization model to calculate ($pmc_f$) and ($\delta^{13}C_f$) for the first down gradient well. This well then becomes the initial well and the corrected (pmc) and ($\delta^{13}C$) are now used as initial activities in the dedolomitization model to correct the next down gradient well on the continuous-curve fit, and so on. The apparent age for each well can then be calculated: $Age = \frac{-t^1/_2}{\ln 2} \times \ln \frac{Af}{Ao}$, where $-t^1/_2$ is the

half life of $\delta^{14}C$, $A_f$ is the dedolomitization model adjusted $\delta^{14}C$ activity, and $A_o$ is the observed $\delta^{14}C$ activity measured from the well.

The dedolomitization model is applied to the $\delta^{13}C$ to test how appropriately the true geochemical evolution is being modeled (figures 8.6 and 8.7). Because $\delta^{13}C$ is a stable isotope, and not subject to radioactive decay, but still undergoes all the same geochemical reactions in the subsurface as $\delta^{14}C$, it can be used as a tracer for changes in carbon isotopes due only to rock/water interactions. This means that if the dedolomitization correction model is a good "fit" then when it is applied to the $\delta^{13}C$, the calculated values should more or less match up with the observed values.

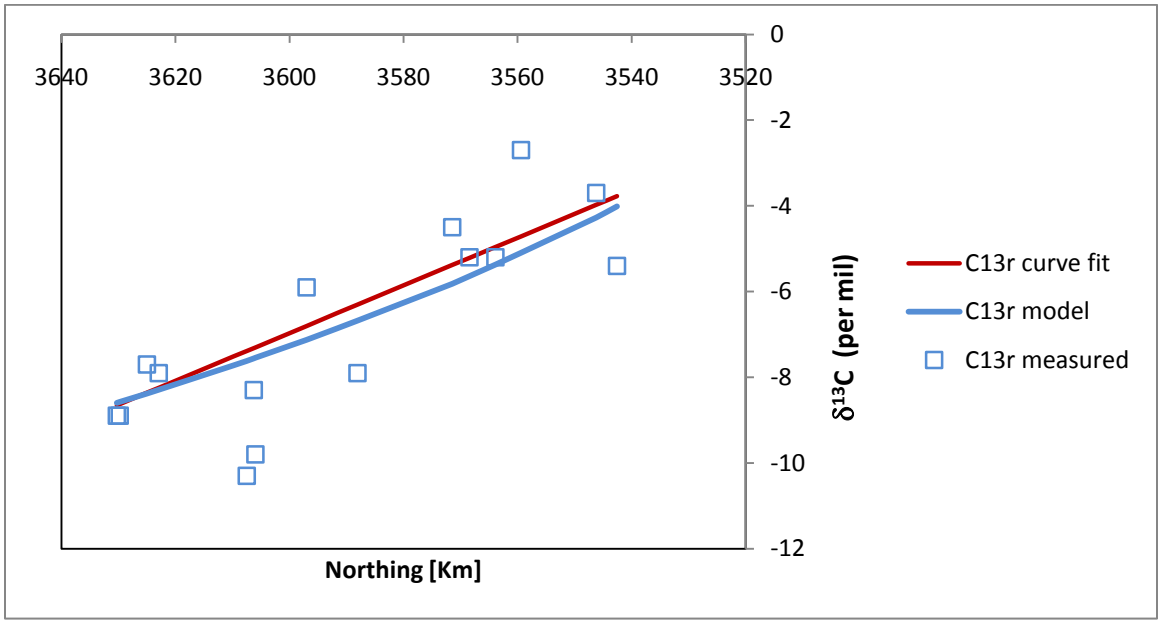


**Figure 8.6** Comparison between the curve fitted $\delta^{13}C$ (red line) compared to the $\delta^{13}C$ modeled by dedolomitization reaction (blue line) and measured from the groundwater (blue squares) for flow path 1. For the $\delta^{13}C$ modeled compared to the curve fit standard deviation is $< 0.2$ and compared to measured value standard deviation is $< 0.7$.

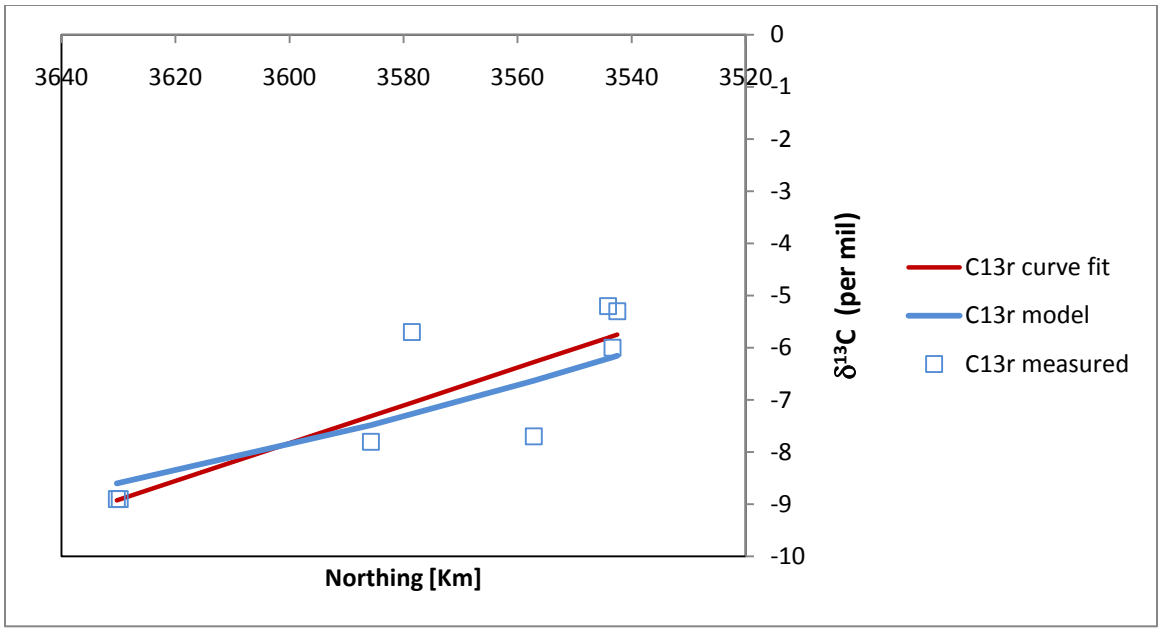


**Figure 8.7** Comparison between the curve fitted $\delta^{13}C$ (red line) compared to the $\delta^{13}C$ modeled by dedolomitization reaction (blue line) and measured from the groundwater (blue squares) for flow path 2. For the $\delta^{13}C$ modeled compared to the curve fit standard deviation is < 0.2 and compared to measured value standard deviation is < 0.7.

The $\delta^{13}C$ from the dedolomitization reaction model show a good match with the continuous curve fit $\delta^{13}C$ data (figures 8.6 and 8.7). The standard deviation between the two is less than 0.2 for both flow path 1 and flow path 2. The standard deviation between the modeled $\delta^{13}C$ and measured $\delta^{13}C$ is slightly higher at 0.7. The dedolomitization reaction model is also generally consistent with the increase in $\delta^{13}C$ measured from the groundwater down the two flow paths. This indicates that the dedolomitization reaction model is adequate as an approximation for the sources and sinks of carbon due to rock/water interactions along the flow paths.

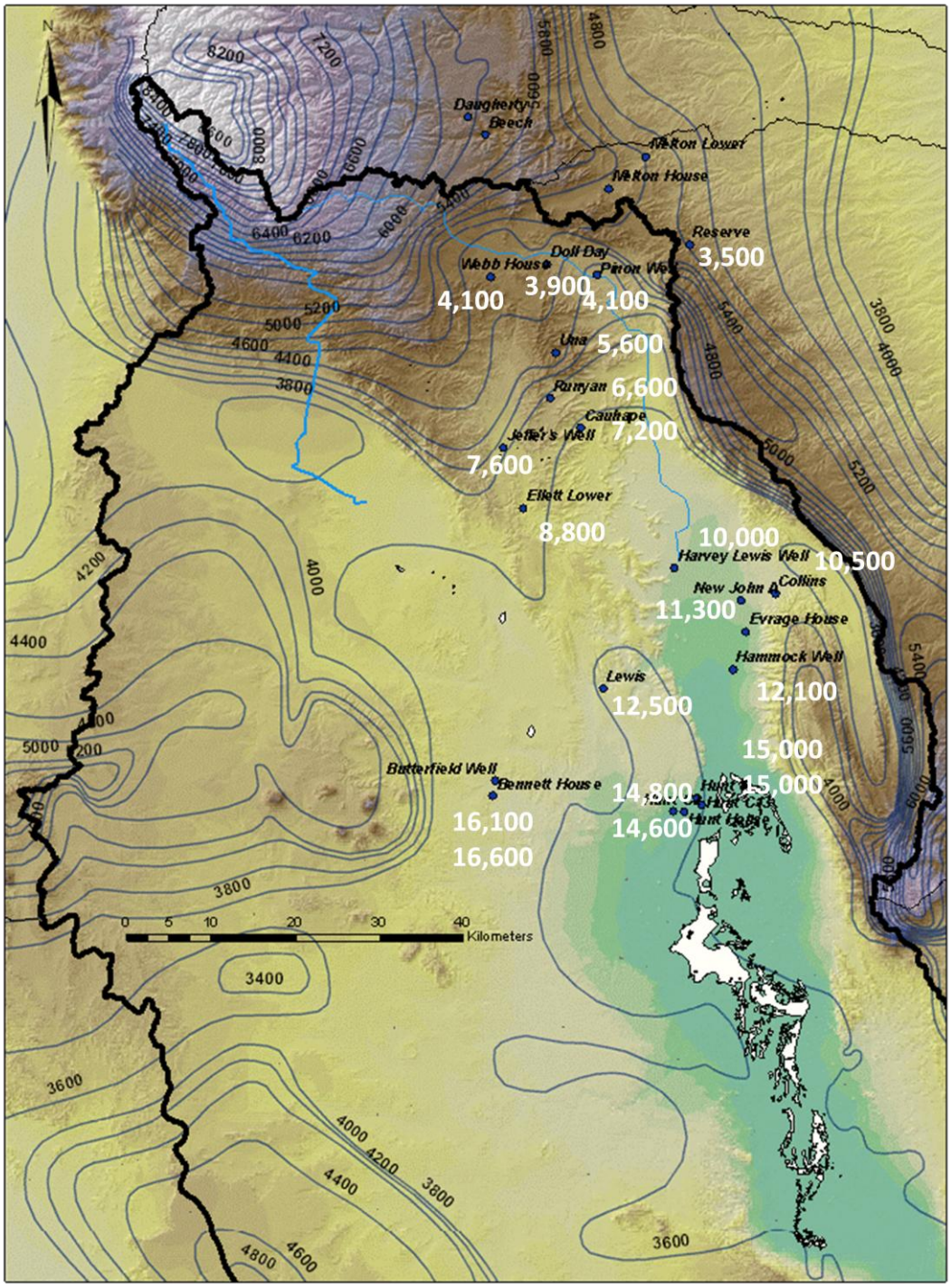


**Figure 8.8** Distribution of apparent groundwater age in the Salt Basin based on geochemical modeling using the dedolomitization reaction model. Ages are expressed in years.

**Table 8.1** Dedolomitization reaction model carbon-14 correction

| Groundwater Sample ID | $\delta^{13}C$ meas. (permil) | $\delta^{13}C$ curve fit (per mil) | $\delta^{13}C$ model (per mil) | STD DEV | $\delta^{14}C$ meas. (pmc) | $\delta^{14}C$ curve fit (pmc) | Ao Corrected model (pmc) | AGE (years) |
|---|---|---|---|---|---|---|---|---|
| *Flow Path 1* | | | | | | | | |
| SM-0140 | -8.9 | -8.7 | -8.6 | 0.0 | 80.9 | 72.8 | 73.0 | 0 |
| SM-0138 | -8.9 | -8.6 | -8.6 | 0.0 | 85.8 | 72.0 | 73.0 | 100 |
| Reserve | | -7.5 | -7.8 | 0.2 | | 48.0 | 73.3 | 3500 |
| Doll Day | -10.3 | -7.4 | -7.6 | 0.2 | 51.7 | 45.7 | 73.3 | 3900 |
| Pinon Well | -8.3 | -7.3 | -7.6 | 0.2 | 44.3 | 44.6 | 73.3 | 4100 |
| Webb House | -9.8 | -7.3 | -7.6 | 0.2 | 67.7 | 44.3 | 73.3 | 4100 |
| Una | -5.9 | -6.8 | -7.2 | 0.2 | 27.7 | 36.9 | 73.4 | 5700 |
| Runyan | | -6.5 | -6.9 | 0.3 | | 33.0 | 73.5 | 6600 |
| Cauhape | -7.9 | -6.3 | -6.7 | 0.3 | 34.8 | 30.8 | 73.5 | 7200 |
| Harvey Lewis Well | -4.5 | -5.4 | -5.8 | 0.3 | 19.7 | 21.9 | 73.9 | 10000 |
| Collins | -5.2 | -5.2 | -5.7 | 0.3 | 19.6 | 20.6 | 73.9 | 10500 |
| Evrage House | -5.2 | -5.0 | -5.4 | 0.3 | 15.4 | 18.8 | 73.9 | 11300 |
| Hammock Well | -2.7 | -4.7 | -5.1 | 0.3 | 22.9 | 17.1 | 74.0 | 12100 |
| Hunt C2 | -5.4 | -3.8 | -4.0 | 0.2 | 26.1 | 12.1 | 74.4 | 15000 |
| *Flow Path 2* | | | | | | | | |
| SM-0140 | -8.9 | -8.9 | -8.6 | 0.2 | 80.9 | 72.8 | 73.0 | 0 |
| SM-0138 | -8.9 | -8.9 | -8.6 | 0.2 | 85.8 | 72.0 | 73.0 | 100 |
| Jeffer's Well | -7.8 | -7.3 | -7.5 | 0.1 | 29.0 | 29.3 | 73.7 | 7600 |
| Ellett Lower | -5.7 | -7.1 | -7.3 | 0.2 | 14.4 | 25.3 | 73.7 | 8800 |
| Lewis | -7.7 | -6.3 | -6.6 | 0.2 | 33.1 | 16.4 | 73.9 | 12400 |
| Hunt 8 | -5.2 | -5.8 | -6.2 | 0.3 | 22.5 | 12.6 | 74.0 | 14600 |
| Hunt C13 | -6.0 | -5.8 | -6.2 | 0.3 | 22.5 | 12.3 | 74.0 | 14800 |
| Hunt House | -5.3 | -5.7 | -6.2 | 0.3 | 22.8 | 12.1 | 74.0 | 15000 |
| Butterfield Well | -3.7 | -4.0 | -4.3 | 0.2 | 8.2 | 13.1 | 74.3 | 16100 |
| Bennett House | | -3.9 | -4.2 | 0.2 | | 12.6 | 74.3 | 16600 |

The apparent age distribution along the two separate flow paths appears to be consistent (fig 8.8). In particular the Dell City area wells that were separated between the two flow paths all come out with about the same apparent ages of about 15,000 years. An interesting observation is that the two wells samples collected to the west of the flow

paths (Bennett and Butterfield) show the lowest pmc and have the oldest apparent groundwater age. The presence of old water in this region has implications for whether or not there is significant recharge from the Cornudas Mountains entering the Salt Basin graben, as well as what the relative groundwater flux from the western side of the Salt Basin is compared to the flow paths on the eastern side. The apparent age distribution is also consistent with the interpretation of $\delta^{18}O$ and $\delta D$, which indicated the presence of Pleistocene age groundwater in Crow Flats and the Dell City area, implying water ages of 10,000 years old or more.

**Section 8.4: Geochemical Modeling using NETPATH**

NETPATH (Plummer et al., 1994) is a geochemical model that uses chemical mass balance, electron balance, and isotope mass balance to define net mass-balance reactions between an initial and final well along a hydrologic flow path. The program uses inverse modeling to ascertain the masses (per kilogram of water) of plausible minerals and gases that must dissolve or precipitate along the flow path to produce the composition of a selected set of chemical and isotopic observations in the final well. It is of critical importance that the wells selected truly share common evolution and lie along well defined flow paths in the aquifer system. The program is exhaustive in that it will out put any number of models so as to include every possible set of geochemical mass-balance reactions between the selected evolutionary waters. The better constrained the flow path and the reactions responsible for the geochemical evolution the more unique the NETPATH model solution. Given sufficient isotopic data, Rayleigh distillation calculations can be applied to mass-balance models that satisfy the constraints to predict changes in isotopic compositions such as carbon. NETPATH is extensively applied to

correct radiocarbon ages of groundwater due to geochemical evolution. NETPATH modeling for radiocarbon dating corrections in the Salt Basin follow examples including Plummer et al. (1991), Plummer and Hanshaw (1983), and Plummer et al. (1994).

### 8.4.a: Modeling Strategy for $^{14}C$ Mass Transfer in NETPATH

This radiocarbon-dating mass-transfer strategy is laid out in Plummer's (1994) NETPATH Manual. As previously discussed, the adjustment for $\delta^{14}C$ needs to account for two complications that result from aqueous geochemistry: (1) definition of the initial $\delta^{14}C$ activity (Ao) in system, (i.e. the recharge zone where the water is isolated from the modern $\delta^{14}C$ reservoir), and (2) adjustment of this initial $\delta^{14}C$ activity for geochemical reactions along the flow path to the final well the $\delta^{14}C$ activity has been measured. Many traditional $\delta^{14}C$ adjustment models combine these two problems so that the model can be applied to a single water analysis at any point in the flow system. NETPATH is different in that it keeps the two problems separate but requires both initial water and final water analysis points along an evolutionary flow path. Traditional adjustments are applied only to the initial water where it will generally be more applicable due to the less complex geochemical evolution. NETPATH then solves for the mass transfer to pertinent phases between the initial water and the final down-gradient water. This mass transfer is then used to adjust the initial $\delta^{14}C$ ($A_o$) for all sources and sinks of carbon that affect the carbon mass transfer between the two wells. This means at the final well the $\delta^{14}C$ activity is adjusted for geochemical reactions but not radioactive decay, thereby giving $A_f$. Again, the apparent age is calculated using: $Age = \frac{-t^{1}/_{2}}{\ln 2} \times \ln \frac{Af}{Ao}$.

All carbon leaving the solution between the initial and the final waters, through carbonate mineral precipitation or outgassing of $CO_2$, is assumed to leave by Rayleigh distillation processes defined by isotopic fractionation. All carbon mass transfer associated with minerals or gases that enter the aqueous phase between the initial and final waters is assumed to enter without isotopic fractionation, and have $\delta^{13}C$ and $\delta^{14}C$ (pmc) compositions that are assigned to the specific phases.

The initial water can be represented by any point along the flow path. This allowed $\delta^{14}C$ activity adjustments down flow paths in the Salt Basin to be carried out in the same fashion as with the dedolomitization model correction. Starting in the recharge area with the initial well on the flow path, the initial carbon-14 activity ($A_o$) is used in the NETPATH model to calculate ($A_f$) for the first down gradient well. This well then becomes the initial well and the corrected (pmc) is now used as the initial activity ($A_o$) in the NETPATH model to correct the next down gradient well, and so on. The modeled $\delta^{14}C$ apparent age of the final water, in this case, represents only the travel time between the initial and final well. To find the actual age of the final water it is necessary to add to this travel time the age of the initial water.

**Section 8.4.b: Selection of Modeling Parameters and Constraints**

Flow paths for geochemical modeling in NETPATH to adjust the $^{14}C$ activity from well measurements in the Salt Basin were defined by two main considerations: (1) the sequence of wells had to be logical relative to groundwater gradients and flow direction; and (2) initial and final well pairs along a flow path were chosen based on the best $^{13}C$ observed versus measured 1:1 fit. This meant, for example, not all the wells in

Crow Flats were interpreted to be evolutionary to one another. If a well pair produced a very poor $^{13}C$ "fit" the initial well was changed to the next nearest up gradient well along the flow path. Allowing for this kind of spatial variability, as well as NETPATH being able to account for much more complex geochemical variability compared to the dedolomitization model, meant that trend lines were not necessary to fit the well chemistry measurements into the NETPATH model.

In NETPATH phases are defined as any mineral or gas that can enter or leave the aqueous solution along the evolutionary path. Important phases are defined by the user and should be based on a predictable geochemical evolution for the flow path. For the flow paths chosen for geochemical modeling in the Salt Basin, dedolomitization as the dominant control on the geochemical evolution is well defined. Some phases can realistically only be precipitated or dissolved, but not both along a flow path. In NETPATH this is acknowledged and phases can be defined as "precipitation only" or "dissolution only". For the Salt Basin the phases included were dissolution of dolomite, dissolution of gypsum, precipitation of calcite, as well as, a $CO_2$ phase.

Defining constraints in NETPATH is necessary to determine the extent of the geochemical reactions. Most constraints are cations and anions typical of aqueous solutions, but redox states and isotopic elements can also be used. For every phase defined within NETPATH there must be a constraint associated with it. For the phases used for geochemical modeling in the Salt Basin, calcium, magnesium, and carbon were used as constraints. Comparing the observed and calculated $\delta^{13}C$ isotopic composition at the final well can, like the dedolomitization model, be used to interpret how appropriate the model "fit" is. Because isotopes of $\delta^{13}C$, like $\delta^{14}C$, are involved in carbonate

reactions with multiple sources and sinks, it is more appropriately treated using isotope evolution calculations as opposed to mass balance in NETPATH , in which case it should not be included as a constraint.

When there is both a source and a sink for an isotope in the reaction, it is treated as a Rayleigh distillation problem. Isotopic data can be entered for pertinent phases in the isotopic evolution. The $\delta^{13}C$ value for the $CO_2$ of the soil gas was set at -25 per mil, at value measured from soil gas in the Sacramento Mountains (Morse, 2010). The $\delta^{13}C$ value for dolomite used was the same as for the dedolomitization model, +5.7 per mil ($1\sigma \pm 0.04$) measured from the San Andres (Wiggins, 1993). The range of $\delta^{13}C$ values for dolomite from this study measured from about 70 samples is from +4 to +7 per mil. The $\delta^{13}C$ value for calcite used was the average value measured from the San Andres and Yeso rock samples collected for this study from outcrops in the Sacramento Mountains, about +2 per mil.

**Table 8.2** $\delta^{13}C$ values for calcite

| ***Formation*** | ***Corrected δ13C*** | ***Std. Dev*** |
|---|---|---|
| San Andres | 3.7 | 0.06 |
| San Andres | 2.6 | 0.07 |
| Yeso | 0.4 | 0.10 |

The calculated radiocarbon ages are not sensitive to varying the input for the $\delta^{13}C$ values assumed for the carbonate rocks over the two ranges presented above. The main difference observed in the NETPATH output is the modeled $\delta^{13}C$ value. Table 8.3 shows

the results of a sensitivity analysis varying the $\delta^{13}C$ value for dolomite and calcite using the lows, averages, and highs.

**Table 8.3** Analysis of the sensitivity of the NETPATH radiocarbon ages to the $\delta^{13}C$ values assumed for carbonate rocks

| *Initial Well* | *Final Well* | *Northing (m)* | *$\delta^{13}C$ meas.* | *$\delta^{13}C$ model* | *$\delta^{14}C$ meas.* | *$\delta^{14}C$ model* | *Age (years)* |
|---|---|---|---|---|---|---|---|
| $\delta^{13}C$ calcite= +2 dolomite = +5.7 (per mil) | | | | | | | |
| SM-0138 | Doll Day | 3607510 | -10.3 | -7.26 | 51.74 | 73.84 | 2900 |
| Doll Day | Una | 3596995 | -5.9 | -5.11 | 27.66 | 45.76 | 7100 |
| Una | Cauahpe | 3588103 | -7.9 | -4.58 | 34.82 | 38.69 | 8000 |
| Cauhape | Harvey Lewis | 3571455 | -4.5 | -6.41 | 19.74 | 32.39 | 12100 |
| Harvey Lewis | Evrage | 3563888 | -5.2 | -3.2 | 15.37 | 26.72 | 16600 |
| *Initial Well* | *Final Well* | *Northing (m)* | *$\delta^{13}C$ meas.* | *$\delta^{13}C$ model* | *$\delta^{14}C$ meas.* | *$\delta^{14}C$ model* | *Age (years)* |
| $\delta^{13}C$ calcite=0 dolomite = +4 (per mil) | | | | | | | |
| SM-0138 | Doll Day | 3607510 | -10.3 | -7.49 | 51.74 | 73.84 | 2900 |
| Doll Day | Una | 3596995 | -5.9 | -5.75 | 27.66 | 45.76 | 7100 |
| Una | Cauahpe | 3588103 | -7.9 | -4.89 | 34.82 | 38.69 | 8000 |
| Cauhape | Harvey Lewis | 3571455 | -4.5 | -4.58 | 19.74 | 32.39 | 12000 |
| Harvey Lewis | Evrage | 3563888 | -5.2 | -3.52 | 15.37 | 26.72 | 16600 |
| *Initial Well* | *Final Well* | *Northing (m)* | *$\delta^{13}C$ meas.* | *$\delta^{13}C$ model* | *$\delta^{14}C$ meas.* | *$\delta^{14}C$ model* | *Age (years)* |
| $\delta^{13}C$ calcite= +4 dolomite = +7 (per mil) | | | | | | | |
| SM-0138 | Doll Day | 3607510 | -10.3 | -7.08 | 51.74 | 73.84 | 2900 |
| Doll Day | Una | 3596995 | -5.9 | -4.61 | 27.66 | 45.76 | 7100 |
| Una | Cauahpe | 3588103 | -7.9 | -4.28 | 34.82 | 38.69 | 8000 |
| Cauhape | Harvey Lewis | 3571455 | -4.5 | -6.19 | 19.74 | 32.39 | 12000 |
| Harvey Lewis | Evrage | 3563888 | -5.2 | -3.02 | 15.37 | 26.72 | 16600 |

Two sets of fractionation factors for the inorganic $^{13}C$ system are available in NETPATH. For modeling in the Salt Basin the set from Mook was applied. "Mook" is a selection of equilibrium factors for carbonate species and calcite from number of studies. All fraction factors in the "Mook set" are based on experimental measurements, except

for values relating to $CO_3^{-2}$, which were derived theoretically by Thode and others (1965). The "Mook" set is given as additive fractionation fractors, $\varepsilon_{i \rightarrow j}$ in per mil.

**Section 8.4.c: Summary of Final Mass Transfer Results/ Apparent Age Distribution**

The phases and constraints used to model the geochemical evolution along flow paths in the Salt Basin provided a unique solution in NETPATH, in that only one model was posed to explain the mass transfer. The solution for each well pair along a flow path defines a balanced chemical reaction and the change in mass for each mineral phase:

$$Groundwater_{initial} + dolomite_{diss.} + gypsum_{diss.} = Groundwater_{final} - calcite_{ppt}$$

In addition to the solution for the mass balance, NETPATH calculates the isotopic fractionation associated with the reaction. This allows model calculated $\delta^{13}C$ to be compared to observed $\delta^{13}C$ values from the final well and also provides a corrected $\delta^{14}C$ (pmc) and a travel time associated with the distance between the initial and final well.

How well the model calculated $\delta^{13}C$ and the observed $\delta^{13}C$ "fit" is a check for how well the true rock/water interactions along the flow path are being model (fig 8.9). The average standard deviation from the modeled $\delta^{13}C$ and the measured $\delta^{13}C$ is about ±1.5 per mil. It is interesting to note that the simple dedolomitization model seems to match the $\delta^{13}C$ better (with an average standard deviation of ± 0.7 per mil) than the more sophisticated NETPATH model. This may be because the generalized trend lines are a better approximation of the actual flow evolution than the well-to-well comparison.

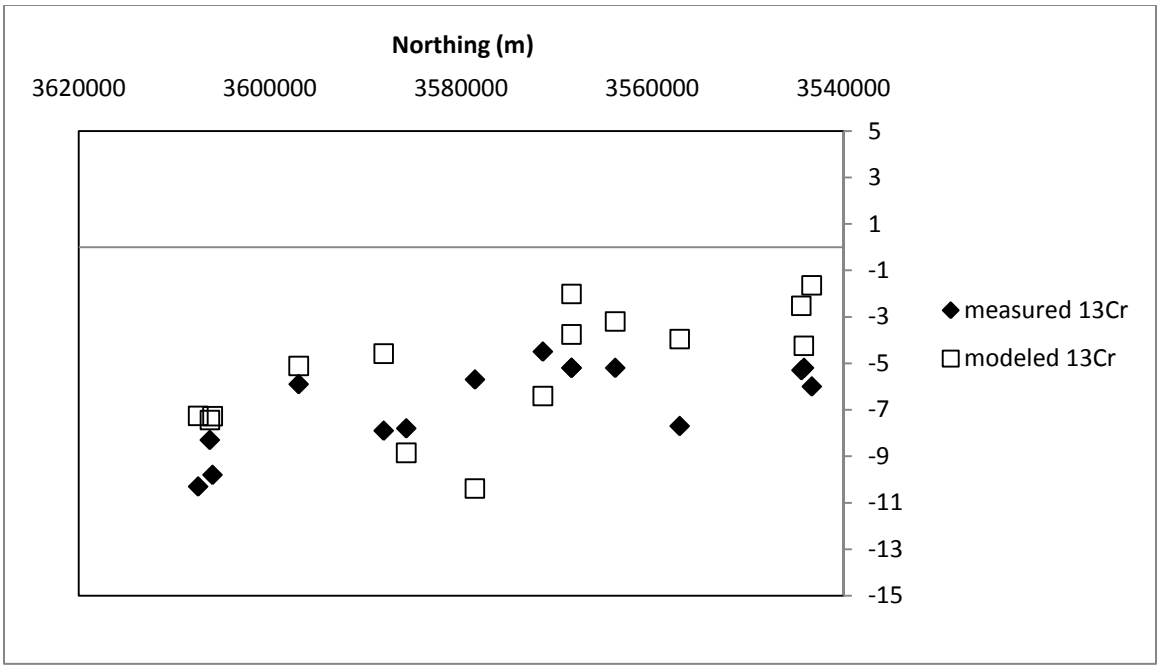


**Figure 8.9** Comparison between the observed $\delta^{13}C$ compared to the $\delta^{13}C$ modeled by NETPATH as a function of distance along flow path.

Deviations in $\delta^{13}C$, as well as other evidence of uncertainty in the model such as precipitation or dissolution inconsistent with saturation indices, may represent modeling error. There are several possible causes for modeling errors. A significant factor is any uncertainty in the analytical data. In NETPATH, mass-balance reaction models combine positive and negative charges in water analyses to compute the masses of uncharged phases. A consequence is that charge-balance errors can contribute to computed masses of one-component phases such as $CO_2$. However, $CO_2$ was not found to play a role in mass transfer in the Salt Basin and so this source of error was likely not a factor. Another obvious source of uncertainty is in defining the composition of the recharge waters. Even though modern groundwater in the Sacramento Mountains was relatively well characterized for this study, uncertainties in $\delta^{14}C$ activity from contamination by bomb

carbon or even natural atmospheric fluctuations in $\delta^{14}C$ always present a problem for confidence in radiocarbon dating. There could also be uncertainties in the $\delta^{13}C$ of dolomite or in the fractionation factors. However, sensitivity analysis indicates these would be minor modeling effects. The most significant source of uncertainty is likely confidence in defining the flow paths. The wells available for sampling do not necessarily lie on an actual well-to-well flow path, and thus provide only approximations to water quality evolution down an actual flow path. In general, the NETPATH results show relatively good fit between the $\delta^{13}C$ modeled and observed values, and there are very few inconsistencies between the mass transfer and the saturation indices.

Back and others (1983) identified another kind of check for whether the NETPATH solutions are consistent with dedolomitization. By combining the $\delta^{14}C$ ages of the groundwater with the mass transfer calculations, rates of dolomite and gypsum dissolution and calcite precipitation can be determined (table 8.4). For dolomite dissolution the mean is about $9.6 \times 10^{-5}$ mmol/yr/kg of $H_20$/yr. The mean gypsum dissolution rate is about $1.95 \times 10^{-4}$ mmol/yr/kg of $H_20$/yr and the average precipitation of calcite is $1.95 \times 10^{-4}$ mmol/yr/kg $H_20$/yr. As previously discussed, dissolution of dolomite and precipitation of calcite are driven irreversibly by the solution of gypsum. If dolomite and calcite maintain approximate equilibrium with constant compositions, then the rate of calcite precipitation should be equal to the gypsum dissolution rate. Stoichiometry dictates that because of the common ion effect, the dolomite dissolution rate should be half the calcite precipitation. The calculated dissolution/precipitation rates in the Salt Basin do follow this pattern.

**Table 8.4** NETPATH mass-transfer

| *Initial Well* | *Final Well* | *Northing* | *Calcite* | *Gypsum* | *Dolomite* | *Calcite* | *Gypsum* | *Dolomite* |
|---|---|---|---|---|---|---|---|---|
| *Flow Path 1* | | *(m)* | *(mmol)* | *(mmol)* | *(mmol)* | *(mmol/yr)* | *(mmol/yr)* | *(mmol/yr)* |
| SM-0138 | Doll Day | 3607510 | -1.23 | 0.90 | 0.41 | -4.2E-04 | 3.0E-04 | 1.4E-04 |
| SM-0138 | Pinon W. | 3606290 | -2.05 | 1.31 | 0.37 | -4.8E-04 | 3.1E-04 | 8.7E-05 |
| Doll Day | Una | 3596995 | -3.29 | 3.31 | 1.15 | -4.6E+00 | 4.7E-04 | 1.6E-04 |
| Una | Cauahpe | 3588103 | 0.74 | -0.53 | 0.04 | 9.3E-05 | -6.6E-05 | 5.2E-06 |
| Cauhape | Collins | 3568454 | -3.37 | 4.30 | 1.07 | -3.5E-04 | 4.4E-04 | 1.1E-04 |
| Cauhape | Evrage | 3563888 | -3.12 | 3.76 | 0.74 | -2.4E-04 | 2.9E-04 | 5.8E-05 |
| Cauhape | Harvey Lewis | 3571455 | -2.14 | 1.72 | 0.41 | -1.8E-04 | 1.4E-04 | 3.4E-05 |
| Harvet Lewis | Collins | 3568454 | -1.24 | 2.57 | 0.66 | -9.3E-05 | 1.9E-04 | 4.9E-05 |
| Harvey Lewis | Hunt C13 | 3543329 | -1.07 | 1.79 | 0.79 | -7.5E-05 | 1.3E-04 | 5.5E-05 |
| Harvey Lewis | Hunt House | 3544407 | -0.50 | 1.25 | 0.49 | -3.2E-05 | 8.2E-05 | 3.2E-05 |
| *Flow Path 2* | | *(m)* | *(mmol)* | *(mmol)* | *(mmol)* | *(mmol/yr)* | *(mmol/yr)* | *(mmol/yr)* |
| SM-0138 | Webb H. | 3606007 | 0.08 | 0.09 | 0.33 | 8.2E-05 | 9.0E-05 | 3.3E-04 |
| Webb H. | Jeffers | 3585742 | -2.30 | 0.96 | 0.29 | -2.8E-04 | 1.2E-04 | 3.5E-05 |
| Webb H. | Ellett | 3578554 | -2.21 | 0.73 | -0.04 | -1.6E-04 | 5.3E-05 | -3.0E-06 |
| Jeffers | Lewis | 3557145 | -1.56 | 3.17 | 0.95 | -1.4E-04 | 2.8E-04 | 8.5E-05 |
| Lewis | Hunt 8 | 3544143 | -2.55 | 2.27 | 0.91 | -1.8E-04 | 1.6E-04 | 6.4E-05 |
| Lewis | Butterfield | 3546210 | -6.66 | 6.27 | 2.39 | -4.1E-04 | 3.9E-04 | 1.5E-04 |

The apparent groundwater ages determined using NETPATH are almost identical to those calculated using the dedolomitization reaction model. Again, there is good agreement between the two flow paths with the Hunt wells at the distal end of flow paths 1 and 2 all having water ages around 15,000 years. The radiocarbon age determined for Ellett Well is somewhat anomalous. However, this well has been singled out as an anomaly in temperature measurement (6.1.a) and chemistry composition (6.2.b) as well. The difference at this well compared to the regional trend is likely the result of vertical upwelling due to a localized fault. The two wells west of the main flow path (Bennett and Butterfield) again show the oldest apparent age.

**Table 8.5** NETPATH radiocarbon correction

| ***Initial Well*** | ***Final Well*** | ***Northing*** | ***$\delta^{13}C$ meas.*** | ***$\delta^{13}C$ model*** | ***d14C meas.*** | ***d14C model*** | ***Age*** |
|---|---|---|---|---|---|---|---|
| *Flow Path 1* | | *(m)* | *(per mil)* | *(per mil)* | *(pmc)* | *(pmc)* | *(years)* |
| SM-0138 | Doll Day | 3607510 | -10.30 | -7.26 | 51.74 | 73.84 | 2900 |
| SM-0138 | Pinon W. | 3606290 | -8.30 | -7.44 | | 73.99 | 4200 |
| Doll Day | Una | 3596995 | -5.90 | -5.11 | 27.66 | 45.76 | 7100 |
| Una | Cauahpe | 3588103 | -7.90 | -4.58 | 34.82 | 38.69 | 8000 |
| Cauhape | Collins | 3568454 | -5.20 | -3.76 | 19.62 | 24.23 | 9700 |
| Cauhape | Evrage | 3563888 | -5.20 | -3.20 | 15.37 | 27.53 | 12800 |
| Cauhape | Harvey Lewis | 3571455 | -4.50 | -6.41 | 19.74 | 32.39 | 12000 |
| Harvet Lewis | Collins | 3568454 | -5.20 | -2.02 | 19.62 | 22.79 | 13300 |
| Harvey Lewis | Hunt C13 | 3543329 | -6.00 | -1.64 | 22.50 | 25.19 | 14200 |
| Harvey Lewis | Hunt House | 3544407 | -5.30 | -2.52 | 22.78 | 29.06 | 15300 |
| *Flow Path 2* | | *(m)* | *(per mil)* | *(per mil)* | *(pmc)* | *(pmc)* | *(years)* |
| SM-0138 | Webb H. | 3606007 | -9.80 | -7.27 | | 76.36 | 1000 |
| Webb H. | Jeffers | 3585742 | -7.80 | -8.85 | 29.04 | 69.36 | 8200 |
| Webb H. | Ellett | 3578554 | -5.70 | -10.39 | 14.37 | 76.90 | 13800 |
| Jeffers | Lewis | 3557145 | -7.70 | -3.96 | 33.09 | 47.56 | 11000 |
| Lewis | Hunt 8 | 3544143 | -5.20 | -4.24 | 22.71 | 32.29 | 14100 |
| Lewis | Butterfield | 3546210 | -3.70 | 0.026 | 8.19 | 14.75 | 16100 |

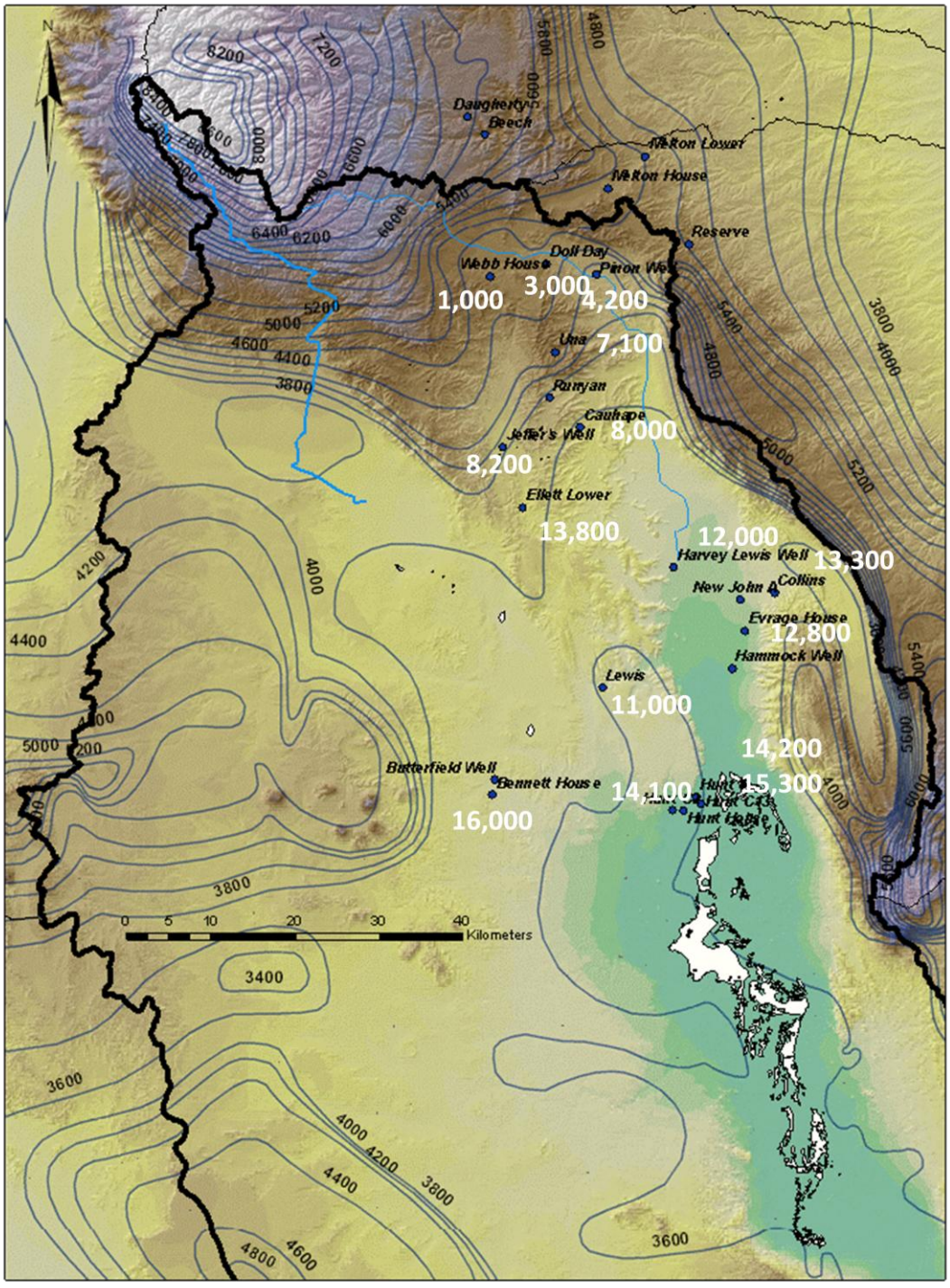


**Figure 8.10** Distribution of apparent groundwater age in the Salt Basin based on geochemical evolution using inverse modeling in NETPATH.

## Section 8.5: Implications for Recharge from Radiocarbon Dating

The apparent age distribution (fig 8.6) based on interpretation of the carbon-14 in the Salt Basin aquifer system is similar to that of the dedolomitization model. The groundwater age is an indication of how long a water particle has been in the aquifer system since recharge. With an understanding of sources of recharge and flow paths, the groundwater age can be directly related to recharge rates in the Salt Basin. Determining the extent of recharging fluxes into the Salt Basin groundwater system is a critical component to proper resource management.

### Section 8.5.a: Seepage Velocity/ Hydraulic Conductivity

Along well-defined flow paths apparent water ages can be used to calculate seepage velocity; *seepage velocity* ($\upsilon$) = $\frac{length\ of\ flow\ path(\Delta L)}{apparent\ age\ (\Delta t)}$. This means the seepage velocity ($\upsilon$) is equivalent to the slope in a plot of distance down the flow path versus groundwater age (fig 8.11). Seepage velocities through the sub-regions of the Salt Basin (fig 6.1) were calculated (table 8.6).

**Table 8.6** Flow velocity and hydraulic conductivity estimated in the Salt Basin

| *Region* | *Seepage Velocity ($\upsilon$)* | *Darcy Velocity (q)* | | *Hydraulic Cond. (K)* | | *Hydraulic Cond. (K)* | |
|---|---|---|---|---|---|---|---|
| | (m/yr) | (m/yr) | | (m/y) | (m/s) | (m/y) | (m/s) |
| | | ne=8% | ne=15% | ne=8% | ne=8% | ne=15% | ne=15% |
| *Pinon Area* | 2.5 | 0.2 | 0.4 | 17.4 | 5.5E-07 | 32.7 | 1.1E-06 |
| *Cornucopia Draw* | 10.2 | 0.8 | 1.5 | 29.7 | 9.4E-07 | 29.7 | 9.7E-07 |
| *Crow Flats* | 8.6 | 0.7 | 1.3 | 294.9 | 9.4E-06 | 294.9 | 9.6E-06 |
| *Salt Basin Average* | 5.1 | 0.4 | 0.8 | 70.3 | 2.2E-06 | 131.8 | 4.3E-06 |

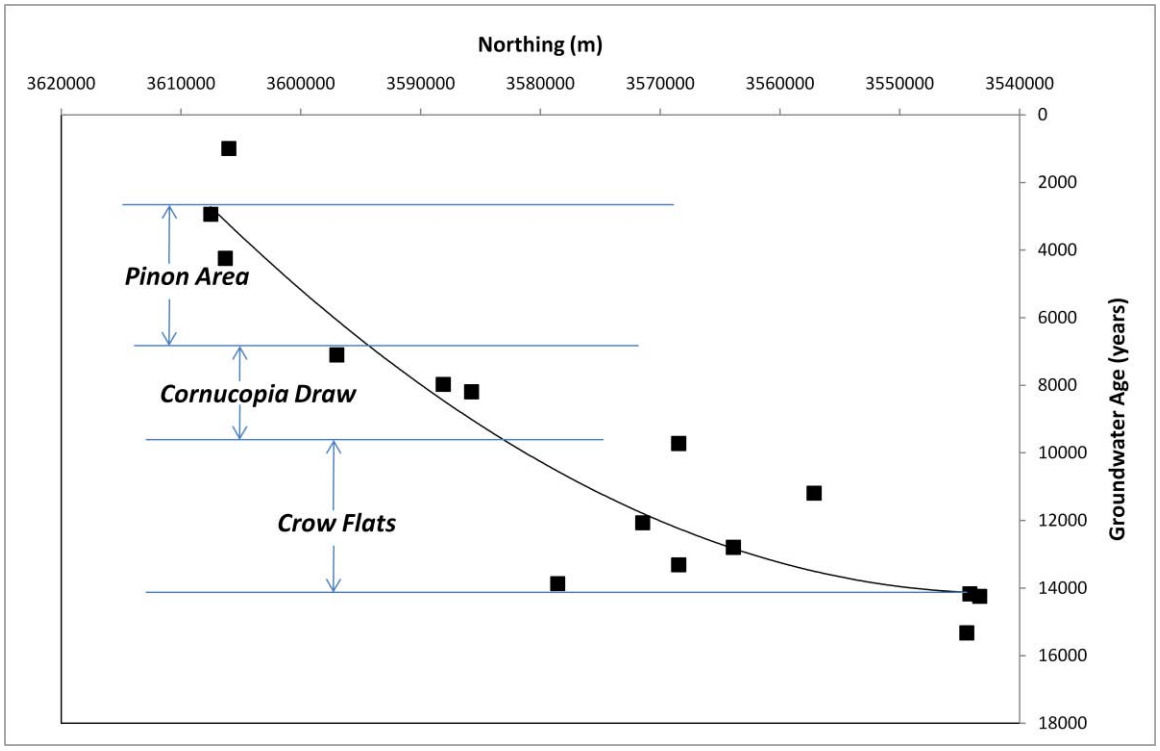


**Figure 8.11** Distance down the flow path versus groundwater age. The slope through each sub-region is equivalent to the seepage velocity (υ) m/yr.

Conservative environmental tracers like $\delta^{14}C$ move with the water and are thus a measure of the actual flow velocity or seepage velocity, which is greater than the Darcy velocity ($q$) (Swartz and Zhang, 2003). Built into the Darcy velocity is an assumption that flow occurs over the entire surface area when water really only flows through the pore space. If the effective porosity ($n_e$) of the aquifer is known or can be accurately estimated, the Darcy velocity can be calculated (table 8.6) where: $q = \upsilon \times n_e$.

To the east of the Salt Basin lies the Permian Delaware Basin where dolomite reservoirs are well known and characterized for their oil production. Porosity and depth relationships for Permian formations such as the San Andres and Abo have been evaluated (Galloway, 1983) and can be used as estimates for porosity of the aquifer

system in the Salt Basin. Based on the distribution of porosity in these dolomite reservoirs a range between 8-15% porosity ($n_e$) seems consistent for the San Andres and Abo formations (fig 8.12). While the Yeso formation is not part of the study, depositionally it is intermediate between the Abo and the San Andres and would likely have a similar porosity range.

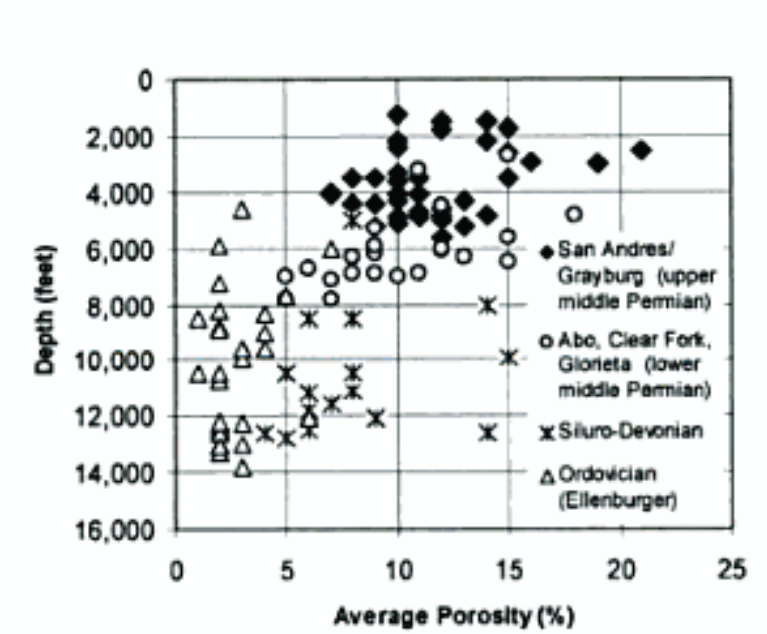


**Figure 8.12** Plot of average porosity versus depth for major west Texas oil field (Galloway, 1983)

The hydraulic conductivity (K) can then be calculated using Darcy's law where:

$q = K\frac{\Delta H}{\Delta L}$, and $\frac{\Delta H}{\Delta L}$ is the hydraulic gradient (table 8.6). The hydraulic conductivities calculated along the flow paths in the Salt Basin are within the range associated with limestone and dolomite commonly reported in the literature (fig 8.13). The estimates for hydraulic conductivity were also compared to previously reported

values for the aquifer units (fig 8.13). In general the estimates are consistent. The hydraulic conductivity through Piñon area and Cornucopia Draw are very similar to values reported for the Yeso (Shomaker, 2002). The average hydraulic conductivity over the entire flow path for the Salt Basin ranges between values reported for the San Andres and Yeso (Shomaker, 2002). The highest hydraulic conductivity is associated with the Crow Flats region due to the very low hydraulic gradient. This estimate is still significantly lower than estimates previously reported. Shomaker (2002) used a hydraulic conductivity of about 3.5 x $10^{-4}$ m/s to model the Crow Flats and Dell City region.

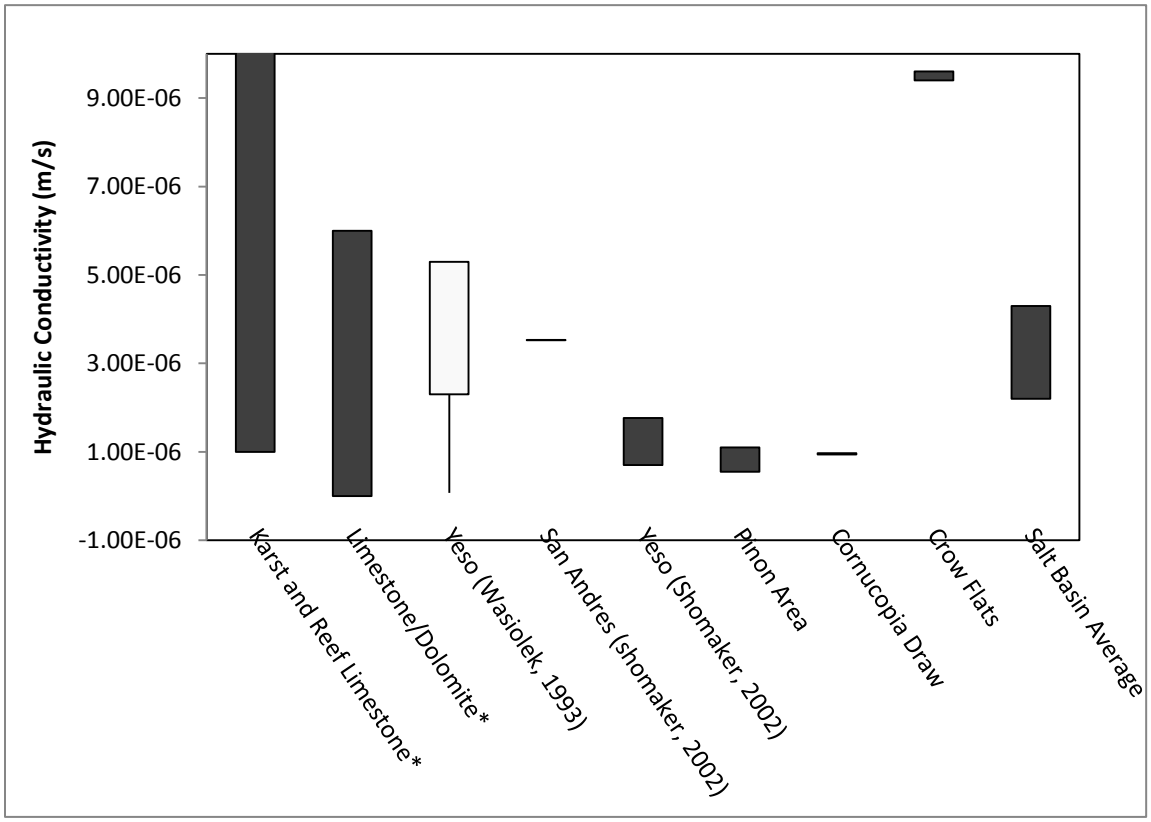


**Figure 8.13** Hydraulic conductivity estimates for the Salt Basin compared to previous reported estimates, as well as literature values* (Schwartz and Zhang, 2003). The tail indicates the drop in conductivity from fractured to unfractured zone of the Yeso (Wasiolek, 1993).

**Section 8.5.b: Piston-flow Approximation**

The trend in groundwater age down the flow path is remarkably consistent with first order exponential decay associated with carbon-14 radioactive decay. This indicates that mixing by dispersion/diffusion along the flow path may be relatively insignificant. If that is the case, the Salt Basin may be appropriately modeled using a simplified approximation such as piston-flow. With piston-flow (or streamtube) analysis (fig 8.14) the age ($\tau$) of groundwater is distance (x) to fluid packet's point of recharge divided by distance-averaged flow velocity ($\upsilon_x$) (Benthke and Johnson, 2002).

$$\frac{d\tau}{dx} = \frac{1}{v_x} \text{ or } \tau(x) = \int_0^x \frac{dx}{v_x} = \frac{x}{\overline{v_x}}$$

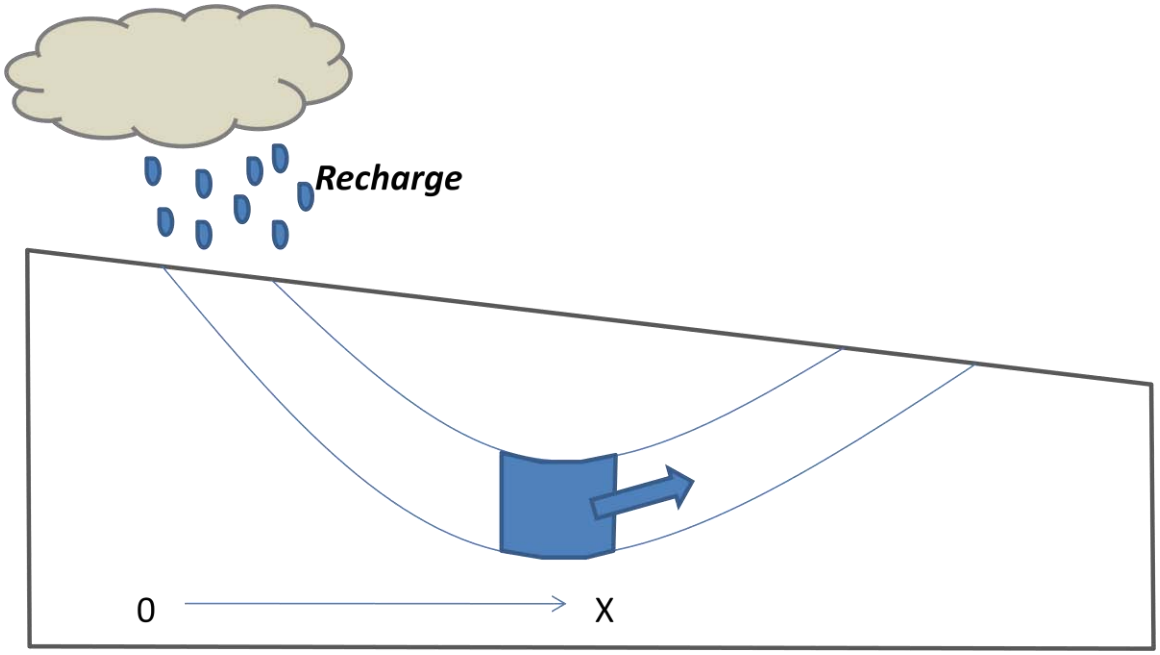


**Figure 8.14** Piston-flow approximation (Bethke and Johnson, 2002).

The piston-flow approximation is very similar to the groundwater ages determined using NETPATH (fig 8.15). This indicates that there is limited mixing along flow paths on the eastern side of the Salt Basin. One reason the piston-flow approximation may be a reasonable conceptual model for the Salt Basin is that water movement through the fracture systems behaves like flow through a streamtube.

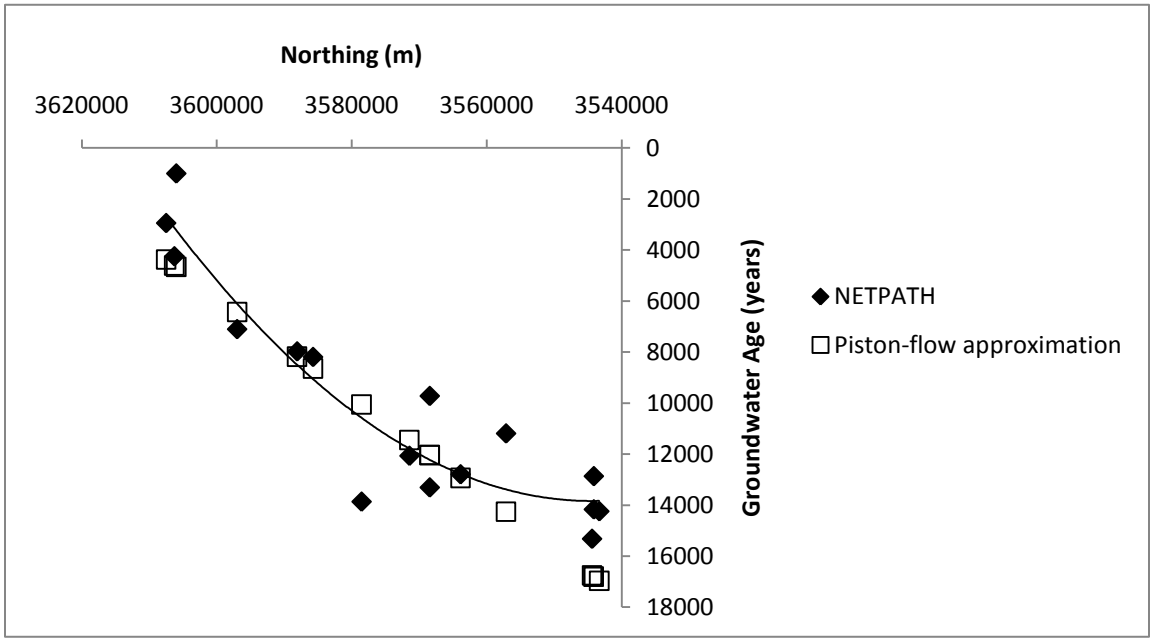


**Figure 8.15** Piston-flow compared to NETPATH groundwater age approximations as a function of Northing (m) along the flow paths.

### Section 8.5.c: Groundwater Flux Calculation

To calculate the subsurface flux from the Sacramento Mountains and northern Salt Basin a cross-section is defined perpendicular to the groundwater flow paths used for geochemical modeling (fig 8.16). The width is about 30 kilometers, encompassing the subsurface flux northeast of the Otero Break.

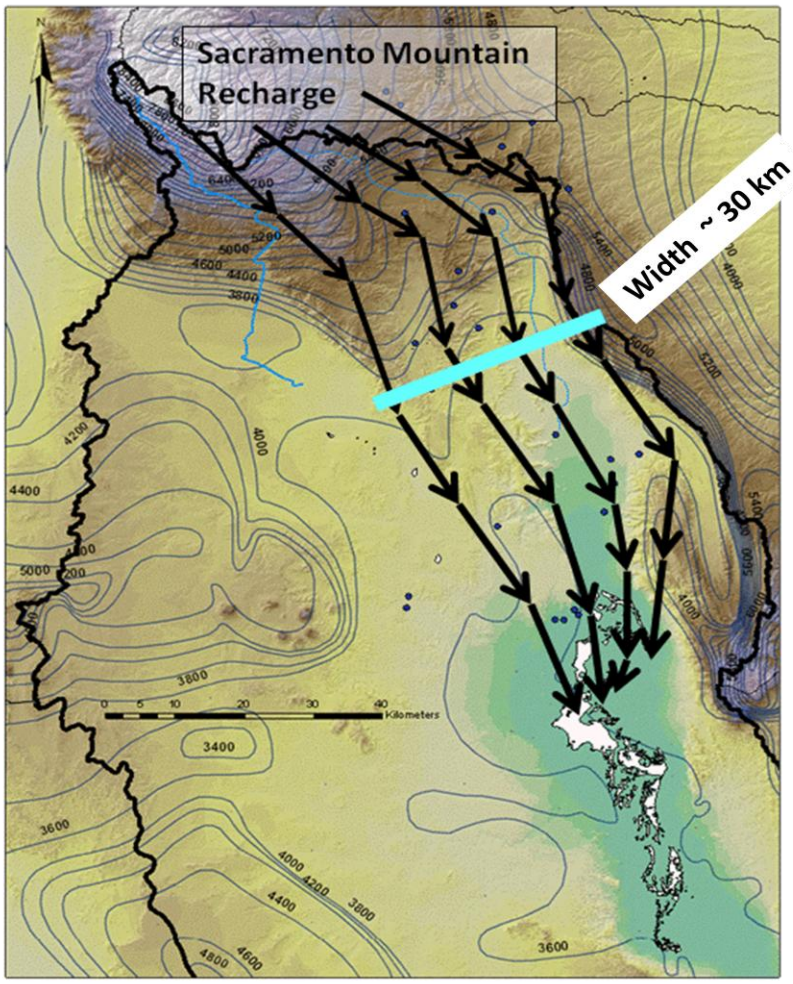


**Figure 8.16** Cross-sectional width for subsurface flux calculation along flow paths northeast of the Otero Break in the Salt Basin.

The $\delta^{34}SO_4$ ratios can be used as lithologic tracers in the Salt Basin (chapter 5.5). Sulfate enrichment in the groundwater of the Salt Basin most likely originates from dissolution of sulfate bearing minerals (i.e. gypsum or anhydrite) caused by meteoric waters that infiltrate in to the extensive carbonate sequences. The Yeso and the San Andres formations have been shown to exhibit distinct ranges of $\delta^{34}SO_4$ composition

(Szynkiewicz, 2009). This distinction can be used as a stratigraphic tracer for water movement through each unit (fig 8.17).

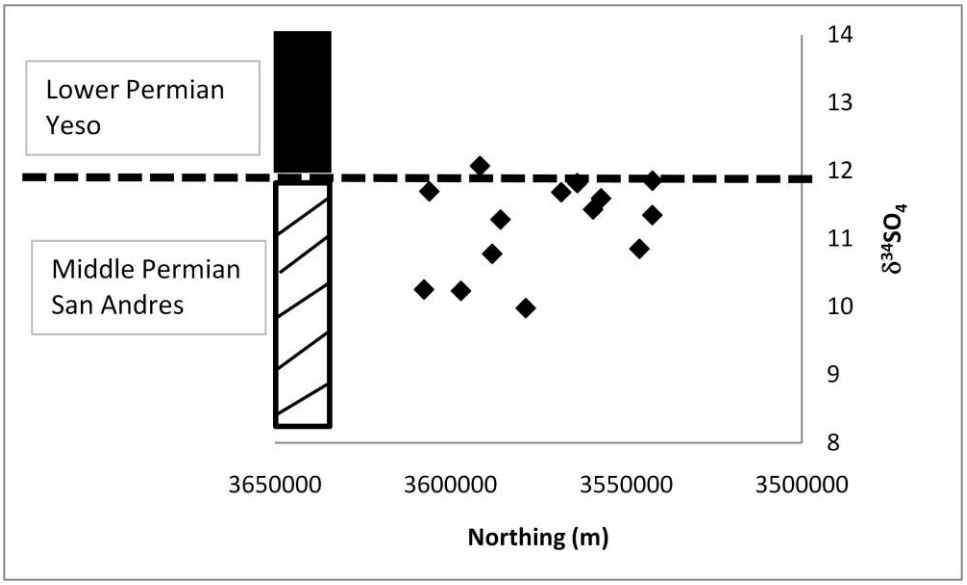


**Figure 8.17** $\delta^{34}SO_4$ isotope compositions (per mil) from Salt Basin groundwater as a function of the well position based on Northing (m). Interpretation of $\delta^{34}SO_4$ isotope signature (Szynkiewicz, 2009).

The San Andres appears to be the dominant influence of the isotopic signature of the $\delta^{34}SO_4$ in the Salt Basin groundwater. This means the water picks up most of the gypsum/anhydrite as dilute rain water infiltrating through the San Andres (the upper stratigraphic unit). Water level correlations with stratigraphic sequences in the Salt Basin (fig 8.18) indicate that the Yeso formation transmits a significant amount of flow through the eastern side of the Salt Basin (Ritchie, 2010). The aquifer thickness for the region where the subsurface flux was calculated across is about 300 m (fig 8.18). With a width of 30 km and a depth of 300 m the total cross-sectional area (A) for the flux calculation is

1.5 x $10^7$ $m^2$. The total subsurface flux through the eastern side of the Salt Basin is a simple multiplication of the cross-sectional area and the Darcy velocity (*q*) in the region.

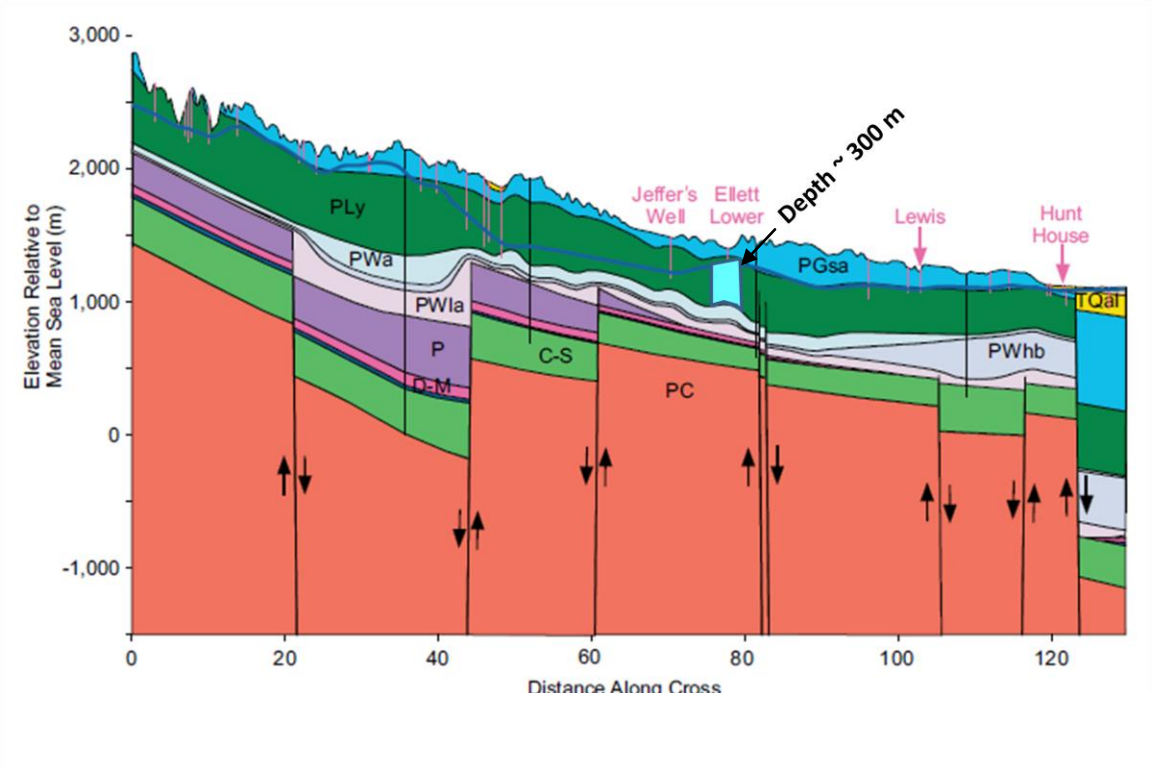


**Figure 8.17** Stratigraphic cross-section down the flow paths on the eastern side of the Salt Basin (Richie, 2010). PGsa (San Andres), Ply (Yeso), PWa (Abo), PWhb (Hueco), Pwla (lower Abo), P (Pennsylvanian), D-M (Devonian-Mississippian), C-S (Cenozoic – Silurian), PC (Pre-Cambrian)

The Darcy velocity (q) through Cornucopia Draw region is 0.8 m/yr and 1.5 m/y for 8% and 15% porosity, respectively (table 8.6). Volume flux (Q) = q x A, giving a subsurface flux through the eastern side of the Salt Basin. Depending the on porosity, the minimum subsurface flux is 7.2 x $10^6$ $m^3$/yr (6,000 acre-ft/yr) and maximum subsurface flux is 1.35 x $10^7$ $m^3$/yr (11,000 acre-ft/yr). This corresponds to annual recharge rates through the eastern side of the Salt Basin from the Sacramento Mountains.

The presence of additional subsurface fluxes along these flow paths, for instance from the Guadalupe Mountains, and other hydrodynamics of the system are not explicitly addressed in the radiocarbon dating model. However, in solving the net mass balance for water along the flow paths, the introduction or the mixing of water cannot not be accounted for explicitly and thus any possible contribution from these sources become incorporated into the overall mass balance solution.

### Section 8.5.d: Water Age Correlations with Evolution along Flow Paths

Correlations between magnesium concentration with age (fig 8.19) and sulfate concentration with age (fig 8.20) confirm that these environmental tracers can be used as proxies for residence time. The increase in aqueous magnesium and sulfate in the groundwater is a time-dependant process related to the dissolution of dolomite and gypsum as the water travels along flow paths. Magnesium is likely the more consistent tracer because the more evaporitic facies of the Yeso formation under Otero Mesa do seem to be associated with much higher sulfate concentrations in the groundwater that may not be a single function of increased residence time.

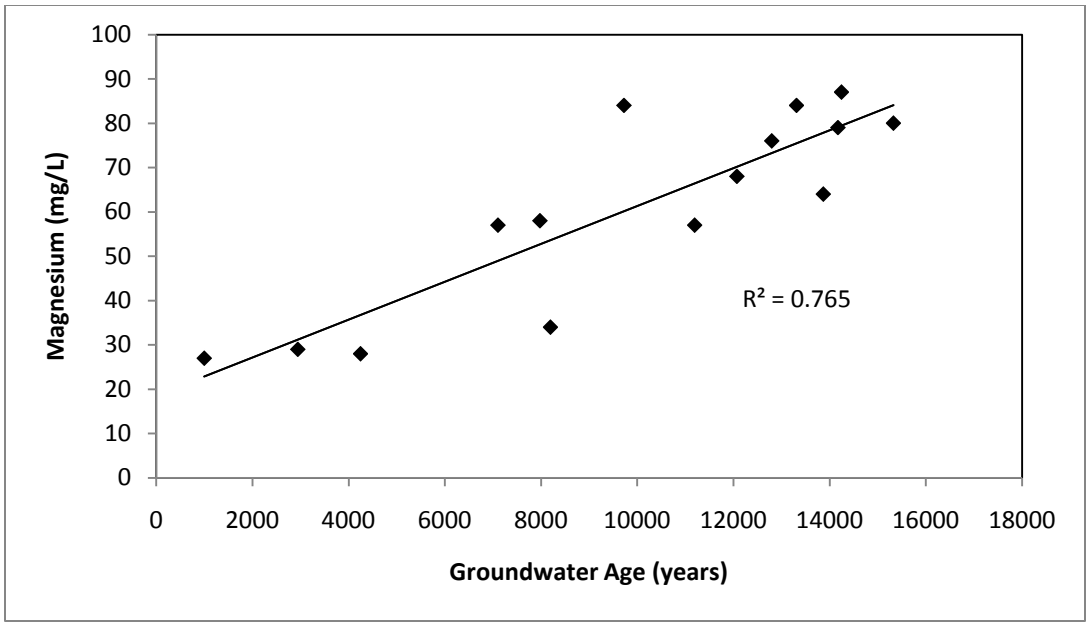


**Figure 8.19** Solute correlations with NETPATH age for magnesium in the Salt Basin.

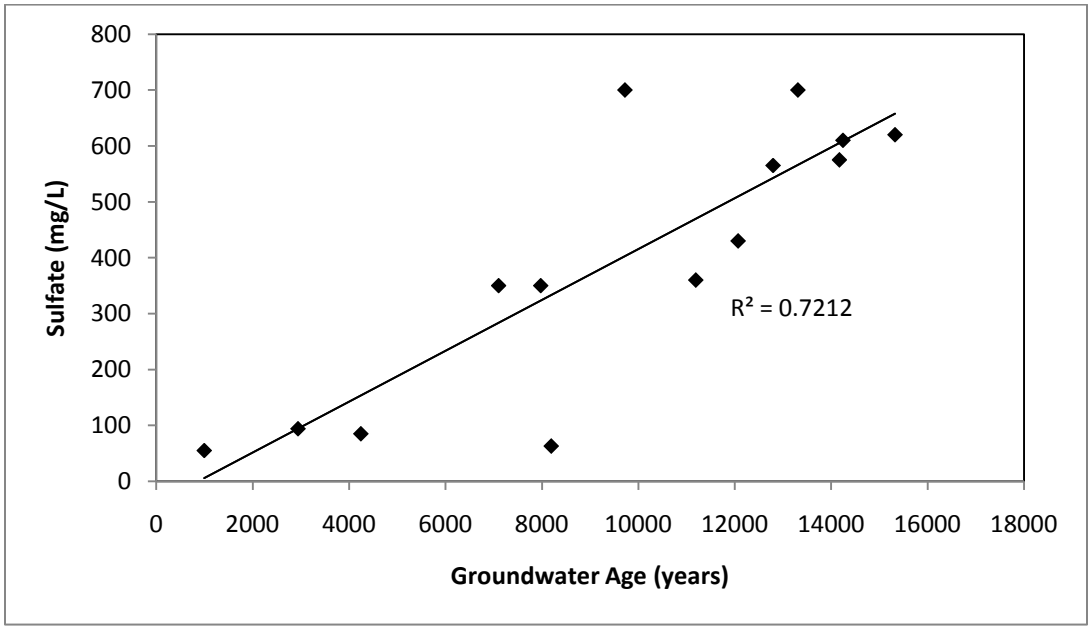


**Figure 8.20** Solute correlations with NETPATH age for sulfate in the Salt Basin.

The correlation between groundwater age and the increase magnesium or sulfate concentration means that although geochemical modeling with radiocarbon data was only performed on flow paths on the eastern side of the Salt, the basin-wide distribution of these constituents (Figures 6.37 and 6.38) have implications for relative fluxes on the western side of the Salt Basin. For example, flow velocities through the Otero Break do appear to be higher than those east of the break. However, flow velocities west of the Otero Break appear to be lower than flow velocities on the eastern side of the Salt Basin. The groundwater ages from Bennett and Butterfield (just east of the Cornudas Mountains) are older than any of the wells on the eastern side of the basin. They also lie within a region of particularly high magnesium and sulfate concentrations (Figures 6.37 and 6.38). The presence of old water in this region has implications for whether or not there is significant recharge from the Cornudas Mountains entering the Salt Basin graben, as well as what the relative groundwater flux from the western side of the Salt Basin is compared to the flow paths on the eastern side.

# CHAPTER IX

## CONCLUSION

Through this geochemical evaluation several characteristics of the Salt Basin aquifer system were revealed that will play a significant role in future resource management. Environmental tracers measured from the Salt Basin aquifer system were used to identify sources recharge, define flow paths, determine the relative amount of mixing from different sources to the groundwater, identify sources of solutes, and estimate flow velocities and recharge rates. The use of environmental traces to determine groundwater ages means that recharge rate and flow velocities can be determined independently of more traditional aquifer tests. In the Salt Basin the result is likely more accurate as hydraulic properties of the aquifer are poorly defined and spatially variable.

The present depositional facies and structure of the Salt Basin is the result of a complex geologic history. Extensive periods of transgression and regression during the deposition of the Permian aquifer units have led to highly heterogeneous formations. These were further complicated by subsequent tectonism resulting in regional fault systems which play a dominant role in groundwater movement in the basin. The distribution of solutes appears to be strongly correlated with fault zones, which in addition to elucidating patterns in groundwater flow, highlight regions within the Salt Basin that are particularly vulnerable in terms of groundwater contamination.

While there are many sources for water entering the Salt Basin graben including Guadalupe Mountain runoff, distributed recharge throughout the basin from storm event

infiltration, as well as, flow across the Diablo Plateau; the main source of recharge is in the Sacramento Mountains. The water chemistry along the flow path on the eastern side of the Salt Basin is consistent with groundwater evolution starting in the Sacramento Mountains and moving south to the Salt Flats near Dell City where it discharges. East of the Otero Break in the Salt Basin are distinct flow paths along which a complete reaction series for the dedolomitization process can be observed. This groundwater reaction involves dissolution and precipitation of carbonate minerals that drive changes in $\delta^{13}C$ and $\delta^{14}C$ (Back, 1983). This means that $\delta^{14}C$ values measured in the laboratory must be adjusted to correct for these rock/water interactions for more accurate age estimations. Along well defined flow paths, groundwater ages can be used to calculate average seepage velocities and estimate recharge rates.

Radiocarbon dating in the Salt Basin indicates that flow velocities through the aquifer system are relatively low along the eastern side of the Salt Basin. Flow velocities (q) range from about 0.5 to 1.5 m/yr. This means that residence times in the Salt Basin are relatively long. The groundwater ages for the Crow Flats and Dell City regions are from about 10,000- 15,000 years old. These ages are consistent with the oxygen and deuterium measured in Crow Flats and Dell City where isotopic signatures indicate Pleistocene aged recharge.

If the effective porosity of the aquifer is known or can be accurately estimated, using the seepage velocity the hydraulic conductivity of the aquifer can be easily estimated. This means across the flow paths on the eastern side of the Salt Basin a subsurface flux could be determined for the aquifer system over a given thickness. The subsurface flux gives an estimate of the annual recharge rate to the Salt Basin from the

Sacramento Mountains. Porosity was estimated between 8 and 15% based on observations from the San Andres and Abo formation. The aquifer thickness was estimated at 300 m through the middle section of the flow path. The subsurface flux or recharge from the Sacramento Mountains through the eastern side of the Salt Basin ranges from about 6,000 to 11,000 acre-ft/yr.

The correlation between groundwater age and increase in magnesium or sulfate concentration in the Salt Basin means that although geochemical modeling with radiocarbon data was only performed on flow paths on the eastern side of the Salt Basin, the basin-wide distribution of these constituents have implications for relative fluxes on the western side of the Salt Basin. Relative to flow through the eastern side of the basin, flow through the Otero Break appears higher and flow on the western side of the basin appears slightly lower. Assuming that the flow path on the eastern side of the Salt Basin constitutes about 1/3 of the total recharge, then a very approximate estimate for total recharge to the Salt Basin would be about 18,000 to 35,000 acre-ft/yr. Roughly estimating that the Sacramento Mountains represent about 30 $km^2$ of recharge area with average precipitation of about 60 cm/yr, then the amount of recharge to the Salt Basin would constitute about 4% to 8% of the total precipitation.

The estimates for recharge to the Salt Basin from this study fall at the lower end of the range (~15,000-100,000 acre-ft/yr) presented by the State Engineer's Office. They are also well below the current rate of groundwater pumping (~100,000 acre-ft/yr) in Dell City. This implies future resource management of the Salt Basin is critically important.

# REFERENCES


Andrews, J. N., and Lee, D. J. (1979) Inert gases in groundwater from the Bunter Sandstone of England as indicators of age and paleoclimate trends, *Journal of Hydrology, 41,* 233-252.

Back, W. (1983) Process and rate of dedolomitization: Mass transfer and 14C dating in a regional carbonate aquifer, *Geological Society of America Bulletin*, *94*, 1415-1429.

Back, W. and Hanshaw, B. (1970) Comparison of chemical hydrogeology of the carbonate peninsulas of Florida and Yucatan, *Journal of Hydrology 10,* 330-368.

Back, W. and Freeze, R. (1983) *Chemical Hydrogeology*, Benchmark Papers in Geology-73, *Hutchinson and Ross, Stroudsburg, Pennsylvania.*

Bakalowicz, M. (2005) Karst groundwater: A challenge for new resources, *Hydrogeology Journal, 13* (1), 148-160.

Bethke, C., and Johnson, T. (2002) Groundwater age, *Groundwater 40,* 337-339.

Bjorklund, L. J. (1957) Reconnaissance of Ground-Water Conditions in the Crow Flats Area, Otero County, New Mexico, *State of New Mexico State Engineer Office Technical Report 8,* 26.

Black, B. A. (1973) Geology of the Northern and Eastern Parts of the Otero Platform, Otero and Chaves Counties, New Mexico, *University of New Mexico, PhD. Geology, Albuquerque NM,* 170.

Black, B. A. (1975) Geology and oil and gas potential of the northeast Otero Platform area, New Mexico, *New Mexico Geological Society Guidebook, 26th Field Conference, Las Cruces Country ,N.M. Bureau of Mines and Mineral Resources,* 323-333.

Black, B. A. (1976) Tectonics of the northern and eastern parts of the Otero Platform, Otero and Chaves Counties, New Mexico, In Woodward, L. A. and Northrop, S. A. (Eds.), *Tectonics and Mineral Resources in Southwestern North America: New Mexico Geological Society Special Publication 61, N.M. Bureau of Mines and Mineral Resources,* 39-45.

Bodine, M. W. and Jones, B. F. (1986) THE SALT NORM: A quantitative chemical-mineralogical characterization of natural waters, *U.S. Geological Survey Water Resources Investigations Report 86-4086,* 130.

Boyd, F. M. (1982) Hydrogeology of the Northern Salt Basin of West Texas and New Mexico, *University of Texas, Master of Arts, Austin T.X.,* 135.

Broadhead, R. F. (2002) Petroleum geology of the McGregor Range, Otero County, New Mexico, *New Mexico Geological Society Guidebook, 53rd Field Conference, Geology of White Sands, N.M. Bureau of Mines and Mineral Resources,* 331-338.

Brook, G., Folkoff, M., and Box, E. (1983) A world model of soil carbon dioxide, *Earth Surface Processes 8,* 79-88.

Buynak, B. (2007) Salt Basin *in Water Matters! (2009), The Utton Center Transboundary Resources, University of New Mexico, N.M.,* 59-62.

Chace, D. A. and Roberts, R. M. (2004) South-central Salt Basin groundwater characterization, *El Paso Geological Society Field Guide Book for the Otero Mesa Area, , New Mexico: El Paso Geologic Society,* 47-61.

Chapman, J. (1984) Hydrogeochemisty of the Unsaturated Zone of a Salt Flat in Hudspeth County, Texas, *University of Texas, Master of Arts, Austin T.X.*, 132.

Chesterman, C., (1979) National Audubon Society Field Guide to North American Rocks and Minerals, *National Audubon Society,* 850-900.

Christophersen, N., and Hooper, R.P. (1992) Multivariate analysis of stream water chemical data: The use of principal component analysis for the end-member mixing problem, *Water Resources Research, 28 (1),* 99-107.

Clark, I., and Fritz, P. (1997) Environmental Isotopes in Hydrogeology, *CRC Press LLC,* Boca Raton FL, 198-199.

Coplen, T., Herczeg, A., and Barnes, C. (2000) Isotope engineering-using stable isotopes of the water molecule to solve practical problems *in* Environmental Tracers in Subsurface Hydrology, Cook, P., and Herczeg, A. *Kluwer Academic Publishers, Boston,* 79-110.

Deines, P., Langmuir, D., and Harmon, R., (1974) Stable carbon isotope ratios and the existence of a gas phase in the evolution of carbonate groundwaters, *Geochim. Cosmochim, Acta. 38,* 1147-1164.

Duffy, C.J. (1997) Density-driven groundwater flow in closed desert basins: field investigations and numerical experiments, *Water Resources Research, 196,* 139-184.

Earman, S., Campbell, A., Phillips, F., Newman, B. (2006) Isotopic exchange between snow and atmospheric water vapor: Estimation of the snowmelt component of groundwater recharge in the southwestern United States, *Journal of Geophysical Research 111, D09302*, doi:10.1029/2005JD006470

Eastoe, C. J. (2002) Isotopes in the Hueco Bolson Aquifer, Texas (USA) and Chihuahua (Mexico): local and general implications for recharge sources in alluvial basins, *Hydrogeology Journal 16 (4),* 737-747.

Edmunds, W., Smedley, P. (1999) Residence time indicators in groundwater; the East Midlands Triassic Sandstone aquifer, *Applied Geochemistry 15*, 737-752.

Edmunds, W., Cook, J., Kinniburgh, D., Miles, D., Bath, A., Morgan-Jones M., and Andrews, J. (1987) Baseline geochemical conditions in the chalk aquifer, Bershire UK: a basis for groundwater quality management, *Applied Geochemistry 2,* 251-274.

Eugster, H. P. (1978) Saline lakes, *Chemistry, Geology, and Physics* ed. A. Lerman, *Springer N.Y.,* 237-293.

Finch, S. T., Jr. (2002) Hydrogeologic Framework of the Salt Basin and Development of Three-Dimensional Ground-Water Flow Model, *John Shomaker & Associates, Inc. Final Report, Prepared for New Mexico Interstate Stream Commission*, 28 p.

Fritz, P., and Fontes, J., (1980) Handbook of Environmental Isotope Geochemistry (vol 1), the Terrestrial Environment, *Elsevier, Amsterdam,* 545.

Galloway, W., Ewing T., Garrett Jr. C., Tyler N., and. Bebout D. (1983) Atlas of major Texas oil reservoirs, *University of Texas, Austin, Bureau of Economic Geology Special Publication*, 139.

Gat, J.R (1980) The isotopes of hydrogen and oxygen in precipitation *in* Handbook of Environmental Isotope Geochemistry (vol 1), Fritz, P., and Fontes, J., *Elsevier, Amsterdam*, 21-47.

Gibbard, P., Head, M., Walker, M., and the Subcommission on Quaternary Stratigraphy (2009) Formal ratification of the Quaternary System/Period and the Pleistocene Series/Epoch with a base at 2.58 Ma., *Journal of Quaternary Science*, DOI: 10.1002/jqs.1338

Godwin, H. (1962) Half-life of radiocarbon, *Nature 195 (4845)*, 984.

Goetz, L. K. (1977) Quaternary Faulting in the Salt Basin Graben, West Texas, *University of Texas, Master of Arts, Austin, T.X.*, 136 p.

Goetz, L. K. (1980) Quaternary faulting in Salt Basin graben, West Texas, *New Mexico Geological Society Guidebook, 31st Field Conference, Trans-Pecos Region, N.M. Bureau of Mines and Mineral Resources*, 83-92.

Goetz, L. K. (1985) Salt Basin graben: A basin-and-range right-lateral transtensional fault zone, some speculations, In Dickerson, P. W. and Muehlberger, R. W. (Eds.), *Structure and Tectonics of Trans-Pecos Texas: West Texas Geological Society Publication 85-81, Midland T.X.*, 165-168.

Hanshaw B. B. (1971) A geochemical hypothesis for dolomitization by groundwater, *Economic Geology, 66*(5), 710-724.

Herczeg, A., Edmunds, M. (2000) Inorganic ions as tracers *in* Environmental Tracers in Subsurface Hydrology, Cook, P., and Herczeg, A., *Kluwer Academic Publishers, Boston,* 31-78.

Hooper, R.P. (2003) Diagnostic tools for mixing models of stream water chemistry, *Water Resources Research, 39 (3),* 1055-1068.

Huff, G. F. and Chace, D. A. (2006) Knowledge and understanding of the hydrogeology of the Salt Basin in south-central New Mexico and future study needs, *U.S. Geological Survey Open-File Report 2006-1358*, 17.

Ingraham, N.L. (1990) Stable isotopes in cave pool systems: Carlsbad Cavern, New Mexico, U.S.A., *Chemical Geology, 86,* 65-75.

Kalin, R. (2000) Radiocarbon dating groundwater systems *in* Environmental Tracers in Subsurface Hydrology, Cook, P., and Herczeg, A., *Kluwer Academic Publisher, Boston,*111-143.

Kaufman, S., and Libby, W. F. (1954) The natural distribution of tritium, *Physics Review, 93*, 1337-1344.

Kelley, V. C. (1971) Geology of the Pecos Country, Southeastern New Mexico, *New Mexico Bureau of Mines & Mineral Resources Memoir 24, Socorro N.M.,* 75.

King, P. B. (1948) Geology of the Southern Guadalupe Mountains, Texas, *U.S. Geological Survey Professional Paper 215*, 183.

King, P. B. (1965) Geology of the Sierra Diablo Region Texas, *U.S. Geological Survey Professional Paper 480*, 185.

King, P. B. (1983) Leonard and Wolfcamp Series of Sierra Diablo, Texas, In Meader-Roberts, S. J. (Eds.), *Geology of the Sierra Diablo and Southern Hueco Mountains West Texas: Permian Basin Section Society of Economic Paleontologists and Mineralogists Field Conference Guidebook 83-22, T.X.*, 80-96.

King, P. B., King, R. E., and Knight, J. B. (1945) Geology of the Hueco Mountains, El Paso and Hudspeth Counties, *U.S. Geological Survey Oil and Gas Inv. Prelim. Map, 36*, 2 sheets.

King, W. E. and Harder, V. M. (1985) Oil and Gas Potential of the Tularosa Basin-Otero Platform-Salt Basin Graben Area, New Mexico and Texas, *New Mexico Bureau of Mines and Mineral Resources Circular 198, Socorro, N.M.*, 36 p.

Kreitler, C. W., Mullican, W. F., and Nativ, R. (1990) Hydrogeology of the Diablo Plateau, Trans-Pecos Texas, In Kreitler, C. W. and Sharp, J. M., Jr. (Eds.), *Hydrology of Trans-Pecos Texas: Texas Bureau of Economic Geology Guidebook 25,T.X.*, 49-58.

Krouse, R., and Mayer, B. (2000) Sulphur and oxygen isotopes in sulphate *in* Environmental Tracers in Subsurface Hydrology, Cook, P., and Herczeg, A., *Kluwer Academic Publisher, Boston,* 195-232.

Langmuir, D. (1997) Aqueous Environmental Geochemistry, *Prentice Hall, U.S.A.*, 30-74.

Loaiciga, H., (2004) Residence time, groundwater age, and solute output in steady-state groundwater systems, *Advances in Water Resources 27*, 681-688

Liu, F., Williams, M.W. (2004) Source water and flow paths in an alpine catchment, Colorado Front Range, U.S.A., *Water Resources Research, 40*, 9401.

Liu, F., Bales, R., Conklin M., and Conrad M. (2008) Streamflow generation from snowmelt in semi-arid, seasonally snow-covered, forested catchments, Valles Caldera, New Mexico, *Water Resources Research, 44.* doi:10.1029/2007WR006728

Mayer, J. R. (1995) The Role of Fractures in Regional Groundwater Flow: Field Evidence and Model Results from the Basin-and-Range of Texas and New Mexico, *University of Texas, PhD., Austin, T.X.,* 218.

Mayer, J. R. and Sharp, J. M., Jr. (1995) The role of fractures in regional groundwater flow, in Rossmanith, H. (Eds.), *Mechanics of Jointed and Faulted Rock, U.S.A.*, 375-380.

Mayer, J. R. and Sharp, J. M., Jr. (1998) Fracture control of regional ground-water flow in a carbonate aquifer in a semi-arid region, *Geological Society of America Bulletin, 110*(2), 269–283.

Mazzullo, S.J. (1995) Permian stratigraphy and facies, Permian basin (Texas-New Mexico) and adjoining areas in the Midcontinent United States, *in* Scholle, P., Peryt, T., and Ulmer-

Scholle, D., eds., The Permian of Northern Pangea (vol 2), *Sedimentary Basins and Economic Resources,Spring-Verlag, N.Y.*,41-60.

McGuire, K., and McDonnell, J., (2006) A review and evaluation of catchment transit time modeling, *Journal of Hydrology 330,* 543-563.

Milner, S. (1976) Carbonate petrology and syndepositional facies of the lower San Andres formation (middle Permian), Lincoln County, NM, *Journal of Sedimentary Petrology, 46( 3)* , 463-482.

Mook, W., and van de Plicht, J. (1999) Reporting 14C activities and concentrations, *Radiocarbon 41,* 227-239.

Muehlberger, W. R., Belcher, R. C., and Goetz, L. K. (1978) Quaternary faulting in Trans-Pecos Texas, *Geology, 6*, 337-340.

Muir, N.J. (1978) Depositional Environments and Diagenesis of the Lower San Andres Formation, Roosevelt and Quay Counties, New Mexico, *Texas Tech University, PhD., Lubbock, T.X.,* 68.

National Elevation Dataset: USGS, 2009, www.ned.usgs.gov/

National Hydrography Dataset: USGS, 2010, www.nhd.usgs.gov/

Nelson, S.T., and Dettman, D. (2001) Improving hydrogen isotope ratio measurements for on-line chromium reduction systems, *Rapid Communications in Mass Spectrometry 15*, 1751-1753.

Nutt, C. J., O'Neill, J. M., Kleinkopf, M. D., Klein, D. P., Miller, W. R., Rodriquez, B. D., and McLemore, V. T. (1997) Geology and Mineral Resources of the Cornudas Mountains, New Mexico, *U.S. Geological Survey Open-File Report 97-282*, 46 p.

Phillips, F., Peeters, L., Tansey, M., and Davis, S. (1986) Paleoclimate inferences from an isotopic investigation of ground water in the central San Juan Basin, New Mexico, *Quaternary Research 26,* 179-192.

Plummer, L. N. (1991) Geochemical evolution of water in the Madison Aquifer in parts of Montana, South Dakota, and Wyoming, *U.S. Geological Survey Professional Paper*, 1273-F.

Plummer, L. N. (1994) An interactive code (NETPATH) for modeling net geochemical reactions along a flow path- version 2.0, *USGS Water Resources Investigation Report, 94-4169.*

Rawling, G., Newton, T., Timmons, S., Partey, F., Kludt, T., Land, L., Timmons, M., Walsh, P., (2008) Sacramento Mountain hydrogeology study, *NM Bureau of Geology and Mineral Resources 518, Socorro, N.M.,* 11-53.

Reiter, M., and Jordan, D. (1996) Hydrogeothermal studies across the Pecos River Valley, southeastern New Mexico, *Geological Society of America Bulletin 108*, 747-756.

Ritchie, A., (2010) Hydrogeologic Framework and Development of a 3-D Finite Difference Groundwater Flow Model of the Salt Basin, New Mexico and Texas, *Master of Science, New Mexico Institute of Mining and Technology, Socorro, N.M.*

Ross, C.A. (1986) Paleozoic evolution of southern margin of Permian basin, *Geologic Society of America Bulletin 97,* 536-554.

Rozanski, K., Araguau-Araguas, L, and Confiantini, R., (1993) Isotopic patterns in modern global precipitation *in* Climate Change in Continental Isotopic Records, Stwart, P., Lohmann, K., McKenzi, J., and Savin, S., *American Geophysical Union, Geophysical Mongraph 78,* 1-36.

Rozanski, K., Johnsen, S. J., Schotterer, U., and Thompson, L. G. (1997) Reconstruction of past climates from stable isotope records of palaeo-precipitation preserved in continental archives, *Hydrologic Sciences- Journal-des Sciences Hydrologiques*, *42*, 725-729.

Scalapino, R. A. (1950) Development of groundwater for irrigation in the Dell City Area, Hudspeth County, Texas, *Texas Board of Water Engineers Bulletin 5004*, *T.X.*, 38 p.

Sharp, J. M., Jr. (1989) Regional ground-water systems in northern Trans-Pecos Texas, In Dickerson, P. W., and Muehlberger, W. R. (Eds.), *Structure and Stratigraphy of Trans-Pecos Texas: American Geophysical Union Field Trip Guidebook* T317, *U.S.A.*, 123-130.

Sharp, J. M., Jr. (2001) Regional groundwater glow systems in Trans-Pecos Texas, In Mace, R. E., Mullican, W. F. III, and Angle, E. S. (Eds.), *Aquifers of West Texas: Texas Water Development Board Report 356*, *T.X.*, 41-75.

Sharp, J. M., Jr., Mayer, J. R., and McCutcheon, E. (1993) Hydrogeologic Trends in the Dell City area, Hudspeth County, Texas, *New Mexico Geological Society Guidebook, 44th Field Conference, N.M. Bureau of Mines and Mineral Resources, Carlsbad,* 327-330.

Sharp, Z. (2007) Principles of stable isotope geochemistry, *Prentice Hall*, 65-100 p.

Solomon, D., and Cook, P. (2000) $^{3}$H and $^{3}$He *in* Environmental Tracers in Subsurface Hydrology, Cook, P. and Herczeg, A., *Kluwer Academic Publisher, Boston*, 397-424.

Stoeser, D. B., Green, G. N., Morath, L. C., Heran, W. D., Wilson, A. B., Moore, D. W., and Van Gosen, B. S. (2007) Preliminary Integrated Geologic Map Databases for the United States: Central States: Montana, Wyoming, Colorado, New Mexico, North Dakota, South Dakota, Nebraska, Kansas, Oklahoma, Texas, Iowa, Missouri, Arkansas, and Louisiana, *U.S. Geological Survey Open-File Report, 2005-1351, Version 1.2*. http://pubs.usgs.gov/of/2005/1351/.

Stute, M., Clark, J., Schlosser, P., Broecker, W., and Bonani, G. (1995) A 30,000 yr continental paleotemperature record derived from noble gases dissolved in groundwater from the San Juan Basin, New Mexico, *Quaternary Research 43,* 209-220.

Stuiver, M., and Polach, H. (1977) Discussion—reporting of $^{14}$C Data, *Radiocarbon 19 (3),* 355-363.

Szynkiewicz, A. (2009) Sulfur isotope signatures in gypsiferous sediments of the Estancia and Tularosa Basin as indicators of sulfate sources, hydrologic processes, and microbial actvitity, *Geochimica et Cosmochimica acta 73, M.O.*, 6162-6186.

Tillery, A. (2010) Estimates of mean annual flow and flow loss for ephemeral channels in the Salt Basin, southern New Mexico, *United States Geologic Survey, Scientific Investigation Report 2010-XXXX, Virginia,* 12-19.

Uliana, M. M. (2000) Delineation of Regional Groundwater Flow Paths and their Relation to Structural Features in the Salt and Toyah Basins, Trans-Pecos Texas, *University of Texas, Ph.D., Austin, T.X.*, 215.

Uliana, M. M. (2001) The Geology and hydrogeology of the Capitan Aquifer: A brief overview, In Mace, R. E., Mullican, W. F. III, and Angle, E. S. (Eds.), *Aquifers of West Texas: Texas Water Development Board Report 356, U.S.A.*, 153-166.

Uliana, M. M. and Sharp, J. M., Jr. (2001) Tracing regional flow paths to major springs in Trans-Pecos Texas using geochemical data and geochemical models, *Chemical Geology, 179, U.S.A.*, 53-72.

Uliana, M. M., Banner, J. L., and Sharp, J. M., Jr. (2007) Regional groundwater flow paths in Trans-Pecos, Texas inferred from oxygen, hydrogen, and strontium isotopes, *Journal of Hydrology 334, U.S.A*, 334-346.

Unterweger, M., Coursey, B., Schima, F., and Mann, W., (1980) Preparation and calibration of the 1978 national bureau of standards tritiated-water standards, *International Journal of Applied Radioactive Isotopes 31,* 611-614.

United States Census Bureau, 2010, www.census.gov/

United States Department of Agriculture, 2010, www.usda.gov/

United States Geologic Survey, 2009, Data: obtained from water-streamflow www.water.usgs.gov/

United States Environmental Protection Agency, 2010, www.epa.gov/

Vogel, J.C. and D. Ehhalt (1963), The use of carbon isotopes in groundwater studies, *Radioisotopes in Hydrology, International Atomic Energy Agency, Vienna*, 383-395.

Vogel, J.C. (1967), Investigation of groundwater flow with radiocarbon, *Isotopes in Hydrology, International Atomic Energy Agency, Vienna*, 355-368.

Vogel, J.C. (1970), Carbon-14 dating of groundwater, *Isotope Hydrology 1970, International Atomic Energy Agency, Vienna*, 235-237.

Wasiolek, M., (1991) The hydrogeoly of the Permian Yeso Formation within the Upper Rio Hondo Basin and the eastern Mescalero Apache Indian Reservation, Lincoln and Otero Counties New Mexico, *New Geologic Society Guidebook, N.M. Bureau of Mines and Mineral Resources, Socorro, N.M.,* 343-351.

Wiggins, W. D. (1993) Geochemistry of Post-uplift Calcite in the Permian Basin of Texas and New Mexico, *Geological Society of American Bulletin*779-790.

Yonge, C. J. (1985) Stable isotope studies of cave seepage water, *Chemical Geology (Isotope Geoscience Section), 58,* 97-105.

APPPENDICES

**Appendix A.** Analytical Chemistry from the Salt Basin Groundwater Samples Collected 2008—2009 (Andre Ritchie and Sophia Sigstedt)

**Appendix B.** General Chemistry from the Sacramento Mountains Groundwater Source: New Mexico Bureau of Geology and Mineral Resources

**Appendix C.** Compiled General Chemistry from Groundwater in the Salt Basin Source: Mayer, 1995

# ABSTRACT

The Salt Basin was declared by the New Mexico State Engineer in 2000, estimates for recharge reported vary anywhere from 20,000 to 100,000 acre-ft/yr. In addition to local demands on water for agricultural purposes, interest has arisen in the groundwater resources of the Salt Basin as a future source of water for a number of competing groundwater appropriations bids. Thus, long-term management of the water resources is needed. In order to inform long-term management strategies, this study seeks to establish a conceptual model of groundwater flow in the Salt Basin.

An adequate conceptual model of groundwater flow in the Salt Basin relies on the development of a hydrogeologic framework, which involves reconstructing the tectonic forcings that have affected the basin during its formation, and identifying the depositional environments that formed and the resultant distribution of facies. The distribution of facies and structural features can then be used to evaluate the distribution of permeability within the basin, and conceptualize the groundwater flow system. The aquifer system is further characterized using a suite of environmental tracers to identify sources of recharge, estimates of recharge rate, flowpaths and directions, flow rates, and sources of solutes in the groundwater. This information is critical for determining volumetric fluxes and estimates for the amount of available water in the Salt Basin.